



National Library  
of Canada

Acquisitions and  
Bibliographic Services Branch

395 Wellington Street  
Ottawa, Ontario  
K1A 0N4

Bibliothèque nationale  
du Canada

Direction des acquisitions et  
des services bibliographiques

395, rue Wellington  
Ottawa (Ontario)  
K1A 0N4

*Your file* *Voire référence*

*Our file* *Notre référence*

## NOTICE

The quality of this microform is heavily dependent upon the quality of the original thesis submitted for microfilming. Every effort has been made to ensure the highest quality of reproduction possible.

If pages are missing, contact the university which granted the degree.

Some pages may have indistinct print especially if the original pages were typed with a poor typewriter ribbon or if the university sent us an inferior photocopy.

Reproduction in full or in part of this microform is governed by the Canadian Copyright Act, R.S.C. 1970, c. C-30, and subsequent amendments.

## AVIS

La qualité de cette microforme dépend grandement de la qualité de la thèse soumise au microfilmage. Nous avons tout fait pour assurer une qualité supérieure de reproduction.

S'il manque des pages, veuillez communiquer avec l'université qui a conféré le grade.

La qualité d'impression de certaines pages peut laisser à désirer, surtout si les pages originales ont été dactylographiées à l'aide d'un ruban usé ou si l'université nous a fait parvenir une photocopie de qualité inférieure.

La reproduction, même partielle, de cette microforme est soumise à la Loi canadienne sur le droit d'auteur, SRC 1970, c. C-30, et ses amendements subséquents.

**UNIVERSITY OF ALBERTA**

**INTERPRETATION OF PRESSUREMETER TESTS USING A CURVE  
FITTING TECHNIQUE**

**BY**

**RONALDO DA SILVA FERREIRA**

A thesis submitted to the Faculty of Graduate Studies and Research in partial fulfillment of the requirements for the degree of **DOCTOR OF PHILOSOPHY**.

**IN**

**GEOTECHNICAL ENGINEERING**

**DEPARTMENT OF CIVIL ENGINEERING**

**EDMONTON, ALBERTA**

**FALL 1992**



National Library  
of Canada

Bibliothèque nationale  
du Canada

Canadian Theses Service    Service des thèses canadiennes

Ottawa, Canada  
K1A 0N4

The author has granted an irrevocable non-exclusive licence allowing the National Library of Canada to reproduce, loan, distribute or sell copies of his/her thesis by any means and in any form or format, making this thesis available to interested persons.

The author retains ownership of the copyright in his/her thesis. Neither the thesis nor substantial extracts from it may be printed or otherwise reproduced without his/her permission.

L'auteur a accordé une licence irrévocable et non exclusive permettant à la Bibliothèque nationale du Canada de reproduire, prêter, distribuer ou vendre des copies de sa thèse de quelque manière et sous quelque forme que ce soit pour mettre des exemplaires de cette thèse à la disposition des personnes intéressées.

L'auteur conserve la propriété du droit d'auteur qui protège sa thèse. Ni la thèse ni des extraits substantiels de celle-ci ne doivent être imprimés ou autrement reproduits sans son autorisation.

ISBN 0-315-77153-4

Canada

**UNIVERSITY OF ALBERTA**

**RELEASE FORM**

NAME OF AUTHOR: **RONALDO DA SILVA FERREIRA**

TITLE OF THESIS: **INTERPRETATION OF PRESSUREMETER TESTS  
USING A CURVE FITTING TECHNIQUE**

DEGREE: **DOCTOR OF PHILOSOPHY**

YEAR THIS DEGREE GRANTED: **FALL 1992**

Permission is hereby granted to the University of Alberta Library to reproduce single copies of this thesis and to lend or sell such copies for private, scholarly or scientific research purposes only.

The author reserves all other publication and other rights in association with the copyright in the thesis, and except as hereinbefore provided neither the thesis nor any substantial portion thereof may be printed or otherwise reproduced in any material form whatever without the author's prior written permission.



Rua Sérgio Gil N° 185  
Estreito, Florianópolis  
Santa Catarina CEP 88075  
**BRAZIL**  
phone: 011-55-482-447798

Date: June 05 1992


UNIVERSITY OF ALBERTA

FACULTY OF GRADUATE STUDIES AND RESEARCH

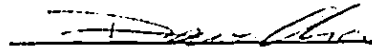
The undersigned certify that they have read, and recommended to the Faculty of Graduate Studies and Research for acceptance, a thesis entitled **INTERPRETATION OF PRESSUREMETER TESTS USING A CURVE FITTING TECHNIQUE** submitted by **RONALDO DA SILVA FERREIRA** in partial fulfillment of the requirements for the degree of **DOCTOR OF PHILOSOPHY** in **GEOTECHNICAL ENGINEERING**.



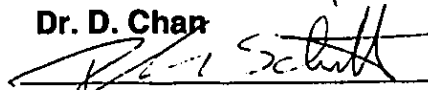
Dr. P.K. Robertson



Dr. Z. Eisenstein



Dr. D. Chan



Dr. D. Schmitt



Dr. D.W. Murray



Dr. B. Ladanyi (External Examiner)

MAY 25, 1992

**To my family**

## **ABSTRACT**

Interpretation of pressuremeter tests is the main subject of this study. For in situ tests, the interpretation of results to yield soil parameters can be very difficult and decisive for their acceptance by the geotechnical engineering community. Fortunately, the pressuremeter test is one of the few geotechnical in situ tests that has well defined boundary conditions. The cavity expansion theory, founded on Solid Mechanics principles, provides the sound theoretical basis to derive the pressuremeter analytical equations. The loading and unloading pressuremeter curves can, therefore, be simulated using analytical equations. Solutions for the drained and undrained problems were developed. The undrained problem was solved using small and large strain analyses, while the drained problem was solved using just the small strain analysis. The solutions were based on the hyperbolic stress-strain relationship with no soil volumetric change for undrained tests and linear volumetric change relationship for drained tests. Based on these solutions, interpretation methodologies for drained and for undrained tests were presented. For both types of tests, the early portion of the pressuremeter loading curve is assumed not to represent the undisturbed soil response. Just the last points of the loading curve are used for soil parameter interpretation purposes. The unloading pressuremeter curve plays a major role in the methodology to interpret undrained tests. On the other hand, due to the soil arching and the free pore water flow phenomena, the unloading portion of the pressuremeter drained test may not be used to derive the drained soil strength. For this reason, the proposed methodologies for interpreting drained SBPT's do not take into account the unloading data. All derived equations are presented and the curve fitting technique is performed using a commercially available microcomputer software. This allows any geotechnical company to use the proposed methods. Simplicity, accuracy, and reliability have been essential features of the proposed methodologies pursued since the conception of this whole work.

## **ACKNOWLEDGEMENTS**

I wish to acknowledge the enthusiastic assistance, encouragement, interest and guidance provided by my advisor, Professor Peter K. Robertson, throughout this work.

Consideration is also due to all academic and administrative staff and graduate students of the Department of Civil Engineering, in particular those belonging to the Geotechnical and Structural groups.

I also would like to express my gratitude to Professor M. Jamiolkowski for providing the pressuremeter data to validate this study.

The research documented in this thesis was conducted under the scholarship provided by CAPES - Brazilian Government Agency, and under the financial assistance provided by Federal University of Santa Catarina, Brazil. This support is greatly appreciated by the author.

To this friendly country, Canada, in particular to the Province of Alberta, and to the friendly people of the city of Edmonton, the author is deeply indebted for the emotional and life support received during this four-year-journey. It was an example for me of how a country and its people can contribute to alleviate the problems of adaptation.

Without the support of my parents, Roberto and Zulma, and my parents-in-law, Moacir and Hilda, it would have been impossible to complete this work. My deep appreciation of their support is acknowledged.

Finally, my deep and very special thanks to my family - Elza (wife), Ronaldo (son), Claudia, Lilian, and Karina (daughters), for their love, emotional support, understanding, and patience throughout this endeavour.



## Table of Contents

1.	<b>INTRODUCTION</b> .....	1
2.	<b>PREVIOUS WORK ON PRESSUREMETER DATA INTERPRETATION</b> .....	7
2.1	Introduction .....	7
2.2	Classification system for pressuremeter interpretation methods .....	8
2.3	Description of the previous interpretation methodologies.....	9
2.3.1	Group I. Pre-conceived stress-strain response .....	9
2.3.2	Group II. Constitutive law derived from pressuremeter data .....	20
2.4	Conclusion .....	26
3.	<b>RESEARCH PROGRAM ON PRESSUREMETER DATA INTERPRETATION</b> .....	27
3.1	Introduction .....	27
3.2	Research on pressuremeter interpretation.....	28
3.3	Important statements for an interpretation methodology.....	29
3.4	Necessary background required .....	32
3.5	Conclusion .....	33
4.	<b>INTERPRETATION OF UNDRAINED SELF-BORING PRESSUREMETER TEST RESULTS INCORPORATING UNLOADING</b> .....	34
4.1	Introduction .....	34
4.2	Previous interpretation procedures of undrained pressuremeter results.....	35
4.3	Proposed methodology to interpret undrained SBPT data.....	37
4.3.1	Assumptions .....	37

4.3.2	Hyperbolic model .....	37
4.3.3	Derivation of the pressuremeter analytical equation....	38
4.3.4	Proposed methodology .....	41
4.3.5	Comments on the proposed methodology .....	42
4.4	Interpretation of SBPT in the Fucino clay.....	43
4.4.1	Initial shear modulus ( $G_i$ ).....	45
4.4.2	Undrained shear strength ( $\tau_{ult}$ ) .....	45
4.4.3	Earth pressure coefficient at rest ( $K_0$ ) .....	47
4.5	Discussion of the interpreted results .....	47
4.5.1	Sensitivity analysis.....	47
4.5.2	Secant shear modulus versus shear strain.....	48
4.6	Comparison of the proposed methodology to the Jefferies (1988) method .....	50
4.6.1	Interpretation of the AF85 P06-15 test using Jefferies' approach.....	50
4.6.2	Interpretation of the AF85 P06-15 using the proposed methodology .....	50
4.6.3	Interpretation of the Fucino-V2P14 test using Jefferies' approach.....	51
4.6.4	Comments on the results.....	54
4.7	Conclusions.....	54
5.	<b>EXTENSION OF THE PROPOSED METHODOLOGY TO OTHER TYPES OF UNDRAINED PRESSUREMETER TESTS</b> .....	72
5.1	Introduction .....	72
5.2	Large strain definitions .....	73
5.2.1	Logarithmic strains (Lagrangian space).....	74

5.2.2	Green strains (Lagrangian space) .....	74
5.2.3	Comparison between small and large strain definitions.....	74
5.3	Pressuremeter analytical equation for large strains.....	75
5.3.1	Assumptions .....	75
5.3.2	Hyperbolic model .....	76
5.3.3	Derivation of the pressuremeter analytical equations..	76
5.4	Capabilities of the pressuremeter large strain analytical equations.....	79
5.4.1	Comparison to the pressuremeter small strain analytical equations .....	79
5.4.2	Large strain analytical curves for different maximum cavity strains .....	81
5.4.3	Interpretation of the Fucino V2P14 SBPT using large strain equations .....	81
5.5	Typical undrained pressuremeter test results .....	81
5.6	Effect of the soil disturbance and the pressuremeter maximum strain .....	83
5.6.1	Radius of the plastic annulus.....	84
5.6.2	Limit pressure and initial disturbance .....	85
5.6.3	Maximum strain and limit pressure .....	85
5.6.4	Calculation of the necessary maximum Green strain ..	86
5.6.5	Proposed methodology to interpret undrained FDPT and PBPT .....	89
5.6.6	Comments on the proposed methodology .....	89
5.7	Interpretation of a SBPT and a FDPT at the same depth (Lulu Island Pile Research Site - BC, Canada) .....	90
5.7.1	Introduction .....	90

5.7.2	Site description .....	91
5.7.3	Self-boring pressuremeter device .....	91
5.7.4	Full-displacement pressuremeter device .....	92
5.7.5	Interpretation of the HPM 87 - 3 test (9.4m) .....	92
5.7.6	Interpretation of the SCPM #1 test (9.4m) .....	93
5.7.7	Comments on test results .....	94
5.8	Initial horizontal stress from a FDPT .....	95
5.9	Interpretation of a FDPT in stiff clays .....	96
5.9.1	Interpretation of the FPC 15 test (4m) .....	96
5.9.2	Interpretation of the FPC 5 test (9m) .....	96
5.9.3	Comments on the derived results .....	97
5.10	Conclusions.....	98
6.	<b>INTERPRETATION OF DRAINED SELF-BORING PRESSUREMETER RESULTS</b> .....	116
6.1	Introduction .....	116
6.2	Previous interpretation methods .....	118
6.3	Soil models for drained response.....	120
6.3.1	Elastic-perfectly plastic model .....	121
6.3.2	Hyperbolic model .....	121
6.4	Pressuremeter analytical equations for elastic perfectly plastic soil response .....	122
6.4.1	Assumptions .....	122
6.4.2	Derivation of the pressuremeter analytical equations..	122
6.4.3	Interpretation of model parameters.....	127

6.4.4	Proposed methodology to interpret drained SBPT data.....	128
6.4.5	Comments on the elastic-perfectly plastic model .....	129
6.5	Pressuremeter analytical equation for hyperbolic soil response .....	130
6.5.1	Assumptions .....	130
6.5.2	Derivation of the pressuremeter analytical loading equation .....	130
6.5.3	Interpretation of the model parameters.....	133
6.5.4	Proposed methodology to interpret drained SBPT data.....	134
6.5.5	Comments on the hyperbolic constitutive model .....	135
6.6	Evaluation of the constant volume friction angle .....	138
6.7	Interpretation of drained SBPT data .....	139
6.7.1	Calibration chamber tests (Bellotti et al, 1987) .....	139
6.7.2	In situ test (Fahey and Carter, 1991) .....	142
6.8	Discussion of the interpreted parameters .....	142
6.8.1	Calibration chamber tests (hyperbolic model) .....	142
6.8.2	Calibration chamber test (elastic-plastic model) .....	145
6.8.3	In situ test (hyperbolic model) .....	146
6.8.4	In situ test (elastic-plastic model).....	146
6.9	Comments on pressuremeter unloading data in sands.....	147
6.10	Conclusions.....	148
7.	<b>CONCLUSIONS AND SUGGESTIONS FOR FURTHER RESEARCH</b> .....	164
7.1	Introduction .....	164
7.2	Proposed methodologies .....	165

7.2.1	Undrained pressuremeter tests interpreted using small strain analysis.....	166
7.2.2	Undrained pressuremeter tests interpreted using large strain analysis.....	167
7.2.3	Drained pressuremeter tests interpreted using small strain definition .....	168
7.3	Summary .....	169
7.4	Suggestions for further research .....	170
7.4.1	Equipment development .....	170
7.4.2	Field test procedures .....	170
7.4.3	Interpretation of pressuremeter data.....	171
	<b>BIBLIOGRAPHY .....</b>	<b>172</b>
	<b>APPENDIX A - TYPES OF PRESSUREMETER DEVICES .....</b>	<b>179</b>
A.1	Pre-bored (Menard type) pressuremeter (PBP).....	179
A.2	Self-boring pressuremeter (SBP).....	180
A.3	Push-in pressuremeter (PIP).....	180
A.4	Full-displacement pressuremeter (FDP) .....	181
	<b>APPENDIX B - PRESSUREMETER RELATED THESES AND DISSERTATIONS.....</b>	<b>184</b>
	<b>APPENDIX C - FUCINO CLAY - V2 SBPT's - INTERPRETATION RESULTS .....</b>	<b>190</b>
C.1	Introduction .....	190
C.2	Interpretation results .....	190
C.3	Comments on the interpreted results.....	190

## List of Figures

Figure 4.1	Proposed hyperbolic model for loading and unloading stages of a pressuremeter test; (a) loading and unloading; (b) loading part; (c) unloading part.....	56
Figure 4.2	Interpretation methodology for a self-boring pressuremeter test (SBPT).....	57
Figure 4.3	Proposed template for interpreting pressuremeter data.....	58
Figure 4.4	Fucino clay test V2P14. Interpretation template.....	59
Figure 4.5	Fucino clay test V2P14. (a) suggested fit to last section of loading curve (final plot); (b) curve fitting for all loading points.....	60
Figure 4.6	Fucino clay test V2P10. Suggested fit to last section of the loading curve (final plot). .....	61
Figure 4.7	Fucino clay borehole V2. Shear modulus versus depth.....	61
Figure 4.8	Fucino clay borehole V2. Undrained shear strength versus depth. ....	62
Figure 4.9	Fucino clay borehole V2. Earth pressure coefficient at rest versus depth. ....	62
Figure 4.10	Fucino Clay - Test V2P14. Sensitivity analysis. Undrained shear strength.....	63
Figure 4.11	Fucino Clay - Test V2P14. Sensitivity analysis. Elastic shear modulus. ....	63
Figure 4.12	Fucino Clay - Test V2P14. Sensitivity analysis. Initial horizontal stress.....	64
Figure 4.13	Fucino Clay - Test V2P14. (a) Secant shear modulus versus shear strain (two curves); (b) Secant shear modulus versus shear strain (combined curve).....	65
Figure 4.14	Test AF85 P06-15. Interpretation template.....	66

Figure 4.15	Test AF85 P06-15. Curve fitting of the unloading stage of the test. ....	67
Figure 4.16	Test AF85 P06-15. Curve fitting of the entire loading stage of the test: (a) for $R_c$ equals to 2.0; (b) for $R_c$ equals to 1.83. ....	68
Figure 4.17	Test AF85 P06-15. Curve fitting of the loading stage for cavity strain greater than 5%: (a) for $R_c$ equals 2.0; (b) for $R_c$ equals 1.83. ....	69
Figure 4.18	Test AF85 P06-15. (a) Final plot; (b) Constitutive laws used in Jefferies (1988) and in the proposed method. ....	70
Figure 4.19	Fucino clay test V2P14. (a) Loading and unloading curve matching; (b) Constitutive laws used in Jefferies (1988) and in the proposed method. ....	71
Figure 5.1	Variation of logarithmic and Green strains with cavity strain. ....	101
Figure 5.2	Test V2P14 Fucino clay - Comparison of large and small strain analytical equations: (a) Loading curve; (b) Unloading curve. ....	102
Figure 5.3	Test AF85 P06-15 - Comparison of large and small strain analytical equations: (a) Loading curve; (b) Unloading curve. ....	103
Figure 5.4	Unloading curves for an idealized soil for several levels of maximum cavity strains. ....	104
Figure 5.5	Test V2P14 Fioravante (1988): Interpretation template using large strain pressuremeter analytical equations. ....	105
Figure 5.6	Test V2P14 Fioravante (1988): (a) Final plot; (b) Curve fitting of all loading points. ....	106
Figure 5.7	Idealized response of undrained pressuremeter tests. ....	107
Figure 5.8	Fucino clay - Fioravante (1988): Profiles of maximum pressure and limit pressure. ....	107



Figure 5.9	Disturbance during pressuremeter insertion: (a) Without consolidation; (b) With consolidation.....	108
Figure 5.10	Variation of the normalized plastic-elastic radius with Green strain. ....	109
Figure 5.11	Madingley Site - Test FPC 5 (9m): (a) Analytical loading curve for many $(p,g)_{max}$ ; (b) Variation of the initial horizontal stress with Green strain. ....	110
Figure 5.12	Lulu Island - Test HPM87-3 (9.4m) Howie (1991): Pressuremeter interpretation template. ....	111
Figure 5.13	Lulu Island - Test HPM87-3 (9.4m) Howie (1991): Final plot. ....	112
Figure 5.14	Lulu Island - Test SCPM#1 (9.4m) Howie (1991): Pressuremeter interpretation template. ....	113
Figure 5.15	Lulu Island - Test SCPM#1 (9.4m) Howie (1991): Final plot. ....	114
Figure 5.16	Lulu Island - Howie (1991): Comparison between SBPT and FDPT original curves.....	114
Figure 5.17	Madingley Site - Test FPC 15 (4m): Curve fitting of the unloading phase of the test. ....	115
Figure 5.18	Madingley Site - Test FPC 5 (9m): Curve fitting of the unloading phase of the test.....	115
Figure 6.1	Soil models for drained response: (a) Elastic perfectly plastic model; (b) Hyperbolic model. ....	150
Figure 6.2	Volumetric strain relationship: (a) In terms of shear strain; (b) In terms of cavity strain. ....	151
Figure 6.3	Hyperbolic model: (a) Stress-strain relationship; (b) Variation of the effective average normal stress. ....	152
Figure 6.4	Test 228 - Ticino sand: Original data.....	153
Figure 6.5	Test 228 - Ticino sand: Hyperbolic stress-strain relationship. ....	153

Figure 6.6	Test 228 - Ticino sand: Mobilized shear stress and effective average normal stress. ....	154
Figure 6.7	Test 228 - Ticino sand: Radial and circumferential stresses. ....	154
Figure 6.8	Test 228 - Ticino sand: (a) Stress path $\sigma_r$ versus $\sigma_\theta$ ; (b) Stress path t versus s. ....	155
Figure 6.9	Test 228 - Ticino sand: (a) All loading points fitted; (b) Only points with $\epsilon > 4\%$ fitted. ....	156
Figure 6.10	Test 238 - Ticino sand: Original data. ....	157
Figure 6.11	Test 238 - Ticino sand: Final curve matching. ....	157
Figure 6.12	Test 246 - Ticino sand: Original data. ....	158
Figure 6.13	Test 246 - Ticino sand: Final curve matching. ....	158
Figure 6.14	Test 247 - Ticino sand: Original data. ....	159
Figure 6.15	Test 247 - Ticino sand: Final curve matching. ....	159
Figure 6.16	Test 252 - Ticino sand: Original data. ....	160
Figure 6.17	Test 252 - Ticino sand: Final curve matching. ....	160
Figure 6.18	Test 260 - Ticino sand: Original data. ....	161
Figure 6.19	Test 260 - Ticino sand: Final curve matching. ....	161
Figure 6.20	Test 260 - Ticino sand: Final curve matching (Elastic-plastic model). ....	162
Figure 6.21	Fahey (1991) test (15.5m): Original data. ....	162
Figure 6.22	Fahey (1991) test (15.5m): Final curve matching. ....	163
Figure 6.23	Fahey (1991) test (15.5m): Final curve matching (Elastic-plastic model). ....	163
Figure A-1	Ideal results of the field PBPT. ....	182
Figure A-2	Ideal results of the field SBPT. ....	182

Figure A-3	Ideal results of the field PIPT. ....	183
Figure A-4	Ideal results of the field FDPT. ....	183
Figure C - 01 (a)	Fucino clay test V2P01: Interpretation template..	193
Figure C - 01 (b)	Fucino clay test V2P01: (b1) Unload fitting; (b2) Final plot. ....	194
Figure C - 02 (a)	Fucino clay test V2P02: Interpretation template..	195
Figure C - 02 (b)	Fucino clay test V2P02: (b1) Unload fitting; (b2) Final plot. ....	196
Figure C - 03 (a)	Fucino clay test V2P03: Interpretation template..	197
Figure C - 03 (b)	Fucino clay test V2P03: (b1) Unload fitting; (b2) Final plot. ....	198
Figure C - 04 (a)	Fucino clay test V2P04: Interpretation template..	199
Figure C - 04 (b)	Fucino clay test V2P04: (b1) Unload fitting; (b2) Final plot. ....	200
Figure C - 05 (a)	Fucino clay test V2P05: Interpretation template..	201
Figure C - 05 (b)	Fucino clay test V2P05: (b1) Unload fitting; (b2) Final plot. ....	202
Figure C - 06 (a)	Fucino clay test V2P06: Interpretation template..	203
Figure C - 06 (b)	Fucino clay test V2P06: (b1) Unload fitting; (b2) Final plot. ....	204
Figure C - 07 (a)	Fucino clay test V2P07: Interpretation template..	205
Figure C - 07 (b)	Fucino clay test V2P07: (b1) Unload fitting; (b2) Final plot. ....	206
Figure C - 08 (a)	Fucino clay test V2P08: Interpretation template..	207
Figure C - 08 (b)	Fucino clay test V2P08: (b1) Unload fitting; (b2) Final plot. ....	208
Figure C - 09 (a)	Fucino clay test V2P09: Interpretation template..	209
Figure C - 09 (b)	Fucino clay test V2P09: (b1) Unload fitting; (b2) Final plot. ....	210

Figure C - 10 (a) Fucino clay test V2P10: Interpretation template..	211
Figure C - 10 (b) Fucino clay test V2P10: (b1) Unload fitting; (b2) Final plot. ....	212
Figure C - 11 (a) Fucino clay test V2P11: Interpretation template..	213
Figure C - 11 (b) Fucino clay test V2P11: (b1) Unload fitting; (b2) Final plot. ....	214
Figure C - 12 (a) Fucino clay test V2P12: Interpretation template..	215
Figure C - 12 (b) Fucino clay test V2P12: (b1) Unload fitting; (b2) Final plot. ....	216
Figure C - 13 (a) Fucino clay test V2P13: Interpretation template..	217
Figure C - 13 (b) Fucino clay test V2P13: (b1) Unload fitting; (b2) Final plot. ....	218
Figure C - 14 (a) Fucino clay test V2P14: Interpretation template..	219
Figure C - 14 (b) Fucino clay test V2P14: (b1) Unload fitting; (b2) Final plot. ....	220
Figure C - 15 (a) Fucino clay test V2P15: Interpretation template..	221
Figure C - 15 (b) Fucino clay test V2P15: (b1) Unload fitting; (b2) Final plot. ....	222
Figure C - 16 (a) Fucino clay test V2P16: Interpretation template..	223
Figure C - 16 (b) Fucino clay test V2P16: (b1) Unload fitting; (b2) Final plot. ....	224
Figure C - 17 (a) Fucino clay test V2P17: Interpretation template..	225
Figure C - 17 (b) Fucino clay test V2P17: (b1) Unload fitting; (b2) Final plot. ....	226
Figure C - 18 (a) Fucino clay test V2P18: Interpretation template..	227
Figure C - 18 (b) Fucino clay test V2P18: (b1) Unload fitting; (b2) Final plot. ....	228
Figure C - 19 (a) Fucino clay test V2P19: Interpretation template..	229

Figure C - 19 (b) Fucino clay test V2P19: (b1) Unload fitting; (b2) Final plot. ....	230
Figure C - 20 (a) Fucino clay test V2P20: Interpretation template..	231
Figure C - 20 (b) Fucino clay test V2P20: (b1) Unload fitting; (b2) Final plot. ....	232

## List of Symbols

### (1) Latin symbols

$D_{RC}$	- relative density
$E_M$	- pressuremeter modulus
$G$	- elastic shear modulus
$G_i$	- initial elastic shear modulus (hyperbolic model)
$G_{ur}$	- shear modulus from unload-reload loops
$G_{ur_0}$	- shear modulus from unload-reload loops corrected for stress level
$G_s$	- secant shear modulus
$G_0$	- small strain shear modulus from seismic measurements
$K_0$	- earth pressure coefficient at rest
$I_r$	- rigidity index
$\dot{L}$	- pressuremeter logarithmic strain
$L_\theta$	- circumferential logarithmic strain
$N$	- friction angle parameter
$N(\varepsilon)$	- friction angle parameter as a function of cavity strain
$R$	- current pressuremeter radius
$R_f$	- reduction factor of the hyperbolic model (failure ratio)
$R_{max}$	- maximum radius of the pressuremeter
$R_\tau$	- ratio of ultimate undrained shear strength on unloading and loading
$R_0$	- initial radius of the pressuremeter
$R_{PE}$	- radius of the plastic-elastic transition
$S$	- slope of the stress-strain law
$S_i$	- initial tangential slope of the hyperbolic relationship
$S_u$	- undrained shear strength
$S_{u mob}$	- mobilized undrained shear strength
$V$	- current volume of the pressuremeter chamber
$V_0$	- initial volume of the pressuremeter chamber
$e$	- basis of the natural logarithm
$e_o$	- total volumetric strain of the soil before failure (Ladanyi, 1963)
$g$	- pressuremeter Green strains

$g_{\max}$	- maximum pressuremeter Green strain at the start of the unloading phase
$g_{L\max}$	- pressuremeter Green strain at the end of the loading phase.
$g^*$	- pressuremeter Green strains in unloading
$g_{\theta}$	- circumferential Green strains
$\log_e$ and $\ln$	- natural logarithm
$n$	- dilation angle parameter
$p$	- pressure at the cavity wall
$p'$	- effective pressure at the cavity wall
$p_l$	- limit pressure
$p_{\max}$	- pressure at the cavity wall at the beginning of the unloading phase
$p_o$	- initial horizontal stress within the soil medium (Ladanyi, 1963)
$p'_o$	- effective lift-off pressure
$r$	- radial coordinate
$r_o$	- initial radial coordinate of a material point
$s_v$	- slope of the volumetric strain relationship
$s$	- effective stress average
$t$	- maximum shear stress
$t/s$	- stress ratio
$(t/s)_{ult}$	- ultimate stress ratio during loading
$u_o$	- static pore water pressure

## (2) Greek symbols

$\beta$	- ratio of undrained strength of clay in extension to that in contraction after principal stress reversal (Jefferies, 1988)
$\gamma$	- engineering shear strain
$\gamma_d$	- dry unit weight
$\Delta R$	- change in pressuremeter radius
$\Delta V/V$	- volumetric cavity strain
$\Delta V$	- change in soil volume
$V_0$	- initial soil volume
$\varepsilon$	- cavity strain in loading
$\varepsilon_{\max}$	- cavity strain at the beginning of unloading

$\varepsilon_r$	- radial strain
$\varepsilon_{EL}$	- cavity strain at the end of the elastic loading
$\varepsilon_{EU}$	- cavity strain at the end of the elastic unloading
$\varepsilon_L _{\max}$	- cavity strain at the end of loading
$\varepsilon_V$	- soil volumetric strain
$\varepsilon'$	- cavity strain in unloading
$\varepsilon_\theta$	- circumferential strain
$\phi'$	- peak friction angle
$\phi'_{CV}$	- constant volume friction angle
$\phi'_{mob}$	- mobilized friction angle
$\phi'_{ult}$	- ultimate friction angle
$\phi_P^{PS}$	- peak friction angle for plane strain mode of deformation
$\phi_P^{TX}$	- peak friction angle for triaxial conditions
$\sigma_r$	- radial stress
$\sigma_{ho}$	- initial horizontal in situ stress
$\sigma'_{ho}$	- effective initial in situ stress
$\sigma_{r \max}$	- maximum radial stress at the beginning of the unloading phase
$\sigma_{r,z,\theta}$	- total normal stresses (radial, vertical and circumferential)
$\sigma'_{r,z,\theta}$	- effective normal stresses
$\sigma_{1,2,3}$	- total principal stresses (major, intermediate, and minor)
$\sigma'_{1,2,3}$	- effective principal stress
$\sigma'_{rEL}$	- radial effective stress at the end of the elastic loading
$\sigma'_{vo}$	- effective initial vertical stress (calibration chamber)
$\tau$ and $\tau_{mob}$	- mobilized shear stress in loading
$\tau_{ult}$	- ultimate undrained shear strength in loading
$\tau^*$	- mobilized shear stress in unloading
$\tau^*_{ult}$	- ultimate shear strength in unloading
$\tau(\varepsilon)$	- shear stress-cavity strain relationship
$v$	- dilation angle



## Acronyms

AF85 P06-15	- Test name (Jefferies, 1988)
AGI	- Associazione Geotecnica Italiana
BC	- Province of British Columbia (Canada)
ENEL-CRIS	- Italian National Electricity Board - Hydraulic and Structural Research Center
FDPT	- Full-displacement pressuremeter test
FDP	- Full-displacement pressuremeter
FPC	- Fugro pressuremeter cone
FPC 15	- Test name (Houlsby, 1988)
HPM	- Hughes pressuremeter
HPM 87 - 3	- Test name (Howie, 1991)
LCPC	- Laboratoire Central des Ponts et Chaussées
OCR	- Overconsolidation ratio
PBPT	- Pre-bored pressuremeter test
PBP	- Pre-bored pressuremeter
PIPT	- Push-in pressuremeter test
PIP	- Push-in pressuremeter
P01	- Test one
SCPM	- Seismic cone-pressuremeter
SCPM #1	- Test name (Howie 1991)
SBP	- Self-boring pressuremeter
SBPT	- Self-boring pressuremeter test
TS-1	- Ticino sand type 1
UBC	- University of British Columbia
V1	- Vertical number one
V1P01	- Test one in the vertical one (Fioravante, 1988)

## CHAPTER 1

### INTRODUCTION

Field and laboratory tests have been used for decades to determine properties and behaviour of soil and rocks. Although both kinds of tests might introduce some degree of disturbance to the material mass, they are considered complementary to one another in most engineering design works. Many authors (Ervin, 1983; Morrison, 1972; Burgess, 1976; Bellotti et al, 1988; Prapaharan 1987; Belkacemi, 1988; and Salgado, 1990) have reported the advantages and disadvantages of laboratory and field tests.

One major disadvantage of laboratory tests is their inability to measure the mass behaviour of the in situ ground. Small samples, that are frequently used, are unable to reflect during the test the true response of a large amount of material that may have features such as fissures, root holes, natural cementing, silt and sand partings, etc. The tendency for testing larger samples is clear in the last decade.

Field tests, on the other hand, present problems of a different kind. Complex and poorly defined boundary conditions, non-uniform stress and strain, variable and unknown drainage conditions, are among the major flaws of even carefully conducted field tests.

To balance those problems, laboratory tests can be performed with pre-defined stress and strain paths and known drainage conditions, while field tests can give the true average response where the mass effect is reflected. The mass effect can have an important role for both soil and rock because the defects often ultimately govern the final behaviour (Ervin, 1983).

For important projects, substantial savings can be achieved if field and laboratory tests can be performed in a balanced and complementary fashion.

Nevertheless, the subsequent development of sophisticated analysis techniques, such as the finite element method, has emphasized the need for

accurate and reliable soil parameters particularly those related to deformation response. In situ tests, which induce unknown changes in the effective stress field and large straining, especially penetration tests, are not suitable for this purpose. The reason, as presented by Bellotti et al (1986), is the significant '...disturbance to the surrounding soil, which can erase all the features related to the stress and strain history of the tested soil.'

In addition, it has been recognized that simple techniques are dominant in geotechnical design practice. Whenever possible, the development of a new technique or a new design approach should be: (a) easy to understand; (b) simple to apply; and (c) reliable in its results. It is worthwhile to recall at this point a quotation presented by Gambin (1990): 'On the overwhelming majority of jobs no more than an approximate forecast is needed, and if such a forecast cannot be made by simple means, it cannot be made at all. If it is not possible to make an approximate forecast, the behaviour of the soil must be observed during construction (Terzaghi and Peck, 1948).' Although almost half a century old, this principle is still governing much of modern geotechnical design practice.

A natural phenomenon usually implies a large number of variables. Physically and mathematically many assumptions have to be considered if a solution to a geotechnical problem has to be reached. The degree of approximation of the solved problem to the real solution depends on how close the results can represent the actual response. Design practice has shown that the forecasted behaviour is not always close to the measured response. Consequently, new techniques need to be developed to improve design methods. These new techniques should necessarily start with a well-understood problem. Then appropriate tests should be performed and interpreted using adequate methodologies that can provide acceptable results.

It has been said by many authors (Baguelin et al, 1978; Wroth, 1982; Ervin, 1983; and Mair and Wood, 1987) that the pressuremeter test is an extremely useful and economical way for obtaining reliable engineering properties of soil and rock. Its results can be used in two basic ways: (a) as input for empirical correlations; and (b) for input to derive constitutive soil or rock parameters.

The French school advocates the use of pressuremeters for foundation design based on empirical correlations. Baguelin et al (1978) stated that foundations can be designed directly from pressuremeter results, without any need for soil strength or deformation parameters. The English school, on the other hand, has considered pressuremeter tests too powerful to be used just as a source of information for empirical purposes. According to Mair and Wood (1987), researchers from the UK and other countries are putting a great deal of effort to obtain measurements of the particular fundamental soil parameters required for geotechnical design.

Today, several types of pressuremeters are available. They can be grouped into four categories: (a) pre-bored pressuremeter (PBP); (b) self-boring pressuremeter (SBP); (c) full-displacement pressuremeter (FDP); and (d) push-in pressuremeter (PIP). A description of each type, including typical ideal results, is presented in Appendix A.

Although different methods of insertion are used for different types of pressuremeters, the testing procedure to obtain the soil response is essentially the same for all types. Automatic data acquisition systems are very common today, resulting in an easier task to perform the test either for the loading stage (cell expansion) or for the unloading stage (cell contraction). Also, some unloading-reloading cycles are commonly performed during a pressuremeter test.

The theoretical background used to interpret pressuremeter data is another attractive aspect of the pressuremeter test. The theory of cylindrical and spherical cavity expansion, using Solid Mechanics principles, can be used to derive soil and soft rock parameters from the pressuremeter response. Theoretically, the pressuremeter boundary conditions are controlled and well defined, as are the stress and strain conditions in the surrounding soil (Mair and Wood, 1987).

It is worthwhile to include here a citation by Baguelin et al (1978) stressing in situ tests as an important requirement of modern Soil Mechanics: 'Unlike

other in situ tests such as penetration or Vane tests, the pressuremeter measures deformation properties of the soils in addition to a rupture or limit resistance. The engineer can now benefit from the considerable advantage of having deformation information available as a matter of routine.'

The pressuremeter test has developed considerably since its first introduction by L.Menard in 1957. A number of publication has chronicled this development (Eisenstein and Morrison, 1973; Baguelin et al, 1978; Briaud and Lytton, 1983; Wroth, 1984; Mair and Wood, 1987; Briaud and Cosentino, 1990; Clough et al, 1990; Gambin, 1990). Initially, pressuremeters have been divided into two main groups: pre-bored and self-boring. The pre-bored pressuremeter test (PBPT) is performed in a pre-drilled hole, whereas the self-boring pressuremeter (SBP) is self-bored into the soil in an effort to minimize soil disturbance. More recently, the full-displacement pressuremeter and the push-in pressuremeter tests (FDPT and PIPT) have been developed (Hughes and Robertson, 1985, Withers et al, 1986; Fyffe et al, 1986; Campanella et al, 1990) where the probe is pushed into the ground. These different pressuremeter tests (PBPT, SBPT, PIPT, and FDPT) are thought of as distinct and separate in situ techniques, with different interpretation methods. The PBPT is usually analyzed using empirical correlations related to specific design rules. The SBPT is generally performed in relatively soft soils and the results are analyzed using theoretical relationships to derive basic soil parameters. The FDPT is relatively new and interpretation techniques are still evolving (Houlsby and Withers 1988, Withers et al 1989). The PIPT has primarily been used by the off-shore industry using wire-line techniques (Lacasse et al, 1990).

The decades of the 70's and the 80's were very prolific with studies on pressuremeter tests. Many graduate students have developed their research work in Universities and Research Institutes, using laboratory and field pressuremeter tests. In laboratories, large triaxial cells and calibration chambers have been used with miniature or full size pressuremeter probes. In this case, the improvement sought is related to: (a) techniques of insertion; (b) techniques of measurement; (c) new types of tests; and (d) calibration of existing interpretation methods. From field tests, improvement of new

interpretation techniques is normally sought.

A list of theses and dissertations related to previous research about pressuremeters is presented in Appendix B. Although limited in number, this survey is useful to identify where and when work on the pressuremeter has been produced.

Recognizing the potential of pressuremeter devices and the limitations of laboratory tests, this study was developed to accomplish the following main objectives:

- (1) Explore a new approach to determine constitutive parameters for soils from pressuremeter data;
- (2) Introduce nonlinear response in the stress-strain constitutive relationship for cohesive and cohesionless soils;
- (3) Keep the new approach as simple as possible, so that engineers can readily apply the method to geotechnical design;
- (4) Provide a contribution to the geotechnical science in terms of an analytical study to interpret field and laboratory pressuremeter results.

The work presented in this research allows the interpretation of SBPT results in clays, and validation of the proposed methodology is done based on SBPT's in Fucino clay reported by AGI (1991). The second contribution of this study is a tentative extension of the proposed methodology to PBPT and FDPT. Finally, following the same approach, an interpretation methodology to interpret SBPT data in sand is developed. Validation of this methodology is provided using calibration chamber results of SBPT's in Ticino sand, reported by Bellotti et al (1987), and one in situ test presented by Fahey and Carter (1991).

This thesis is organized in seven chapters. In chapter one an introduction to the pressuremeter problem is presented allowing a brief comparison to other field and laboratory tests. In Appendices A and B respectively, there is a brief presentation of the four types of pressuremeter devices and a list of dissertations and theses on many aspects of pressuremeter research.

Interpretation of pressuremeter test results is the major concern of this work. A review of previous work on pressuremeter interpretation for cohesive and cohesionless soils is provided in chapter two. In chapter three the organization of the complete research program is presented. A proposed methodology to interpret SBPT data in clays is presented in chapter four. Results of interpretation of 20 in situ SBPT's performed in Fucino clay, Italy, are presented in Appendix C. These results were used to validate the proposed methodology. Chapter five provides a tentative extension of the proposed methodology to other types of pressuremeter tests, namely PBPT and FDPT. Some additional validation of this extension is still necessary. In chapter six a methodology to interpret SBPT data in sands is developed for two soil models: (a) hyperbolic stress-strain relationship; and (b) elastic-perfectly plastic relationship. Finally, in chapter seven, discussion of the proposed methodologies and the main conclusions drawn from this work are presented. Some suggestions on further research in this area are also included.

It is believed that the contribution to the geotechnical science in this thesis will help engineers design more economical and safer structures based on soil parameters derived from pressuremeter tests.

## CHAPTER 2

### PREVIOUS WORK ON PRESSUREMETER DATA INTERPRETATION

#### 2.1 Introduction

As a field device, the pressuremeter has been used to obtain information of soil response according to the type of test procedure used. Inflation of a rubber cylindrical membrane in soil or rock, can be considered quite similar to the procedure of loading a foundation structure (Baguelin et al, 1978), especially the lateral loading of foundations. The pressuremeter test results are commonly expressed in terms of a plot with the corrected cavity pressure as the ordinate axis and the cavity strain (the change in radius divided by the initial radius) as the abscissa axis. The great majority of interpretation methodologies assume that the measured pressure-deformation curve is the true response of the loaded material. However, it has been shown by many authors (Denby, 1978; Battaglio et al, 1981; Ghionna, 1983; Prapaharan, 1987; Ferreira and Robertson, 1992) that this is not always the case mainly because of the influence on the result by: (a) disturbance during installation and operation; (b) rate of soil stressing or soil straining; (c) unknown drainage conditions; and (d) stress and strain paths followed during the test. Nevertheless, interpreted pressuremeter data have been used not only to yield information for empirical correlations, but also to derive strength and deformation parameters of the soil.

The pressuremeter test is commonly understood as an expansion of a cylindrical cavity within the soil. The physical problem has well-defined boundary conditions and can be solved theoretically using Solid Mechanics principles. For instance, Lamé's theory (thick hollow cylinder) dating from 1852, can be used to compute the elastic deformation modulus of a linear elastic material for plane strain conditions. For other stress-strain responses, such as elasto-plastic response, a solution proposed by Bishop, Hill and Mott in 1945 for metals could be adapted for geomaterials. Interpretation methodologies have been developed based on the above statements to derive soil parameters that govern the measured pressuremeter response.



## **2.2 Classification system for pressuremeter interpretation methods**

There are many interpretation methods to obtain the required information from pressuremeter results. Therefore, it is not a simple task to classify such a variety of interpretation methods because they differ not only in the physical concepts used but also in the mathematical procedures to obtain the solution. In most cases the solution is a set of strength and deformation soil parameters, and some initial stress condition (in situ horizontal stress).

From the physical point of view, the methodologies available to interpret pressuremeter data could be classified by the type of:

- (a) Constitutive law used;
- (b) Geomaterial tested;
- (c) Information used from the pressuremeter data (loading and/or unloading curve); and
- (d) Volumetric response of the soil during shearing.

The first classification based on different constitutive laws has at least half a dozen types, whereas the others have only two or three.

Related to the type of geomaterial tested, three types of soil can be considered:

- (a) Purely cohesive (clay behaviour);
- (b) Purely frictional (sand behaviour); and
- (c) Both cohesive and frictional (natural soil).

Depending upon the type of information required from the pressuremeter data, also three options are possible:

- (a) Loading curve only;
- (b) Unloading curve only; and
- (c) Loading and unloading curves together.

Finally, for the volumetric strain response of the soil two situations during the shearing process are possible:

- (a) No volumetric strain occurs; and
- (b) Some volumetric strain takes place.

From the mathematical point of view, the classification can be as follows:

- (a) Closed-form solutions with or without curve fitting;
- (b) Graphical solutions by geometrical constructions using the originally plotted pressuremeter data;
- (c) Graphical solutions by plotting pressuremeter data using special axes' coordinates and scales;
- (d) Approximate solutions using finite difference or finite element techniques.

For the purpose of this work, a main classification of interpretation methods based on the type of constitutive law employed is presented. There are two main groups further divided into subgroups:

**Group I. Pre-conceived stress-strain response**

- (1) Linear elastic;
- (2) Rigid plastic;
- (3) Linear elastic perfectly plastic;
- (4) Nonlinear elastic perfectly plastic; and
- (5) Elasto-plastic with strain hardening or strain softening.

**Group II. Constitutive law derived from pressuremeter data**

- (1) General shape;
  - (1.1) Interpretation using graphical construction;
  - (1.2) Interpretation using a numerical technique;
- (2) Shape defined by a mathematical function derived from a fitted pressuremeter curve.

For each interpretation method classified according to constitutive law, additional information will be presented later in this chapter.

All interpretation methodologies have assumptions and limitations. The mathematical development of each existing method will not be presented here. The reader is referred to the original reference if more information is needed to understand a specific method. Mapping of the space occupied by each methodology can help to make a comparison between existing methods and the proposed method developed in this study.

## **2.3 Description of the previous interpretation methodologies**

### **2.3.1 Group I. Pre-conceived stress-strain response**

#### **(1) Linear elastic constitutive law**

Presented by Baguelin et al (1978) and Mair and Wood (1987), this is the most simplistic solution to the pressuremeter problem.

The basic assumptions of this method are:

- (a) Cylindrical cavity expansion theory applies;
- (b) Axisymmetry and plane strain are assumed;
- (c) Soil is isotropic and homogeneous; and
- (d) Soil behaves linearly elastically.

The state of stress and strain around the pressuremeter can be determined with just two soil parameters: Young's modulus and Poisson's ratio. Because of the magnitude of strain imposed during the pressuremeter test (cavity strain generally greater than 10%), this method is not acceptable for the interpretation of the whole test due to its unrealistic representation of the soil at these strain levels.

#### **(2) Rigid perfectly plastic constitutive law**

##### **A. Hughes et al (1977) method**

Presented by Hughes et al (1977), this methodology has been well accepted by the engineering community because of its simplicity and reasonable results for granular materials. The method by Hughes et al (1977) is applicable to self-boring pressuremeter tests.

The basic assumptions for this method are:

- (a) Cylindrical cavity expansion theory applies;
- (b) Axisymmetry and plane strain are assumed;
- (c) Soil is homogeneous and isotropic;
- (d) Soil behaviour is rigid plastic;

(e) Soil has a constant linear rate of dilation.

Allowing for volume change during the shearing process, sand strength parameters can be determined (peak friction angle) from plotting pressuremeter loading curve in a bi-logarithmic plot. Using cavity strain (change in radius divided by initial radius) as abscissa and effective cavity stress as ordinate, a straight line is obtained which has the slope dependent on the mobilized friction and dilation angles at failure. These angles can be determined using Rowe's dilatancy law assuming a known constant volume friction angle (steady state). The complete interpretation also includes estimation of shear modulus from unload-reloading cycles (Hughes, 1982), and initial in situ horizontal stress from lift-off pressure (SBPT).

Some comments on the Hughes (1977) method:

- The method is currently very popular for dense sands. However, the constant linear rate of dilation is too restrictive for general behaviour of sands;
- As shown by the authors, interpretation of sand data is too sensitive to the disturbance during pressuremeter installation. Hence, the loading portion of the test is likely to be influenced by such disturbance and may not represent the response of the undisturbed material.

### (3) Linear elastic perfectly plastic constitutive law

The tested material is considered to behave linearly elastically until a yield or failure criterion is reached. During this elastic phase, shearing is governed by the shear modulus. For the plastic phase the ultimate shear stress is kept constant and equal to the shear stress defined by the failure criterion.

#### A. Gibson and Anderson (1961) method

The method proposed by Gibson and Anderson (1961), has been used by the engineering community mainly for clay soils. It was initially developed to interpret PBPT results, although it can also be used to interpret SBPT results. The basic assumptions of this method are:

- (a) Cylindrical cavity expansion theory holds;
- (b) Axisymmetry and plane strain are assumed;
- (c) Soil is infinite in extension, isotropic and homogeneous;
- (d) Soil's behaviour is linear elastic perfectly plastic;
- (e) No volumetric strain occurs within the soil medium.

A solution in the form of an analytical equation was developed for the elastic and plastic phases of the pressuremeter test. This closed-form solution could be called analytical pressuremeter equation. The Tresca criterion was used to define the beginning of the plastic stage for tests in clays. The analytical equation derived expresses the applied pressure in terms of the Neperian (natural) logarithm of the measured strain (change of pressuremeter cell volume divided by current volume). Then, by plotting pressuremeter loading data in a semi-logarithmic plot using these coordinates (applied pressure in arithmetic scale and the measured strain in logarithm scale) the undrained shear strength of the clay can be determined from the slope of the straight line (plastic stage) that follows the curved line (elastic stage). The elastic parameters (Young's modulus and Poisson's ratio) and the initial stress must be determined from the original pressuremeter curve or obtained from other sources. The authors also suggest that reasonable value of the initial horizontal stress can be determined from the same straight line (semi-logarithmic plot) if an estimation of the elastic parameters and the shear strength can be made. An estimation of the limit pressure (pressure for infinite strain) can also be obtained from this plot. The essence of this method is the special plot generated from the original pressuremeter data.

Some comments on this methodology are pertinent:

- The main attraction of this method is its capability to determine clay parameters from field data using a simple and understandable procedure, without any empirical factors;
- The value of the undrained shear strength determined by this method is usually higher than of the one determined from other in situ or laboratory tests (Wroth, 1984);

Following the same approach and assumptions as for clays, an analytical pressuremeter equation was derived for sands by Gibson and Anderson (1961). The Mohr-Coulomb criterion was used in the Gibson and Anderson (1961) method to identify the beginning of the plastic stage. The final equation derived shows that the cavity pressure applied versus the measured cavity strain plots as a straight line in a bi-logarithmic plot. The shear strength parameter (friction angle) is determined from the slope of this line. Although the value of the friction angle appears reasonable (Wroth, 1984), the assumption of constant volume used for the derivation can not be accepted. It is well known that, unless the sand is at steady state (constant volume) during the shearing process, there is change in the soil volume (dilatancy property).

A comment on this methodology can be made:

- The use of this methodology to interpret the pressuremeter test in sands was, unlike the clay solution, not so popular. The reason was the unrealistic assumed soil response.

#### B. Vesic (1972) method

Vesic (1972) proposed a methodology that takes into account the volumetric change of the soil around the pressuremeter during the shearing process. The method uses the general Mohr-Coulomb failure criterion. Both spherical and cylindrical solutions were developed. The assumptions are essentially the same as used by Gibson and Anderson (1961), with the exception of the volumetric change. The methodology is complex and cumbersome to apply. The major drawback is the requirement to evaluate the average volumetric strain at failure for a range of confining pressures from laboratory tests. To interpret pressuremeter test data to derive the friction angle, an iterative procedure is necessary. The final friction angle is a function of two factors. The first factor is called the cavity expansion factor and is related to the mean normal stress in the soil around the pressuremeter and to the friction angle. This factor is calculated for both an ultimate pressure defined from the pressuremeter data and an initial value of the friction angle (first iteration).

This ultimate pressure can be understood as a limit pressure (pressure for infinite strain). The second factor is called the reduced rigidity index. It is calculated from the shear modulus determined from the beginning of the pressuremeter curve, the average volumetric strain expected at failure, and the friction angle. A table or a plot correlating these two factors is then used to yield the friction angle for this first iteration. The iterative process is complete when the calculated friction angle is approximately equal to the previous value.

Some comments on Vesic (1972) method can be made:

- Using this methodology, the ultimate pressure to expand a cylindrical or spherical cavity in natural soils is determined in terms of strength parameters and deformation parameters;
- The methodology itself is cumbersome to use mainly because of the necessity for the average volumetric strain that has to be determined from laboratory tests. These special laboratory tests must take into account: (a) sample with comparable relative density to the natural soil; (b) stress path similar to the pressuremeter test (e.g. triaxial plane strain test); and (c) range of confining stress dependent on the depth of the pressuremeter test;
- Consideration of volumetric strain within the soil medium is complex and troublesome.

#### C. Jefferies (1988) method

Jefferies (1988), developed an extension of the Gibson and Anderson (1961) method to include the unloading phase of a self-boring pressuremeter test in clays. The assumptions are the same as for the 1961 method. Four analytical equations were derived to simulate a pressuremeter test. Two equations for the loading stage (elastic and plastic phases) and two equations for the unloading stage (elastic and plastic phases). The mathematical procedure to derive the soil parameters was by visual curve matching on the microcomputer screen. The method was called Computer-Aided Modeling

(CAM). Visual matching is used to check if the assumed soil parameters make the analytical equations fit the experimental curve. Three parameters are considered for clays: (a) initial horizontal stress; (b) undrained shear strength; and (c) elastic shear modulus. The best fit identifies the most appropriate set of soil parameters. Jefferies (1988) method was one of the first methods to incorporate interpretation of the unloading phase of a pressuremeter test. The method assumes no soil disturbance and is therefore only applicable to ideal self-boring pressuremeter tests in clay soils.

Some comments on Jefferies (1988) method can be made:

- The methodology is straightforward if a specially written code is available to do the calculations and plot the curves;
- There is no improvement on the assumptions required to do the interpretation. The constitutive relationship used is not continuous and the equivalent elastic shear modulus derived is meaningless for practical purposes;
- The linear elastic response is extended too far and does not realistically simulate the response of the natural clays. The elastic perfectly plastic model is too restrictive.

#### D. Houlsby and Withers (1988) method

Proposed by Houlsby and Withers, (1988), this interpretation methodology is based on a hybrid consideration of a small strain (elastic stage) and a large strain (plastic stage). Developed for the FDPT results the method assumes all the same assumptions as Gibson and Anderson (1961) method. The main difference from other methodologies is that this method considers only the unloading stage of the test. Because of the full displacement manner of pressuremeter insertion, the loading stage cannot be considered a true response of the natural undisturbed soil. From the unloading FDPT data, three parameters can be derived: (a) undrained shear strength; (b) shear modulus; and (c) initial in situ horizontal stress. While the first two have



realistic values, the last one is not recommended by the authors due to its unacceptable high values. The undrained shear strength is determined from a graphical procedure using the unloading stage of the FDP test. The equation derived is complicated due to the simulation of the unloading behaviour. Some approximations allow for a simple graphical method to be used. The elastic shear modulus is determined from the beginning part of the unloading curve.

Some comments on the Houlsby and Withers (1988) method:

- Although dealing with complex equations, the methodology has a sound theoretical basis. The mixture of small strain definition (Cauchy strain) and large strain definition (Hencky strain) may cause some confusion when performing the graphical procedure, although for small strains no difference between the two definitions exists. The derivation of shear modulus uses small strain (elastic stage) and the determination of undrained shear strength uses the large strain (plastic portion);
- Because of the assumption of linear elastic perfectly plastic constitutive model, the Tresca yield criterion allows the elastic portion of the test to extend far beyond the acceptable limit for this response. Moreover, the derived equivalent elastic shear modulus is difficult to apply for practical application purposes.

E. Houlsby et al (1986) method

Proposed by Houlsby et al (1986), this interpretation method follows the same assumptions as Hughes (1977) but includes the unloading stage of the test. SBPT data was used to validate the proposed methodology. The entire self-boring pressuremeter test is divided into four portions: (a) elastic loading; (b) plastic loading; (c) elastic unloading; and (d) plastic unloading. Following the same reasoning as in Gibson and Anderson's method, the point where there is the change in response from elastic to plastic was determined for both loading and unloading. Afterwards, a curve fitting technique, using an optimization routine, was applied to derive sand parameters for the plastic

portion of the test, again for both loading and unloading. Finally, shear moduli for the two elastic portions were directly measured from the experimental data. Altogether two shear moduli and two friction angles were determined. Rowe's dilatancy law can be used if dilation angles are to be determined. The initial horizontal stress was evaluated from the lift-off pressure.

Some comments on this methodology:

- The sand parameters were determined from SBPT data based on sound theoretical statements. Analytical equations were derived which govern the elastic and plastic phases of loading and unloading portions of the pressuremeter curve. Acceptable parameters were obtained only when unloading friction angle was assumed to be the constant volume friction angle (steady state value). This assumption implies, using Rowe's law, that the unloading stage occurs with no volume change, which is too restrictive (Jewell et al, 1980);
- The shear moduli determined were considered lower than the unload-reload shear modulus. Again, this is a consequence of using linear elastic perfectly plastic models which cause elastic region to extend too far from where it should be (very small strain). The Mohr-Coulomb failure criterion was used in this case to identify the end of the elastic stage.

#### (4) Nonlinear elastic perfectly plastic constitutive law

##### A. Denby (1978) method

Based on hyperbolic stress-strain relationship within the elastic region, Denby (1978) presented an interpretation method for self-boring pressuremeter data in clays. The assumptions of this study were the same as made by Gibson & Anderson for clays. However, rather than linear elastic, this method assumes nonlinear elastic soil response during the early stage of a pressuremeter test. From a special coordinate plot associated with a curve fitting technique, shear modulus and undrained shear strength were estimated. Specially chosen coordinates are used to generate a two-straight line plot. The ordinate is the

inverse of the slope determined from the loading portion of the pressuremeter test. Cavity strain is plotted as the abscissa axis. Initial horizontal stress can be calculated using the derived analytical equation for the elastic phase of the loading pressuremeter curve. The final interpreted results were considered reasonable by the author, since they were comparable to the results from other tests performed in the same San Francisco Bay mud.

Some comments on the Denby (1978) method:

- This methodology is seldom used in practice to derive deformation and strength parameters from pressuremeter tests in clays. The most probable reason is the need for the slope of the loading pressuremeter curve. The method becomes cumbersome to apply because of the dispersion of the field data, and for some types of soft clays it does not give reasonable results (Prapaharan, 1987);
- Another important drawback of this method is the reliance on the loading phase of the test, which likely has been affected by disturbance during the insertion process. Therefore, the measured response during the loading phase of the pressuremeter test represents the behaviour of the disturbed soil and not the response of the natural material.

(5) Elasto-plastic with strain hardening or strain softening constitutive law

A. Prevost and Hoeg (1975) method.

Plasticity theory was used to derive analytical equations which govern the self-boring pressuremeter expansion phase (Prevost and Hoeg, 1975). The analysis was developed for strain hardening and strain softening clay soils (undrained behaviour) using two sets of constitutive equations.

Besides the first three assumptions related to the cavity expansion problem (Gibson and Anderson, 1961), the following suppositions were also considered:

- (a) Strain hardening soil with hyperbolic plastic response;
- (b) Strain softening soil with a particular function governing the stress-strain

relationship;

(c) No volumetric strain.

The Von Mises yield criterion was used to represent the undrained behaviour of the saturated material. The solution to the problem was reached in a closed-form manner, with the final equations correlating pressure and deformation as in a pressuremeter test. Also equations governing stress distribution around the expanded cavity were derived. To represent the strain-hardening material three parameters were considered: (a) initial in situ stress (assumed known); (b) ultimate undrained strength; and (c) initial shear modulus (hyperbolic model). For strain softening material, three parameters were considered: (a) initial in situ stress (assumed known); and (b) two experimental parameters with no commonly used physical meaning.

Some comments on the Prevost and Hoeg (1975) method:

- The sound theoretical basis of this interpretation method is very attractive, increasing its potential of being more popular in the future if simpler mathematical technique (e.g. curve fitting) can be used;
- Although the derivation of soil parameters was not explicitly shown, it could be done if the slope of the pressuremeter loading curve was calculated. Similarly as for Denby's method, this procedure is not adequate for practical application.

B. Juran and Mahmoodzadegan (1989) method

Proposed by Juran and Mahmoodzadegan (1989), this method was developed to derive basic sand parameters from self-boring pressuremeter data. This was accomplished by using plasticity and cavity expansion theories to incrementally derive a shear curve, defined by the shear stress and the circumferential strain. The assumptions of this study were essentially the same as for Prevost's method, with the exception of the one related to the volumetric strain response. A particular plastic potential function is used in this case, allowing for volumetric strains during the shearing process. The total strain, which has two components - elastic and plastic, is considered to

be formed by the plastic strain only. Two different yield functions (Mohr-Coulomb type) and two different volumetric strain responses are adopted depending on sand relative density: dense dilating sand and loose contracting sand. Starting from a known initial horizontal stress and from a direct measurement of the slope of the pressuremeter loading curve at a certain strain level, an equation relating shear stress to the circumferential strain is established. With this equation plus the other equations that govern the plastic response in terms of stress (yield function) and volumetric strain (plastic potential function), both the shear curve and the effective stress path at the cavity wall can be incrementally obtained. Then the following sand parameters are determined: (a) friction angle at peak; (b) dilation angle; and (c) shear modulus. Triaxial hollow-cylinder tests were used to validate this methodology.

Some comments on the Juran and Mahmoodzadegan (1989) method:

- Similarly to all other interpretation methods of self-boring pressuremeter data, the physical problem is completely defined using the well-known cavity expansion theory (Solid Mechanics equations). Hence, the solution (generally in a closed-form manner) has a sound theoretical basis. In this method plasticity theory is used in addition to the cavity expansion theory to derive the equations which simulate the soil response to the pressuremeter loading;
- Interpretation methodologies based on the direct determination of the slope of the loading pressuremeter curve have two important drawbacks: (a) pressuremeter field tests have the loading curve determined by points which do not allow incremental analysis (Manassero, 1989; Baguelin et al, 1972); and (b) loading pressuremeter curve, mainly for sands, is likely to have been influenced by disturbance during the pressuremeter installation procedure. Soil parameters derived from such a curve will be influenced by the amount of disturbance.

### 2.3.2 Group II. Constitutive law derived from pressuremeter data

Since the early 70's, contributions to pressuremeter research have pointed

out two other approaches to interpret pressuremeter data, both giving a derived constitutive law of the soil tested as a result. The first one, called a general shape constitutive law, was the solution for the interpretation of pressuremeter data in clays and sands. For clayey soils, a geometric construction known as the sub-tangent method, was developed based on the cavity expansion theory. For sandy soils, a numerical approximation method was applied to self-boring pressuremeter data and a constitutive law as well as stress and strain paths were derived. The second approach had its origin based on the first one but using a pre-defined shape for the pressuremeter curve. Using a curve fitting technique, a particular function was fitted to the pressuremeter loading data. The constitutive law was then derived based on the cavity expansion theory.

#### (1) General shape constitutive law

##### (1.1) Interpretation using a graphic construction

###### A. Baguelin et al (1972), Palmer (1972), Ladanyi (1972) method

The interpretation of the self-boring pressuremeter data in clays using a general type relationship between shear stress and shear strain, was developed simultaneously and independently by Palmer (1972), Ladanyi (1972) and Baguelin et al (1972). Apart from slight differences in the physical conception, the principles and the mathematical techniques used were the same.

In addition to the first three assumptions commonly used in the cavity expansion theory (Gibson and Anderson, 1961), two other assumptions were stated:

- (a) No volume change occurs in the surrounding soil (undrained conditions);
- (b) Every element follows the same stress-strain curve.

Mathematical derivation using cavity expansion theory principles, has led to an analytical equation expressing a shear stress function in terms of a product between the slope of the loading pressuremeter curve and the cavity strain, generally defined as the change in radius divided by initial radius. This product represents the well-known sub-tangent graphical construction. Small

strain definition was used for that derivation. At the time of its presentation, this interpretation method was well accepted by the engineering community as a tool to derive the undrained shear strength of the soil tested. However, as pointed out by Wroth (1984), this method was very sensitive to disturbance and to the datum considered for the measured cavity strain. Derived values of the undrained shear strength tend to be higher than the values determined by other field tests (e.g. Vane test) or laboratory tests (AGI, 1991). In fact, there is no reason for the undrained shear strength to have a unique value (Wroth, 1984). Its dependency on stress or strain path followed, as well as the stress or strain rate applied during the test, is well recognized. The initial horizontal stress is measured directly from the lift-off pressure of the original pressuremeter curve, and the shear modulus is evaluated from unload-reloading cycles that may exist in the same curve.

Some comments on the Baguelin et al (1972), Palmer (1972), Ladanyi (1972) method:

- The approach to the pressuremeter problem used by this method is powerful, and represents the major attraction of the method. However, some concerns still remain regarding the high values of the undrained shear strength derived. This tendency was aggravated by drainage during the test and the presence of disturbance during the insertion stage;
- Reliance on the loading curve (soil normally disturbed) and use of graphical construction directly on the field data (high dispersion) are perhaps major weaknesses of this methodology.

#### B. Wroth and Windle (1975) method

This methodology was presented by Wroth and Windle (1975). Based on the same approach as the Palmer - Baguelin - Ladanyi's method, a graphical construction was used to derive the complete stress-strain curve of soils which undergo volumetric changes during the shearing process. Although the proposed method was meant to be an extension of the last method presented (Palmer, 1972; Baguelin et al, 1972; Ladanyi, 1972), it turned to be a more

general one, being applicable for sands and clays. The assumption of a known linear relationship between volumetric strain and cavity strain, and the equations of the cavity expansion theory, allowed a derivation of a relationship between shear stress and cavity strain in the form of an equation, which could be called the general sub-tangent method. The word 'general' is used to refer to the capability of the equation to handle expansion of cavities with and without volumetric strain. If no volume change occurs in the soil around the pressuremeter, the analysis reduces to the previous methodology. On the other hand, if some volumetric strain occurs, dilation properties can be derived (dilation angle). However, no method to derive the friction angle was presented.

A comment on the Wroth and Windle (1975) method can be made:

- The same comments as those made for the previous methodology apply to this method. In addition, the lack of information on how to derive the friction angle for granular material, constitutes strong weakness.

## (1.2) Interpretation using numerical methods

### A. Ladanyi (1963) method

A methodology to derive the strength and volumetric characteristics of granular materials, which undergo to volume changes during the shearing process, was presented by Ladanyi (1963). Based on a similarity condition between the problem of expanding a cylindrical cavity with an initial finite radius and with a zero initial radius, an analytical equation to calculate the stress distribution around the pressuremeter was derived. The relationship between shear strain and the pressuremeter volumetric strain accounting for soil volumetric strain during shear was presented. A simplified solution, which considers no additional volumetric change within the soil medium after the failure has taking place, was recommended. Only the total volumetric strain before failure is considered. No assumption about the soil stress-strain relationship was made. A finite difference methodology was used to integrate the equilibrium equation. The stress-strain law used was a general stress ratio



versus radial coordinate relationship, numerically approximated. To derive the correct failure envelope of the tested soil a trial and error procedure, related to the value of the soil volumetric strain, was used. The value of the volumetric strain that gives a straight line in the Mohr diagram, passing through the graphic origin is the actual soil volumetric strain. An alternate procedure following a similar reasoning of the Gibson and Anderson (1961) method, is also presented by Ladanyi (1963). The total volumetric strain before failure is chosen by trial and error such that the plot  $\log(\Delta V/V + e_o)$  versus  $\log(p/p_o)$  is a straight line (using Ladanyi's notation:  $\Delta V/V$  - pressuremeter volumetric strain;  $e_o$  - total volumetric strain of the soil before failure;  $p$  - pressure at the cavity wall;  $p_o$  - initial horizontal stress within the soil mass). The method was validated using an analytical pressuremeter loading curve. This method was only a simplified version of the numerical method presented by Ladanyi (1961).

#### Comment on Ladanyi (1963) method

- No information on soil parameters derived from in situ PBPT's was presented by Ladanyi (1963). The derived method has not been commonly used in geotechnical design.

#### B. Manassero (1989) method

In the late 80's the lack of a methodology to interpret self-boring pressuremeter data in sand, directly from the measured field curve was filled by Manassero's method (Manassero, 1989). Based on the finite difference method, the loading pressuremeter curve can be followed step by step (piece wise manner), providing the starting point of the curve is known. For the SBPT this starting point is identified by the lift-off pressure with zero circumferential and radial strains. Although cumbersome in its derivation (extremely long equation) the method is easy to understand. The assumptions and the principles used were essentially the same as used by Hughes (1977). The mathematical technique and the approach, however, were innovative. As a result, the complete nonlinear nature of the stress and volume change behaviour during shearing could be derived. Hence, the sand parameters

were determined: (a) shear modulus; (b) friction angle; and (c) dilation angle (from Rowe's law). Also the stress and strain paths followed by any element at the cavity wall during the expansion phase of the pressuremeter, were numerically determined.

Some comments on the Manassero (1989) method:

- For sandy soils, the complete nonlinear nature of the constitutive and volumetric strain relationships during shearing was derived based on the loading stage of a pressuremeter test. However, the direct use of the experimental data makes the method a bit troublesome to apply mainly because of the data dispersion. Some improvement was reached when the original pressuremeter curve was fitted by a polynomial function, as pointed out by the author;
- Even for the SBPT the loading curve from tests in sands is likely to be disturbed by the installation process. Relying on such experimental data to derive undisturbed soil parameters is susceptible to some criticism, even though the reported results could be considered reasonable.

## (2) Constitutive law derived from fitted pressuremeter curve

The use of the sub-tangent graphical construction, generates a considerable amount of scatter in the constitutive law derived (Baguelin et al, 1972). If a particular function can be fitted to the original pressuremeter loading data, an equation for the constitutive law could be derived mathematically using the sub-tangent definition equation. Many authors have proposed different equations to fit self-boring pressuremeter data in clays (Baguelin et al, 1972; Arnold, 1981; Prapaharan, 1987). From these methods the mobilized undrained shear strength of the tested clay can be evaluated.

Some comments on this approach

- An interpretation methodology based on such approach is very simple and easy to apply in practice. However, the derived parameters from this curve

fitting technique are physically meaningless, resulting in lack of confidence in its use. Those methods are currently rarely used ;

- The same comment related to the use of the loading curve made for the previously presented method is applicable here.

## **2.4 Conclusion**

More than one dozen interpretation methodologies have been presented and commented. All of them use the cavity expansion theory (cylindrical or spherical). This theory constitutes the core of the theoretical background used to solve the pressuremeter problem. Interpretation methods should consider the following important points: (a) the actual soil response is nonlinear; (b) the complete pressuremeter test has loading and unloading phases as well as some unload-reload cycles; (c) the loading curve is likely to be influenced by disturbance during pressuremeter installation. This review has shown few interpretation methods, within the group of the pre-defined constitutive law (Group I), which deal with nonlinear aspect of the stress-strain relationship. Also, only two of the presented approaches are concerned with the unloading stage of the pressuremeter test (Houlsby et al, 1986; Houlsby and Withers, 1988; Jefferies, 1988). Additionally, the reliance on the entire loading curve of the SBPT is another point for criticism. Although the self-boring technique can theoretically eliminate soil disturbance during the installation phase, some unknown degree of perturbation exists in the soil around the probe after insertion. All these three aspects - soil non linearity, loading and unloading data, and possible disturbance during the pressuremeter installation, will be considered by the interpretation methodology developed and proposed in this work.

## CHAPTER 3

### RESEARCH PROGRAM ON PRESSUREMETER DATA INTERPRETATION

#### 3.1 Introduction

When the pressuremeter first appeared in the late 50's it was designed to be a special device for testing soil and rock in place. One of the first pressuremeter, known as the Menard pressuremeter (pre-bored pressuremeter), produced a great deal of disturbance to the ground. However, the pre-drilled technique proved to be adequate for stiff or compact soils and weak rocks, even though there was a significant change in the stress state due to pre-drilling. The test results were presented in the form of a pressure-deformation plot and showed a characteristic s-shape curve for the loading stage. The disturbance caused by pre-drilling was somewhat similar to the disturbance experienced during sampling used for laboratory tests. No improvement in this respect was achieved. Mainly for this reason small importance was given to this field device during the 60's, at least outside France. The self-boring technique was developed in the early 70's in an effort to avoid disturbance. Hence, the derived parameters should represent the response of undisturbed natural soil. Although being an important improvement to the old technique, Ghionna et al (1983) showed that the SBP still has some flaws. Unfortunately, not all SBP problems are easily corrected. Research on the pressuremeter test should continue mainly due to its potential to yield valuable information of the material tested.

Three complementary areas of research can be identified when dealing with the pressuremeter test. One area would be the development of the equipment itself. A lot of laboratory and field work has been done in this respect in England, France, Canada, the USA, Australia, Italy and other countries around the world (Withers et al, 1986; Baguelin et al, 1978; Briaud et al, 1986; Campanella et al, 1990; Fahey and Carter, 1991; Ghionna et al, 1982). The second area of research on the pressuremeter test would deal with the test procedures. Strain controlled, stress controlled and holding tests constitute the focus of past studies on test techniques (Fioravante, 1988, Pyrah et al,

1985; Bellotti et al, 1986). Finally, the third area of pressuremeter related research is the development of interpretation methods to derive soil or design parameters from the pressuremeter data. The work developed in this thesis refers to the third area. Analytical equations are derived and soil parameters are determined using a curve fitting technique.

### **3.2 Research on pressuremeter interpretation**

Many researchers have been working in this area for the last two decades. The English and French schools have given important contributions (Wroth, 1984; Baguelin et al, 1978). Nevertheless, researchers from other countries have contributed to a better understanding of the pressuremeter test itself and the interpretation of its results (Fahey and Carter, 1991; Robertson and Hughes, 1986; Briaud, 1986; Denby, 1978; Manassero, 1989; Lacasse et al, 1990). However, the first attempt to theoretically develop an interpretation method was done by Gibson and Anderson (1961). Since that time, the general response of the soil during a pressuremeter test has been split into two groups: (a) undrained response (fine grained soil), and (b) drained response (granular soil). In the 70's, many interpretation methodologies were developed and some are still under development. For undrained type of soils the methodologies developed by Gibson and Anderson, (1961) and by Palmer-Baguelin et al-Ladanyi (1972) are the most popularly used for geotechnical design. Both methodologies are used to determine the undrained shear strength of the soil tested. However, the undrained shear strength from the pressuremeter is generally larger than the shear strength from other in situ tests (Vane test, flat dilatometer test) and laboratory tests. Such comparison is not always recommended since the undrained shear strength is not a fundamental soil parameter (no-unique value), and is highly dependent on the type of test. Stress or strain path, as well as stress or strain rate, are the most important influences on the undrained shear strength value. Moreover, disturbance during insertion and consolidation during the test, frequently contribute to the overestimation of the soil undrained strength (Wroth, 1984). For the other group, granular soils, the response to the pressuremeter loading and unloading is necessarily drained and influenced by the volumetric change in the soil around the opened cylindrical cavity. The

research undertaken by Hughes et al (1977) resulted in the most practical interpretation method of the pressuremeter test in sands. However, reliance on the loading curve only and approximation of the soil response by a rigid plastic model constitute the main sources of criticism of the Hughes et al (1977) method. Recently another method for interpretation of the pressuremeter test in sands has been developed (Houlsby et al, 1986; Houlsby and Yu, 1990). This method is based on the loading and unloading portions of a SBPT and analytical equations were derived to simulate the pressuremeter test in elastic perfectly plastic material. The large strain theory was used for this purpose. A graphical construction was suggested to determine the friction angle.

So far, despite a large number of pressuremeter interpretation methods, a simple, practical and repeatable method is still being sought. Jefferies (1988) gave an important contribution in this direction, although the dependency on a specially written computer code might discourage engineers from applying such a method to the geotechnical design. There is no question that pressuremeter test results carry important and useful information of the soil behaviour. Research in this area should continue searching for practical and simple ways to accurately derive reliable soil parameters from pressuremeter soil response.

### **3.3 Important statements for an interpretation methodology**

Research on the methods of pressuremeter data interpretation should consider at least the following five important statements:

- (a) The soil must be modeled by a realistic constitutive law;
- (b) A complete pressuremeter test has soil response information in both loading and unloading;
- (c) The insertion of any device into the soil medium will necessarily cause some disturbance;
- (d) The methodology derived must be consistent, repeatable and simple to apply; and
- (e) All the necessary mathematical calculations may be performed with the help of commercially available software.

An interpretation method that considers the above statements in a balanced fashion has a greater chance of contributing effectively to an improved engineering construction based on realistically determined soil parameters.

The constitutive law has been a major concern for many contributions to research into pressuremeter data interpretation. Based on either pre-defined stress-strain response or pressuremeter derived constitutive law response, interpretation methodologies have been developed to determine soil parameters. It has been shown (Baguelin et al, 1978; Fahey and Carter, 1991; Wood, 1990 and 1991) that the soil behaviour is highly nonlinear even for the earliest part of most pressure-deformation measurements. Linear elasticity is not able to represent such response, unless for really small shear strains (less than  $10^{-3}\%$ ). The hyperbolic soil model is a nonlinear model that has proven to be a simple and realistic representation of most soil stress-strain relationships (Duncan and Chang, 1970). For undrained response the shear stress can be considered to follow a hyperbolic relationship as a function of the measured cavity strain during a pressuremeter test. For drained response, due to the increase of the mean normal stress before failure, the stress ratio ( $t/s$ ) can be considered to follow a hyperbolic relationship as a function of the measured cavity strain during the pressuremeter test. To describe the soil response with this model requires only two parameters. Hence, the solution of the inverse boundary value problem becomes feasible using a mathematical technique such as curve fitting. This type of model has not been used before to interpret the entire pressuremeter curve. Denby (1978) has used the hyperbolic model to describe just the elastic response of the soil during the early part of the pressuremeter expansion. His method is classified as nonlinear elastic perfectly plastic type and is not suitable for the derivation of a closed-form solution that represents the entire loading stage of the pressuremeter test where a discontinuity is imposed to the stress-strain law.

Another aspect of the problem is the amount of mathematical computation to reach the solution. A simple technique, even involving some judgement by the user, is usually desirable when the interpretation methodology is intended to be used by engineering practitioners. Numerical techniques, such as finite

element and finite difference methods, are seldom used to solve day to day problems mainly because of the computational infrastructure required. Software to perform curve fitting techniques is currently available and easy to use. These types of applications require only non-specialized hardware (regular microcomputers) and a very small amount of previous data processing experience. Nowadays, any engineering can easily fulfill such requirements.

As said by Wroth (1975), it is impossible to insert any device into the soil mass without causing some amount of disturbance. Highly experienced technicians and field engineers can obtain SBPT data of a very good quality. However, this is very expensive and does not represent the general situation. Typical pressuremeter loading data have always an unknown amount of disturbance embedded. It means that the measured response does not represent the natural undisturbed material. However, the unloading curve starts at a point where the maximum pressure inside the pressuremeter was defined by a large amount of failed surrounding soil. This pressure is commonly referred as the limit pressure (pressure for infinite strain). Hence, there is no apparent reason for the unloading portion of the pressuremeter test to be different for different types of devices (PBP, SBP, PIP, and FDP). The unloading curve, therefore, must be understood as an important piece of information when pressuremeter data interpretation is concerned. Recently, this feature has been recognized by Houlsby et al (1986) and by Jefferies (1988). The natural trend is to provide interpreted soil parameters based on both loading and unloading portions of the pressuremeter test.

However, it is not a recommended practice to put the same emphasis on loading and unloading portions of a pressuremeter test. Because of the inevitable disturbance during installation the initial loading data are influenced more than the unloading data. For this reason the later part of the loading stage is more reliable than the earlier portion. Since the amount of disturbance is unknown, only the last measured data points during the loading stage should be considered by any interpretation methodology. Until now, this has not been the case, most techniques are based on the interpretation of the complete loading part of a pressuremeter test. Frequently, the unloading



portion of the test is not presented. Houlsby and Withers (1988) and Jefferies (1988) were the first to incorporate the unloading part of the test into interpretation.

The last aspect to be addressed here are features such as consistency, simplicity, and repeatability. Firstly, to be consistent a method must take into account soil parameters that are physically meaningful, directly related to the nature of the tested material. When dealing with the solution of an inverse boundary value problem, the uniqueness of the solution is always a concern. However, when basic soil parameters are sought (shear modulus, shear strength, initial horizontal stress) the solution is, in the great majority of cases, well conditioned and consistent (Jefferies 1988). It means that changes in the interpreted set of parameters, will cause the derived analytical equation no longer represent the experimentally measured response. Mathematically, many sets of numbers are possible. However physically, just small variation of the interpreted set ( $\pm 10\%$ ) is acceptable because the analytical response will deviate from the experimental measurements. The second essential feature of an interpretation method is its simplicity. If the method is complex and cumbersome to apply to practical engineering work, there is a small probability that the proposed method will be used for geotechnical design purposes. Sound theoretical basis and adequate mathematical technique will result in acceptance of the method by the engineering community. Finally, the method's repeatability should be considered. A methodology to interpret pressuremeter data should not be heavily dependent on the user's judgement. This is the case for almost all graphical methods to derive soil parameters from pressuremeter field data. If some judgement is left to the user, the variation of the results should lie within a narrow range around the average ( $\pm 5\%$ ). The method then can be considered repeatable.

### **3.4 Necessary background required**

For research on pressuremeter interpretation, the following background should be provided: (a) good infrastructure for analytical work; and (b) a variety of pressuremeter data to validate the method. The necessary infrastructure is commonly available in Universities and Research Institutes.

However, pressuremeter data is available only where access to the equipment is possible. For this work, the pressuremeter data was provided by private companies, government agencies and other universities.

### **3.5 Conclusion**

The development of an interpretation methodology to derive soil parameters from pressuremeter data is the subject of this work. Many researchers have developed methods to interpret pressuremeter results since the early 60's. Some methodologies have become popular in geotechnical design. However, restrictive assumptions and not repeatable mathematical techniques are important drawbacks of these interpretation methods. Nonlinear soil behaviour in the form of a hyperbolic function relating shear stress and cavity strain is proposed in this work in order to have a more realistic representation of the soil response. Analytical equations are derived for both loading and unloading portions of the pressuremeter test. Using curve fitting technique as the mathematical tool, soil parameters are then derived from pressuremeter experimental data. The approach is applied for both sand and clay responses. Some soil disturbance is assumed to exist in the initial loading stage of all pressuremeter tests.

## CHAPTER 4

### INTERPRETATION OF UNDRAINED SELF-BORING PRESSUREMETER TEST RESULTS INCORPORATING UNLOADING

#### 4.1 Introduction

Anderson et al (1986) have pointed out that in situ tests have been increasingly preferred by geotechnical engineers due to their capability to: (a) decrease physical disturbance; (b) decrease stress relief; and (c) increase the amount of tested soil. Therefore, pressuremeter tests have become very popular. The self-boring version of the pressuremeter has been frequently used to test normally consolidated clays in the search for specific geotechnical parameters (Yeung and Carter, 1990; Fukagawa and Iizuka, 1990; Anderson et al, 1986; Benoit et al, 1990). The main attraction of the self-boring technique is the possibility of minimum disturbance (Wroth, 1984).

Interpretation procedures have been developed since the early 60's to allow derivation of soil parameters from pressuremeter test results in clays (Gibson and Anderson, 1961; Palmer, 1972; Ladanyi, 1972; Baguelin et al, 1972; Houlby and Withers, 1988; Jefferies, 1988). Generally, the most commonly sought parameters are: (a) undrained shear strength; (b) shear modulus; (c) initial horizontal stress; and (d) consolidation parameters (from holding tests). One important assumption of these interpretation methods is the undrained response of the soil during pressuremeter loading. Although it is very difficult to assure that no drainage will take place during the test, Fukagawa and Iizuka (1990) has shown that it is theoretically possible to adjust the test rate to the soil permeability, so that undrained behaviour can be achieved. Rate dependent processes, such as creep and consolidation, have an important influence on the derived undrained shear strength of the tested soil.

Until 1988, the unloading stage of a pressuremeter test (PBPT, SBPT, and PIPT) has been considered just the necessary stage to contract the pressure cell to advance the equipment to the next test depth. In other words, just the loading portion of the pressuremeter test has been considered to derive the soil parameters. However, a comparison of the unloading portions of

pressuremeter tests (PBPT, SBPT, FDPT, and PIPT) show great similarity. The unloading portion of the test is the least influenced by any disturbance created during pressuremeter insertion. Moreover, due to the low permeability of clay soils the unloading stage is more likely to be undrained than the loading stage. Houlsby and Withers (1988) and Jefferies (1988) were the first to recognize the importance of the unloading curve in the derivation of soil parameters from pressuremeter tests in clays.

#### **4.2 Previous interpretation procedures of undrained pressuremeter results**

One of the earliest pressuremeter interpretation methods was developed by Gibson and Anderson (1961) to define a limit pressure for pressuremeter expansion in an ideal elastic-perfectly plastic material. Commonly, the pressuremeter results are plotted in terms of radial pressure ( $\sigma_r$ ) versus  $\log_e(\Delta V/V)$ , where  $(\Delta V/V)$  is a measurement of the cavity strain related to the deformed configuration. The results of the plastic phase of the test should lie on a straight line with a gradient equal to the undrained shear strength ( $S_u$ ). The method is still very popular for interpreting pressuremeter tests (both PBPT and SBPT's) in clays, partly due to its reliance on the large strain (plastic) portion of the test which is less affected by soil disturbance.

In 1972, analytical solutions (Palmer, 1972; Ladanyi, 1972; Baguelin et al, 1972) were developed that allowed the complete undrained stress-strain curve of the soil to be derived from SBPT results of an undrained test. The solution by Palmer-Ladanyi-Baguelin et al (1972) uses the slope of the pressuremeter loading curve and assumes the soil to have a unique, but not pre-defined stress-strain relationship. Experience gained with this approach showed that in many cases the derived stress-strain curve has an irregular shape due to the difficulty in obtaining the slope of the field pressure-expansion curve. Therefore, several methods were developed (Jamiolkowski and Lancellotta, 1977a, and 1977b; Denby, 1978; Arnold, 1981) to smooth the measured pressure-expansion curve using different curve fitting techniques. All these techniques were developed to interpret the loading portion of the pressuremeter test. Hence, any soil disturbance caused by installation was

reflected in some unknown manner in the interpreted results.

Houlsby and Withers (1988) suggested that full-displacement pressuremeter tests in clay could be analyzed using the unloading portion of the test results. The soil was assumed to be elastic-perfectly plastic; principal stress rotation due to unloading was assumed to occur when reverse plasticity takes place and a large strain analysis was applied. A closed-form solution was developed and the undrained shear strength was determined from a geometric construction using the unloading curve, somewhat similar to the sub-tangent construction used in the Palmer (1972) method. This method represents the first attempt to obtain information on soil parameters using the complete unloading portion of a pressuremeter test.

Jefferies (1988) proposed a method to interpret SBPT results in clays incorporating the complete loading and unloading portion of the test. The method was also based on an elastic-perfectly plastic soil model. The ratio of the unloading strength of the clay to its loading strength was assumed to be known. Jefferies' method assumed that the installation was carried out with minimum disturbance (i.e. perfect self-boring process) so that the loading portion of the test represented the true undisturbed response of the soil. Jefferies (1988) used computer aided modeling techniques to visually compare the measured response with the numerically derived curves. The method required specialized interactive software operating on an engineering workstation (or microcomputer with high resolution screen monitor). The primary objective of the method was to derive the in situ horizontal stress, although the undrained shear strength ( $S_u$ ) and an equivalent linear elastic shear modulus ( $G$ ) were also derived. The Jefferies' approach represents one of the first attempts to use all the information contained in the loading and unloading portions of the SBPT to derive the required soil parameters. However, the technique required specialized interactive software and perfect SBPT results. Also the simplified elastic-perfectly plastic soil model made it difficult to understand the meaning of the equivalent linear elastic shear modulus to apply to engineering design problems.

### **4.3 Proposed methodology to interpret undrained SBPT data**

The proposed method is an extension of the method developed by Jefferies (1988). However, soil non linearity is incorporated assuming the soil stress-strain response can be represented by a hyperbolic function.

#### **4.3.1 Assumptions**

The method has the following assumptions:

- (1) The pressuremeter test is performed undrained from the start of expansion to complete contraction;
- (2) The test is treated as an expansion and contraction of an infinitely long cylindrical cavity (i.e. radially symmetric and plane strain);
- (3) The vertical stress remains the intermediate principal stress during the test;
- (4) The unique soil stress-strain behaviour can be represented by a hyperbolic function in both loading and unloading;
- (5) The ratio of the unloading strength of the clay to the loading strength is known; and
- (6) The strains are considered to be small.

These assumptions are essentially the same as those made by Jefferies (1988) and Gibson and Anderson (1961), except for the hyperbolic representation of the stress-strain behaviour.

#### **4.3.2 Hyperbolic model**

The range of soil models used to represent the soil response is fairly large. Models ranging from simple linear elastic to general elastic-plastic could be used to describe the soil response. Each one has advantages and limitations. The selection of the hyperbolic representation of soil behaviour was made for the following reasons:

- (1) The hyperbolic stress-strain model (Kondner, 1963; Kondner and Zelasko, 1963) has proven effective in describing soil behaviour under a variety of loading conditions (Duncan and Chang, 1970);

- (2) The need to keep the soil model simple and to avoid generating a method that requires a solution for many unknown parameters;
- (3) The parameters that define the soil model have some engineering significance, so that when the interpretation process is completed the parameters derived can be understood and applied to the design.

#### 4.3.3 Derivation of the pressuremeter analytical equation

##### • Sign convention and strain definition

Compressive normal strains and compressive normal stresses are positive. For pressuremeter testing the circumferential strain ( $\varepsilon_\theta$ ) is often referred as the cavity strain ( $\varepsilon$ ) ( $\varepsilon = -\varepsilon_\theta$ ).

For pressuremeter expansion, the cavity strain is defined as:

$$\varepsilon = \frac{\Delta R}{R_0} \text{-----(4.1)}$$

where:  $\varepsilon$  - cavity strain in loading  
 $R_0$  - initial radius of the pressuremeter  
 $\Delta R$  - change in pressuremeter radius ( $\Delta R = R - R_0$ )  
 $R$  - current pressuremeter radius

For pressuremeter contraction, the cavity strain is defined as:

$$\varepsilon^* = \frac{\Delta R}{R_{\max}} \text{-----(4.2)}$$

where:  $\varepsilon^*$  - cavity strain in unloading  
 $R_{\max}$  - maximum radius of the pressuremeter  
 $\Delta R$  - change in pressuremeter radius ( $\Delta R = R - R_{\max}$ )  
 $R$  - current pressuremeter radius

The derived relationship between  $\varepsilon$  and  $\varepsilon^*$  is:

$$\varepsilon^* = \frac{\varepsilon - \varepsilon_{\max}}{1 + \varepsilon_{\max}} \text{-----(4.3)}$$

where:  $\varepsilon_{\max}$  - maximum cavity strain at the start of the unloading

##### • Governing equations

(1) Baguelin et al (1972), Palmer (1972), Ladanyi (1972)

$$\frac{d\sigma_r}{d\varepsilon} = \frac{2\tau(\varepsilon)}{\varepsilon(2+\varepsilon)(1+\varepsilon)} \text{-----(4.4)}$$

where:  $\sigma_r$  - radial stress applied to the soil element  
 $\tau(\varepsilon)$  - constitutive relationship

For small strains the equation reduces to:

$$\frac{d\sigma_r}{d\varepsilon} = \frac{\tau(\varepsilon)}{\varepsilon} \text{-----(4.5)}$$

(2) Constitutive relationship (hyperbolic model)

(a) Loading:

$$\tau = \frac{\varepsilon}{\frac{1}{2G_i} + \frac{\varepsilon}{\tau_{ult}}} \text{-----(4.6)}$$

where:  $\tau$  - mobilized shear stress  
 $2G_i$  - initial shear modulus  
 $\tau_{ult}$  - ultimate shear strength (asymptote)

The complete soil stress-strain curve followed during the pressuremeter loading phase can then be defined using equation (4.6) and the two parameters  $G_i$  and  $\tau_{ult}$ . The parameter  $G_i$  represents the initial tangent shear modulus at small strains. The level of strain that  $G_i$  is applicable to is dependent on the strain range over which the hyperbolic function adequately fits the stress-strain response of the soil. One approximation would suggest that  $G_i$  is applicable from a shear strain level of approximately 0.1%.

(b) Unloading:

$$\tau^* = \frac{\varepsilon^*}{\frac{1}{2G_i} - \frac{\varepsilon^*}{\tau_{ult}^*}} \text{-----(4.7)}$$

where:  $\tau^*$  - mobilized shear stress  
 $\varepsilon^*$  - circumferential strain (negative under unloading)  
 $\tau_{ult}^*$  - ultimate shear strength (asymptote)



The hyperbolic model is usually applied in terms of shear stress ( $\tau$ ) and shear strain ( $\gamma$ ). However, for undrained cylindrical cavity expansion the following relationship holds:

$$\gamma = 2\varepsilon \text{ -----(4.8)}$$

Hence, the term  $2G_i$  in equations (4.6) and (4.7) stems from the use of cavity strain ( $\varepsilon$ ) instead of the more conventional engineering shear strain ( $\gamma$ ). The resulting loading and unloading model is illustrated in figure 4.1.

• Boundary conditions at the cavity wall

(a) Loading:

$$\varepsilon = 0 \Rightarrow \sigma_r = \sigma_{h_0} \text{ -----(4.9)}$$

(b) Unloading:

$$\varepsilon^* = 0 \Rightarrow \sigma_r = \sigma_{r \max} \text{ -----(4.10)}$$

• Pressuremeter analytical equation

(a) Loading:

$$p = \sigma_{h_0} + \frac{\tau_{ult}^*}{R_\tau} \cdot \ln \left( 1 + \frac{2G_i \cdot R_\tau \cdot \varepsilon}{\tau_{ult}^*} \right) \text{ -----(4.11)}$$

valid for  $0 \leq \varepsilon \leq \varepsilon_{L \max}$

where:  $p = \sigma_r$  - pressure at the cavity wall  
 $\sigma_{h_0}$  - initial horizontal stress  
 $R_\tau = \tau_{ult}^* / \tau_{ult}$  - ratio of the ultimate undrained shear strength on unloading and loading  
 $\varepsilon_{L \max}$  - cavity strain at the end of loading

(b) Unloading:

$$p = p_{\max} + \tau_{ult}^* \cdot \ln \left( \frac{1}{1 - \frac{2G_i \cdot (\varepsilon - \varepsilon_{\max})}{(1 + \varepsilon_{\max}) \cdot \tau_{ult}^*}} \right) \quad (4.12)$$

valid for  $0 \geq \varepsilon^* \geq -(\varepsilon_{\max}/(1 + \varepsilon_{\max}))$

where:  $p_{\max} = \sigma_{r_{\max}}$  - pressure at the cavity wall at the beginning of unloading

#### 4.3.4 Proposed methodology

As discussed earlier, the unloading part of the pressuremeter curve is less influenced by disturbance during installation. Hence, it is logical to first analyze the unloading part of the test to derive  $\tau_{ult}^*$  and  $G_i$ . If a value for the ratio  $R_r$  is assumed, the ultimate undrained shear strength in loading  $\tau_{ult}$  is therefore determined. Using these values of  $\tau_{ult}^*$ ,  $G_i$  and  $R_r$  the loading part of the test can then be analyzed to derive  $\sigma_{h_0}$ .

If the loading part of the test is influenced by disturbance, the early part of the loading portion will not agree with the derived curve. Hence, the loading part of the test should only be analyzed over the last part of the curve, which will, in general be less influenced by disturbance. Based on this logic, the following steps are prescribed for the proposed interpretation methodology:

- (a) Use the unloading analytical equation (4.12) to fit the unloading portion of the pressuremeter test. Two parameters are derived from the best fit:  $\tau_{ult}^*$  and  $G_i$ .
- (b) Assume a value for  $R_r (= \tau_{ult}^*/\tau_{ult})$  and use the equation (4.11) applying the derived values of  $\tau_{ult}^*$  and  $G_i$  to fit the last part of the loading pressuremeter curve to determine  $\sigma_{h_0}$ .

This interpretation methodology is shown schematically in figure 4.2.

This process accepts that the initial loading portion of the pressuremeter test is influenced by some amount of disturbance. If the self-boring installation process has resulted in very little disturbance the analytical curve should match closely the entire measured pressuremeter curve. The proposed

method (equations 4.11 and 4.12) is based on small strains and would not be applicable to large strain pressuremeter expansion.

#### 4.3.5 Comments on the proposed methodology

- Ratio of undrained strength in loading and unloading ( $R_\tau$ )

As presented in the interpretation methodology, the parameter  $R_\tau$  is required to obtain the value of the undrained shear strength  $\tau_{uk}$  and the horizontal in situ initial stress,  $\sigma_{h_0}$ . Ideally, the parameter  $R_\tau$  should be obtained from laboratory testing on high quality undisturbed samples, tested under stress paths similar to those experienced during undrained pressuremeter expansion and contraction, as suggested by Jefferies (1988). However, for the initial interpretation of most pressuremeter tests this is not always possible, and an estimate of  $R_\tau$  should be made. The parameter  $R_\tau$  affects the value of the: (a) undrained shear strength in loading, and (b) initial horizontal stress.

Undrained pressuremeter expansion and contraction can be considered to be a plane strain problem where the stress path in unloading is the reverse of loading. Hence, since the plane strain strength envelope is the same in loading and unloading, it is reasonable to assume that  $R_\tau = 2.0$ . Both Jefferies (1988) and Houlsby and Withers (1988) also assumed that the strength in loading equals the strength in unloading. Therefore, for the soil model used in this methodology the value of the ratio  $R_\tau$  is assumed to be 2.0.

- Software to perform curve fitting

Several approaches can be used to fit an equation to experimental data. Rather than develop a specific software to perform the curve fitting process using an optimization routine, it is preferable to use available application software developed for personal computers. The software selected for this study was Kaleidagraph™ (version 2.1) developed for a Macintosh™ microcomputer. This application is a powerful tool to perform calculations, graphs and curve fitting.

The experimental data, from the field, after being corrected for membrane stiffness, is copied to a Kaleidagraph™ worksheet, so the data becomes available for analyses. The only manipulation needed is to separate the loading and unloading portions of the test, eliminate any unload-reload loop data, and arrange both sets of remaining data in ascending order. The data are then ready to be analyzed.

The least square error curve fitting method was used to fit a general function to a set of experimental data. This is a very simple and well-understood method and can be used readily when the data does not present a large scatter and has a defined trend. This is the case of the data from pressuremeter tests.

Loading and unloading analytical equations are entered and the curve fitting is performed. As a result, a graph is automatically displayed on the monitor screen, and a visual check of the match between the experimental and analytical curves can be made. It is noteworthy to mention at this point, that the first set of parameter values to be tested must be given by the user. For fitting the unloading curve the only requirement for this first set is that the parameters should have the same order of magnitude as the set that will give the best curve fitting. Hence, one can avoid divergence of the analysis. However, for fitting the loading curve the first set must consider: (a) minimum number of experimental points used; and (b) minimum range of pressure for those points. Experience with this software has shown that the minimum number of points must be greater than 15 and the range of pressure must be sufficient to obtain a correlation factor from the curve fitting between 0 and 1.0. The reader is referred to the Kaleidagraph™ manual for more information on using the application and curve fitting capabilities. A suggested interpretation template is presented in figure 4.3.

#### **4.4 Interpretation of SBPT in the Fucino clay**

The proposed methodology has been applied to high quality SBPT results performed in a uniform clay deposit, reported by Fioravante (1988) and A.G.I.- Associazione Geotecnica Italiana (1991). Fioravante (1988) presented 36

self-boring pressuremeter test results performed in the Fucino clay in two boreholes at the same site. A complete geotechnical characterization of the Fucino clay is presented by AGI (1991). The clay deposit, located within the central Apennines, is described as a soft, homogeneous, highly structured  $\text{CaCO}_3$  cemented, lacustrine clay. The cementation with calcium carbonate plays an important role in the mechanical behaviour of the clay, being responsible for some discrepancies shown by different tests, mainly when disturbance is present.

From the SBPT results presented by Fioravante (1988), 20 tests from borehole V2, have been interpreted and the results presented. The first test was performed at 2m and the last one at 38m. All tests have been interpreted using the methodology described earlier. The template shown in figure 4.4 was used to interpret the V2P14 test (depth 26m). Figures 4.5 (a) and (b) respectively present the final plot and the curve fitting for all loading points of the V2P14 test.

Test V2P14 appears to represent a good SBPT with little disturbance. Figure 4.5 (a) shows that the analytical solution with  $R_c = 2.0$  provides an excellent fit to all points of the measured loading curve. For the final interpretation, shown in figure 4.5 (a), only the very last points of the loading curve have been chosen to apply the curve fitting technique. The good agreement of the fit to all the loading data points and the fit to only the last loading points implies the test has suffered little disturbance due to the installation process. Figure 4.4 illustrates the suggested process to yield the full interpretation.

Figure 4.6 presents the interpretation for the V2P10 test (depth 18m). This test appears to have some disturbance since the analytical solution does not provide a good match to the complete loading curve. Note that the solution shown in figure 4.6 was obtained by matching only the final portion of the loading curve. When the fit was performed over the complete loading curve, the match was poor over the last part of the experimental curve.

Interpretation templates and final plots for all 20 tests in the Fucino clay are presented in Appendix C.

#### 4.4.1 Initial shear modulus ( $G_i$ )

The interpreted initial shear modulus values for all twenty tests are presented in figure 4.7. The interpreted values of  $G_i$  are very close to the shear modulus values calculated from unload-reload loops presented by AGI (1991), and approximately one third of the values determined from in situ shear wave velocity measurements.

The shear modulus ( $G_0$ ) determined from in situ shear wave velocity measurements represents the elastic shear modulus at a strain level of less than  $10^{-4}\%$ . The unload-reload modulus ( $G_{ur}$ ) represents the average modulus over an average shear strain level of about  $10^{-1}\%$  (Robertson, 1982; Bellotti et al 1986). The interpreted shear modulus ( $G_i$ ) derived from the proposed interpretation is based on an assumed hyperbolic stress-strain relationship. Experience has shown that the hyperbolic expression is a reasonable representation of the stress-strain response of many soils over a variety of strain ranges (Vucetic and Dobry, 1991). Hardin and Drnevich (1972) suggested that the hyperbolic expression could represent the stress-strain response of many soils from the very small shear strain of  $10^{-4}\%$  to about  $10^{-1}\%$ . Also, Duncan and Chang (1970) showed that the hyperbolic expression was very good to describe the stress-strain response from an initial shear strain of around  $10^{-1}\%$  to failure ( $>1\%$ ).

The results shown in figure 4.7 suggest that the hyperbolic expression is a reasonable representation of the stress-strain response from around  $10^{-1}\%$  to failure for Fucino clay.

#### 4.4.2 Undrained shear strength ( $\tau_{ult}$ )

When using the hyperbolic relationship to describe the nonlinear stress-strain behaviour of soil, the ultimate shear stress or undrained shear strength is only reached at infinite strain. Traditionally, this has been overcome by incorporating a reduction factor ( $R_f$ ) to allow the undrained shear strength to be attained at a known strain level. However, if a reduction factor is

incorporated into the proposed interpretation method, the following problems occur:

- (1) Additional parameter is needed to define the reduction factor ( $R_f$ );
- (2) Closed form solution is difficult to obtain because of the discontinuity in the stress-strain curve due to the reduction factor cut-off.

Although the ultimate shear stress is not attained in the hyperbolic representation, it is possible to calculate the mobilized pressuremeter undrained shear stress ( $S_{u|mob}$ ) reached at any strain level in the pressuremeter test. Figure 4.8 shows the interpreted range for the mobilized pressuremeter undrained shear stress ( $S_{u|mob}$ ) at the maximum cavity strain for the Fucino clay compared to the undrained shear strength from the field Vane, flat dilatometer and laboratory undrained triaxial tests (UU). Also shown are the undrained shear strengths derived from the SBPT results using only the loading portion of the pressuremeter test. The results are in good agreement at the depth around 5m. At a depth greater than 5m the interpreted values using the SBPT results are significantly higher than the values from above mentioned tests. High undrained shear strengths from pressuremeter tests have been frequently observed. Wroth (1984) showed that the undrained shear strength derived from the SBPT should be larger than the strength derived from the field Vane test due to the different stress paths followed. Wroth (1984) suggested that the SBPT  $S_u$  values should be larger than the field Vane by about 40% depending on the friction angle of the clay. If the SBPT  $S_u$  values in figure 4.8 were corrected based on the suggestion by Wroth (1984), the SBPT  $S_u$  values would remain larger than the field Vane values.

It has been recognized by many researchers (Wroth, 1984; Anderson and Pyrah, 1986; Williams, 1986) that some drainage and creep take place during many pressuremeter tests in clays. This drainage and creep can result in an overestimated undrained shear strength (Wroth and Windle, 1975). Partial drainage and strain rate effects (e.g. creep) are common problems when interpreting in situ tests in fine grained soils.

#### 4.4.3 Earth pressure coefficient at rest ( $K_0$ )

Figure 4.9 shows the interpreted values for the earth pressure coefficient at rest using the proposed methodology, compared to values determined from flat dilatometer tests and from the observed lift-off pressure of the SBPT. In general, the interpreted values of  $K_0$  using the proposed interpretation methodology are slightly higher than the values obtained from the lift-off pressure.

Wroth (1975) stated that it is impossible to measure the in situ stress at rest with any device that depends upon the insertion of any type of instrument into the soil mass. However, providing a careful insertion and minimum disturbance, it has been recognized that the self-boring pressuremeter data should carry useful information on the initial horizontal stress. For a pre-defined value for ratio  $R_r$  it appears possible to derive acceptable values for  $\sigma_{h_0}$  using the proposed interpretation method even if the loading curve has been somewhat influenced by disturbance during installation. This pre-defined value for the ratio  $R_r$  can be assumed to be 2.0 or determined from laboratory tests, as proposed by Jefferies (1988).

### 4.5 Discussion of the interpreted results

#### 4.5.1 Sensitivity analysis

To illustrate the sensitivity of the proposed interpretation method, V2P14 test has been re-analyzed varying one of the three variables by  $\pm 10\%$  of the interpreted value. The parameters selected were those derived from the interpretation (figure 4.4) to provide the best fit using the proposed methodology.

Figure 4.10 presents the variation in the analytical loading curves for a  $\pm 10\%$  change in  $\tau_{ult}$ . The initial horizontal stress and shear modulus values were kept constant. It is evident from figure 4.10 that a small change in the value of the ultimate shear strength can influence the shape of the loading curve. Although the influence is not dramatic, a noticeable change is evident in the



value of the maximum pressure.

Figure 4.11 presents the variation in the analytical loading curves for a  $\pm 10\%$  change in  $G_i$ . The initial horizontal stress and the undrained shear strength were kept constant. Figure 4.11 shows that a small change in the value of shear modulus has little influence on the final analytical loading curve.

Figure 4.12 presents the variation in the analytical loading curves for a  $\pm 10\%$  change in  $\sigma_{h_0}$ . The shear modulus and undrained shear strength were kept constant. Figure 4.12 shows that a small change in the value of the horizontal stress results in a large change in the analytical loading curve. The initial horizontal stress is, therefore, an important parameter used by this method. Hence, it should be possible to evaluate in-situ stress with an acceptable degree of accuracy using curve fitting techniques.

#### 4.5.2 Secant shear modulus versus shear strain

The hyperbolic model used in this interpretation method as the stress-strain relationship allows calculation of the secant shear modulus as a function of the shear strain. The normalized equation can be written as follows:

$$\frac{G_s}{G_0} = \frac{G_i}{G_0} \left( \frac{1}{1 + \frac{G_i \gamma}{\tau_{ult}}} \right) \text{-----(4.13)}$$

where:

- $G_s$  - secant shear modulus ( $G_s = \tau(\epsilon)/\epsilon$ )
- $G_0$  - small strain shear modulus seismically determined

The small strain shear modulus ( $G_0$ ) is determined by seismic techniques. The parameters  $G_i$  and  $\tau_{ult}$  are determined by the proposed interpretation method. Hence, using this equation and varying the shear strain ( $\gamma$ ) from  $10^{-4}\%$  to the maximum value reached during the test, the complete curve describing the variation of the secant shear modulus with the shear strain can be obtained. Using a similar procedure with a pre-defined value for  $G_0$  a new value for  $\tau_{ult}$  can be determined from the proposed method. Hence, another

equation can be derived to correlate the normalized secant shear modulus to the shear strain:

$$\frac{G_s}{G_0} = \frac{1}{1 + \frac{G_0 \gamma}{\tau_{ult}}} \text{-----(4.14)}$$

Figure 4.13 (a) shows the functions defined by equations (4.13) and (4.14) for the V2P14 SBPT in the Fucino clay. The maximum shear modulus ( $G_0$ ) for this depth (26m) is 31,500 kPa (AGI, 1991).

Vucetic and Dobry (1991) have studied the influence of the soil plasticity on cyclic response. Figure 4.13 (b) shows the proposed curves describing the change of the secant shear modulus with shear strain for a variation of the plasticity index (PI) from 0% to 200%. It also shows a combined curve which could represent the change of the secant shear modulus with shear strain for the V2P14 test (PI=70%). This curve was obtained by linking the top portion of the  $G_s/G_0$  (from  $G_0$ ) curve (equation 4.14) and the bottom portion of the  $G_s/G_0$  (from  $G_1$ ) curve (equation 4.13) which are presented in figure 4.13 (a).

Some conclusions can be drawn from this theoretical exercise:

- (a) The analysis of the two curves presented in figure 4.13 (a) shows that two stress-strain relationships are necessary to describe the soil response from very small strains (10<sup>-4</sup>%) to the maximum strain during the test. This is consistent with the analysis of the derived shear modulus for the Fucino clay using the proposed methodology. The derived shear modulus from the SBPT was approximately one third of the maximum shear modulus and correspond to a strain level around 0.1%;
- (b) The combined curve representing the variation of the secant shear modulus for the entire range of shear strain agrees well with the range proposed by Vucetic and Dobry (1991) for PI between 0% and 200%. Besides that, this combined curve presented in figure 4.13 (b) extends the soil response up to 20% of shear strain. The plastic index of the Fucino clay at the depth of 26m (the V2P14 test) is around 70%.

## 4.6 Comparison of the proposed methodology to the Jefferies (1988) method

### 4.6.1 Interpretation of the AF85 P06-15 test using Jefferies' approach

A methodology for interpreting the self-boring pressuremeter test was presented by Jefferies (1988). This method was based on elastic-perfectly plastic soil model. Analytical equations for pressuremeter loading and unloading curves were derived and used to visually match experimental data from the SBPT. The interpretation yields: (a) shear modulus; (b) undrained shear strength; and (c) initial in-situ horizontal stress. Jefferies (1988) analyzed a self-boring test, named AF85 P06-15, which was carried out in the Canadian Beaufort Shelf, at a site known as Amauligak F-24. The tested soil was a stiff clay, and the depth of the test was 48m below the mudline, a total of 80m below the mean sea level. Applied to this test, Jefferies' approach gave the following results for  $\beta = 0.83$  (where  $\beta$  is the ratio of undrained strength of clay in extension to that in contraction after principal stress reversal as defined by Jefferies, 1988):

- (a) Equivalent elastic shear modulus ( $G$ ): 18,000.0 kPa
- (b) Undrained shear strength ( $S_u$ ): 160.0 kPa
- (c) Initial in-situ horizontal stress ( $\sigma_{h_0}$ ): 1690.0 kPa

Additional information shows that the unload-reload shear modulus is about 45,000.0 kPa and the expected initial horizontal stress should be  $1670 \pm 30$  kPa (Jefferies, 1988). A laboratory anisotropically consolidated undrained stress-controlled triaxial test performed on a similar clay obtained from the same region a ratio between extension and compression undrained shear strength of 0.83. It is interesting to compare the proposed methodology to the Jefferies' approach for this self-boring pressuremeter test AF85 P06-15.

### 4.6.2 Interpretation of the AF85 P06-15 using the proposed methodology

The interpretation template for the test AF85 P06-15 is presented in figure 4.14. Figure 4.15 shows the curve fitting of the unloading portion of the test with the very last points which deviate from the expected contraction curve being discarded. The matching is very good, and the parameters derived

using the proposed method are:  $G_i = 65,500.0$  kPa, and  $\tau_{ult}^* = 262.8$  kPa. Figures 4.16 (a) and (b) show the curve fitting of the entire pressuremeter loading curve for  $R_\tau$  equals 2.0 and 1.83. As could be expected, the analytical curve does not match the experimental curve closely when all loading points are considered in the curve fitting technique. The most probable reason for this response is the disturbance caused by the pressuremeter installation. Assuming that some unknown amount of disturbance has influenced the early portion of the SBPT loading curve, the curve fitting technique is performed based on the data at cavity strains greater than 5%. Figures 4.17 (a) and (b) show the curve matching for  $R_\tau$  equals 2.0 and 1.83.

The final interpreted parameters using the proposed methodology can be summarized as follows:

- (a) Shear modulus ( $G_i$ ): 65,727.0 kPa
- (b) Undrained shear strength ( $S_u|_{mob}$ ): 143.9 kPa
- (c) Initial in-situ horizontal stress ( $\sigma_{ho}$ ): 1690.1 kPa

The final plot including the loading and unloading portions of the AF85 SBPT is presented in figure 4.18 (a). Comparison between the interpreted stress-strain curves are shown in figure 4.18 (b).

The final interpreted parameters determined by both methodologies are presented in the following table:

Methodology	$G$ kPa	$S_u$ kPa	$\sigma_{ho}$ kPa	Remarks
Jefferies (1988)	18,000	160	1690.0	$\beta = 0.83$
Proposed Method	65,727	143.9	1690.1	$R_\tau = 1.83$

#### 4.6.3 Interpretation of the Fucino-V2P14 test using Jefferies' approach

The method proposed by Jefferies (1988) was used to interpret the Fucino-V2P14 test. The objective of this study was to provide a basis for comparison the results of both methodologies when applied to SBPT performed in soft normally consolidated clay. The software developed by Jefferies (1988) was not available, his approach, called GAM (Computer-Aided Modeling), was

used in a spreadsheet calculation. The elastic-perfectly model used by Jefferies (1988) to derive the following pressuremeter analytical equations:

• Loading phase

(1) Elastic response

$$p = \sigma_{ho} + 2G\varepsilon \text{ -----(4.15)}$$

valid for  $0 \leq \varepsilon \leq S_u/2G$ .

(2) Plastic response

$$p = \sigma_{ho} + S_u \left[ 1 + \ln \left( \frac{G}{S_u} \cdot \left( 1 - \frac{1}{(1 + \varepsilon)^2} \right) \right) \right] \text{ -----(4.16)}$$

valid for  $S_u/2G \leq \varepsilon \leq \varepsilon_{max}$

• Unloading phase

(1) Elastic response

$$p = p_{max} + 2G \left( \frac{\varepsilon - \varepsilon_{max}}{1 + \varepsilon_{max}} \right) \text{ -----(4.17)}$$

valid for  $\varepsilon_{max} \geq \varepsilon \geq \left( \varepsilon_{max} - \frac{S_u}{G} \cdot (1 + \varepsilon_{max}) \right)$ .

(2) Plastic response

$$p = p_{max} - 2S_u \left[ 1 + \ln \left( \frac{G}{2S_u} \left( \frac{1 + \varepsilon_{max}}{1 + \varepsilon} - \frac{1 - \varepsilon}{1 + \varepsilon_{max}} \right) \right) \right] \text{ -----(4.18)}$$

valid for  $\left( \varepsilon_{max} - \frac{S_u}{G} \cdot (1 + \varepsilon_{max}) \right) \geq \varepsilon \geq 0$ .

The soil parameters derived from the best curve matching are:

- (a) Initial horizontal stress ( $\sigma_{ho}$ )
- (b) Equivalent elastic shear modulus ( $G$ )
- (c) Undrained shear strength mobilized during loading and unloading ( $S_u$ )

In addition to these parameters another test dependent parameter is also considered - the maximum cavity strain reached during the SBPT ( $\varepsilon_{max}$ ).

Based on this four-parameter model the following routine was executed:

- (1) Guess the first set of parameters ( $\sigma_{ho}$ ,  $G$ ,  $S_u$ , and  $\epsilon_{max}$ );
- (2) Calculate the strain intervals for elastic and plastic responses for both loading and unloading;
- (3) Generate the analytical curves using equations (4.15) to (4.18);
- (4) Plot the analytical and experimental curves for both loading and unloading simultaneously in a single plot;
- (5) Two options are available:
  - (5.1) The interpretation is finished if the curve matching is considered acceptable; or
  - (5.2) Guess another set of parameters and re-start at step (2) if the curve matching is considered poor.

Using this procedure the Fucino-V2P14 test was interpreted to yield after 12 trials the parameters listed in the following table:

<b>Trial</b>	<b><math>G</math> kPa</b>	<b><math>S_u</math> kPa</b>	<b><math>\sigma_{ho}</math> kPa</b>	<b><math>\epsilon_{max}</math> dec</b>	<b><math>P_{max}</math> kPa</b>	<b><math>\epsilon_{EL}</math> %</b>	<b><math>\epsilon_{EU}</math> %</b>	<b>Remarks</b>
12	6,000	100	450	0.109	791.7	0.8	9.0	Good

The final curve matching is presented in figure 4.19 (a). Figure 4.19 (b) presents the constitutive laws used in both methodologies to interpret the Fucino-V2P14 test. For the interpreted test the equivalent linear elastic shear modulus is equal to the secant hyperbolic mode at a cavity strain of about 0.43%.

The final interpreted parameters determined by both methodologies are presented in the following table:

<b>Methodology</b>	<b><math>G</math> kPa</b>	<b><math>S_u</math> kPa</b>	<b><math>\sigma_{ho}</math> kPa</b>	<b>Remarks</b>
<b>Jefferies (1988)</b>	6,000	100	450	$\beta = 1.0$
<b>Proposed Method</b>	11,188	116	442	$R_t = 2.0$

#### 4.6.4 Comments on the results

- A comparison between the results of both methodologies for test AF85 P06-15, shows the consistency of the set of parameters derived. The undrained shear strength and the initial horizontal stress are very close, but a discrepancy exists in the value of the shear modulus. The derived stress-strain curves using both methodologies are presented in figure 4.18 (b). The interpreted initial shear modulus ( $G_i$ ) is greater than the measured unload-reloading shear modulus, and is almost four times the equivalent linear elastic shear modulus derived by Jefferies (1988). The value of the small strain shear modulus  $G_s$  (seismically determined) is not reported by Jefferies (1988). For the analyzed test, the equivalent linear elastic modulus is equal to the secant hyperbolic model at a cavity strain of about 0.3%.
- The interpretation of the Fucino-V2P14 test followed the same trend as the AF85 P06-15 test. The undrained shear strength and the initial horizontal stress results are very close. However, the shear modulus are quite different as could be expected because the type of model used. The unload-reload shear modulus for this test is 13,900 kPa and the small strain shear modulus determined by seismic tests is 31,500 kPa.
- Summarizing, the interpreted result shows the adequacy of the hyperbolic model in representing the non-linear response of the tested soil either for stiff or soft clays. On the other hand, the elastic-perfectly plastic model can be considered quite poor in reproducing the deformation response of the clay.

#### 4.7 Conclusions

A method to interpret undrained pressuremeter results in clay has been presented. The method incorporates the unloading portion of the pressuremeter test to derive the initial shear modulus and undrained shear strength. The soil response is represented by a hyperbolic relationship between the shear stress and circumferential strain. The method accepts that some level of disturbance may exist for the SBPT results and, hence, only the later part of the loading curve should be used to derive the in situ stress.

Pre-bored and full-displacement undrained pressuremeter test results can also be analyzed by the proposed method providing the loading portion of the test has taken sufficient volume of undisturbed soil to failure. This may require a large expansion in some soils. The current method is based on small strains and will, therefore, not apply to large pressuremeter expansions.

To apply the proposed interpretation methodology a value for the ratio of the undrained shear strength in unloading and loading ( $R_{\tau}$ ) must be known. A value of 2.0 is recommended. To improve the interpretation of in-situ stress and undrained shear strength the ratio of undrained shear strength in unloading and loading ( $R_{\tau}$ ) should be measured on undisturbed samples, following stress paths similar to those in the pressuremeter test.

The proposed interpretation method involves comparison of the measured loading and unloading pressuremeter curves with analytically derived curves. This comparison can be achieved using commercially available microcomputer application software. For this study, the software used was Kaleidagraph™ (version 2.1) developed for the Macintosh™ microcomputer. Hence, it should be possible for practicing engineers to apply this proposed method to undrained SBPT results without the need of special customized software.

The proposed interpretation method has been evaluated using 20 high quality self-boring pressuremeter results performed in the Fucino clay in Italy. The interpreted soil parameters had reasonable values when compared to other in situ and laboratory test results.

The proposed interpretation method presents an acceptable framework to derive soil parameters from undrained pressuremeter tests in fine grained soils. This framework includes the complete loading and unloading portions of the test, and it incorporates non linearity of the soil response in a simple closed-form manner.



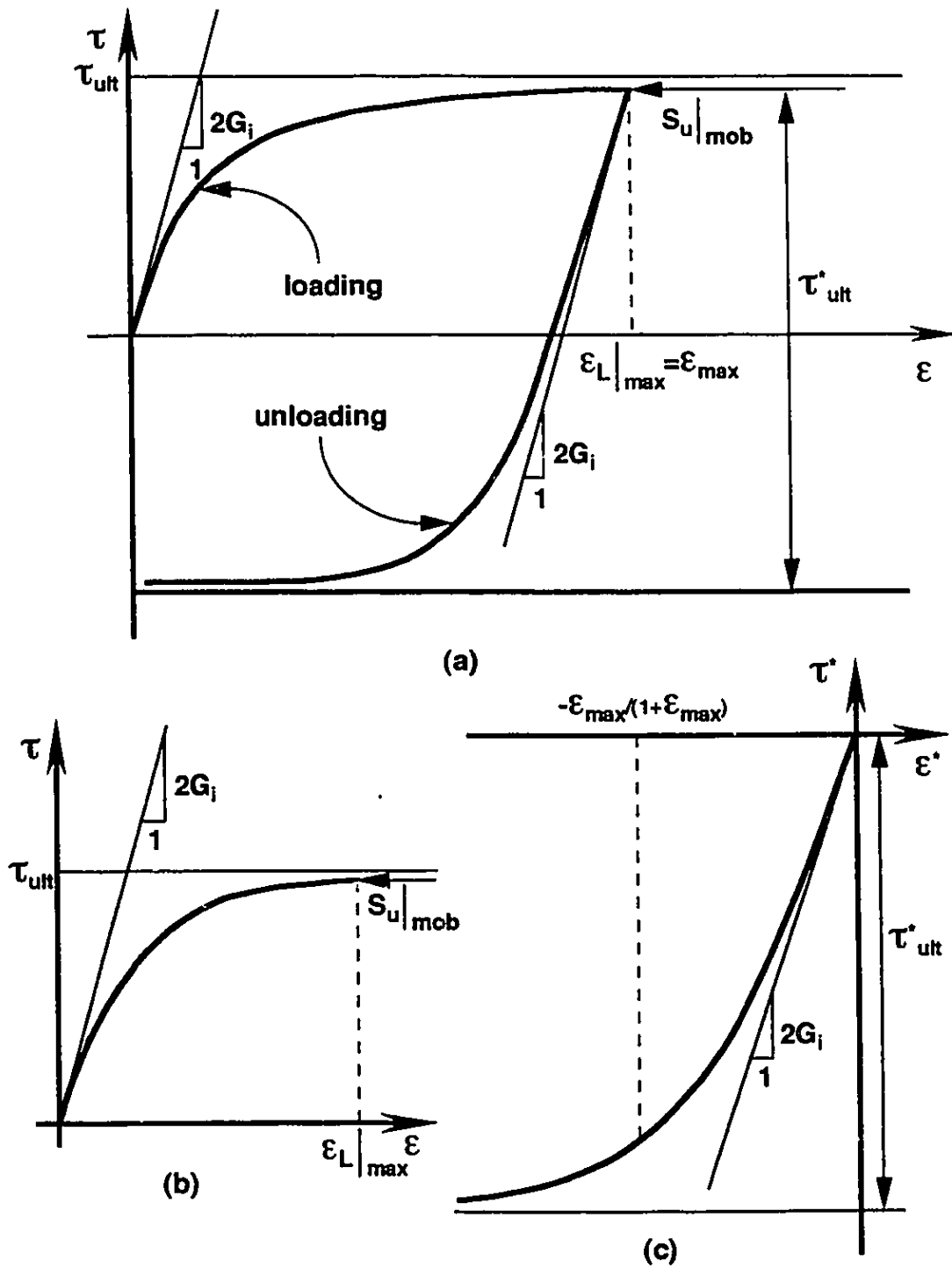
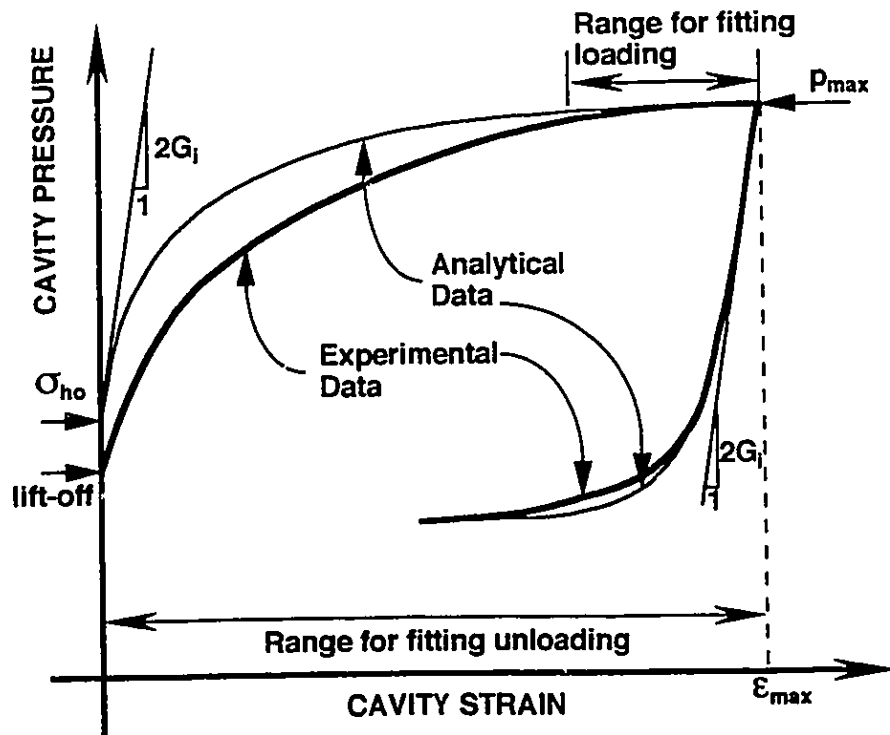


FIGURE 4.1 Proposed hyperbolic model for loading and unloading stages of a pressuremeter test: (a) Loading and unloading together; (b) Loading part; (c) Unloading part.



**FIGURE 4.2** Interpretation methodology for a self-boring pressuremeter test (SBPT).

## PRESSUREMETER INTERPRETATION TEMPLATE - CLAYS

TEST ID \_\_\_\_\_

DEPTH [m] \_\_\_\_\_ LIFT-OFF [kPa] \_\_\_\_\_

Loading :  $p_{max}$  [kPa] \_\_\_\_\_  $\epsilon_{max}$  [dec] \_\_\_\_\_

Unloading :  $p_{max}$  [kPa] \_\_\_\_\_  $\epsilon_{max}$  [dec] \_\_\_\_\_

**STEP # 1 - UNLOADING (Best fit with two parameters)**

(a) All unloading points

$\tau_{ult}^* =$  \_\_\_\_\_ Graph Page \_\_\_\_\_

$2G_i =$  \_\_\_\_\_

(b) (some data points removed) e.g. Discard the last unloading points

$\tau_{ult}^* =$  \_\_\_\_\_ Graph Page \_\_\_\_\_

$2G_i =$  \_\_\_\_\_

**STEP # 2 - LOADING (Best fit with one parameter  $R_c=2.0$ )**

(a) All loading points

$\sigma_{ho} =$  \_\_\_\_\_ Graph Page \_\_\_\_\_

(b) Strain range (first option) Last half

$\sigma_{ho} =$  \_\_\_\_\_ Graph Page \_\_\_\_\_

(c) Strain range (second option) Last quarter

$\sigma_{ho} =$  \_\_\_\_\_ Graph Page \_\_\_\_\_

(d) Strain range (third option) Interpolate points at the very last end

$\sigma_{ho} =$  \_\_\_\_\_ Graph Page \_\_\_\_\_

**STEP # 3 - SUMMARY**

(a) First strain range selected: e.g. Step #2 option (d)

$\tau_{ult}^* =$  \_\_\_\_\_  $\tau_{ult} =$  \_\_\_\_\_ Graph Page \_\_\_\_\_

$2G_i =$  \_\_\_\_\_  $\sigma_{ho} =$  \_\_\_\_\_

(b) Second strain range selected

$\tau_{ult}^* =$  \_\_\_\_\_  $\tau_{ult} =$  \_\_\_\_\_ Graph Page \_\_\_\_\_

$2G_i =$  \_\_\_\_\_  $\sigma_{ho} =$  \_\_\_\_\_

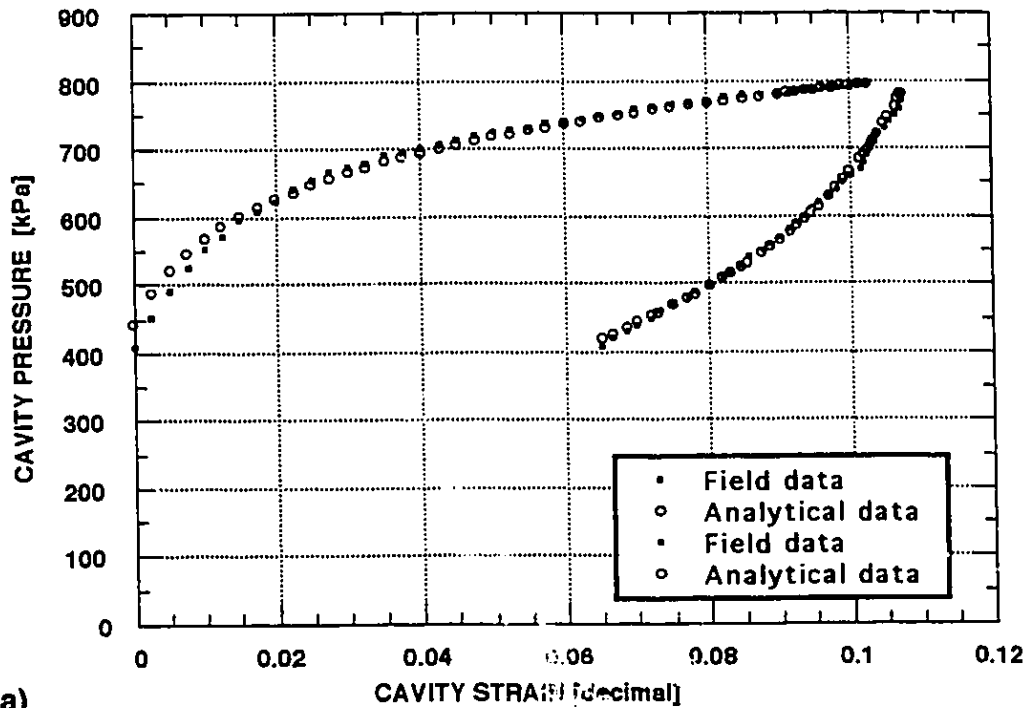
**FIGURE 4.3** Proposed template for interpreting SBPT data in clays.

## PRESSUREMETER INTERPRETATION TEMPLATE - CLAYS

TEST ID	Fucino clay - Test V2P14		
DEPTH [m]	26.0	LIFT-OFF [kPa]	409.93
Loading :	p <sub>max</sub> [kPa] 792.93	ε <sub>max</sub> [dec]	0.1025
Unloading :	p <sub>max</sub> [kPa] 779.93	ε <sub>max</sub> [dec]	0.1074
<b>STEP # 1 - UNLOADING (Best fit with two parameters)</b>			
<b>(a) All unloading points</b>			
	τ <sub>ult</sub> <sup>*</sup> = 233.0	Graph Page	Figures 4.5 (a) and (b)
	2G <sub>i</sub> = 22,377.0		
<b>(b) (some data points removed)</b>			
	τ <sub>ult</sub> <sup>*</sup> =	Graph Page	_____
	2G <sub>i</sub> =		
<b>STEP # 2 - LOADING (Best fit with one parameter R<sub>c</sub>=2.0)</b>			
<b>(a) All loading points</b>			
	σ <sub>ho</sub> = 441.9	Graph Page	Figure 4.5 (b)
<b>(b) Strain range (first option) Last half</b>			
	σ <sub>ho</sub> = 444.4	Graph Page	not shown
<b>(c) Strain range (second option) Last quarter</b>			
	σ <sub>ho</sub> = 443.0	Graph Page	not shown
<b>(d) Strain range (third option) Interpolate points at the very last end</b>			
	σ <sub>ho</sub> = 441.7	Graph Page	Figure 4.5 (a)
<b>STEP # 3 - SUMMARY</b>			
<b>(a) First strain range selected: Step #2 option (d)</b>			
	τ <sub>ult</sub> <sup>*</sup> = 233.0	τ <sub>ult</sub> = 116.5	Graph Page <span style="border-bottom: 1px solid black;">Figure 4.5 (a)</span>
	2G <sub>i</sub> = 22,377.0	σ <sub>ho</sub> = 441.7	
<b>(b) Second strain range selected</b>			
	τ <sub>ult</sub> <sup>*</sup> =	τ <sub>ult</sub> =	Graph Page <span style="border-bottom: 1px solid black;">_____</span>
	2G <sub>i</sub> =	σ <sub>ho</sub> =	

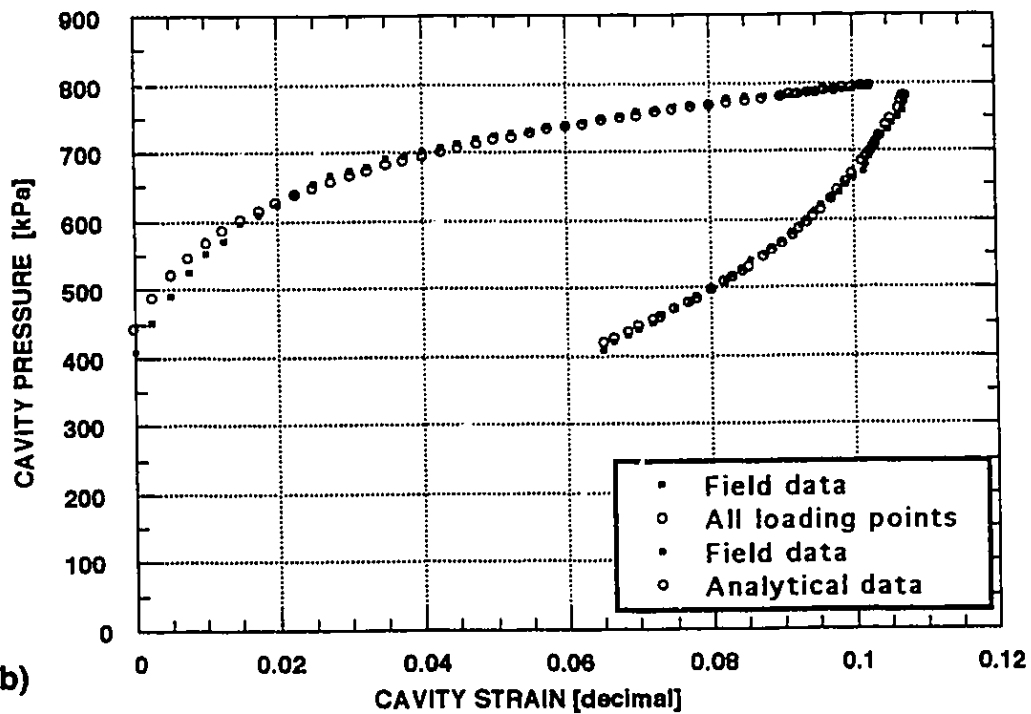
**FIGURE 4.4** Fucino clay test V2P14: Interpretation template.

## FUCINO CLAY - TEST V2P14 - FINAL PLOT



(a)

## FUCINO CLAY - TEST V2P14 - FITTING ALL LOADING POINTS



(b)

**FIGURE 4.5** Fucino clay test V2P14. (a) Suggested fit to last section of loading curve (final plot); (b) curve fitting for all loading points.

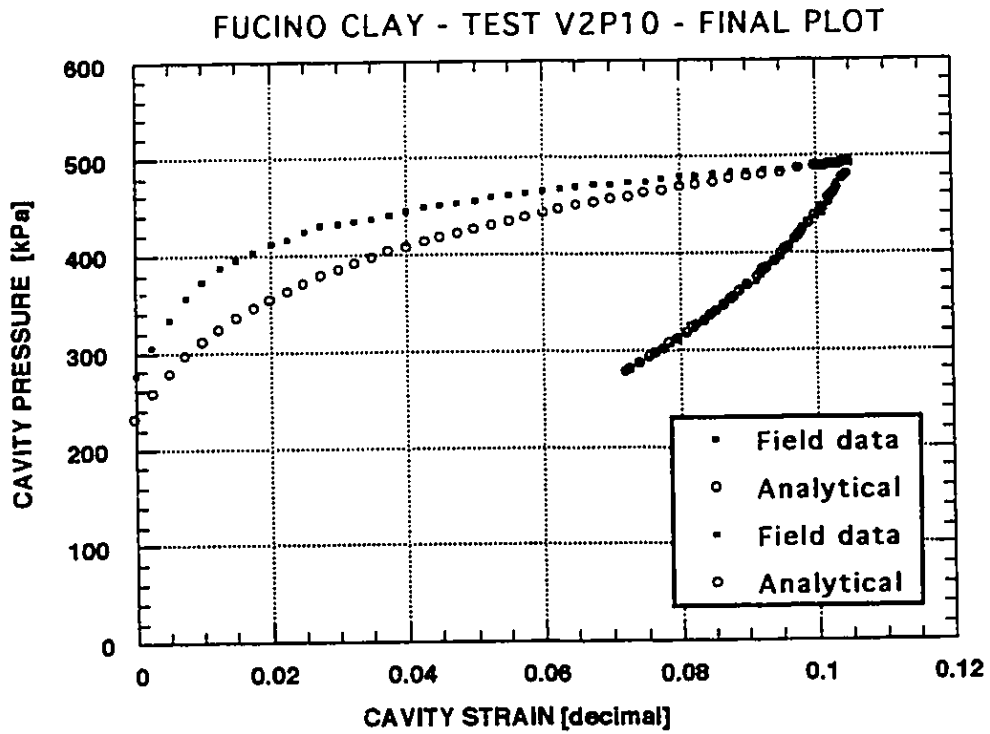


**FIGURE 4.6** Fucino clay test V2P10. Suggested fit to last section of the loading curve (final plot).

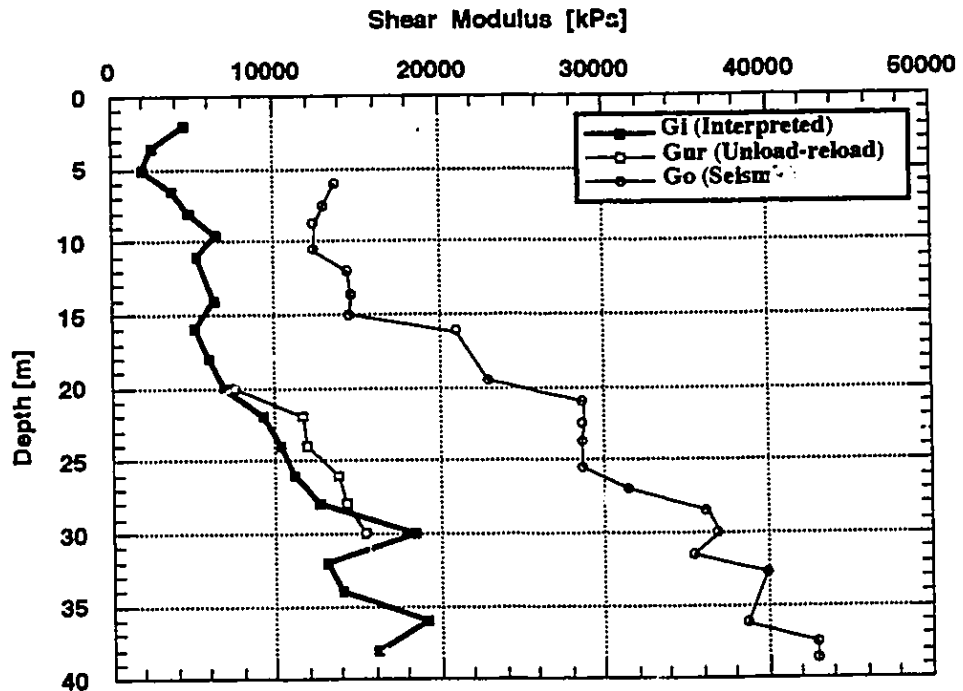


**FIGURE 4.7** Fucino clay borehole V2. Shear modulus versus depth.

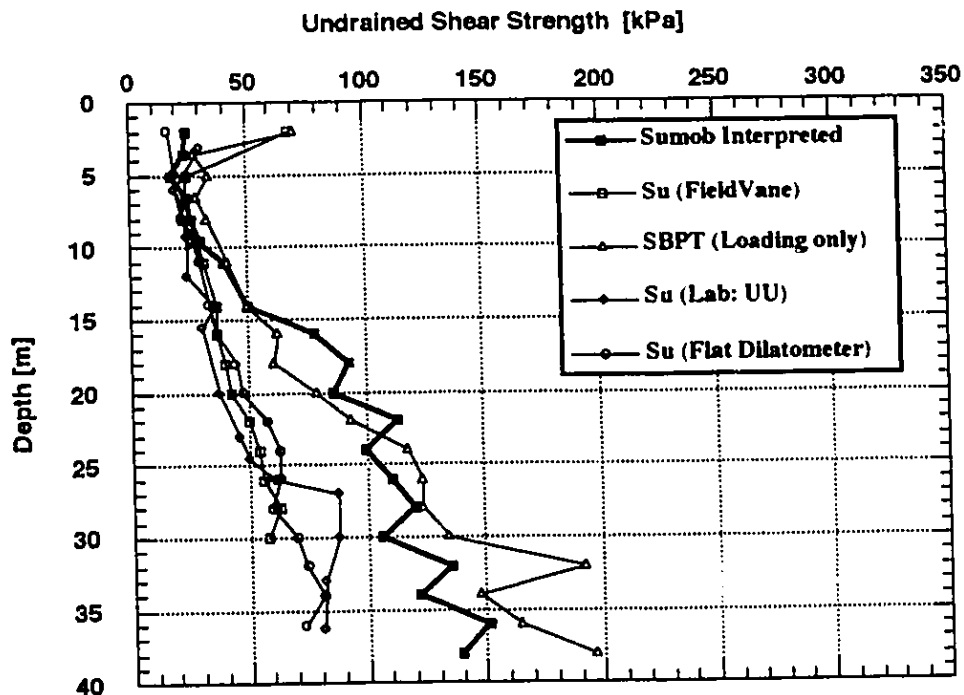


FIGURE 4.8 Fucino clay borehole V2. Undrained shear strength versus depth.

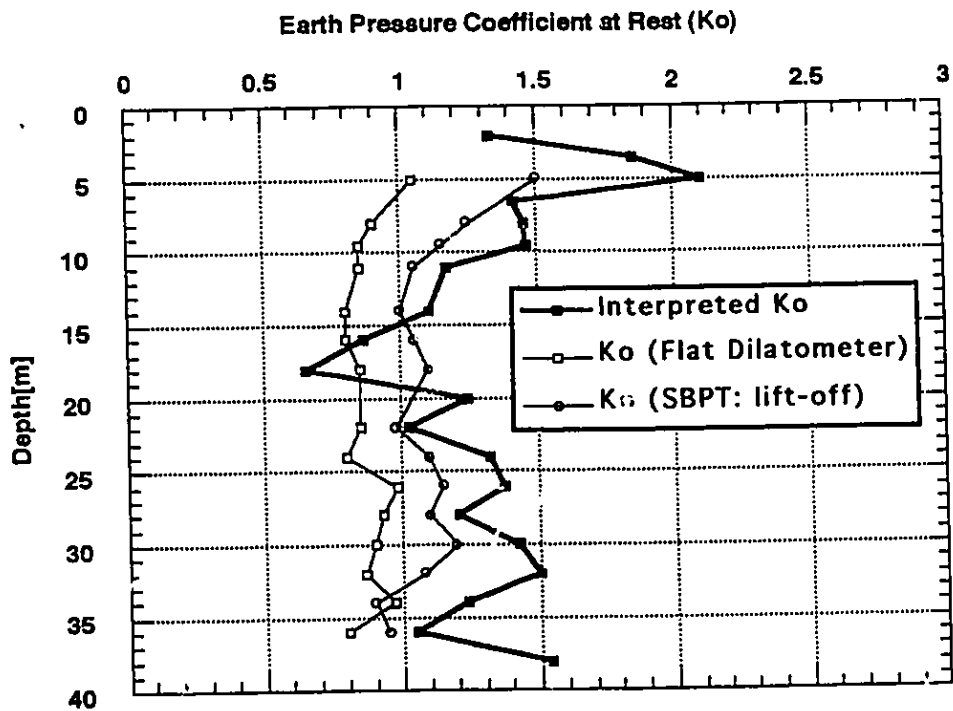
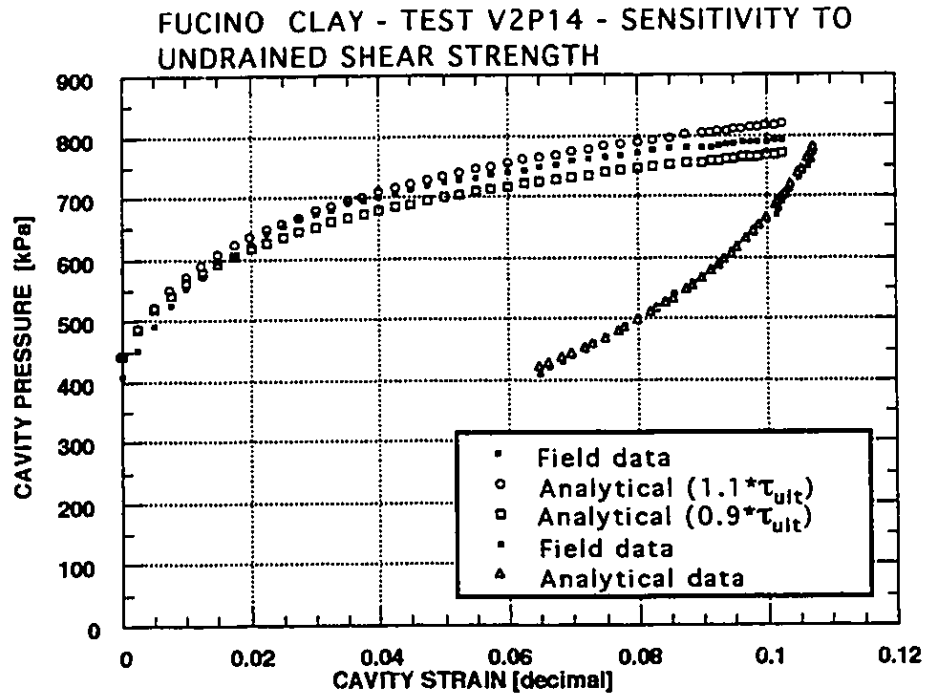
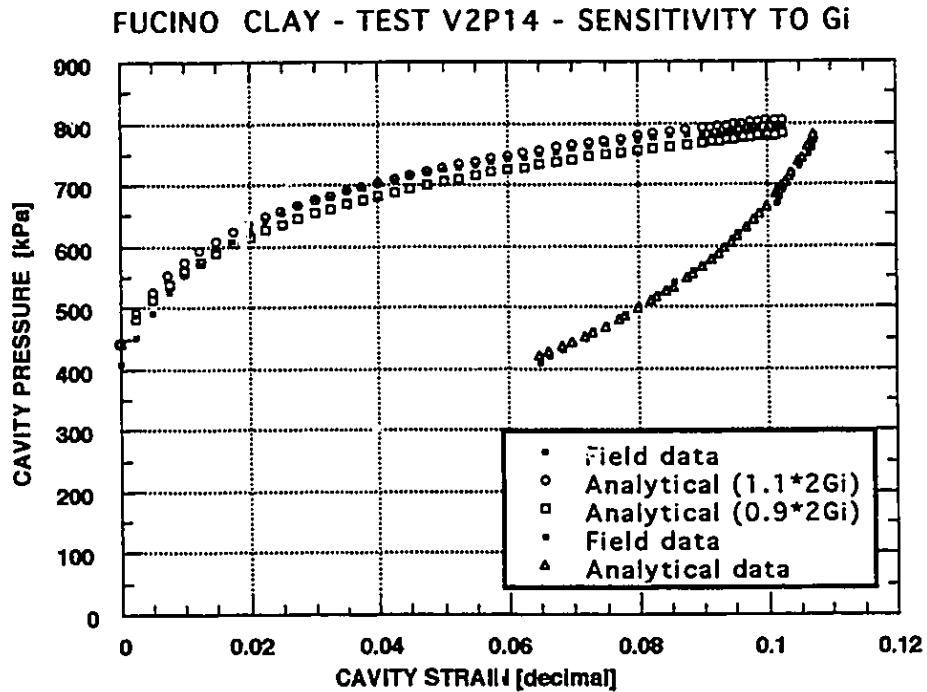


FIGURE 4.9 Fucino clay borehole V2. Earth pressure coefficient at rest versus depth.



**FIGURE 4.10** Fucino clay test V2P14. Sensitivity analysis - Undrained shear strength.



**FIGURE 4.11** Fucino clay test V2P14. Sensitivity analysis - Elastic shear modulus.



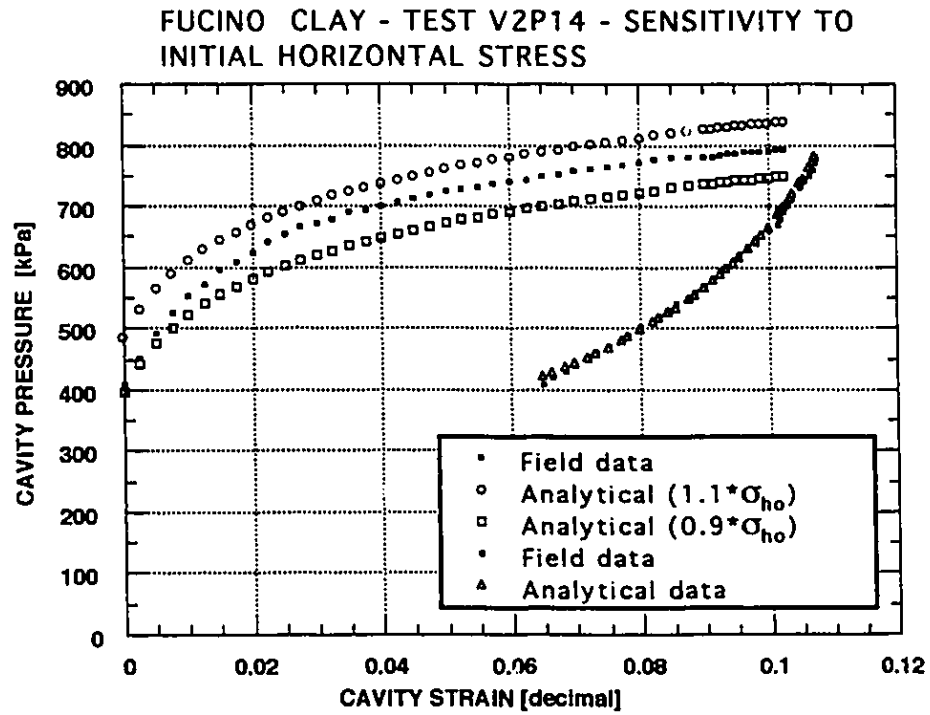


**FIGURE 4.12** Fucino clay test V2P14.Sensitivity analysis - Initial horizontal stress

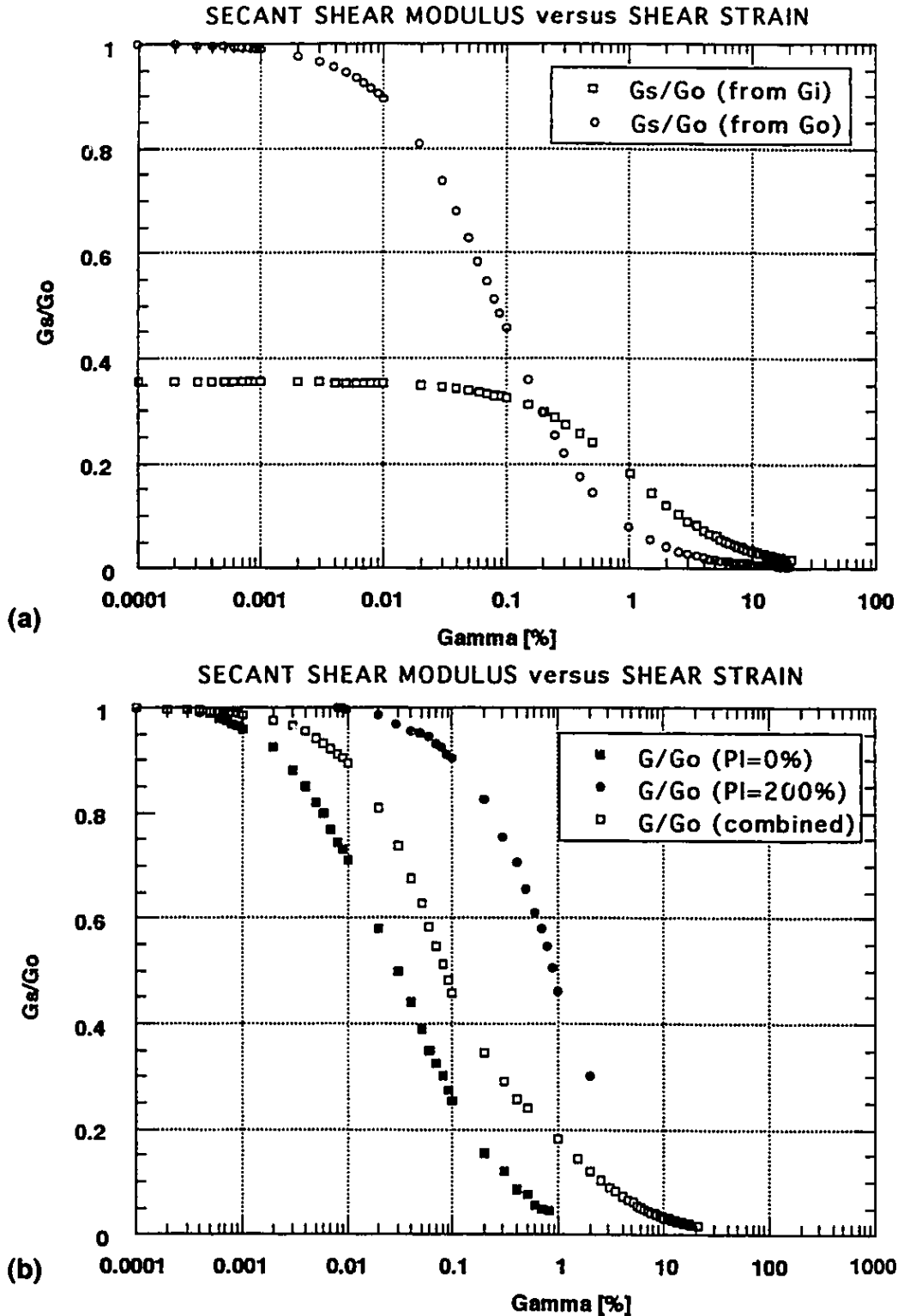


**FIGURE 4.13** Fucino clay test V2P14. (a) Secant shear modulus versus shear strain (two curves); (b) Secant shear modulus versus shear strain (combined curve).

## PRESSUREMETER INTERPRETATION TEMPLATE - CLAYS

<b>TEST ID</b>	<u>Test AF85 P06-15 (stiff clay) Jefferies (1988)</u>		
<b>DEPTH [m]</b>	<u>80 (below sea level)</u>	<b>LIFT-OFF [kPa]</b>	<u>1500</u>
<b>Loading :</b>	$p_{\max}$ [kPa] <u>2,297.0</u>	$\epsilon_{\max}$ [dec]	<u>0.0775</u>
<b>Unloading :</b>	$p_{\max}$ [kPa] <u>2,297.0</u>	$\epsilon_{\max}$ [dec]	<u>0.0775</u>
<b>STEP # 1 - UNLOADING (Best fit with two parameters)</b>			
<b>(a) All unloading points</b>			
$\tau_{ult}^*$ =		Graph Page	
$2G_i$ =			
<b>(b) (some data points removed) At the very last end</b>			
$\tau_{ult}^* = 262.8$		Graph Page	<u>Figure 4.15</u>
$2G_i = 131,454.0$			
<b>STEP # 2 - LOADING</b>			
<b>(a) All loading points (<math>R_{\tau}=2.0</math>)</b>			
$\sigma_{ho} = 1690.6$		Graph Page	<u>Figure 4.16 (a)</u>
<b>(b) All loading points (<math>R_{\tau}=1.83</math>)</b>			
$\sigma_{ho} = 1660.8$		Graph Page	<u>Figure 4.16 (b)</u>
<b>(c) Cavity strain greater than 5% (<math>R_{\tau}=2.0</math>)</b>			
$\sigma_{ho} = 1728.9$		Graph Page	<u>Figure 4.17 (a)</u>
<b>(d) Cavity strain greater than 5% (<math>R_{\tau}=1.83</math>)</b>			
$\sigma_{ho} = 1690.1$		Graph Page	<u>Figure 4.17 (b)</u>
<b>STEP # 3 - SUMMARY</b>			
<b>(a) First strain range selected: Step #2 option (d)</b>			
$\tau_{ult}^* = 262.8$	$\tau_{ult} = 146.0$ ( $R_{\tau}=1.83$ )		
$2G_i = 131,454.0$	$\sigma_{ho} = 1690.1$	Graph Page	<u>Figure 4.19 (a)</u>
<b>(b) Second strain range selected</b>			
$\tau_{ult}^* =$	$\tau_{ult} =$	Graph Page	
$2G_i =$	$\sigma_{ho} =$		

**FIGURE 4.14 Test AF85 P06-15. Interpretation template .**

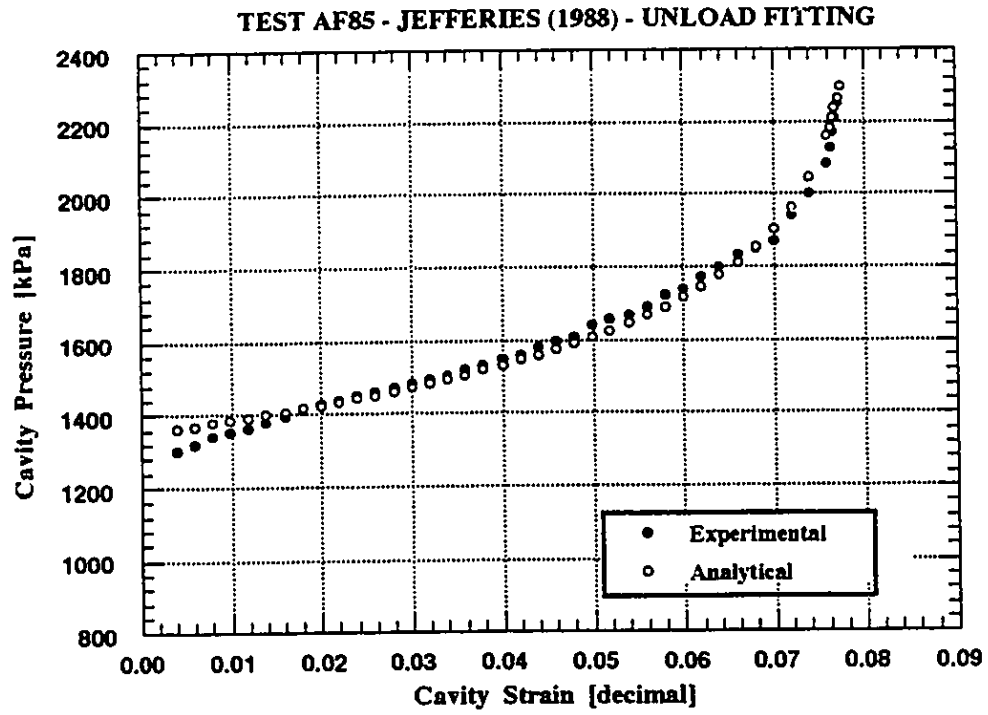
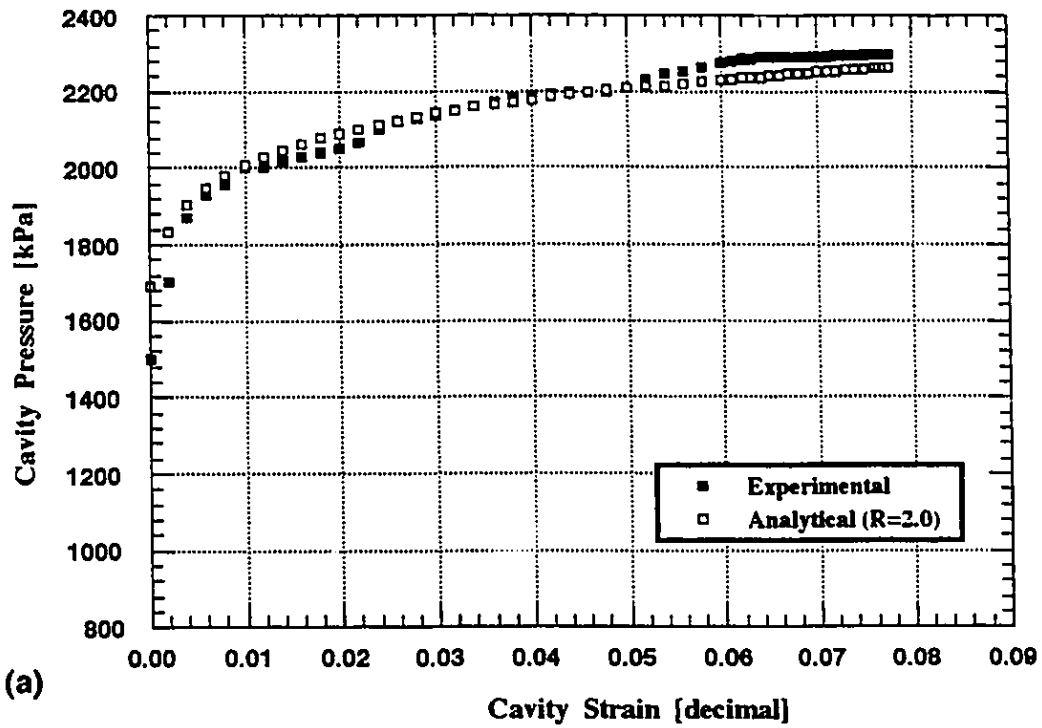


**FIGURE 4.15** Test AF85 P06-15. Curve fitting of unload stage of the SBPT.

## TEST AF85 JEFFERIES (1988) - ALL LOADING POINTS



## TLST AF85 JEFFERIES (1988) - ALL LOADING POINTS

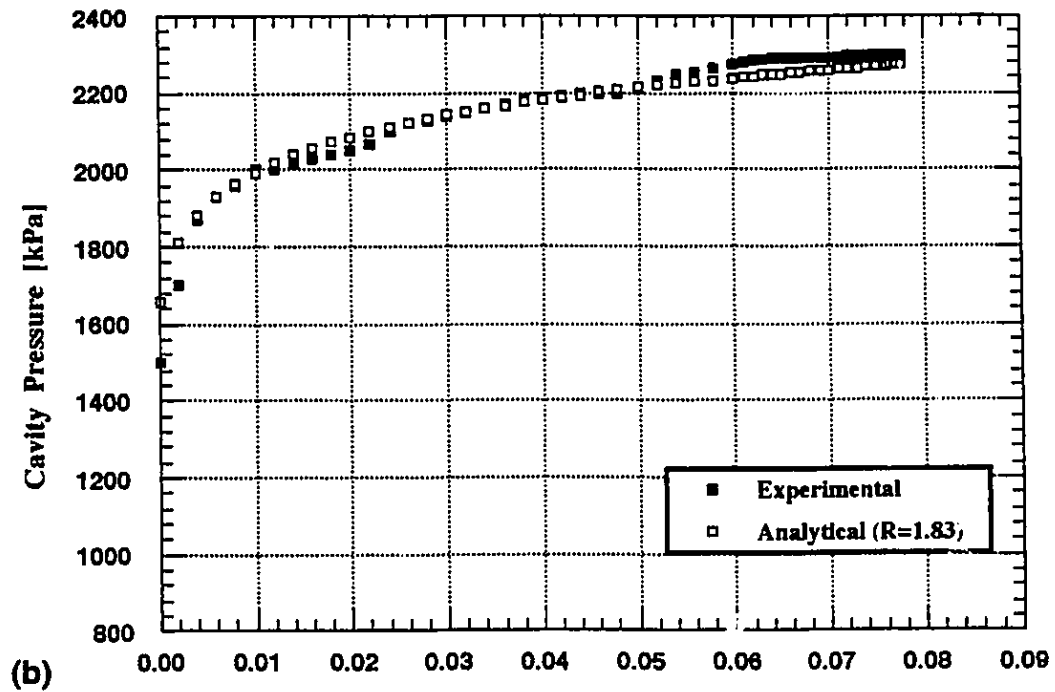
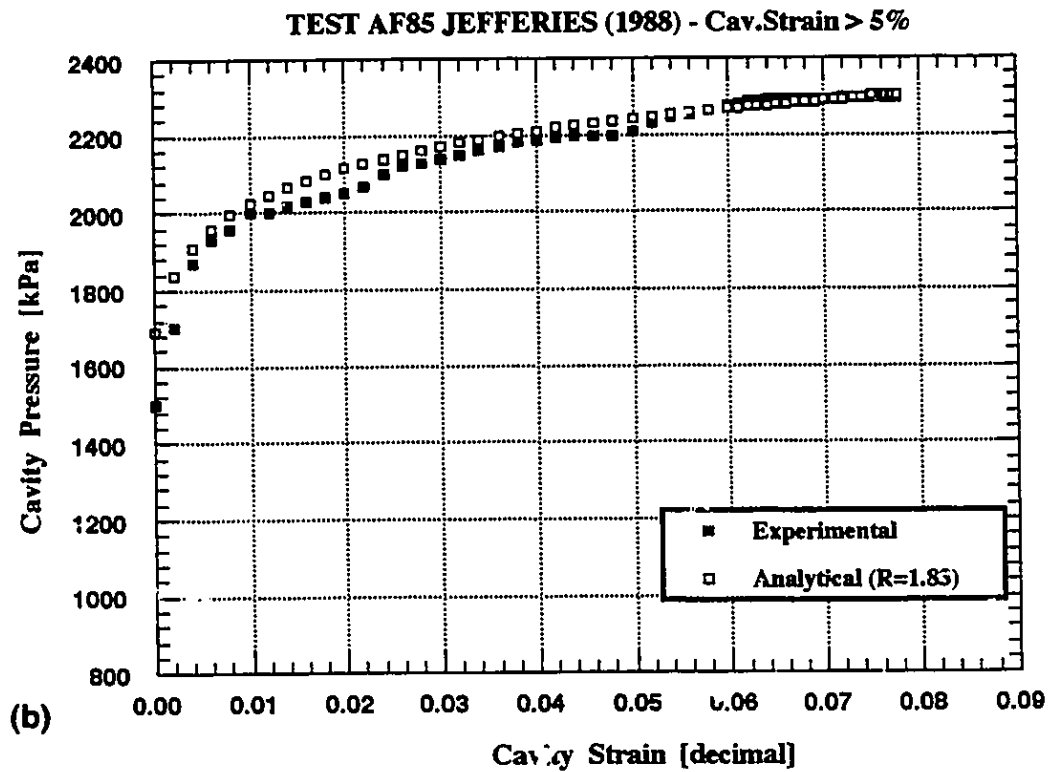
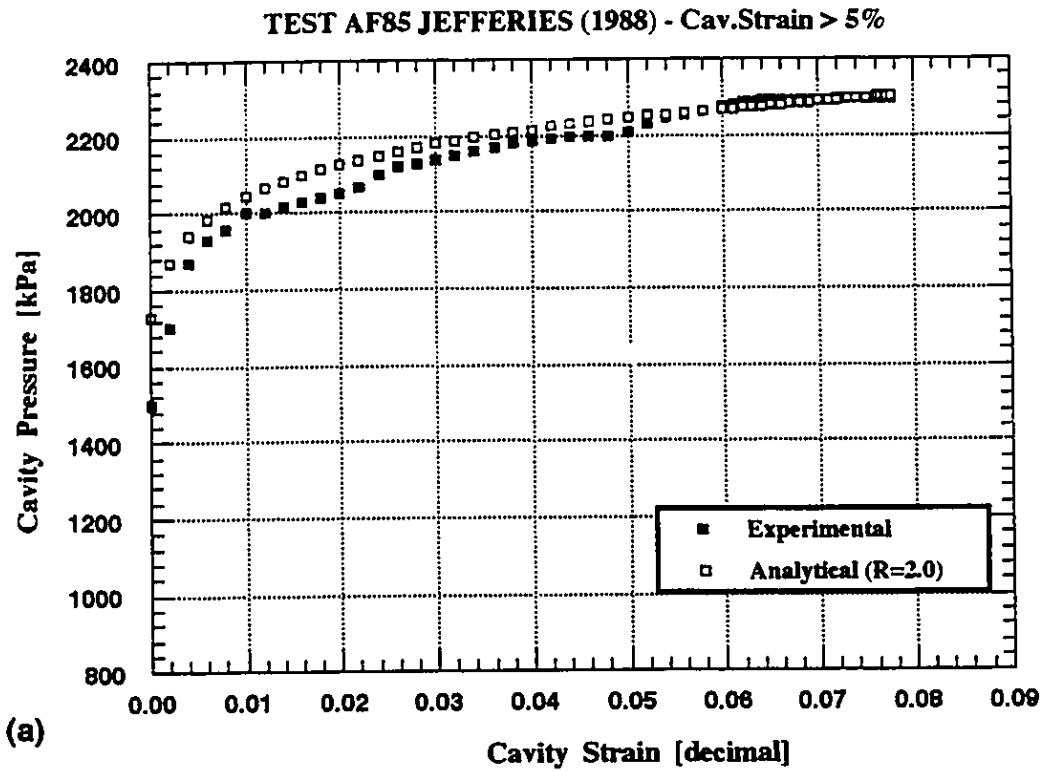
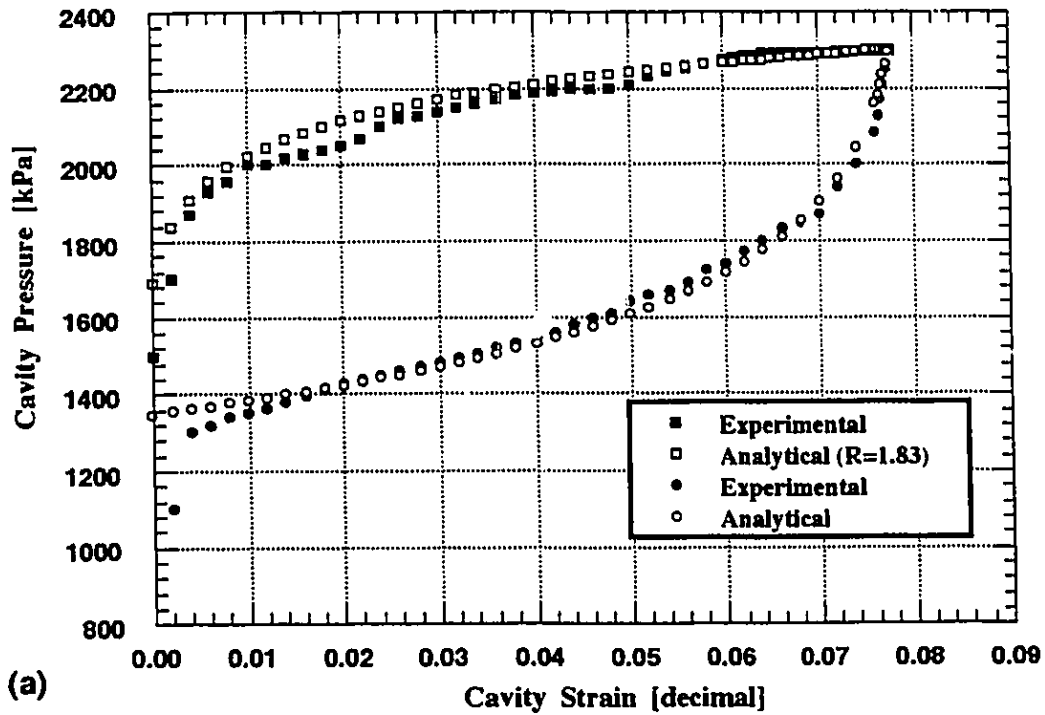


FIGURE 4.16 Test AF85 P06-15. Curve fitting of the entire loading stage of the test: (a) for  $R_t=2.0$ ; (b) for  $R_t=1.83$ .



**FIGURE 4.17** Test AF85 P06-15. Curve fitting of the loading stage for strains greater than 5%: (a) for  $R_c=2.0$ ; (b) for  $R_c=1.83$ .

## TEST AF85 - JEFFERIES (1988) - FINAL PLOT



## Test AF85 Jefferies (1988) - Constitutive Laws

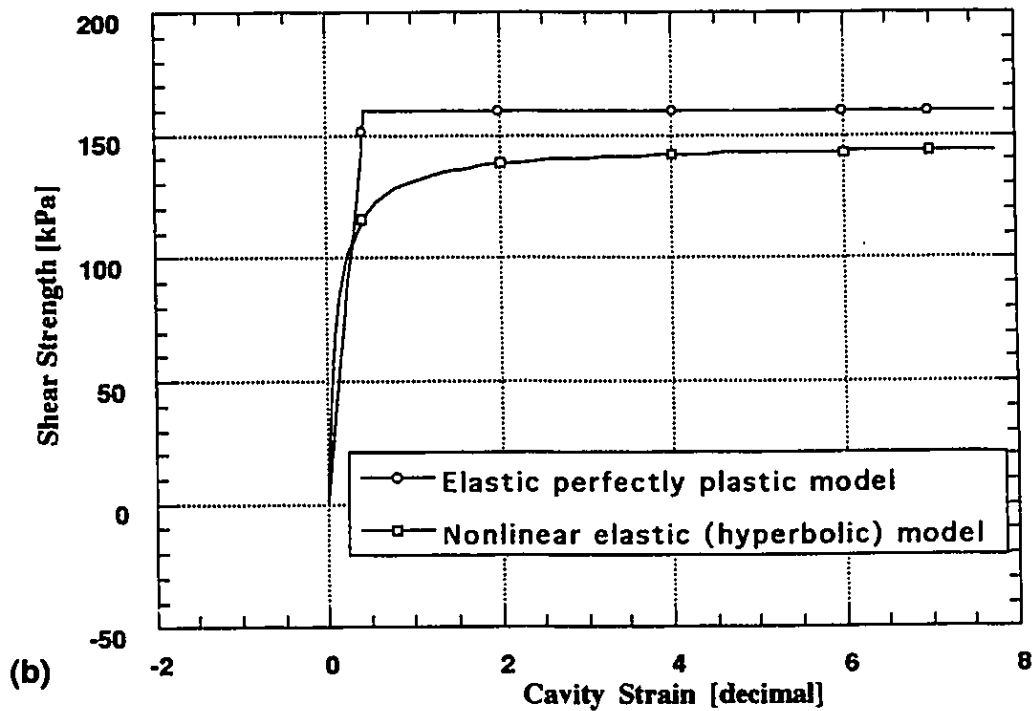
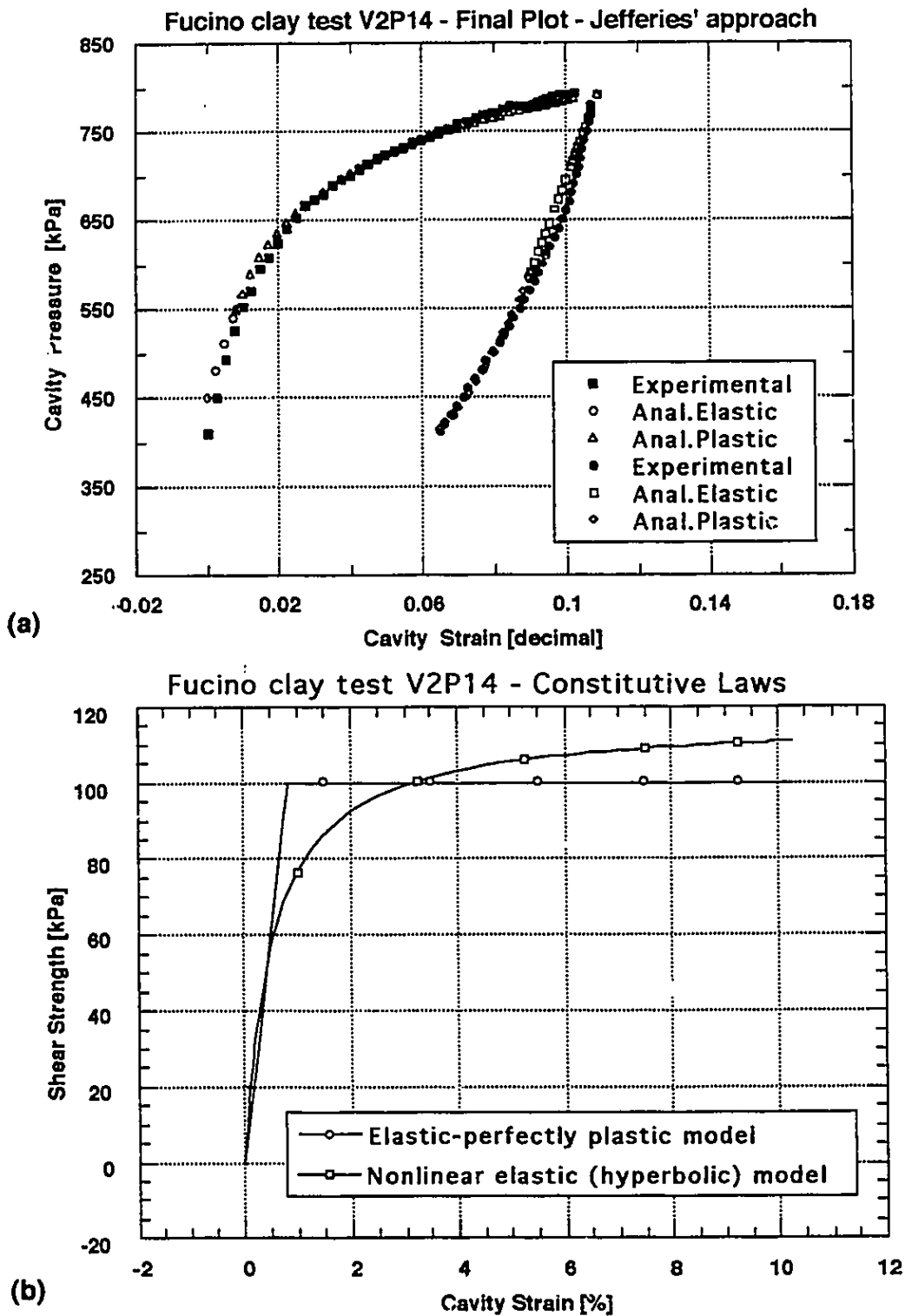


FIGURE 4.18 Test AF85 P06-15. (a) Final plot; (b) Constitutive laws used in Jefferies (1988) and in the proposed method.



**Figure 4.19** Fucino clay - Test V2P14. (a) Loading and unloading curve matching; (b) Constitutive laws used in Jefferies (1988) and in the proposed method.



## CHAPTER 5

### EXTENSION OF THE PROPOSED METHODOLOGY TO OTHER TYPES OF UNDRAINED PRESSUREMETER TESTS

#### 5.1 Introduction

As presented in chapter 4, small strain definition was used to derive the pressuremeter analytical equations to simulate both pressuremeter expansion and contraction curves. The commonly used version of the self-boring pressuremeter is limited to soil deformations that rarely exceed 15%, measured as cavity strain (change in pressuremeter radius divided by its initial radius). It is generally accepted that the self-boring technique can be used to install the pressuremeter and cause a very small disturbance to the surrounding soil. Consequently, it is believed that the early part of the expansion curve is the true response of the natural undisturbed soil. However, it has been recognized that this is seldom the case (Ghionna et al, 1983). The proposed interpretation method, presented in chapter 4, does not rely on the early part of the loading phase because the amount of soil perturbation caused by pressuremeter installation is difficult to evaluate. As pointed out, if no disturbance has occurred during the insertion, a good match should exist between the analytical and the entire experimental loading curves, even if just the last portion of the experimental loading curve is used to fit the analytical pressuremeter equation. A good match is expected if the actual soil response is similar to the assumed hyperbolic stress-strain relationship.

If the disturbance due to installation is small a cavity expansion of 15% may be adequate to capture the natural soil response. However if the degree of disturbance is high a larger cavity expansion is required. A PBPT requires a pre-drilled hole for device installation. The pre-drilling procedure always causes some soil unloading, even though water or another stabilizing fluid may be used to prevent any collapse of the borehole wall. An annulus of perturbed soil is formed and larger deformations during the subsequent pressuremeter test are required until the natural soil response can be recorded. The s-shape loading curve is typical for a PBPT. The opposite

occurs with a FDPT, also called the cone-pressuremeter test. During installation of the FDP the soil is displaced from its original position and a large annulus of disturbed soil can be formed. The size of the disturbed zone will be a function of the soil characteristics. In this case a large pressuremeter cavity expansion during the test may be necessary to measure the natural soil response. The updated versions of the FDP are able to expand to around 50% of their original initial radius. For a PIPT the annulus of the disturbed soil is expected to be smaller than the one for a FDPT mainly due to its sampler like body (hollow cylinder). Compared to a SBPT, a PIPT still requires a larger deformation to measure the undisturbed soil response.

In summary, when dealing with a PBPT, a FDPT or a PIPT large strain definitions must be used to interpret their results. It is important to point out that the most common way to present pressuremeter experimental curves is in a graph with cavity strain in the x-axis (small strain definition). The cavity strains are calculated directly from the membrane displacements measured by the equipment. Transformation of small strains to large strains is necessary in this case. The only exceptions are the devices where the definition of strain is based on the change in volume of the cell (hydraulically inflated). In this case the volumetric cavity strain (change in the cell volume divided by initial volume) is already a definition of large strains, provided the cavity expands as a right cylinder.

## **5.2 Large strain definitions**

A definition of strain must always be referred to a frame of reference, also called space. There are two frames of reference: (a) Lagrangian space, and (b) Eulerian space. The Lagrangian space is based on the undeformed configuration, which is always known in advance. The Eulerian space is based on the current (deformed) configuration, which is unknown in advance. For small strains, however, both references give equivalent results since the location of a material point in the deformed space can be considered coincident with its initial position. However, for large strains this approximation is not possible, and the change in position of a material point must be taken into account.

### 5.2.1 Logarithmic strains (Lagrangian space)

Houlsby and Withers (1988) have used the logarithmic definition of strains to account for the large magnitude of strains developed during a FDPT. For the axially symmetric problem the logarithmic strains can be defined using cylindrical coordinates, as follows:

$$L_{\theta} = -L = -\ln\left(\frac{r}{r_0}\right) \text{-----(5.1)}$$

where:  $L_{\theta}$  - circumferential logarithmic strain  
 $L$  - pressuremeter logarithmic strain  
 $r$  - current radial coordinate of a material point  
 $r_0$  - initial radial coordinate of a material point

### 5.2.2 Green strains (Lagrangian space)

Baguelin et al (1978) have used the Green's definition of strain to solve the problem of large strains that can be developed in any pressuremeter test. For the axially symmetric problem the Green strains can be defined using cylindrical coordinates, as follows:

$$g_{\theta} = -g = -\frac{1}{2} \cdot \frac{r^2 - r_0^2}{r_0^2} \text{-----(5.2)}$$

where:  $g_{\theta}$  - circumferential Green strains  
 $g$  - pressuremeter Green strains

### 5.2.3 Comparison between small and large strain definitions

Cauchy strains were used in the derivations shown in chapter 4. The Cauchy's definition involves just the first derivatives of the displacement vector with respect to the cartesian coordinates. Therefore, Cauchy strains can only form a tensor if they are small, i.e. if the second order or higher order terms can be neglected. For the axially symmetric problem in the Lagrangian space, Cauchy strains can be defined using cylindrical coordinates, as follows:

$$\varepsilon_{\theta} = -\varepsilon = -\frac{r - r_o}{r_o} \text{-----(5.3)}$$

where:  $\varepsilon_{\theta}$  - circumferential Cauchy strains  
 $\varepsilon$  - pressuremeter Cauchy strains (cavity strains)

In the case of large strains, higher order terms can not be neglected so Cauchy strains do not form a tensor, which means that they do not plot as circles in Mohr diagrams (Baguelin et al, 1978).

The relationship correlating the three definitions of strains presented in the equations (5.1), (5.2) and (5.3) is the following:

$$(1 + \varepsilon)^2 = e^{2L} = 1 + 2g \text{-----(5.4)}$$

where:  $e$  - basis of the natural logarithms

Figure 5.1 shows the variation of the three strain definitions with the commonly used cavity strain. A quick analysis of this figure shows that the numeric values of the pressuremeter Green strains are bigger than the corresponding values of the pressuremeter cavity strains, while the opposite occurs with the pressuremeter logarithmic strains. Also, for cavity strains of up to 15% the difference between each definition is small.

### 5.3 Pressuremeter analytical equation for large strains

Following a similar procedure used in the derivation of the pressuremeter analytical equation for small strains, the equations that describe the variation of pressure with strain can be derived for large strains. The Green's definition of strains will be used in this study to define the large strains developed during any pressuremeter test. The reason for this choice is the basic equation presented by Baguelin et al (1978) which constitutes the starting point of the entire mathematical derivation developed in this chapter.

#### 5.3.1 Assumptions

The derivation considers the following assumptions:

- (1) The pressuremeter test is performed undrained from the start of the expansion to the complete contraction;

- (2) The test is treated as an expansion of an infinitely long cylindrical cavity (i.e. radially symmetric and plane strain);
- (3) The vertical stress remains the intermediate principal stress during the test;
- (4) The soil stress-strain behaviour can be represented by a hyperbolic function in both loading and unloading;
- (5) The ratio of the unloading strength of the clay to the loading strength is known.

These assumptions are essentially the same as those made by Jefferies (1988) and Gibson and Anderson (1961), except for the hyperbolic representation of the stress-strain behaviour and the absence of any restriction about the strain magnitude.

### 5.3.2 Hyperbolic model

The description of the soil stress-strain behaviour is made by the same hyperbolic equations used for small strain analysis. The cavity strain ( $\varepsilon$ ) is replaced by the Green pressuremeter strain ( $g$ ).

### 5.3.3 Derivation of the pressuremeter analytical equations

#### • Sign convention and strain definitions

The sign convention used defines compressive strains as positive.

The Green's definition of strain is used in the derivation.

For pressuremeter expansion (loading stage) the strains at the cavity wall are defined as follows:

$$g = \frac{1}{2} \cdot \frac{R^2 - R_o^2}{R_o^2} = \frac{1}{2} \cdot \frac{V - V_o}{V_o} = \frac{1}{2} \cdot ((1 + \varepsilon)^2 - 1) \text{-----(5.5)}$$

where:  $g$  - pressuremeter Green strains in loading

$$\varepsilon = \frac{R - R_o}{R_o} \text{ - cavity strains}$$

$R$  - current pressuremeter radius

$R_o$  - initial pressuremeter radius

$V$  - current volume of the pressuremeter chamber

$V_o$  - initial volume of the pressuremeter chamber

For pressuremeter contraction (unloading phase) the strains at the cavity wall are defined as follows:

$$g^* = \frac{1}{2} \cdot \frac{R^2 - R_{\max}^2}{R_{\max}^2} \text{-----(5.6)}$$

where:  $g^*$  - pressuremeter Green strains in unloading  
 $R_{\max}$  - maximum radius of the pressuremeter

The derived relationship between  $g^*$  and  $g$  is:

$$g^* = \frac{g - g_{\max}}{1 + 2g_{\max}} \text{-----(5.7)}$$

where:  $g_{\max}$  - maximum pressuremeter Green strain at the start of the unloading phase

• Governing equations

(1) Baguelin et al (1978)

$$\frac{d\sigma_r}{dg} = \frac{\tau(g)}{g(1 + 2g)} \text{-----(5.8)}$$

where:  $\sigma_r$  - radial stress

$$\tau(g) = \frac{\sigma_r - \sigma_\theta}{2} \text{ - shear stress}$$

For the sake of simplicity, Cauchy stresses are used in the derivation of the analytical pressuremeter equations for large strains.

(2) Constitutive relationship (hyperbolic model)

(a) Loading:

$$\tau = \frac{g}{\frac{1}{2G_i} + \frac{g}{\tau_{ult}}} \text{-----(5.9)}$$

where:  $\tau$  - mobilized shear stress

$G_i$  - shear modulus

$\tau_{ult}$  - ultimate shear strength (asymptote)

The complete stress-strain soil response during the pressuremeter loading phase is defined by equation (5.9) with just two parameters:  $G_i$  and  $\tau_{ult}$ . The

parameter  $G_i$  represents the initial tangent shear modulus of the hyperbolic model. The level of strain that  $G_i$  is applicable is dependent on the strain range within which the hyperbolic function adequately fits the stress-strain response of the soil. One approximation would suggest that  $G_i$  is applicable from a shear strain level of approximately 0.1% as suggested in chapter 4.

(b) Unloading:

$$\tau^* = \frac{g^*}{\frac{1}{2G_i} - \frac{g^*}{\tau_{ult}^*}} \text{-----(5.10)}$$

where:  $\tau^*$  - mobilized shear stress

$\tau_{ult}^*$  - ultimate shear strength (asymptote)

The hyperbolic model is usually applied in terms of shear stress ( $\tau$ ) and shear strain ( $\gamma$ ). However, for undrained cylindrical cavity expansion the following relationship holds:

$$\gamma = 2g \text{-----(5.11)}$$

Hence, the term  $2G_i$  in equations (5.9) and (5.10) stems from the use of pressuremeter Green strain ( $g$ ) instead of the more conventional engineering shear strain ( $\gamma$ ).

• Boundary conditions at the cavity wall

(a) Loading:

$$g = 0 \Rightarrow \sigma_r = \sigma_{ho} \text{-----(5.12)}$$

(b) Unloading:

$$g^* = 0 \Rightarrow \sigma_r = \sigma_{r_{\max}} \text{-----(5.13)}$$

where:  $\sigma_{r_{\max}}$  - maximum radial stress at the beginning of the unloading phase

$\sigma_{ho}$  - initial horizontal stress

• Pressuremeter analytical equations

(a) Loading:

$$p = \sigma_{ho} + \frac{G_i \cdot \tau_{ult}^*}{R_\tau G_i - \tau_{ult}^*} \cdot \ln \left( \frac{1}{1 + 2g} + \frac{2G_i \cdot R_\tau \cdot g}{\tau_{ult}^* \cdot (1 + 2g)} \right) \text{-----(5.14)}$$

where:  $p$  - pressure at the cavity wall

$$R_\tau = \frac{\tau_{ult}^*}{\tau_{ult}} \text{ - ratio of the ultimate undrained shear strength in}$$

unloading and loading

This equation is valid within the range  $0 \leq g \leq g_{L_{max}}$  where  $g_{L_{max}}$  is the pressuremeter Green strain at the end of the loading phase.

(b) Unloading:

$$p = p_{max} + \frac{G_i \cdot \tau_{ult}^*}{G_i + \tau_{ult}^*} \cdot \ln \left| \frac{\tau_{ult}^* \cdot \left( 1 + 2 \cdot \left( \frac{g - g_{max}}{1 + 2g_{max}} \right) \right)}{\tau_{ult}^* - 2G_i \cdot \left( \frac{g - g_{max}}{1 + 2g_{max}} \right)} \right| \text{-----(5.15)}$$

where:  $p_{max}$  - pressure at the cavity wall at the beginning of the unloading phase

## 5.4 Capabilities of the pressuremeter large strain analytical equations

Equations (4.11) and (4.12), derived in chapter 4, are the pressuremeter small strain analytical equations, and the equations (5.14) and (5.15) are the derived pressuremeter analytical equations for a large strain definition. It is interesting to see how they compare for different soils (stiff and soft clays) and for different levels of maximum strain.

### 5.4.1 Comparison to the pressuremeter small strain analytical equations

The maximum cavity strain for a typical SBP is commonly smaller than 15%. For a FDPT, however, the maximum cavity strain has been extended up to 50%. These two levels of maximum strains will be used to analyze the large strain pressuremeter equations for two different rigidity indices. The AF85 P06-15 test performed in the Beaufort Sea and presented by Jefferies (1988) will be used as an example of stiff clays. The parameters for the stiff clay used in this exercise are presented in figure 4.14 (step #3 - Summary). The



V2P14 test presented by Fioravante (1988) will be used as an example for soft to medium clays. The soil parameters of this test are presented in figure 4.4 (step #3 - Summary). The data is summarized in the following table:

<b>Parameters</b>	<b><math>G_i</math> kPa</b>	<b><math>\tau_{ult}^*</math> kPa</b>	<b><math>R_\tau</math></b>	<b><math>\sigma_{ho}</math> kPa</b>
<b>AF85 P06</b>	65,727	262.8	1.83	1,690.1
<b>V2P14</b>	11,188	233.0	2.0	441.7

Figures 5.2 (a) and (b) present the theoretical pressuremeter curves for loading and unloading for the soft Fucino clay. As would be expected, there is a very small difference in the equations' results for the first 15% of cavity strain for both loading and unloading. The equation (5.4) was used to convert Green strains to cavity strains (Cauchy strains). The results show that for soft clay either the equations derived using the small strain theory or the equations derived using the large strain theory are suitable for interpretation of pressuremeter tests where the maximum strain does not exceed 15%. At this level of strain the difference between the calculated loading pressures is smaller than 2.5% of the pressure calculated using the small strain equation for this soft soil. On the other hand, for cavity strains greater than 15% the theoretical curves are too far from each other. The greater the cavity strain, the higher is the distance between both curves.

Figures 5.3 (a) and (b) present the theoretical pressuremeter curves for loading and unloading for the stiff Beaufort Sea clay. The results follow the same trend as for the soft soil. But, in this case the distance between the loading curves for 15% of cavity strain is even smaller (1.2%).

The conclusion that can be drawn from these results is that the interpretation of large cavity expansions (>15%) in clays must be done using the equations for large strains. Large strain equations were used by Houlsby and Withers (1988) for interpretation of FDPT results, but using the logarithmic definition rather than the Green's definition of large strains.

#### 5.4.2 Large strain analytical curves for different maximum cavity strains

Equation (5.15) can be used to generate theoretical pressuremeter unloading curves for different levels of maximum cavity strains. This simple exercise shows the capability of the large strain equation to fit pressuremeter unloading curves irrespective of the level of maximum strain reached during the test. Figure 5.4 shows theoretical unloading curves for an idealized soil for several levels of maximum cavity strain.

#### 5.4.3 Interpretation of the Fucino V2P14 SBPT using large strain equations

The V2P14 test in Fucino clay was interpreted in chapter 4 using small strain equations. The same test is now interpreted using large strain equations. The interpretation template is presented in figure 5.5. Figures 5.6 (a) and (b) show the final plot and the curve fitting for all loading points. A comparison between figures 5.5 and 4.4 (step #3 - Summary) shows very similar results and confirms that the large strain pressuremeter analytical equations are also adequate to interpret small strain pressuremeter tests, as suggested in 5.4.1.

<b>Parameters</b>	$G_f$ <b>kPa</b>	$\tau_{ult}^*$ <b>kPa</b>	$R_\tau$	$\sigma_{ho}$ <b>kPa</b>
<b>Small strain</b>	11,188	233.0	2.0	441.7
<b>Large strain</b>	11,314	222.3	2.0	464.1

### 5.5 Typical undrained pressuremeter test results

There are basically four types of pressuremeter devices: (a) SBP; (b) PBP; (c) FDP; and (d) PIP. The expected disturbance during the procedure of device installation into the ground is different for each type. Depending on the operator ability the SBP can cause the least soil disturbance of all the types. The PIP can also cause small soil disturbance during the insertion into soft soil. But when soil stiffness increases the amount of disturbance increases rapidly. On the other hand, the PBP and the FDP cause large soil disturbance during the installation procedure. While the pre-drilling operation unloads the

soil, the full-displacement operation overstresses the soil around the pressuremeter. Generally speaking, there is a relationship between the amount of disturbance during insertion and the required value of the maximum pressuremeter cavity strain to ensure a measured response that is controlled primarily by the undisturbed soil. The greater the disturbance the bigger the value of the maximum strain necessary to ensure that the measured response is dominated by the natural undisturbed material. Only in this case can the maximum pressure reached during the test be assumed to be close to the limit pressure response of the undisturbed soil. The issue of how close the pressures should be will be addressed later in this chapter. Figure 5.7 shows a sketch of the idealized response of undrained pressuremeter tests. It can be seen that all types of pressuremeter tests will ultimately reach approximately the same maximum pressure during the loading phase of the test which is close to the undisturbed soil limit pressure (pressure for infinite strain). Hence, the unloading curves will have a similar shape for all the tests, provided the probe has been expanded to a sufficiently large strain. If the pressuremeter test does not reach a maximum pressure which is close to the limit pressure of the undisturbed soil, the interpreted parameters obtained using curve fitting techniques will be meaningless. The limit pressure equation can be derived from the pressuremeter loading analytical equation for large strains:

$$P_l = P(g \rightarrow \infty) = \sigma_{ho} + \frac{G_i \cdot \tau_{ult}^*}{R_c G_i - \tau_{ult}^*} \cdot \ln \left( \frac{G_i \cdot R_c}{\tau_{ult}^*} \right) \text{-----}(5.16)$$

Figure 5.8 shows a comparison between the profile of the maximum pressure reached during the test and the limit pressure calculated using equation (5.16) for the SBPT's in Fucino clay (parameters from Appendix C). On the average, the maximum pressure reached during each test in this soft cemented clay is around 80% of the calculated theoretical limit pressure. Since equation (5.16) is based on a hyperbolic relationship, it requires an infinite strain to reach the limit pressure.

## 5.6 Effect of the soil disturbance and the pressuremeter maximum strain

For all types of pressuremeter test the amount of disturbance during device installation has an important influence on the shape of the measured loading curve. The SBPT performed in soft clays is the least susceptible to disturbance during insertion, compared to the other pressuremeter tests. On the other hand, the FDP generally causes the highest degree of disturbance to the adjacent soil during device installation. In any case, an annulus of disturbed soil (soil already failed) is formed around the pressuremeter. Although the exact size of the disturbed zone is unknown, the diameter of the disturbed annulus is a function of the type of pressuremeter and type of material being tested. The rigidity index, introduced by Vesic (1972), is the material property that has a direct relationship with the amount of disturbance caused by pressuremeter installation. Defined as a ratio between the shear modulus and the undrained shear strength ( $I_r = G/S_u$ ), the value of the rigidity index of most clay soils lies within a limited range from about 100 to 500.

In general, disturbance due to pressuremeter installation will cause the experimental measured curve to follow one of the two possible responses: (a) disturbance with no consolidation, or, (b) disturbance with consolidation. In both cases, during the initial stage of pressuremeter expansion the disturbed material has a dominant effect on the measured response. As pressuremeter expansion continues, the failed annulus starts growing and the path of the measured response will depend whether consolidation has occurred in the disturbed region.

If there was no consolidation during pressuremeter insertion, i.e. the insertion was undrained, the failed annulus will be softer and weaker than the natural soil. The soil sensitivity plays an important role in this case. Theoretically, this case can be understood as a cavity expansion of a two-layered system, one softer close to the pressuremeter and another stiffer around the first layer. The pressuremeter measured curve will follow initially the path defined by the weaker and softer annulus. Afterwards, as the failed annulus grows, the response will be influenced by the natural undisturbed soil. For this case, the analytical curve, which was generated based on undisturbed one-layered

system, will tend to be above the measure experimental curve. Figure 5.9 (a) shows the idealization of such response.

On the other hand, if consolidation has occurred during pressuremeter installation, i.e. some drainage has been allowed, the disturbed annulus will be stiffer and stronger than the natural soil. In this case, the pressuremeter curve will follow initially the path defined by the stronger and stiffer annulus. The two-layered system can be represented by one layer of stronger material close to the pressuremeter and another layer of weaker material around the first layer. Figure 5.9 (b) shows the idealization of such response.

Either for disturbance with or without consolidation the limit pressure, governed by the intact soil, is reached when the failed zone has grown enough such that the initial disturbed annulus is just a fraction of the final failed annulus. Unfortunately, the hyperbolic model used to derive the pressuremeter analytical equations cannot allow the calculation of the failed zone because the nonlinear response modeled reaches the ultimate load only when the cavity strain is infinite.

The effect of disturbance is less critical for SBPT results since it is assumed that a cavity expansion of about 15% is generally sufficient to measure predominantly undisturbed soil response. However, for FDPT and PBPT results the disturbance is larger and hence, the required cavity expansion to measure predominantly undisturbed soil response must be larger. The following sections attempt to address the amount of cavity expansion required for FDPT's and PBPT's.

### 5.6.1 Radius of the plastic annulus

To illustrate the grows of the plastic zone, an elastic-perfectly plastic model will be used here. This type of model has been used by several authors to study the pressuremeter problem (Gibson and Anderson, 1961; Houlsby and Withers, 1988; Jefferies, 1988). The plastic-elastic boundary can be calculated using the following equation (undrained loading):

$$\frac{R_{PE}}{R_0} = \sqrt{\varepsilon I_r (2 + \varepsilon)} \text{-----(5.17)}$$

Where:  $R_{PE}$  - radius of the plastic-elastic transition  
 $I_r = G/S_u$  - rigidity index

Figure 5.10 shows the variation of the normalized plastic-elastic radius with the Green strain for a range of the rigidity index from 100 to 500. Figure 5.10 illustrate that to produce a radius of plastic soil 10 times larger than the initial pressuremeter radius it requires a cavity strain of only 10% for a stiff soil ( $I_r = 500$ ) but up to 50% for a soft soil ( $I_r = 100$ ). Also, it would appear that stiff soils will reach their limit pressure at smaller strains than soft soils with the same shear strength.

### 5.6.2 Limit pressure and initial disturbance

The concept of limit pressure was introduced in section 5.5. Assuming that a unique limit pressure can be reached for different types of pressuremeter tests, the amount of initial disturbance can delay the approaching of this pressure. This reasoning assumes that the pressuremeter test is undrained. A large amount of initial disturbance requires a large cavity strain expansion in order to ensure that the limit pressure reached is the response of the undisturbed material around the pressuremeter prior to the expansion. If the pressuremeter installation produces a disturbance equivalent to a cavity strain of say 1%, the size of the plastic zone produced will be approximately  $1 \cdot R_0$  for  $I_r = 100$  and  $3 \cdot R_0$  for  $I_r = 500$ . Hence, the pressuremeter expansion required to produce an annulus of plastic soil five times larger than the initial disturbed zone will be about 14% for  $I_r = 100$  and 22% for  $I_r = 500$ . It appears that 'stiffer' soils may require larger pressuremeter expansion to overcome the effects of initial disturbance. It has been recognized by many authors that disturbance either during pressuremeter installation or during pressuremeter operation can influence significantly the derived soil parameters (Ladanyi, 1972; Sayed and Hamed, 1988; Law and Eden, 1982; Huang et al, 1991).

### 5.6.3 Maximum strain and limit pressure

Using the analytical pressuremeter loading curve for large strains, equation (5.14), the initial horizontal stress can be calculated for any pair of stress and strain ( $p, \epsilon$ ) assumed to be the maximum level reached during a pressuremeter test. A FDPT in stiff clay will be used to illustrate this

reasoning. Houlsby and Withers (1988) presented a cone pressuremeter test FPC 5 (9m) performed in a very stiff glacial clay at Madingley, Cambridge-England. Figures 5.11 (a) and (b) show respectively the analytical loading curves for many (p,g) points and the variation of the initial horizontal stress with the maximum Green strain chosen. The soil parameters used to generate these analytical pressuremeter curves were:

- (a) Initial tangent shear modulus ( $G_t$ ) = 78200 kPa
- (b) Ultimate undrained shear strength in unloading ( $\tau_{ult}^*$ ) = 303 kPa
- (c) Ratio of ultimate undrained strength ( $R_\tau$ ) = 2.0

The chosen pairs (p,g) and the determined initial horizontal stresses are presented in the following table:

<b>Simulation</b>	<b>1</b>	<b>2</b>	<b>3</b>	<b>4</b>
<b><math>g_{max}</math> (dec)</b>	0.105	0.196	0.300	0.400
<b><math>p_{max}</math> (kPa)</b>	1380.0	1411.0	1419.0	1421.3
<b><math>\sigma_{ho}</math> (kPa)</b>	696.3	654.3	619.2	595.8

Figure 5.11 (b) shows that the derived value of the initial horizontal stress decreases as the maximum Green strain increases. The reason for this response is partly due to the hyperbolic model used to derive the pressuremeter analytical loading equation. If the Green strain tends to infinity the value of the initial horizontal stress will reach its minimum value. It means that the curve  $\sigma_{ho}$  versus  $g_{max}$  has an asymptote at the  $\sigma_{ho}$  minimum. Theoretically this minimum value could be interpreted as the in situ initial horizontal stress, once when the Green strain is infinite the maximum pressure is the theoretical limit pressure (equation (5.16)). However, the pressuremeter test has to stop at a finite strain. Hence, two essential questions remain to be answered:

- (1) How much strain is needed to the maximum pressure reaches a level close to the limit pressure?
- (2) How close should be considered close enough?

#### 5.6.4 Calculation of the necessary maximum Green strain

In fact, the limit pressure is the key parameter for the FDPT and the PBPT. If

this pressure is not reached, at least closely, during the pressuremeter test the interpretation based on curve fitting of the experimental results cannot yield acceptable results. Two main procedures to calculate the maximum Green strain will be presented here.

- Calculation based on the hyperbolic model

The calculation is based on the concept of the parameter  $R_f$  (failure ratio) introduced by Duncan and Chang (1970). Two possible calculations are available: (a) Cut-off to the  $\sigma_{ho}$  versus  $g_{max}$  curve; or (b) Minimum  $p_{max}/p_l$  ratio acceptable.

If the first possible calculation is chosen, the minimum value of the initial horizontal stress can be calculated if the maximum pressure reached during the test is assumed to be very close to the limit pressure. Equation (5.16) can be used for this calculation. The soil parameters needed are determined from the pressuremeter unloading curve. A cut-off is defined at the level of Green strain that corresponds to the initial horizontal stress 10% greater than the minimum horizontal stress calculated. The Green strain determined in the  $\sigma_{ho}$  versus  $g_{max}$  curve is the minimum level of straining necessary to guarantee that the maximum pressure reached during the loading phase of the pressuremeter test is close to the theoretical limit pressure. This procedure is troublesome since it requires the construction of the  $\sigma_{ho}$  versus  $g_{max}$  curve. Because of the hyperbolic model used in the equation derivation, Green strains of 100% or even larger are sometimes calculated as the necessary strain to reach the limit pressure. This is unreal and constitutes another drawback of this procedure.

Rather than generating a  $\sigma_{ho}$  versus  $g_{max}$  plot to determine the minimum required strain, a similar but easier procedure will be used here. This is the second possible calculation of the minimum required strain and is based on the minimum  $p_{max}/p_l$  ratio acceptable. Using the procedure described in 5.6.3 the horizontal stress correspondent to the pair (p,g) at the end of the experimental loading curve can be calculated (equation (5.14)). Assuming that this calculated value of the initial horizontal stress is the minimum value, a limit pressure can be calculated using equation (5.16). The ratio  $p_{max}/p_l$  can now be calculated. If the ratio is greater than 90% the pressuremeter was



expanded far enough and consequently the maximum pressure reached is close to the limit pressure. In this case, the maximum pressure can be used in equation (5.16) to calculate the final value of the initial horizontal stress. On the other hand, if the ratio  $p_{max}/p_l$  is smaller than 90% the pressuremeter was not expanded far enough and the data is not adequate to be interpreted by curve fitting methods. For instance, this procedure was applied to the FPC 5 (9m) test. For a maximum pressure of 1421.3 kPa and a maximum Green strain of 40% (Cauchy strain 34%) the initial horizontal stress calculated is 595.8 kPa. The limit pressure calculated with this value of the initial horizontal stress and the soil parameters derived from the experimental unloading curve is 1544.0 kPa. Hence, the ratio  $p_{max}/p_l$  is 92%. Consequently, based on the above criterion, the test was expanded far enough and the final value of the initial horizontal stress is 472 kPa. To check the consistency of this procedure, the four simulations previously presented were tested. The results are presented in the following table:

<b>Simulation</b>	<b>1</b>	<b>2</b>	<b>3</b>	<b>4</b>
$\delta_{max}$ (dec)	0.105	0.196	0.300	0.400
$p_{max}$ (kPa)	1380.0	1411.0	1419.0	1421.3
$\sigma_{ho}$ (kPa)	696.3	654.3	619.2	595.8
$p_l$ (kPa)	1644.4	1602.5	1567.4	1544.0
$p_{max}/p_l$ (%)	83.9	88.0	90.0	92.0

- Calculation based on the elastic-perfectly model

The minimum required strain during a FDPT or a PBPT can also be evaluated based on the radius of the plastic-elastic annulus around the pressuremeter. Figure 5.10 shows that for a large initial disturbance, say 10% measured in Green strains, the plastic-elastic boundary will be 10 times the initial pressuremeter radius for a rigidity index of 500 (stiff soils). In order to double the radius of the already failed material, the pressuremeter must be expanded at least to 40% in terms of Green strains. However, assuming that the initial disturbance expressed in terms of strains is very difficult to evaluate, if possible, this procedure is far less attractive than the one previously

presented, which is based on the ratio of the maximum and limit stresses.

### 5.6.5 Proposed methodology to interpret undrained FDPT and PBPT

Based on the concept of limit pressure a methodology to interpret FDPT and PBPT results can be proposed. The methodology consists of the following steps:

- (1) Correct the field data based on the calibration results and arrange the data in a Kaleidagraph™ worksheet in two separate curves - loading and unloading;
- (2) Use equation (5.15) to perform the curve fitting technique on the unloading experimental points. Some points at the end of the unloading curve might be discarded if there is an improvement in the curve fitting of the remaining points. Two parameters are derived from this curve matching: (a) initial tangent shear modulus ( $G_i^*$ ); and (b) ultimate undrained shear strength ( $\tau_{ult}^*$ );
- (3) Assume an undrained strength ratio ( $R_\tau$ ) equal 2.0 and the maximum pressure ( $p_{max}$ ) reached during the loading phase equals the theoretical limit pressure ( $p_l$ ), the value of the initial horizontal stress can be calculated using equation (5.14);
- (4) Calculate the limit pressure ( $p_l$ ) using equation (5.16);
- (5) Calculate the ratio  $p_{max}/p_l$ . If the ratio is greater than 90% the maximum pressure is very close to the limit pressure and hence, it could be used to estimate the final value of the initial in situ horizontal stress. On the other hand, if the ratio  $p_{max}/p_l$  is smaller than 90% the maximum pressure is not close to the limit pressure and the test cannot be used to yield soil parameters by curve fitting interpretation.

### 5.6.6 Comments on the proposed methodology

- It is clear that the hyperbolic model cannot be used to evaluate the radius of the failed zone around the pressuremeter because the ultimate strength will be mobilized only at infinite strain. However, this weakness can be overcome if a cut-off level is assumed, as proposed by Duncan and Chang (1970). They found that the value of the failure ratio was between 0.75 and 1.0 for a large

number of different soils. Following a similar approach, the ratio between the maximum and the limit pressures can be acceptable if it lies within a range of 90% and 100%. In this case, the maximum pressure during the loading phase of a pressuremeter test can replace the limit pressure in the calculation of the final value of the initial horizontal stress.

- The PBPT is often used to test stiff to hard clay. In very stiff clays a limit pressure is rarely achieved with most conventional PBP device. Hence, the test results are not adequate to be interpreted by curve fitting technique. It is also uncommon for the unloading data to be recorded during most standard PBPT. Therefore, no PBPT was interpreted in this work. One possible solution for this problem is to avoid the s-shape curve at the beginning of the pressuremeter expansion. This can be accomplished by drilling a hole with a diameter slightly smaller than the pressuremeter diameter. In this case, the equipment must be forced to penetrate inside the hole and consequently the expansion curve starts with a positive slope rather than the traditional s-shape curve.
- A complete validation of this methodology should be provided before any attempt to apply it to any geotechnical design. FDPT and PBPT results from several experimental sites, where the soil properties are known from other in situ or laboratory tests, are necessary to completely evaluate the proposed methodology. Those results were not available to be included in this work.

## **5.7 Interpretation of a SBPT and a FDPT at the same depth (Lulu Island Pile Research Site - BC, Canada)**

### **5.7.1 Introduction**

As theoretically presented in figure 5.7, SBPT results (pressuremeter curve) are expected to be different from FDPT results. Due to the smaller degree of disturbance caused during insertion, the SBPT is expected to reach a pressure close to the soil limit pressure at a smaller cavity strain than the FDPT. It would be of great interest if the results of these two tests were obtained at the same site and at the same depth. Specialized geotechnical

literature has mentioned few places around the world where different pressuremeter tests have been performed at the same depth. One of these places is a test site of the Department of Civil Engineering of the University of British Columbia in Vancouver, BC, Canada. Howie (1991) reported a program of pressuremeter tests undertaken at four sites in the Vancouver region. In one of these sites, namely the Lulu Island Pile Research Site, 23 SBPT's and 19 FDPT's were performed. Two representative tests performed at that site will be interpreted using the large strain pressuremeter analytical equations and the methodology presented in chapter 4. Although this proposed method was developed to interpret a SBPT, an attempt will be made to extend this method to interpret a FDPT in soft clay.

#### 5.7.2 Site description

As reported by Howie (1991) the Pile Research Site is located on Lulu Island on the north side of the Annacis Channel which is a portion of the South Arm of the Fraser River in Richmond, BC. Heterogeneous fill of sands and silts covers the site to a depth of 2 to 4m. Specifically at the pile site, a rectangular area of 5m by 12m, the fill was excavated and replaced by clean river sand. On top of that 0.6m to 1m of pit-run sand and gravel was placed over the whole site including the pile site. Underlying the fill is a 12m thick deposit of organic silt and clay formed by the deltaic deposition of the Fraser River. Following this thick organic layer, a medium dense fine to medium sand forms a strata of approximately 10 to 15m thick. All the tests were performed in these two layers (organic silt clay and fine sand).

#### 5.7.3 Self-boring pressuremeter device

The equipment used to perform the SBPT was the Hughes pressuremeter. As described by Howie (1991), this type of SBP was modeled on the Cambridge, England Camkometer. The diameter of the SBP was 74mm and the expandable cell had a slenderness ratio of 6 (length/diameter). Three strain arms located at the mid-height of the probe were used to monitor the cavity strains. Two effective stress cells were installed in the membrane to monitor the pore pressure during the test. The analogue signals from the pressure

transducers and strain arms were transmitted to the surface through a cable which was put inside the gas line. The urethane membrane protected by a 'chinese lantern' was inflated using nitrogen fed from the surface through a plastic tube which was taped to the rods as the pressuremeter was drilled in. With this device, 23 SBPT's were performed and the pressuremeter curves were obtained. The final pressures were corrected based on the calibration results.

#### 5.7.4 Full-displacement pressuremeter device

The equipment used to perform the full-displacement pressuremeter tests was the UBC seismic cone-pressuremeter. (SCPM). As described by Howie (1991), the pressuremeter expansion unit was 220mm long and the membrane made of natural rubber was protected by a 'chinese lantern' consisting of overlapping stainless steel strips. A new clamping mechanism was designed to allow the membrane protection to move during expansion and contraction as well as during insertion and extraction. With a diameter of 44mm the UBC probe had a slenderness ratio of 5. The membrane was expanded by pumping oil from a pressure developer into the pressuremeter cell. Light silicon oil was selected due to its low viscosity ensuring rapid movement through the narrow channels between the pressure developer and the pressuremeter cell. This type of oil does not cause any deterioration to the rubber membrane. Three strain arms located at the mid height of the cell pressure were used to monitor the cavity strains. The arms were capable of measuring deflections of up to 6mm which means a cavity strain of about 27%. The pressure was provided by a piston and reservoir system. The maximum pressure generated was about 7,000 kPa. A solid 44mm diameter cone tip was used to allow the pressuremeter insertion. With this device, 19 FDPT's were performed and the pressuremeter curves were obtained. The final pressures were corrected based on the calibration results.

#### 5.7.5 Interpretation of the HPM 87 - 3 test (9.4m)

The HPM 87 - 3 test (9.4m) was performed on Feb.19, 87 using the self-boring pressuremeter developed by John Hughes and described in 5.7.3.

After the pressure has been corrected based on the calibration results, the data were plotted using the average strain from the three arms. The definition of strain used to obtain the pressuremeter curve was the logarithmic strain presented in 5.2.1. Since the definition of large strain used in this work is the Green's definition, a transformation was provided using the equation (5.4). The maximum pressure reached during the test was 271.0 kPa. Figure 5.13 shows the final plot after the curve fitting. The final interpreted parameters are shown in Figure 5.12, and are:

- (1) Undrained shear strength mobilized ( $g_{max} = 192\%$ ): 21 kPa
- (2) Initial shear modulus: 7,787 kPa
- (3) Initial in situ horizontal stress: 170 kPa

The limit pressure calculated using equation (5.16) and the parameters showed in figure 5.12 - step #3 - Summary, was 295.6 kPa. Hence, the maximum pressure reached was 92% of the theoretical soil limit pressure. The large strain pressuremeter analytical equations (5.14) and (5.15) were used in the test interpretation. Figure 5.13 shows that the unloading curve fitting is excellent. On the other hand, the loading analytical curve is above the experimental curve indicating some disturbance possibly due to an oversize cutting shoe. It can be noticed that, during the interpretation procedure, just the last points of the experimental loading curve were used.

#### 5.7.6 Interpretation of the SCPM #1 test (9.4m)

The SCPM #1 test (9.4m) was performed on Apr.03, 87 using the UBC seismic cone-pressuremeter described in 5.7.4. After the pressure has been corrected based on the calibration results, the data were plotted using the average strain from the three arms. The definition of strain used to obtain the experimental pressuremeter curves was the logarithmic strain presented in 5.2.1. A transformation to Green's definition of strain was made using equation (5.4). Figure 5.15 shows the final plot and the curve fitting. The final interpreted parameters are shown on Figure 5.14, and are summarized below:

- (1) Undrained shear strength mobilized ( $g_{\max} = 28.4\%$ ): 19 kPa
- (2) Initial shear modulus: 7,996 kPa
- (3) Initial in situ horizontal stress: 180 kPa

The maximum pressure reached during the test was 279.0 kPa. The interpretation template used to derive the soil parameters is presented in figure 5.14. The theoretical limit pressure was calculated using equation (5.16) and the parameters showed in figure 5.14 - step #3 - Summary. Its value was 298.4 kPa. Hence, the maximum pressure reached during the test was 93% of the theoretical soil limit pressure. The large strain pressuremeter analytical equations (5.14) and (5.15) were used in the test interpretation procedure. Figure 5.15 shows that the unloading curve fitting is very good for strains greater than 10%. The loading analytical curve is above the loading experimental curve. It is possible that the solid cone tip ahead of the pressuremeter element may have been slightly larger than the pressuremeter resulting in some unloading and hence, reduced pressuremeter loading response.

The lift-off stress from the cone-pressuremeter is approximately 170 kPa compared to the value of 110 kPa for the SBPT. It can be noticed from figure 5.15 that during the interpretation procedure just the last loading points of the experimental loading curve were used.

#### 5.7.7 Comments on test results

A comparison between the shape of the original SBPT (HPM 87 - 3 (9.4m)) and the original FDPT (SCPM #1 (9.4m)) is presented in figure 5.16. Although the type of pressuremeter installation for both tests is totally different, the plotted results are not so different. On the other hand, due to the difference in the values of the maximum strain reached during the tests, the unloading curves appear to be different. However, the final interpreted parameters based primarily on the unloading curves are very close for both tests as shown in the following table:

Parameters	$G_i$ kPa	$\tau_{ult}^*$ kPa	$R_\tau$	$\sigma_{ho}$ kPa
HPM87-3	7,787	42.3	2.0	170.3
SCPM#1	7,997	39.2	2.0	180.3

This confirms the consistency of the interpretation methodology presented in chapter 4, using large strain pressuremeter analytical equations, to interpret FDPT and SBPT in soft clay. However, to assess the adequacy of the hyperbolic model to derive soil parameters from large strain FDPT further validation is necessary. The procedure can be similar to the one adopted in chapter 4 to show the adequacy of the hyperbolic model for small strain analysis.

### 5.8 Initial horizontal stress from a FDPT

As shown in figure 5.7, the FDPT must be extended to large strains so that the limit pressure, which is function of the undisturbed soil parameters, can be closely reached. As a consequence, FDPT results can only be interpreted using the large strain theory, as shown before in this chapter. Furthermore, the degree of disturbance generated during the pressuremeter insertion is so high that the information on the initial in situ horizontal stress is so poor that it is almost impossible to derive its value from the loading phase of the FDPT. This conclusion is specially true for medium to stiff clays. However, the information on the initial horizontal stress still remains embedded in the value of the limit pressure. Using the hyperbolic model the theoretical limit pressure can be determined by equation (5.16) as a function of the initial in situ horizontal stress, the shear modulus and the undrained shear strength. Hence, if the limit pressure can be determined experimentally from large strain FDPT an estimate of the horizontal stress can be obtained. This procedure was used by Houlsby and Withers (1988). The proposed methodology presents an alternate procedure to calculate the in situ initial horizontal stress.



## 5.9 Interpretation of a FDPT in stiff clays

Houlsby and Withers (1988) presented two FDPT's performed at Madingley, Cambridge/England, with a prototype of the Fugro Pressuremeter Cone: (a) FPC 15 test at 4m depth, and (b) FPC 5 test at 9m depth. To interpret these tests using the large strain pressuremeter analytical equations the proposed methodology presented in section 5.6.5 was used.

### 5.9.1 Interpretation of the FPC 15 test (4m)

Assuming that the experimental pressuremeter curve presented by Houlsby and Withers (1988) has used the logarithmic strain definition, a transformation for Green strains using equation (5.4) is necessary, so that equation (5.15) can be used to execute the curve fitting technique. Figure 5.17 shows the curve fitting of the unloading phase of the test. Notice that the unloading points with strains smaller than 36% were discarded. The reason was a significant improvement in the curve matching of the remaining points. The derived parameters were: (a) Shear modulus: 27,947 kPa; and (b) Ultimate undrained shear strength for unloading: 233 kPa.

For a ratio  $R_\tau$  equal 2.0, the ultimate undrained shear strength for loading is 116.5 kPa. Hence, using equation (5.16) and assuming the soil limit pressure equals to the maximum pressure reached during the test ( $p_{max}$ ) that is 914.5 kPa, the derived value for the initial in situ horizontal stress is 343 kPa.

In summary, the parameters derived from the FPC 15 test (4m) using the proposed methodology are:

- (1) Undrained shear strength mobilized ( $g_{max} = 60.9\%$ ): 115.7 kPa
- (2) Initial shear modulus: 27,947 kPa
- (3) Initial in situ horizontal stress: 343 kPa

### 5.9.2 Interpretation of the FPC 5 test (9m)

Using a similar procedure as described in 5.9.1, the FPC 5 test (9m) was interpreted to yield the following parameters:

- (1) Undrained shear strength mobilized ( $g_{max} = 49.1\%$ ): 152 kPa
- (2) Initial shear modulus: 57,877 kPa
- (3) Initial in situ horizontal stress: 618.5 kPa

The curve fitting of the unloading phase of the test is presented in figure 5.18. Notice that the unloading points with strains smaller than 25% were discarded to improve the curve matching of the remaining points.

### 5.9.3 Comments on the derived results

The following table shows the parameters derived from the FDPT at Madingley Site reported by Houlsby and Withers (1988) and the interpreted parameters using the proposed methodology. The analysis of the results shows that the undrained shear strength derived by both methodologies are in very good agreement. These values also agree well with the undrained shear strength determined from other in situ and laboratory tests (Houlsby and Withers, 1988).

<b>Method</b>	<b>Houlsby and Withers (1988)</b>		<b>Proposed methodology</b>	
	<b>FPC 15(4m)</b>	<b>FPC 5(9m)</b>	<b>FPC 15(4m)</b>	<b>FPC 5(9m)</b>
<b><math>G</math> (MPa)</b>	14.8	33.5	27.9	57.9
<b><math>S_u</math> (kPa)</b>	111.0	150.0	115.7	152.2
<b><math>\sigma_{ho}</math> (kPa)</b>	239.0	465.0	343.1	618.5

On the other hand, the values of the shear modulus are totally different. The reason is the type of soil model assumed by each methodology. Houlsby and Withers (1988) used an elastic perfectly plastic model; consequently, the value of the shear modulus determined should be called equivalent elastic shear modulus. The proposed methodology used a hyperbolic model so that the shear modulus is the initial tangent shear modulus. Therefore, the discrepancy of these shear modulus values could be expected. While the equivalent elastic shear modulus is meaningless for deformation analysis in soils subjected to shear strains above the elastic threshold (approximately  $10^{-3}\%$ ), the hyperbolic model can be used with any level of shear strains, in

the way described in chapter 4 (4.5.2). Finally, a comparison between the values of the initial in situ horizontal stress determined by both methodologies shows that the values derived from the hyperbolic model are almost 50% greater than the values from the elastic-perfect plastic model. For both tests the ratio between the limit pressure (equation 5.16) and the maximum pressure reached during pressuremeter expansion was 93%. Considering that the pressuremeter was expanded far enough, one possible explanation for the high values of the initial horizontal stress is the use of the hyperbolic model which requires infinite expansion to mobilize the ultimate undrained strength. However, as stated by Houlsby and Withers (1988), even for elastic-perfectly plastic model the derived values for the initial horizontal stress appear to yield higher earth pressure coefficient at rest than the expected values at the Madingley Site.

### **5.10 Conclusions**

The required amount of soil straining during a pressuremeter test to evaluate undisturbed soil parameters is a direct function of the amount of disturbance caused to the soil during the pressuremeter installation procedure. The SBPT requires small strains during the test to capture the response of the natural undisturbed material. The main reason is the expected small amount of disturbance caused during the pressuremeter insertion. On the other hand, the FDPT requires large strains during the test to ensure that the maximum pressure reached is the response of the undisturbed soil. Small strain theory is, therefore, adequate to analyze the SBPT when the maximum strain does not exceed 15% (cavity strain). For strains greater than 20% the deformed configuration is not close enough to the initial configuration so that the coincidence of both configurations cannot be assumed and large strain theory must be used. Updated versions of the FDP allow cavity strains up to around 50%. For slenderness ratios less than 4.0 the spherical cavity expansion theory may be more appropriate to analyze this problem than the cylindrical cavity expansion theory. Some discussion still exists on this issue (Houlsby and Withers, 1988).

At least two definitions of large strains in the Lagrangian space have been

used: (a) Logarithmic strains; and (b) Green strains. The latter was used in this work to derive the large strain pressuremeter analytical equations. In this derivation the hyperbolic stress-strain relationship was assumed to be the soil constitutive law, for both pressuremeter loading and unloading. The complete soil behaviour using this model is very simple and is dependent on just two parameters - initial tangent shear modulus and ultimate undrained shear strength. Nonlinear stress-strain relationship, like the hyperbolic model, has proved to be powerful in describing the stress-strain response of a large number of soils. Furthermore, the parameters used to describe soil behaviour are meaningful in terms of engineering application. The derived large strain pressuremeter analytical equations - one for loading and one for unloading, require four parameters to simulate a complete pressuremeter test: (a) initial tangent shear modulus, (b) initial in situ horizontal stress; (c) ultimate undrained shear strength during loading; and (d) ultimate undrained shear strength during unloading. If a relationship between the undrained shear strength in unloading and loading is assumed known, three soil parameters can be derived from a large strain pressuremeter test. The interpretation methodology considers the experimental unloading pressuremeter curve as the least disturbed by the device insertion. The shear modulus and the undrained shear strength in unloading can be estimated using the least square error curve fitting technique. Assuming that the maximum pressure is the true limit pressure, the third parameter (initial horizontal stress) can be evaluated using the limit pressure equation. Further validation is necessary to confirm this latter step since horizontal stresses derived by this method have shown to be overestimated (Houlsby and Withers, 1988). On the other hand, the shear modulus and the undrained shear strength derived from the unloading curve by the proposed methodology appear to be useful parameters for engineering design.

A final consideration related to the shape of the FDPT curve is necessary when soft and stiff soils are tested. As presented by Howie (1991) the shape of the FDPT curve for soft soils may not be much different from the shape of the SBPT curve. In this case, the large strain pressuremeter analytical equations can be used in conjunction with the interpretation philosophy presented in chapter 4. All three parameters can then be derived. On the

other hand, if the FDPT is performed in stiff soils, the loading curve appears not to present any information on the initial horizontal stress. In this case, the limit pressure has to be used according to the methodology described in 5.6.5 if the horizontal stress is to be evaluated. Hence, it is important that the pressuremeter be expanded to a strain level sufficient to be close to the limit pressure of the undisturbed soil.

Finally, it is worthwhile to emphasize the importance of this simple methodology to interpret large strain pressuremeter tests. Although further validation is necessary to confirm the applicability of the derived analytical equations, the proposed methodology has a potential to be used by geotechnical engineers due to its accessibility, simplicity, and repeatability.

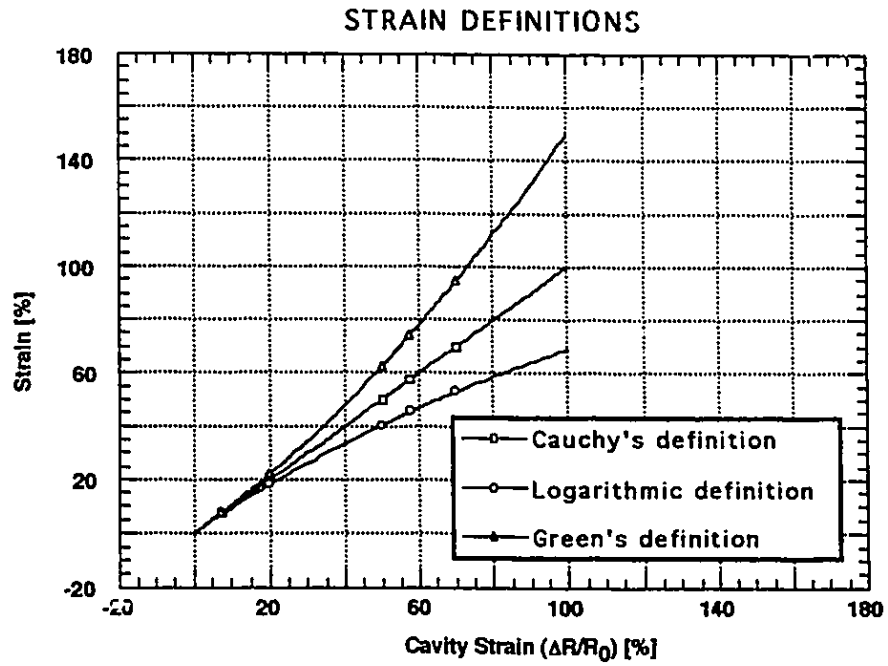
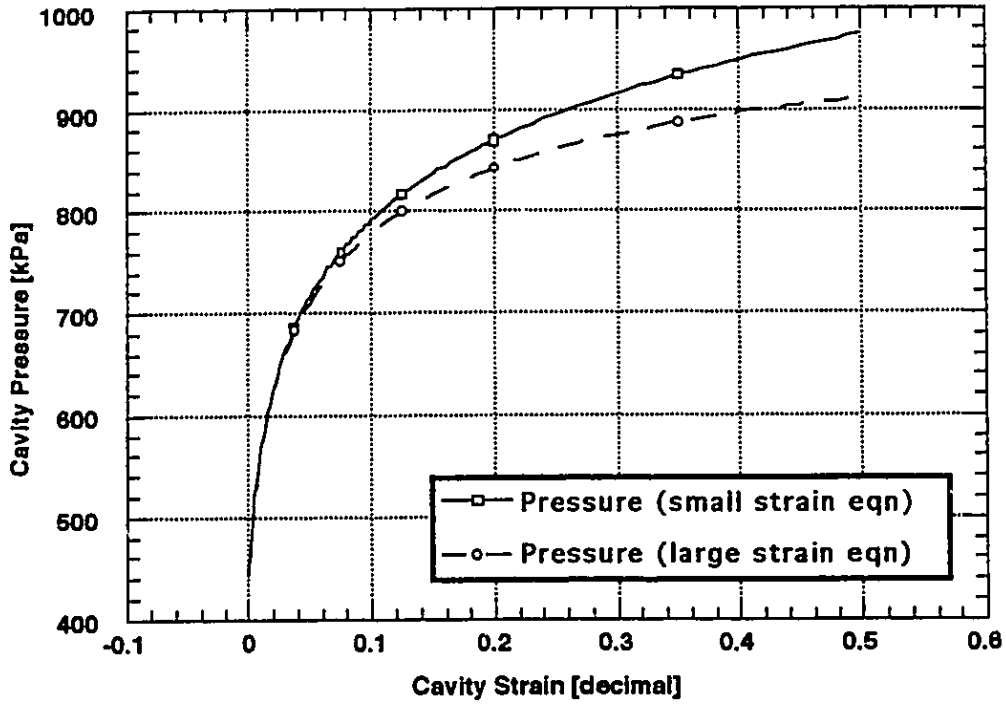


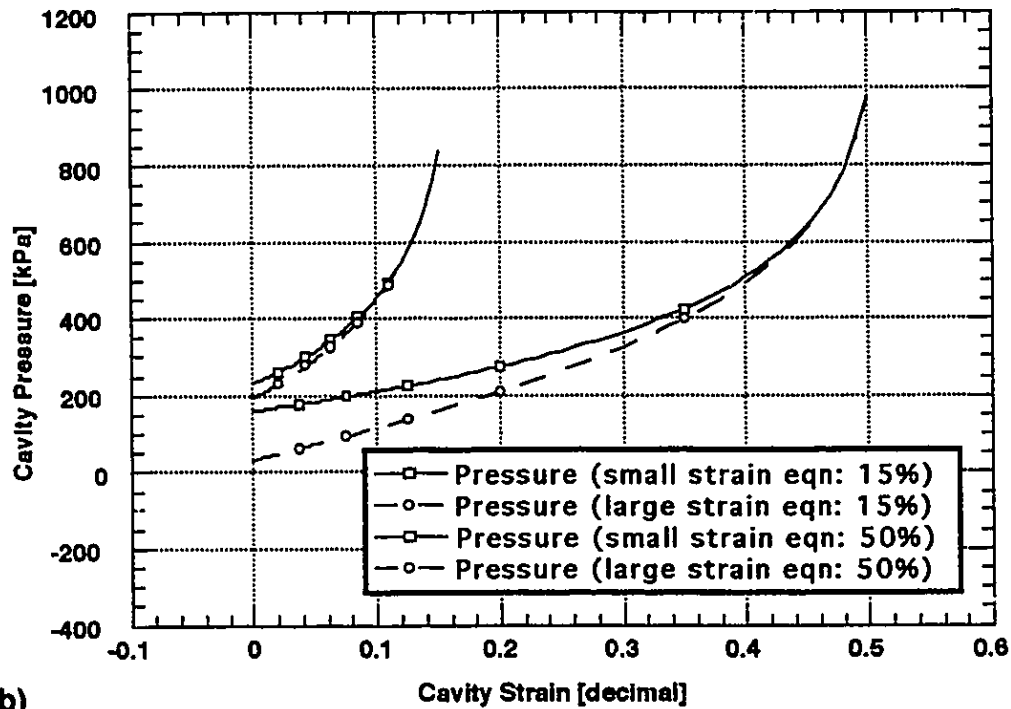
**Figure 5.1** Variation of logarithmic and Green strains with cavity strain

Test V2P14 - Large and small strain equations



(a)

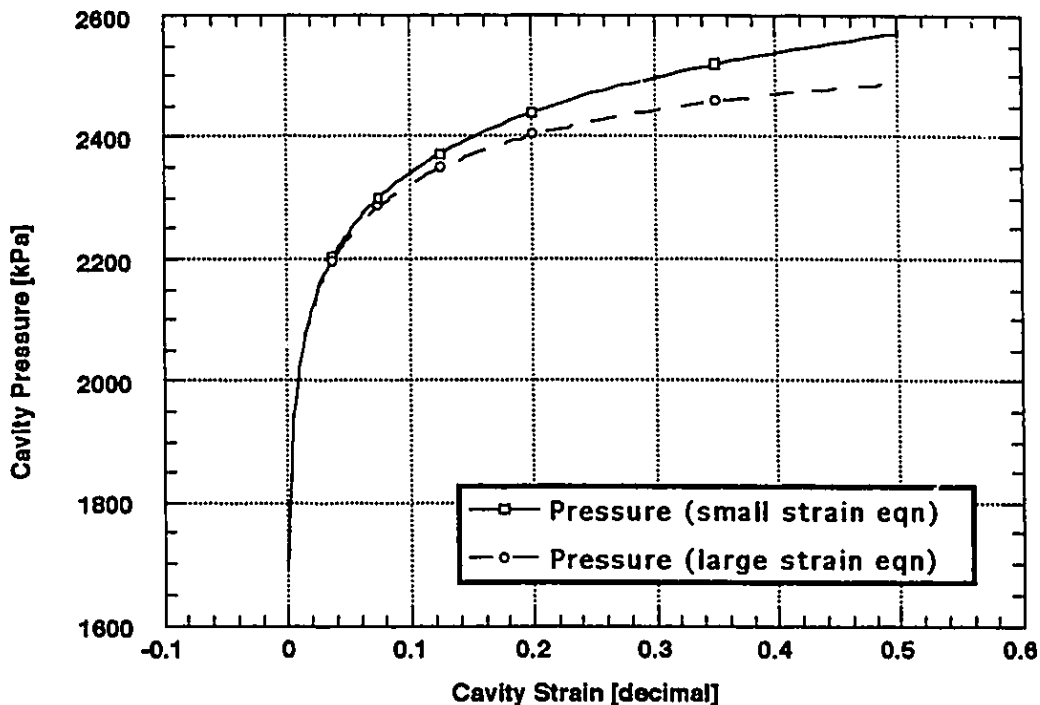
Test V2P14 - Large and small strain equations



(b)

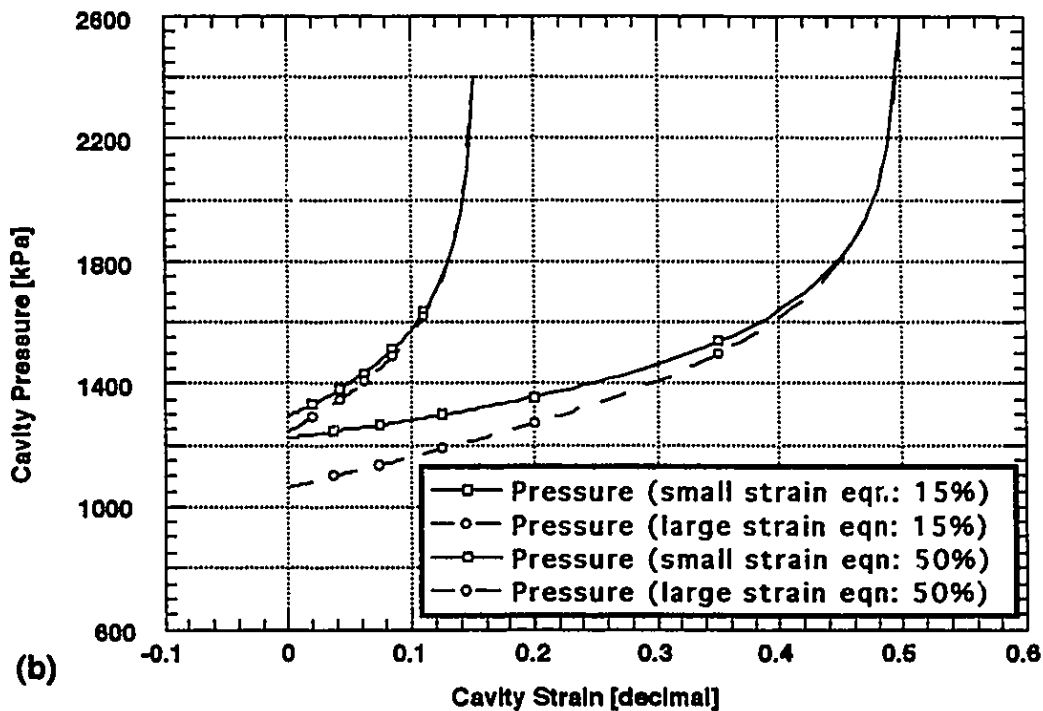
Figure 5.2 Test V2P14 Fucino clay - Comparison of large and small strain equations: (a) Loading curve; (b) Unloading curve.

Test AF85 - Large and small strain equations



(a)

Test AF85 - Large and small strain equations



(b)

Figure 5.3 Test AF85 P06-15 - Comparison of large and small strain equations: (a) Loading curve; (b) Unloading curve.



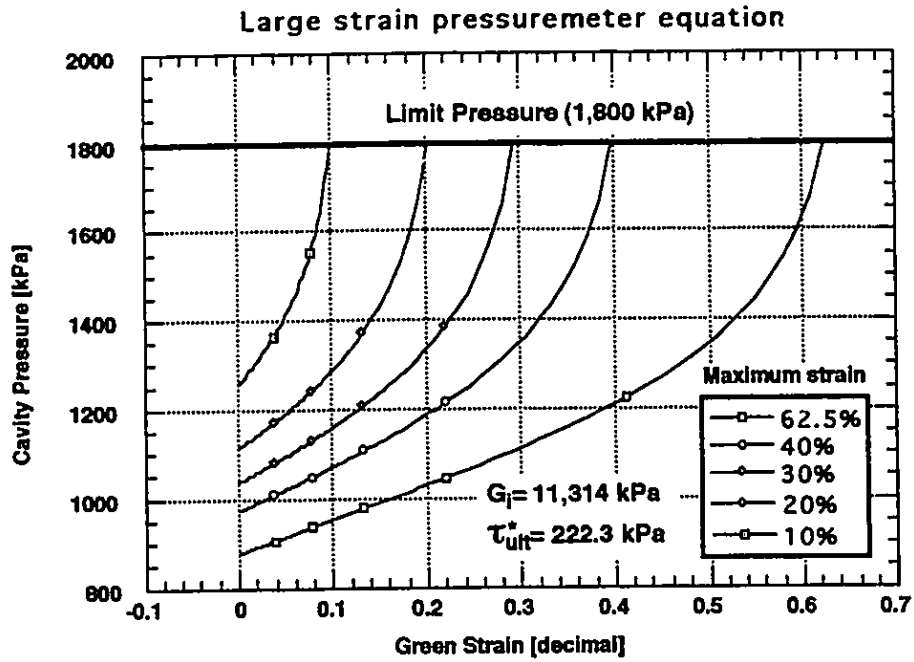


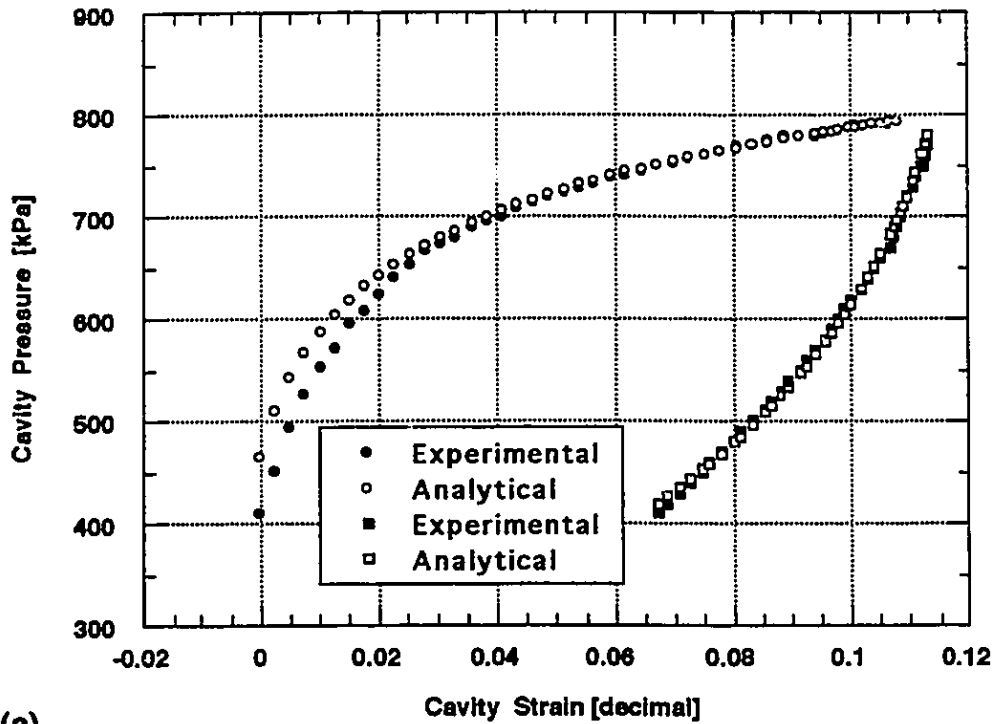
**Figure 5.4 Unloading curves for an idealized soil for several levels of maximum strain.**

## PRESSUREMETER INTERPRETATION TEMPLATE - CLAYS

TEST ID	Fucino clay - Test V2P14 (Large strain equations)		
DEPTH [m]	26.0	LIFT-OFF [kPa]	409.93
Loading :	p <sub>max</sub> [kPa] 792.93	g <sub>max</sub> [dec]	0.10775
Unloading :	p <sub>max</sub> [kPa] 779.93	g <sub>max</sub> [dec]	0.11317
<b>STEP # 1 - UNLOADING (Best fit with two parameters)</b>			
<b>(a) All unloading points</b>			
	$\tau_{ult}^* = 222.3$	Graph Page	Figure 5.6 (a)
	$2G_i = 2*11,313.9$		
<b>(b) (some data points removed)</b>			
	$\tau_{ult}^* =$	Graph Page	_____
	$2G_i =$		
<b>STEP # 2 - LOADING (Best fit with one parameter <math>R_c=2.0</math>)</b>			
<b>(a) All loading points</b>			
	$\sigma_{ho} = 455.2$	Graph Page	Figure 5.6 (b)
<b>(b) Strain range (first option) Last half</b>			
	$\sigma_{ho} = 463.4$	Graph Page	Not shown
<b>(c) Strain range (second option) Last quarter</b>			
	$\sigma_{ho} = 464.1$	Graph Page	Not shown
<b>(d) Strain range (third option) Interpolate points at the very last end</b>			
	$\sigma_{ho} = 464.1$	Graph Page	Figure 5.6 (a)
<b>STEP # 3 - SUMMARY</b>			
<b>(a) First strain range selected: Step # 2 option (d)</b>			
	$\tau_{ult}^* = 222.3$	$\tau_{ult} = 111.15$	Graph Page
	$2G_i = 2*11,313.9$	$\sigma_{ho} = 464.1$	Figure 5.6 (a)
<b>(b) Second strain range selected</b>			
	$\tau_{ult}^* =$	$\tau_{ult} =$	Graph Page
	$2G_i =$	$\sigma_{ho} =$	_____

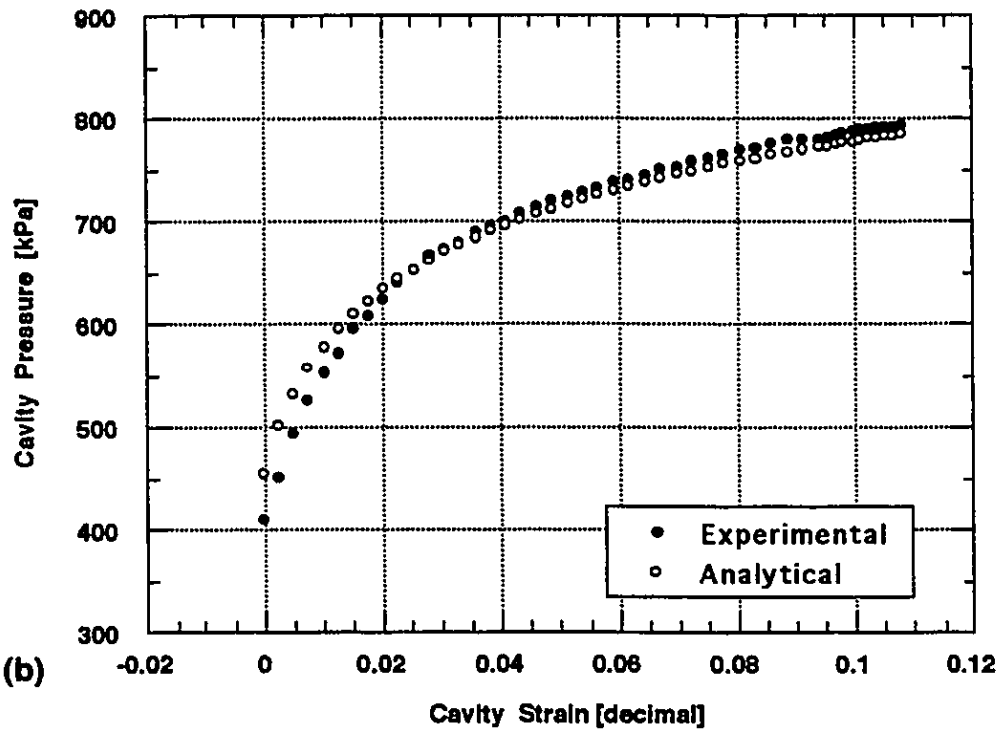
**Figure 5.5 Test V2P14 Fioravante (1988): Interpretation template using large strain pressuremeter analytical equations.**

Fucino Clay - Test V2P14 - Final Plot



(a)

Fucino Clay - Test V2P14 - All loading points



(b)

Figure 5.6 Test V2P14 Fioravante (1988) - Large strain equations: (a) Final plot; (b) Curve fitting of all loading points.

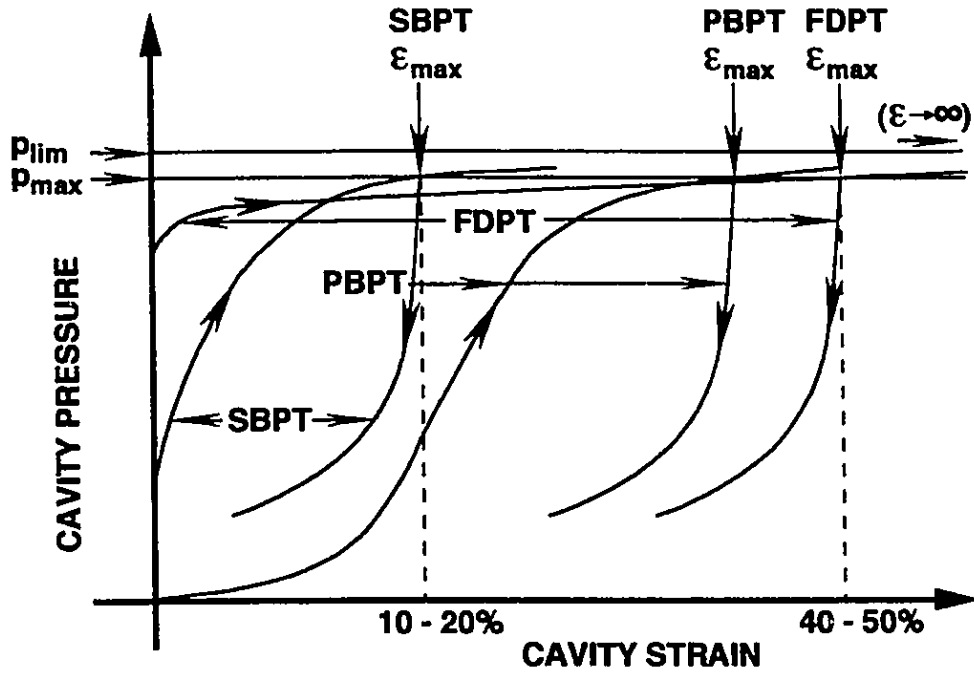


Figure 5.7 Idealized response of undrained pressuremeter tests.

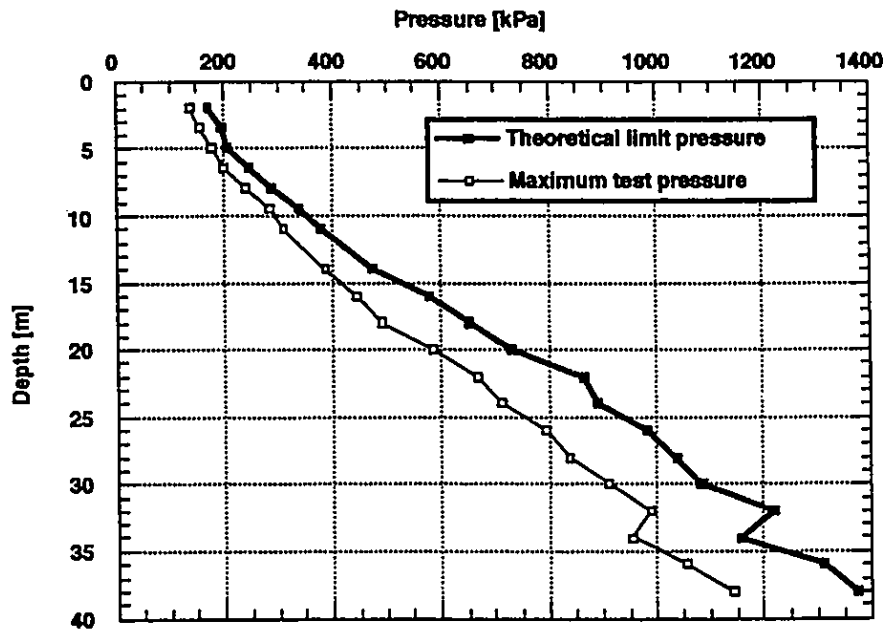


Figure 5.8 Fucino clay: Profiles of maximum pressure and theoretical limit pressure.

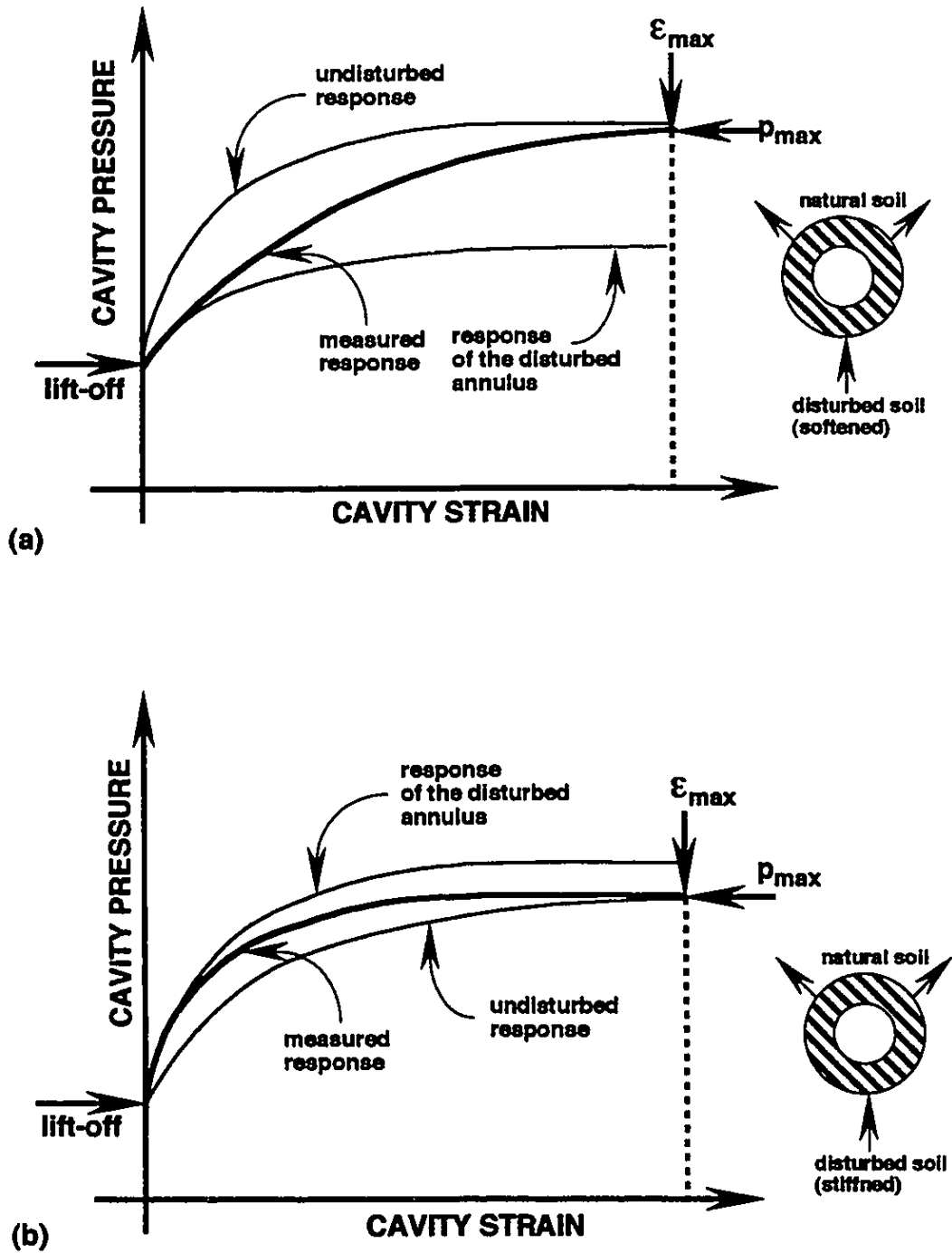
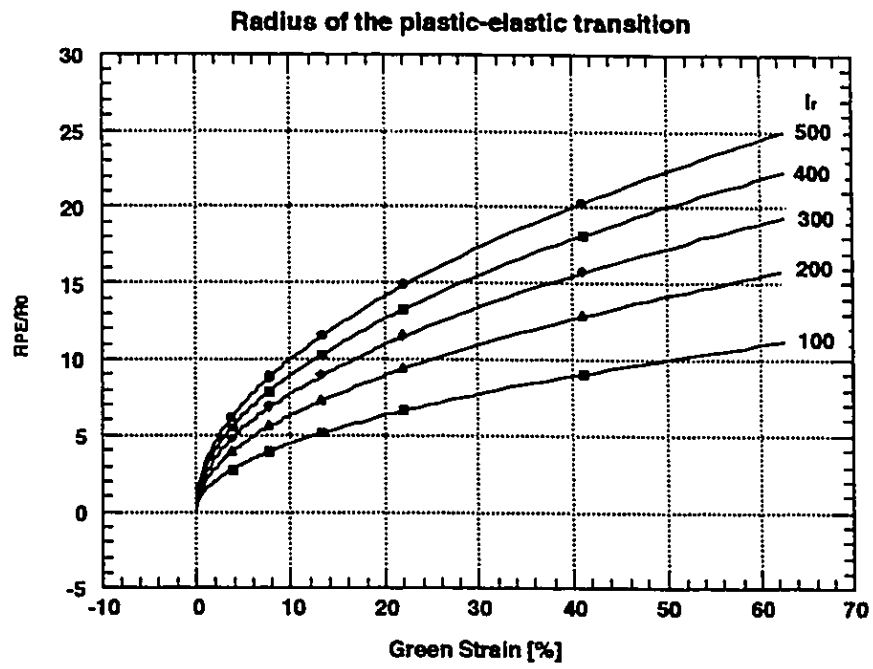
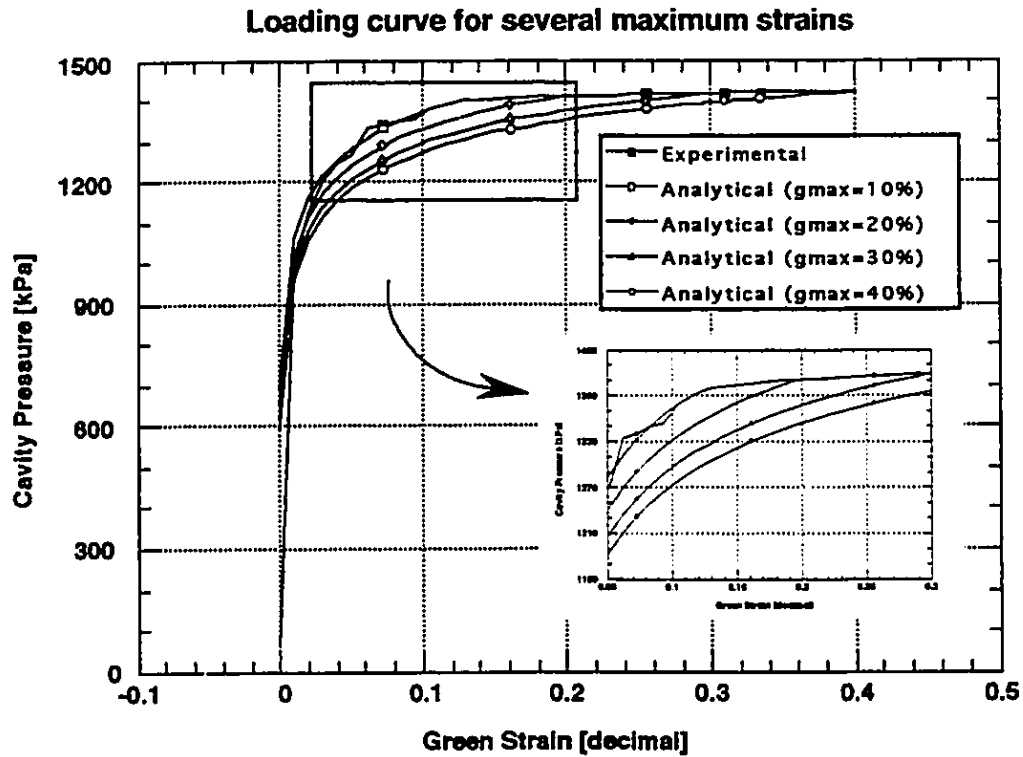


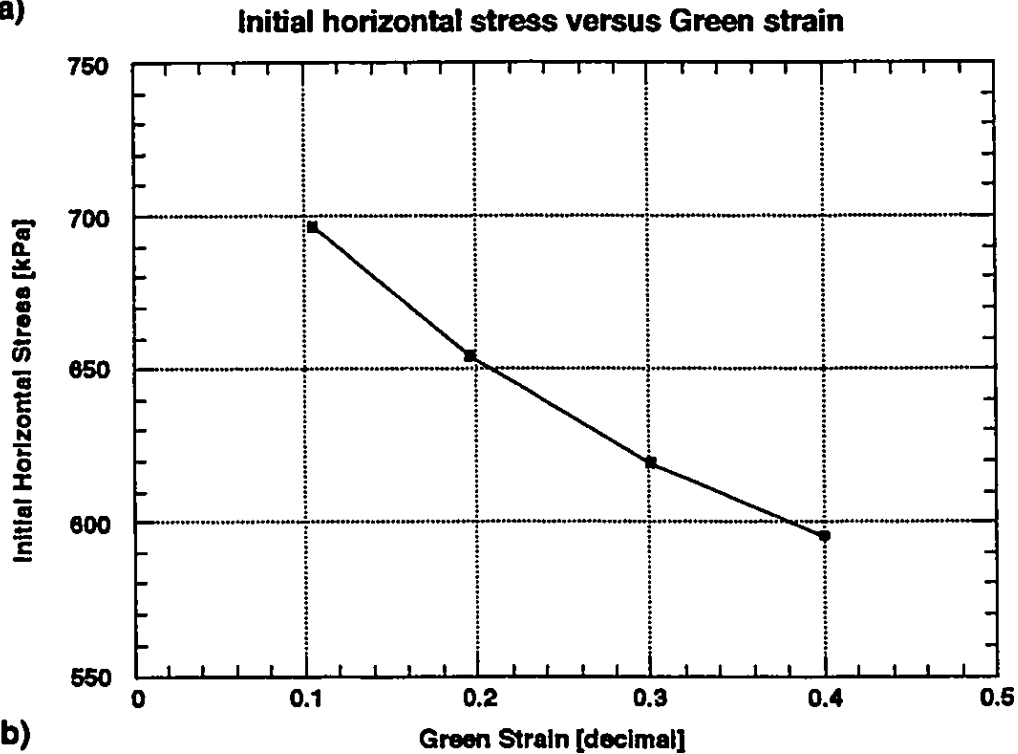
Figure 5.9 Disturbance during pressuremeter insertion: (a) Without consolidation; (b) With consolidation.



**Figure 5.10** Variation of the normalized plastic-elastic radius with Green strain.



(a)



(b)

**Figure 5.11 Madingley Site - Test FPC 5 (9m): (a) Analytical loading curve for many  $(p,g)_{max}$ ; (b) Variation of the initial horizontal stress with Green strain.**

## PRESSUREMETER INTERPRETATION TEMPLATE - CLAYS

TEST ID	Lulu Island - Test HPM-3 (Large strain equations)		
DEPTH [m]	9.4	LIFT-OFF [kPa]	110.0
Loading :	$p_{max}$ [kPa] 271.0	$g_{max}$ [dec]	0.19202
Unloading :	$p_{max}$ [kPa] 265.0	$g_{max}$ [dec]	0.1934
<b>STEP # 1 - UNLOADING (Best fit with two parameters)</b>			
<b>(a) All unloading points</b>			
	$\tau_{ult}^* = 42.3$	Graph Page	Figure 5.13
	$2G_i = 2*7,787.0$		
<b>(b) (some data points removed)</b>			
	$\tau_{ult}^* =$	Graph Page	
	$2G_i =$		
<b>STEP # 2 - LOADING (Best fit with one parameter <math>R_c=2.0</math>)</b>			
<b>(a) All loading points</b>			
	$\sigma_{ho} = 150.5$	Graph Page	Not shown
<b>(b) Strain range (first option) Last half</b>			
	$\sigma_{ho} = 166.4$	Graph Page	Not shown
<b>(c) Strain range (second option) Last quarter</b>			
	$\sigma_{ho} = 169.3$	Graph Page	Not shown
<b>(d) Strain range (third option) Interpolate points at the very last end</b>			
	$\sigma_{ho} = 170.3$	Graph Page	Figure 5.13
<b>STEP # 3 - SUMMARY</b>			
<b>(a) First strain range selected: Step # 2 option (d)</b>			
	$\tau_{ult}^* = 42.3$	$\tau_{ult} = 21.15$	Graph Page Figure 5.13
	$2G_i = 2*7,787.0$ $\sigma_{ho} = 170.3$		
<b>(b) Second strain range selected</b>			
	$\tau_{ult}^* =$	$\tau_{ult} =$	Graph Page
	$2G_i =$ $\sigma_{ho} =$		

**Figure 5.12** Lulu Island - Test HPM87 - 3: Interpretation template using large strain pressuremeter analytical equations.



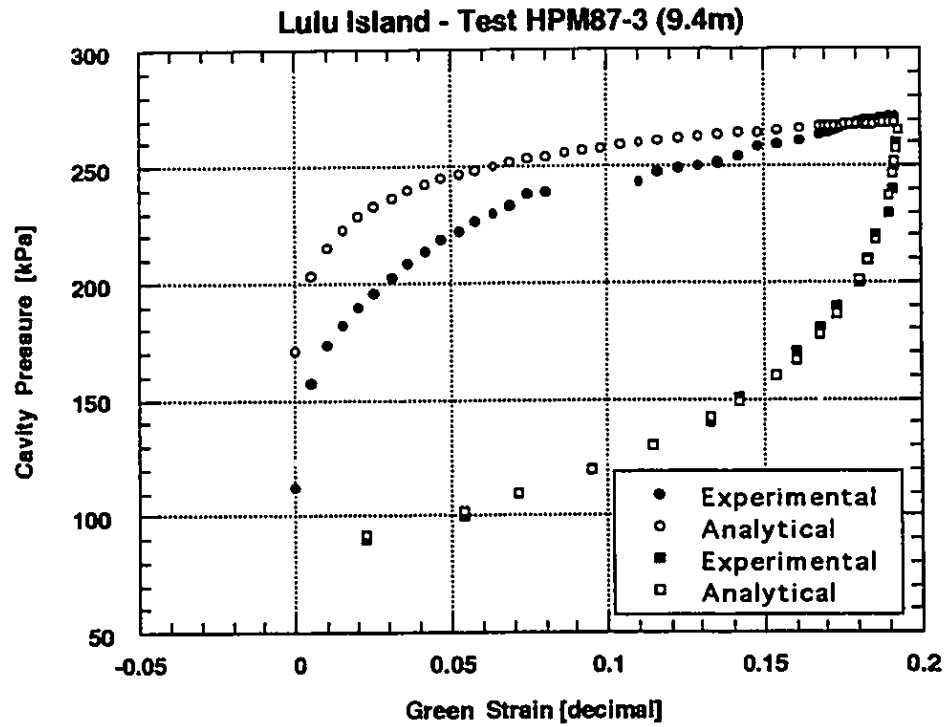


**Figure 5.13 Lulu Island - Test HPM87 - 3 Large strain equations: Final plot.**

## PRESSUREMETER INTERPRETATION TEMPLATE - CLAYS

TEST ID	Lulu Island - Test SCPM#1 (Large strain equations)		
DEPTH [m]	9.4	LIFT-OFF [kPa]	170.0
Loading :	$p_{max}$ [kPa] 279.0	$g_{max}$ [dec]	0.28416
Unloading :	$p_{max}$ [kPa] 279.0	$g_{max}$ [dec]	0.28416
<b>STEP # 1 - UNLOADING (Best fit with two parameters)</b>			
<b>(a) All unloading points</b>			
$\tau_{ult}^*$ = 34.3		Graph Page	Not shown
$2G_i$ = 2*9,707.4			
<b>(b) (some data points removed)</b>			
$\tau_{ult}^*$ = 39.2		Graph Page	Figure 5.15
$2G_i$ = 2*7,996.6			
<b>STEP # 2 - LOADING (Best fit with one parameter <math>R_\tau=2.0</math>)</b>			
<b>(a) All loading points</b>			
$\sigma_{ho}$ = 171.6		Graph Page	Not shown
<b>(b) Strain range (first option) Last half</b>			
$\sigma_{ho}$ = 178.9		Graph Page	Not shown
<b>(c) Strain range (second option) Last quarter</b>			
$\sigma_{ho}$ = 180.2		Graph Page	Not shown
<b>(d) Strain range (third option) Interpolate points at the very last end</b>			
$\sigma_{ho}$ = 180.3		Graph Page	Figure 5.15
<b>STEP # 3 - SUMMARY</b>			
<b>(a) First strain range selected: Step # 2 option (d)</b>			
$\tau_{ult}^*$ = 39.2	$\tau_{ult}$ = 19.6	Graph Page	Figure 5.15
$2G_i$ = 2*7,996.6	$\sigma_{ho}$ = 180.3		
<b>(b) Second strain range selected</b>			
$\tau_{ult}^*$ =	$\tau_{ult}$ =	Graph Page	
$2G_i$ =	$\sigma_{ho}$ =		

**Figure 5.14** Lulu Island - Test SCPM#1 (9.4m): Interpretation template using large strain pressuremeter analytical equations.

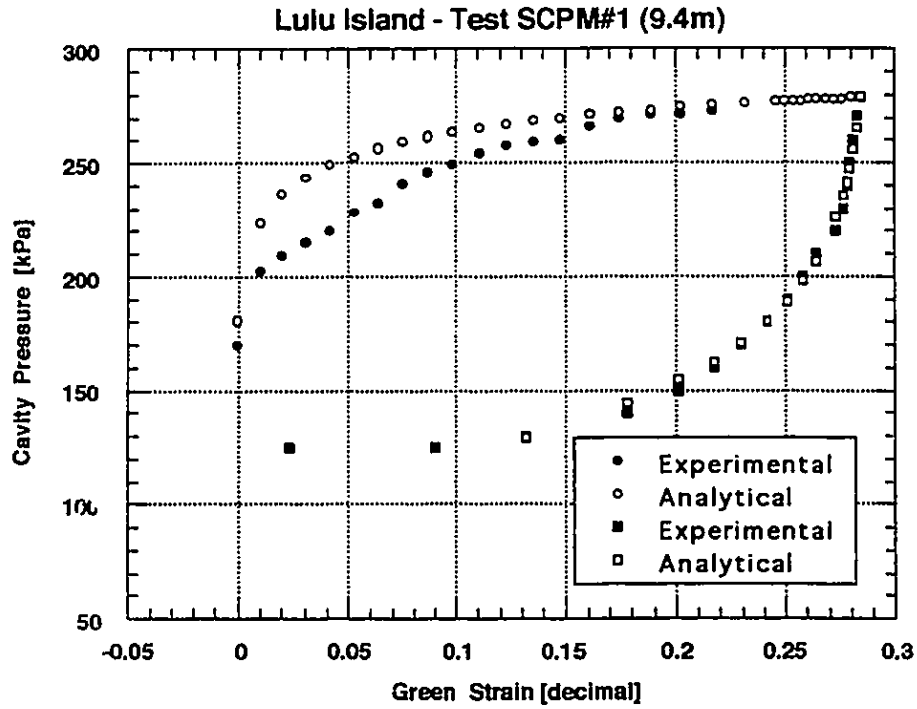


**Figure 5.15 Lulu Island - Test SCPM#1 - Large strain equations: Final plot.**

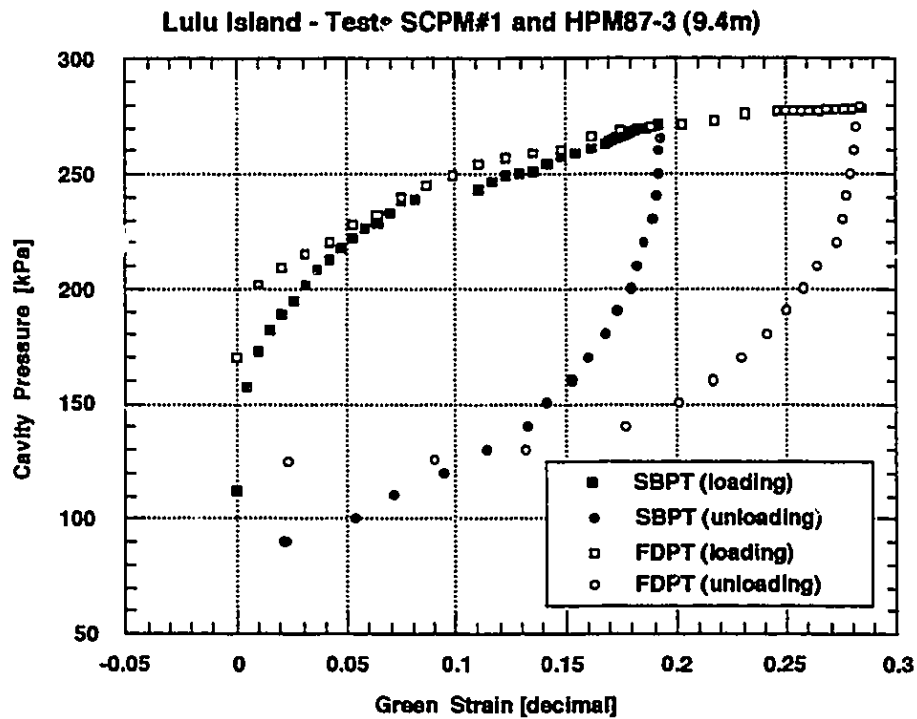


**Figure 5.16 Lulu Island - Howie (1991): Comparison between SBPT and FDPT original curves**

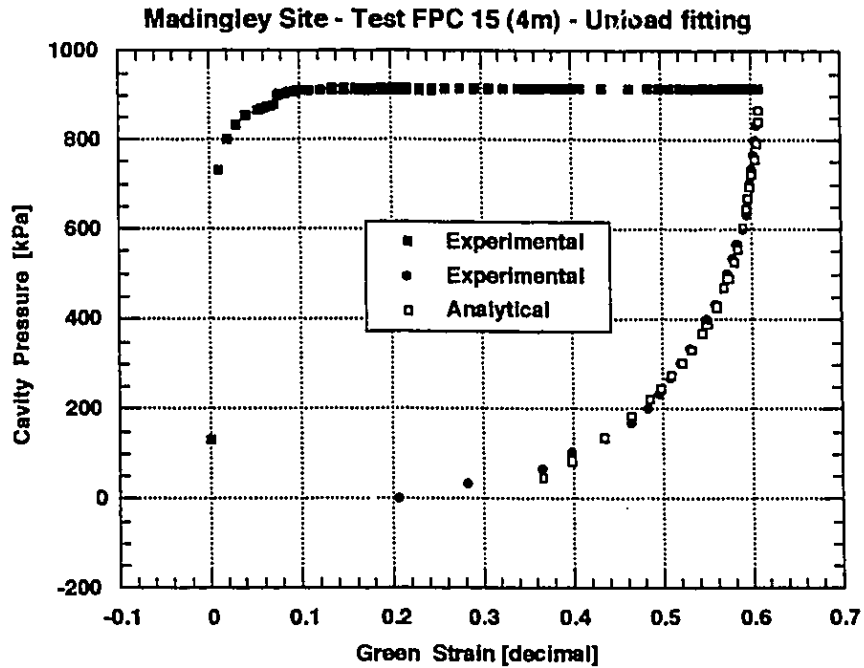


**Figure 5.17** Madingley Site - Test FPC15 (4m): Curve fitting of the unload phase of the test.

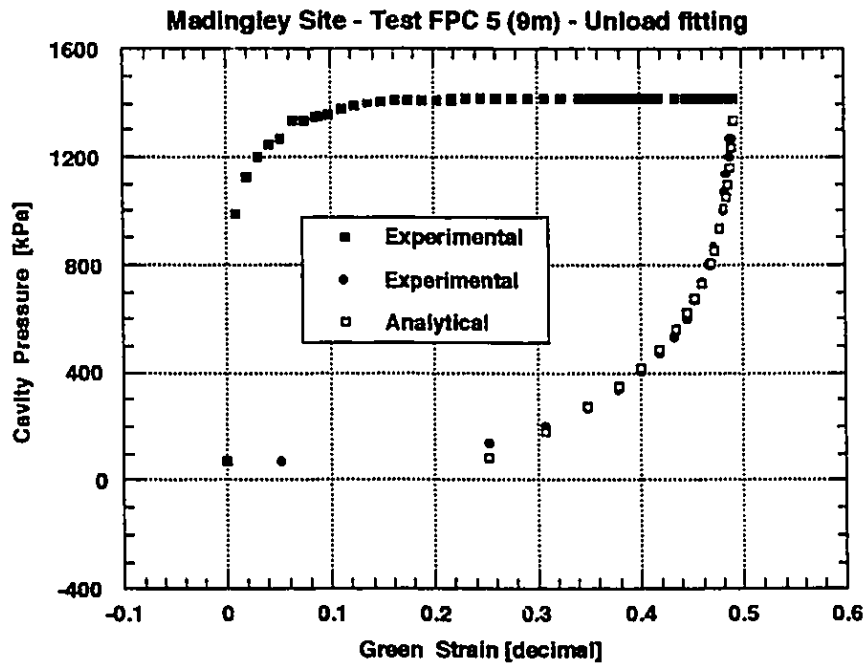


**Figure 5.18** Madingley Site - Test FPC5 (9m): Curve fitting of the unload phase of the test.

**CHAPTER 6****INTERPRETATION OF DRAINED SELF-BORING PRESSUREMETER RESULTS****6.1 Introduction**

One important assumption considered in the derivation of the pressuremeter analytical equations in Chapters 4 and 5 was the undrained response of the soil during pressuremeter expansion and contraction. The consequence of such soil behaviour was no volumetric change within the soil medium during the test. In addition, the mean normal stress was considered to remain constant before the stress path reached the undrained strength envelope. The radial and circumferential strain increments, measured in cylindrical coordinates, had opposite directions and a pure shear condition was achieved. The closed form solution for the undrained problem was developed and basic soil parameters were derived using a curve fitting technique. The interpreted results were promising and additional validation may confirm the applicability of this simple and ready to use methodology to geotechnical design.

The problem now is to deal with drained soil response. The immediate question that appears is: Is the philosophy of interpretation used for undrained tests adequate to analyze drained tests? The drained response has additional variables, which must be accounted for, such as volumetric strain and change of the mean normal stress. Moreover, the problem is no longer pure shearing.

Although drained response is typical of sandy material, a pressuremeter test is considered drained or undrained depending on the test speed. Even clayey soils would show a drained response if the test was performed with no increase in pore water pressure. However, it is common to group the natural soil response into two types: (a) undrained response; and (b) drained response. The former occurs if no drainage is considered during the test and the mobilized soil strength is cohesive (undrained shear strength). On the other hand, drained response occurs when the pore water is free to move

within the soil voids and the mobilized strength is based on the friction of soil particles (friction angle).

For drained pressuremeter tests the soil response is no longer dependent only on the material strength and deformation properties. Another physical response has to be considered - the material volumetric change. When the pressuremeter cell is expanded during a drained test, the total volumetric change has two components: (a) compressibility due to the normal stress increase, and (b) dilation or contraction due to the shearing process. For medium to dense sands the first component is smaller than the second component and is commonly not considered in the calculations. For loose sands, the compressibility and the contraction during shear result in volume reduction, which makes it difficult to separate them. In this case, the contraction during shear is considered to be responsible for all the volumetric change during the pressuremeter test.

The change in the soil volume during shear is called dilatancy and the magnitude of this property is expressed by the angle of dilation. Conventionally, in Soil Mechanics, the positive dilation angle means expansion and is characteristic of medium to dense sands. Negative dilation angle means contractive behaviour during shear and is typical of loose sands. When dealing with drained pressuremeter tests the consideration of volume change is mandatory. Baguelin et al (1978) presented a table showing the error in the estimated friction angle if properties such as sensitivity (strength reduction after peak), compressibility and dilatancy are not considered during the calculations. While omission of sensitivity and compressibility cause a fairly small underestimation of the friction angle in loose deposits, omission of dilatant response greatly overestimates the friction angle for dense sands. If dilatancy is not considered during the interpretation of pressuremeter tests in loose deposits, the friction angle is underestimated (Mair and Wood, 1987).

The main objective of this chapter is to verify the adequacy of the philosophy of interpretation used for undrained tests to analyze drained tests. Hyperbolic constitutive law and a linear volumetric strain relationship will be considered for this purpose. The Mohr-Coulomb failure criterion will be used to define the

relationship between shear and normal stresses.

## **6.2 Previous interpretation methods**

The interpretation of drained pressuremeter tests has been the subject of research since the early 60's. Chapter 2 presented an overview on the previous work on pressuremeter data interpretation. The following methodologies related to drained tests were presented:

- (a) Gibson and Anderson (1961);
- (b) Ladanyi (1963);
- (c) Vesic (1972);
- (d) Wroth and Windle (1975);
- (e) Hughes et al (1977);
- (f) Houlsby et al (1986);
- (g) Manassero (1989); and
- (h) Juran and Mahmoodzadegan (1989) method.

The first four methods have not been popularly used because they present some important weaknesses. The Gibson and Anderson (1961) method does not consider the volumetric change of the soil surrounding the pressuremeter during a drained test. The Ladanyi (1963) method extended one step further the Gibson and Anderson (1961) method considering the volumetric changes that occur in granular materials prior to failure. No assumption about the soil stress-strain relationship was made. The pressuremeter analytical equation derived includes another variable - the soil volumetric change before failure. However, if the material behaves elastically before failure, the volumetric change will be very small. In this case, the analysis becomes similar to Gibson and Anderson (1961) method. The Vesic (1972) method requires laboratory tests to evaluate the average volumetric strain at failure with a confining stress that corresponds to the depth of the pressuremeter test. In addition, the iterative process is complicated and cumbersome to apply. The Wroth and Windle (1975) method does not show how to derive the sand parameters from drained pressuremeter tests.

The fifth method is the most popularly used to derive the friction and dilation angles from drained pressuremeter tests. The Hughes et al (1977) method assumes the soil response is rigid-perfectly plastic and volumetric changes

are linear with shear strain. The Hughes et al (1977) method requires that the pressuremeter data be plotted using bi-logarithmic axis scales. The straight line obtained has its slope dependent on the friction and dilation angles. If the constant volume friction angle is pre-determined, Rowe's dilatancy law can be used to calculate the peak friction angle and the dilation angle. This method can only be used for good quality pressuremeter tests, where disturbance during pressuremeter installation is minimum. Data from disturbed tests may not yield the straight line in the log-log plot. In addition, values of the friction angle determined from SBPT data using this methodology have been shown to be higher than those determined from other tests (Mair and Wood, 1987). The possible reason for this finding could be the differences in the test deformation modes and the presence of a disturbed annulus formed around the pressuremeter during the equipment insertion.

The Houlsby et al (1986) method considered, for the first time, the use of the unloading pressuremeter curve in the soil parameters' derivation procedure. The Houlsby et al (1986) method assumes a linear elastic perfectly plastic soil response and linear volumetric changes with shear strain. For SBPT, the unloading portion of the test can be regarded as important as the loading portion. Chapters 4 and 5 considered this statement for undrained pressuremeter tests. However, for drained tests the static pore water pressure and the arching phenomenon make the unloading portion of the test difficult to reproduce analytically. It has been observed that SBPT's in clean saturated sands show a well-defined closing pressure during unloading. This closing pressure is generally equal to the static pore pressure around the probe. The sand appears to arch during unloading and the static water pressure pushes the membrane to the closed position.

The Manassero (1989) method uses a numerical procedure that does not require any pre-definition of the soil stress-strain relationship followed during the pressuremeter expansion. Instead, this constitutive law is derived from the SBPT loading curve. A polynomial function must be fitted to the experimental loading data so that the derived stress-strain law is not affected by the scattering of the experimental data during the numerical calculations. This method can only be used in good quality SBPT data.

The Juran and Mahmoodzadegan (1989) method is also based on a numerical incrementally determined solution for the pressuremeter problem.



Soil plasticity and cavity expansion theories are used for this purpose. The method requires the calculation of the experimental curve slope and, therefore, is subjected to the scattering of the experimental data. In addition, the method was validated using a miniature pressuremeter prototype in sand sample within laboratory triaxial cells. No in situ tests were interpreted using this method. The requirement of the soil volumetric strain behaviour known in advance constitutes another important weakness of this method. Furthermore, only undisturbed tests can be interpreted to yield the sand parameters.

A conclusion that can be drawn from these interpretation methods is that besides the experimental pressuremeter data some information on the soil volumetric response must be provided to derive the sand parameters. The mathematical treatment of the problem is very complex and a closed form solution for the pressuremeter problem has been developed just for the simple elastic perfectly plastic model.

### **6.3 Soil models for drained response**

Dealing with soil modeling and in particular with sand modeling, it is worthwhile to recall some essential statements presented by Drucker (1987):

- (a) The modeling of material properties is governed as much by the problem to be solved as by the actual properties of the material;
- (b) Simple models are needed to obtain useful understandable answers to complex problems;
- (c) Materials are essentially infinitely complex in their inelastic response;
- (d) Be sure to include in the framework of any model the well-known qualitative aspects of the material behaviour that clearly are important to the problem to be solved; and
- (e) If the material model captures just the essence of the physical behaviour of importance in your problem, you have done exceedingly well.'

With these principles in mind and knowing that the interpretation of a drained

pressuremeter test is more complex and less developed than undrained tests (Mair and Wood, 1987; Baguelin et al, 1978) a solution for drained SBPT will be developed, modeling the material nonlinear behaviour with a hyperbolic law and accounting for material volumetric changes with a linear relationship. Because of the reasons presented in the previous section, only the loading stage of the test will be considered in the derivations.

### 6.3.1 Elastic perfectly plastic model

The representation of the soil stress-strain relationship by an elastic perfectly plastic response was the most frequently used in the past to solve the pressuremeter problem. Gibson and Anderson (1961) derived analytical pressuremeter equations for the loading part of the test using the elastic perfectly plastic model and assuming that no volumetric strain would occur in the soil medium. Hughes et al (1977) and Coutinho (1990) used the rigid-plastic model to derive the soil friction angle. Hughes (1977) assumed a linear volumetric strain relationship. Houlsby et al (1986) analyzed the unloading curve of a pressuremeter test in sands also considering the elastic perfectly plastic response and assuming a linear volumetric strain rate.

The derivation presented in this work will follow the same approach as presented by Hughes et al (1977) and Houlsby et al (1986). However, the mathematics will be based on Wroth and Windle (1975). The only reason to include the elastic plastic modeling in this work is to provide a basis for comparison of the elastic perfectly plastic response with the hyperbolic response. Figure 6.1 (a) shows the elastic plastic representation of the normalized shear stress versus the engineering shear strain.

### 6.3.2 Hyperbolic model

The hyperbolic representation of the drained behaviour of the soil was selected for the same reasons as presented for the undrained soil response (Chapter 4 section 4.3.2). However, for the drained response there is no longer a unique shear stress curve to describe the soil stress-strain relationship. Instead, there is a family of shear curves, each one being a

function of the effective mean normal stress which changes throughout the pressuremeter test. During the pressuremeter expansion and contraction stages there is a movement from one curve to another depending on the level of the mean normal stress reached. Figure 6.1 (b) shows an idealized representation of the shear stress versus cavity strain relationship with four levels of mean normal stress. In order to avoid this jumping from one shear curve to another curve, the current shear stress can be normalized by the respective effective mean normal stress. Hence, a unique hyperbolic curve will be considered to govern the loading part of the pressuremeter test. Figure 6.1 (b) shows the unique hyperbolic curve followed by a soil particle during the loading phase of the SBPT.

#### **6.4 Pressuremeter analytical equations for elastic perfectly plastic soil response**

##### **6.4.1 Assumptions**

The derivation of the pressuremeter equations considers the following assumptions:

- (1) The pressuremeter test is performed drained during the loading phase;
- (2) The test is treated as an expansion of an infinitely long cylindrical cavity (i.e. radially symmetric and plane strain);
- (3) The vertical stress remains the intermediate principal stress during the test;
- (4) The soil is homogeneous, isotropic and elastic during the early part of the pressuremeter expansion;
- (5) The soil becomes perfectly plastic, with constant friction angle, after the failure criterion is reached;
- (6) The strains are considered to be small.

##### **6.4.2 Derivation of the pressuremeter analytical equations**

###### **• Sign convention**

Compressive normal strains and compressive normal stresses are positive. Volumetric strains are positive when contraction takes place (decreasing in

soil volume).

• Normal strain definition

For pressuremeter testing the circumferential strain ( $\varepsilon_\theta$ ) is often replaced by the cavity strain ( $\varepsilon$ ). The relationship between the circumferential (hoop) strain and the cavity strain is:

$$\varepsilon = -\varepsilon_\theta \text{-----(6.1)}$$

The cavity strain is defined as the ratio between the change in pressuremeter radius (radial displacement at the cavity wall) and the initial pressuremeter radius. According to the sign convention the cavity strain is defined as follows:

$$\varepsilon = \frac{\Delta R}{R_0} \text{-----(6.2)}$$

• Volumetric strain definition

A linear relationship is considered between the volumetric and the cavity strains. According to the sign convention the definition is:

$$\varepsilon_v = -\frac{\Delta V}{V_0} = -s_v \varepsilon \text{-----(6.3)}$$

where:  $\varepsilon_v$  - soil volumetric strain  
 $\Delta V = V - V_0$  - change in soil volume  
 $s_v$  - slope of the volumetric strain relationship

The parameter  $s_v$  is positive during dilation and negative during contraction. Figures 6.2 (a) and (b) show respectively the idealized volumetric strain relationship in terms of the engineering shear strain and the assumed relationship in terms of the cavity strain. Notice that the positive ordinate axis is pointing downwards and the negative sign is necessary to maintain consistency with the volumetric strain sign convention. Wroth and Windle (1975) used the same linear volumetric strain relationship presented in equation (6.3). Using the dilation angle definition ( $\nu$ ), the volumetric strain is defined as follows:

$$d\varepsilon_v = d\left(-\frac{\Delta V}{V_0}\right) = -\sin\nu d\gamma \text{-----(6.4)}$$

where:  $\nu$  - dilation angle

The dilation angle is the soil property most commonly used to express the soil tendency to dilate or contract during the shearing process. Using Rowe's dilatancy law (Rowe, 1962 and 1972) a relationship between the peak friction

angle, the dilation angle, and the constant volume friction angle can be derived (Manassero, 1989; Baguelin et al, 1978; Hughes et al, 1977; Mair and Wood, 1987). The positive dilation angle means that the sand tends to dilate during shear, and the negative dilation angle means that the sand tends to contract during shear. If the sand sample is dilative at failure the mobilized friction angle at failure is bigger than the constant volume friction angle. No volumetric strain is expected if the dilation angle is zero.

- Constitutive relationship

The stress-strain relationship used to represent the elastic perfectly plastic model is defined in terms of the stress ratio ( $t/s$ ) and the engineering shear strain ( $\gamma$ ). For elastic expansion the relationship is:

$$t/s = S \gamma \text{ -----(6.5)}$$

where:  $t/s$  - stress ratio

$S$  - slope of the stress-strain law

$t = \frac{\sigma_1 - \sigma_3}{2}$  - maximum shear stress

$s = \frac{\sigma_1' + \sigma_3'}{2}$  - effective normal stress average

For plastic expansion the stress-strain relationship is:

$$t/s = \text{constant} = \sin \phi' \text{ -----(6.6)}$$

where:  $\phi'$  - peak friction angle

- Boundary conditions at the cavity wall

For elastic expansion, the essential boundary condition in terms of cavity strain is:

$$\varepsilon = 0 \Rightarrow \sigma_r' = \sigma_{ho}' \text{ -----(6.7)}$$

For plastic expansion, the boundary condition at the beginning of the plastic response is:

$$\varepsilon = \varepsilon_{EL} \Rightarrow \sigma_r' = \sigma_{rEL}' \text{ -----(6.8)}$$

where the subscript 'EL' represents the end of the elastic phase.

- Pressuremeter analytical equation during the elastic loading

Assuming pure shear, there is no volumetric strain during the linear elastic response, implying that the mean normal stress remains constant. The

constitutive relationship, equation (6.5), can be used to yield the following relationship between the circumferential and radial stresses:

$$\sigma'_\theta = \sigma'_r \left( \frac{1 - 2S\varepsilon}{1 + 2S\varepsilon} \right) \text{-----}(6.9)$$

The equilibrium equation in terms of the effective stresses is:

$$\frac{d\sigma'_r}{dr} + \frac{\sigma'_r - \sigma'_\theta}{r} = 0 \text{-----}(6.10)$$

For no volumetric strain, Wroth and Windle (1975) presented the following relationship between the strain at any point and the radial coordinate:

$$-\frac{dr}{r} = \frac{d\varepsilon}{\varepsilon(1 + \varepsilon)(2 + \varepsilon)} \text{-----}(6.11)$$

Combining equations (6.9), (6.10), (6.11) and neglecting the high order cavity strain terms ( $\varepsilon^2$  and higher) the following differential equation is obtained:

$$\frac{d\sigma'_r}{\sigma'_r} = S d\varepsilon \text{-----}(6.12)$$

Equation (6.12) is valid for any radial coordinate. At the cavity wall the solution of the differential equation yields the pressuremeter analytical equation for elastic loading:

$$p' = \sigma'_{ho} e^{S\varepsilon} \text{-----}(6.13)$$

where 'e' is the basis of the natural logarithm.

Equation (6.13) is valid only within the elastic strain range. Using the Mohr-Coulomb failure criterion the strain at the end of the elastic phase can be determined by the following equation:

$$\varepsilon_{EL} = \frac{\ln\left(\frac{2}{N+1}\right)}{S} \text{-----}(6.14)$$

where:  $N = \frac{1 - \sin\phi'}{1 + \sin\phi'}$  - friction angle parameter

Equations (6.13) and (6.14) can be used to simulate the pressuremeter curve within the elastic range.

- Pressuremeter analytical equation during plastic loading

The consideration of plastic response of cohesionless soils implies in consideration of volumetric strains. In this study the simplest volumetric strain law will be used, which is the linear relationship between the volumetric strain and the engineering shear strain, passing through the origin of the coordinate

system (Hughes et al, 1977).

$$-\varepsilon_v = \gamma \sin \nu \text{ -----(6.15)}$$

A relationship between radial strain and cavity strain can be derived from equation (6.15) to yield:

$$\frac{\varepsilon_r}{\varepsilon} = n \text{ -----(6.16)}$$

where:  $n = \frac{1 - \sin \nu}{1 + \sin \nu}$  - dilation angle parameter

For perfect-plastic material the stress ratio ( $t/s$ ) is constant. Hence, the relationship between radial and circumferential effective stresses is:

$$\frac{\sigma'_r}{\sigma'_\theta} = \frac{1 + \sin \phi'}{1 - \sin \phi'} = \frac{1}{N} \text{ -----(6.17)}$$

Wroth and Windle (1975) presented a relationship between the cavity strain ( $\varepsilon$ ) and the radial coordinate ( $r$ ) when volumetric strain occurs according to equation (6.3). The equation is:

$$-\frac{dr}{r} = \frac{(1 + s_v \varepsilon) d\varepsilon}{\varepsilon(1 + \varepsilon)(2 + \varepsilon - s_v)} \text{ -----(6.18)}$$

Combining equations (6.16), (6.15), and (6.3) the following relation is obtained (Wroth and Windle, 1975):

$$s_v = \frac{2 \sin \nu}{1 + \sin \nu} = 1 - n \text{ -----(6.19)}$$

Combining equations (6.10), (6.18), and (6.19) and neglecting the high order cavity strain terms ( $\varepsilon^2$  and higher), the following differential equation is obtained:

$$\frac{d\sigma'_r}{\sigma'_r} = \frac{1 - N}{1 + n} \cdot \frac{d\varepsilon}{\varepsilon} + \frac{1 - N}{1 + n} \cdot d\varepsilon - \frac{n(1 - N)}{1 + n} \cdot d\varepsilon \text{ -----(6.20)}$$

The integration process requires the appropriate boundary condition defined by equation (6.8), which now has the following form:

$$\varepsilon_{EL} = \frac{\ln\left(\frac{2}{N+1}\right)}{S} \Rightarrow \sigma'_{rEL} = \sigma'_{ho} e^{1n(2/(N+1))} \text{ -----(6.21)}$$

Equation (6.20) is valid for any radial coordinate. At the cavity wall the solution of the differential equation yields the pressuremeter analytical equation for plastic loading:

$$p' = \sigma'_{ho} e^{1n(2/(N+1))} \cdot \left[ \frac{S\varepsilon}{\ln(2/(N+1))} \right]^{\left(\frac{1-N}{1+n}\right)} \cdot e^{\frac{(1-n)(1-N)}{S(1+n)}(S\varepsilon - 1n(2/(N+1)))} \text{ -----(6.22)}$$

where 'e' is the basis of the natural logarithm.

Equation (6.22) can be used to simulate the pressuremeter curve within the plastic strain range.

### 6.4.3 Interpretation of model parameters

To simulate the complete pressuremeter loading curve, four parameters are necessary: (a) the initial effective horizontal stress ( $\sigma'_{ho}$ ); (b) the slope of the stress-strain relationship ( $S$ ); (c) the friction angle parameter ( $N$ ); and (d) the constant volume friction angle ( $\phi'_{CV}$ ). The friction angle parameter ( $N$ ) and the dilation angle parameter ( $v$ ) are related through Rowe's dilatancy law (Rowe, 1962 and 1972) using the constant volume friction angle ( $\phi'_{CV}$ ). Further information on the constant volume friction angle will be presented later in this chapter.

The soil parameters derived from this analysis are: (a) the initial effective horizontal stress ( $\sigma'_{ho}$ ); (b) the peak friction angle ( $\phi'$ ); (c) the elastic shear modulus ( $G$ ); and (d) the dilation angle ( $v$ ).

#### • Elastic shear modulus ( $G$ )

The equivalent elastic shear modulus is determined from the slope of the stress-strain relationship ( $S$ ). The relation between  $G$  and  $S$  is (Juran and Mahmoodzadegan, 1989):

$$G = S\sigma'_{ho} \text{-----(6.23)}$$

#### • Peak friction angle ( $\phi'$ )

The peak friction angle is determined from the friction angle parameter ( $N$ ). The relationship between  $\phi'$  and  $N$  is:

$$\phi' = \sin^{-1}\left(\frac{1-N}{1+N}\right) \text{-----(6.24)}$$

#### • Dilation angle ( $v$ )

The dilation angle is determined from the peak friction angle and the constant volume friction angle using the Rowe's dilatancy law. The relationship is:

$$v = \sin^{-1}\left(\frac{K_A^{CV} - N}{K_A^{CV} + N}\right) \text{-----(6.25)}$$



where:  $K_A^{CV} = \frac{1 - \sin\phi'_{CV}}{1 + \sin\phi'_{CV}}$  - constant volume friction angle parameter

#### 6.4.4 Proposed methodology to interpret drained SBPT data

Equations (6.13), (6.14), and (6.22) can be used to derive the soil parameters from a drained SBPT data. The procedure assumes that the early portion of the loading pressuremeter curve does not represent the natural soil response because of the inevitable disturbance during pressuremeter insertion. If the test has been performed with no disturbance, a good curve matching over the entire loading range is expected. For elastic perfectly plastic model, where three equations are necessary to completely simulate the loading pressuremeter curve, the procedure of guessing the soil parameters and visually matching the analytical curve to the experimental curve may be adequate. The soil parameters that give the best match are inferred to be the actual soil parameters. The following steps are necessary to do the interpretation:

- (1) Copy the experimental pressuremeter loading data to a spreadsheet. The pressure must be corrected for the membrane stiffness (calibration phase). Since the analysis is performed in terms of effective stress, the static pore water pressure must be known and subtracted from the total pressure measured during the test. The cavity strain, defined by equation (6.2), is the commonly used to define the pressuremeter strains;
- (2) Guess a set of soil parameters ( $\sigma'_{ho}$ ,  $\phi'$ ,  $\phi'_{CV}$  or  $\nu$ , and  $G$ );
- (3) Calculate the model parameters ( $\sigma'_{ho}$ ,  $N$ ,  $S$ , and  $n$ );
- (4) Calculate the end of the elastic loading using equation (6.14);
- (5) Determine the analytical pressuremeter curve for the elastic strain range  $[0, \varepsilon_{EL}]$  using equation (6.13). For medium to compact sands this range is rather small;
- (6) Determine the analytical pressuremeter curve for the plastic strain range  $[\varepsilon_{EL}, \varepsilon_{max}]$  using equation (6.22). The maximum cavity strain during the loading phase of the pressuremeter test is called  $\varepsilon_{max}$ ;
- (7) Plot the experimental and the analytical curves together in the same graph. If the matching is visually acceptable the guessed set of soil parameters can be considered to represent the actual soil parameters. If

the matching is unacceptable, go back to step 2 for another trial.

The curve matching is considered acceptable if at least the last loading points of the experimental curve coincide with the last points of the analytical curve. Considering the subjectivity of this method, additional information on the soil tested may be necessary to ensure that the derived parameters can in fact represent the in situ material. For instance, the unload-reload shear modulus can be used to indicate the magnitude of the soil shear modulus. A small computer code can be developed to speed up the calculations and plotting although this is not essential for the proposed method. This methodology will be used to interpret SBPT's in sands.

#### 6.4.5 Comments on the elastic perfectly plastic model

- The existence of three equations (two for pressure and one for strain) precludes the use of a curve fitting technique to reach a better match between the experimental and the analytical curves. However, an alternative procedure exists. In most situations the initial portion of the experimental loading curve will not match the initial portion of the analytical loading curve because of the disturbance during insertion. Hence, in such case, the elastic loading curve can be discarded and the plastic equation can be used with a curve fitting technique to determine the model parameters that give the best matching. The least square error is a commonly used curve fitting technique. The equation (6.22) must be modified to include the relationship between the friction angle parameter ( $N$ ) and the dilation angle parameter ( $n$ ) through Rowe's dilatancy law. This equation is:

$$n = \frac{N}{K_A^{CV}} \text{-----(6.26)}$$

The constant volume friction angle must be determined or estimated in advance as suggested by Hughes et al (1977), Houlsby et al (1986), Manassero (1989).

- The equivalent elastic shear modulus derived in this manner is meaningless to geotechnical design, since the elastic strain range determined is unrealistically large. Therefore, the elastic shear modulus is underestimated

when the soil response is modeled elastically-perfectly plastically. To overcome this problem, the unload-reload shear modulus corrected for stress level (Robertson, 1982) can be used in conjunction with the elastic plastic model.

## **6.5 Pressuremeter analytical equation for hyperbolic soil response**

### **6.5.1 Assumptions**

The derivation of the pressuremeter equation based on the hyperbolic model considers the following assumptions:

- (1) The pressuremeter test is performed drained during the loading phase;
- (2) The test is treated as an expansion of an infinitely long cylindrical cavity (i.e. radially symmetric and plane strain);
- (3) The vertical stress remains the intermediate principal stress during the test;
- (4) The soil stress-strain response during loading can be represented by a hyperbolic function;
- (5) The strains are considered to be small.

Most of these assumptions were also considered by other methods to interpret drained pressuremeter tests, the hyperbolic constitutive law being the only exception.

### **6.5.2 Derivation of the pressuremeter analytical loading equation**

- **Sign convention**

The sign convention is the same as presented in section 6.4.2.

- **Normal strain definition**

The definition of the normal strain is the same as presented in section 6.4.2.

- **Volumetric strain definition**

The definition of the volumetric strain is the same as presented in section 6.4.2.

• Constitutive relationship

The stress-strain relationship is defined in terms of stress ratio ( $t/s$ ) as function of the cavity strain ( $\epsilon$ ):

$$\frac{t}{s} = \frac{\epsilon}{S_i + \frac{\epsilon}{(t/s)_{ult}}} \text{-----(6.27)}$$

where:  $\frac{t}{s} = \frac{\sigma_1 - \sigma_3}{\sigma_1 + \sigma_3}$  - mobilized stress ratio  
 $S_i$  - initial tangent slope of the hyperbolic model  
 $(t/s)_{ult}$  - ultimate stress ratio during loading

As said before, if just the mobilized shear strength is taken as a function of the cavity strain, there will be a family of hyperbolic curves and the one followed by a soil particle during loading will depend on the level of the effective mean normal stress ( $\sigma'_m$ ) acting on the soil during the test. The effective mean normal stress is defined as follows:

$$\sigma'_m = \frac{\sigma'_1 + \sigma'_2 + \sigma'_3}{3} = \frac{\sigma'_r + \sigma'_z + \sigma'_\theta}{3} \text{-----(6.28)}$$

where:  $\sigma'_m$  - effective mean normal stress  
 $\sigma'_{1,2,3}$  - effective principal stresses  
 $\sigma'_{r,z,\theta}$  - effective normal stresses

Hence, the actual value of the mobilized shear stress ( $\tau_{mob}$ ) is not only function of the cavity strain but also function of the effective mean normal stress. To overcome this complexity, a normalized shear stress is considered and the stress ratio ( $t/s$ ) is adopted to represent the unique stress-strain curve followed during the test. The shear stress is defined as the semi-difference between the major and the minor principal stresses, and the effective mean normal stress is defined as the arithmetic average between the major and the minor effective principal stresses. Figures 6.3 (a) and (b) show, respectively, the idealized representation of the hyperbolic constitutive law and the variation of the average effective normal stress ( $s$ ) with cavity strain during a pressuremeter loading test.

• Boundary condition at the cavity wall

$$\epsilon = 0 \Rightarrow \sigma'_r = \sigma'_{ho} \text{-----(6.29)}$$

• Pressuremeter analytical equation during loading

The relationship between the effective radial and circumferential stresses can be derived from the stress ratio ( $t/s$ ) as follows:

$$\frac{\sigma'_r}{\sigma'_\theta} = \frac{1+t/s}{1-t/s} = \frac{1+\sin\phi'}{1-\sin\phi'} = \frac{1}{N(\varepsilon)} \quad \text{-----(6.30)}$$

where:  $N(\varepsilon)$  - friction angle parameter as a function of cavity strain

The function  $N(\varepsilon)$  is defined based on the hyperbolic stress-strain relationship as follows:

$$N(\varepsilon) = \frac{1/S_i + \varepsilon/(t/s)_{ult} - \varepsilon}{1/S_i + \varepsilon/(t/s)_{ult} + \varepsilon} \quad \text{-----(6.31)}$$

From the equilibrium equation (6.10) and the effective radial and circumferential stress ratio (equation (6.30)), the following differential equation is obtained:

$$\frac{d\sigma'_r}{\sigma'_r} = -\frac{dr}{r}(1-N(\varepsilon)) \quad \text{-----(6.32)}$$

Equations (6.18) and (6.19), used in section 6.4.2, are also valid for the hyperbolic model. Combining equations (6.31) and (6.32) with equations (6.18) and (6.19) and neglecting the high order cavity strain terms ( $\varepsilon^2$  and higher), the following differential equation is obtained:

$$\frac{d\sigma'_r}{\sigma'_r} = \frac{2}{1+n} \cdot \frac{d\varepsilon}{1/S_i + \varepsilon/(t/s)_{ult} + \varepsilon} + \frac{2(1-n)}{1+n} \cdot \frac{\varepsilon d\varepsilon}{1/S_i + \varepsilon/(t/s)_{ult} + \varepsilon} \quad \text{-----(6.33)}$$

The dilation angle parameter ( $n$ ) is considered to be constant throughout the loading expansion because of the simplified volumetric strain relationship. In addition, parameter  $n$  is related to the friction angle parameter ( $N$ ) through the Rowe's dilatancy law presented in equation (6.26). Hence, the constant value of  $n$  can be determined using the ultimate value of the stress ratio ( $(t/s)_{ult}$ ), as follows:

$$n = \frac{1 - (t/s)_{ult}}{K_A^{CV} (1 + (t/s)_{ult})} \quad \text{-----(6.34)}$$

Integrating equation (6.33) with the pre-defined boundary condition presented in equation (6.29), and replacing the value of  $n$  by equation (6.34), the final pressuremeter analytical loading equation is obtained as follows:

$$p' = \sigma'_{ho} \cdot \left[ 1 + \left( \frac{1 + (t/s)_{ult}}{(t/s)_{ult}} \right) \cdot S_i \varepsilon \right]^4 \cdot e^B \text{-----(6.35)}$$

where:

$$A = \frac{2S_i \left( \frac{1 + (t/s)_{ult}}{(t/s)_{ult}} \right) - 2 \left( 1 - \frac{1 - (t/s)_{ult}}{K_A^{CV} (1 + (t/s)_{ult})} \right)}{S_i \left( \frac{1 + (t/s)_{ult}}{(t/s)_{ult}} \right)^2 \cdot \left( 1 + \frac{1 - (t/s)_{ult}}{K_A^{CV} (1 + (t/s)_{ult})} \right)}$$

$$B = \frac{2 \left( 1 - \frac{1 - (t/s)_{ult}}{K_A^{CV} (1 + (t/s)_{ult})} \right) \varepsilon}{\left( \frac{1 + (t/s)_{ult}}{(t/s)_{ult}} \right) \cdot \left( 1 + \frac{1 - (t/s)_{ult}}{K_A^{CV} (1 + (t/s)_{ult})} \right)}$$

where 'e' is the basis of the natural logarithm. Equation (6.35) is the pressuremeter analytical loading equation and is valid for the entire pressuremeter loading curve.

### 6.5.3 Interpretation of the model parameters

The complete loading simulation of a drained pressuremeter test depends on four parameters: (a) the initial tangent slope of the hyperbolic relationship ( $S_i$ ); (b) the ultimate ratio of the hyperbolic relationship during loading ( $(t/s)_{ult}$ ); (c) the initial effective horizontal stress ( $\sigma'_{ho}$ ); and (d) the constant volume friction angle parameter ( $K_A^{CV}$ ). In order to simplify the interpretation procedure, the constant volume friction angle parameter is assumed to be known. Additional information on the constant volume friction angle will be presented later in this chapter.

The soil parameters derived from this analysis are: (a) the initial tangent shear modulus ( $G_i$ ); (b) the ultimate friction angle ( $\phi'_{ult}$ ); (c) the dilation angle ( $\nu$ ); and (d) the initial effective horizontal stress ( $\sigma'_{ho}$ ).

- Initial tangent shear modulus ( $G_i$ )

The initial tangent shear modulus is determined from the initial tangent slope of the hyperbolic relationship ( $S_i$ ). A comparison between the  $t/s$  versus  $\varepsilon$

hyperbolic curve and the  $t/s$  versus  $\gamma$  hyperbolic curve yields the following relationship:

$$G_i = \frac{S_i \sigma'_{ho}}{2 - s_v} \text{-----(6.36)}$$

- Ultimate, mobilized and peak friction angle ( $\phi'_{ult}$ ,  $\phi'_{mob}$ ,  $\phi'$ )

Using the Mohr-Coulomb failure criterion the following relationship can be derived:

$$\phi'_{ult} = \sin^{-1}(t/s)_{ult} \text{-----(6.37)}$$

At any level of strain the mobilized stress ratio can be used to calculate the mobilized friction angle:

$$\phi'_{mob} = \sin^{-1}(t/s)_{mob} \text{-----(6.38)}$$

The maximum mobilized friction angle, called peak friction angle, can be calculated using the maximum mobilized stress ratio (equation (6.27) with  $\varepsilon = \varepsilon_{max}$ ):

$$\phi' = \sin^{-1}(t/s)_{max} \text{-----(6.39)}$$

- Dilation angle ( $\nu$ )

Rowe's dilatancy law is commonly used to calculate the dilation angle as long as the constant volume friction angle is known (Hughes et al, 1977; Robertson, 1982; Houlsby et al, 1986; Manassero, 1989).

$$\nu = \sin^{-1} \left( \frac{\left( K_A^{CV} - \frac{1 - \sin \phi'_{ult}}{1 + \sin \phi'_{ult}} \right)}{\left( K_A^{CV} + \frac{1 - \sin \phi'_{ult}}{1 + \sin \phi'_{ult}} \right)} \right) \text{-----(6.40)}$$

#### 6.5.4 Proposed methodology to interpret drained SBPT data

A philosophy of interpretation similar to that applied to undrained tests will be used to interpret drained tests. However, for drained tests just the loading phase of the test will be considered. Disturbance during pressuremeter insertion is also a concern when interpreting the loading portion of the SBPT. Granular materials are more susceptible to disturbance during pressuremeter installation than frictionless materials. Hence, like for clays, only the final part

of the loading curve can be fitted with the derived analytical equation. Equation (6.35) will be used to fit the last loading points of the SBPT data to yield three soil parameters: (a) the effective initial horizontal stress ( $\sigma'_{ho}$ ); (b) the ultimate friction angle ( $\phi'_{ult}$ ); and (c) the initial tangent shear modulus ( $G_i$ ).

The following steps are necessary to perform the interpretation:

- (1) Copy the experimental pressuremeter loading data to a spreadsheet. The pressure must be corrected for the membrane stiffness (calibration phase). Since the analysis is performed in terms of effective stress, the static pore water pressure must be known and subtracted from the total pressure measured during the test. The cavity strain, defined by equation (6.2), is commonly used to define the pressuremeter strains;
- (2) Assume a value for the constant volume friction angle and use the equation (6.35) to fit the loading points of the SBPT. Firstly, take all loading points. Afterwards, take the last half, last quarter and, finally, just the very last loading points. Linear interpolation can be used to add some more points at the end of the loading curve if the number of discrete points is smaller than 10. The reader is referred to section 4.3.5 if additional information on the curve fitting technique is needed;
- (3) For each portion of the loading curve a set of model parameters is determined by the curve fitting technique. Generally, the last quarter or the very last loading points will have the best curve fitting and, so, they will yield the set of model parameters more suitable to simulate the entire pressuremeter loading curve;
- (4) The soil parameters will be determined using the information presented in section 6.5.3.

This methodology will be used to interpret the SBPT in sands.

#### 6.5.5 Comments on the hyperbolic constitutive model

- The general idea for solving the problem of a drained pressuremeter test came from Chapter 4 where the solution for the undrained problem was developed. However, as explained before, the shear stress defined as the principal stress difference, no longer can be considered to reach an ultimate value due to the variation of the effective mean normal stress during the pressuremeter test. The shear stress increases continuously while the cell



pressure increases. Hence, a normalized shear stress was used with the hyperbolic model. If the pressure applied during the pressuremeter test is assumed to be the radial stress at the cavity wall, the complete stress path followed during the test depends on four parameters: (a) the initial hyperbolic slope ( $S_i$ ); (b) the ultimate value of the stress ratio ( $(t/s)_{ult}$ ); (c) the effective initial horizontal stress ( $\sigma'_{ho}$ ); and (d) the constant volume friction angle ( $\phi'_{CV}$ ).

To analyze the stress path followed by any soil element at the cavity wall during the loading phase of a drained pressuremeter test, the calibration chamber test 228 performed in Ticino sand was chosen as an example. Bellotti et al (1987) presented results of 48 SBPT's performed under strictly controlled boundary conditions on pluvially deposited Ticino and Hokksund sand samples in the calibration chamber at ENEL-CRIS (Milan, Italy). Test 228 was performed after a so called ideal installation, where the pressuremeter is placed inside the chamber before filling it with pluvially deposited sand. The reader is referred to Bellotti et al (1987) if additional information is necessary. Three unload-reload loops were performed during the loading phase of the test 228. The measured unload-reload shear modulus varied from 67,297 kPa to 77,793 kPa, depending on the stress level reached. The unload-reload shear modulus corrected for stress level varied from 64,621 kPa to 69,555 kPa. The maximum dynamic shear modulus determined from resonant column tests was reported to be 139,715 kPa. The peak friction angles were calculated based on three pressuremeter interpretation methodologies: (a) Hughes et al (1977); (b) Robertson and Hughes (1986); and (c) Manassero (1989). Assuming the value of  $34^\circ$  for the constant volume friction angle, the dilation angle was calculated using the Rowe's dilatancy law. The final parameters of Ticino sand determined from test 228 are presented in the following table:

Meth.	Hughes(77)		Robertson(86)		Manassero(89)		Average	
	$\phi'$	$v$	$\phi'$	$v$	$\phi'$	$v$	$\phi'$	$v$
228	41.9°	10°	44.3°	13.5°	43.9°	12.7°	43.4°	12.0°

In order to evaluate the initial slope of the hyperbolic relationship (equation (6.24)) the initial horizontal stress was assumed to be 207.9 kPa (average lift-off pressure) and the slope of the linear volumetric strain relationship was

calculated based on the equation presented by Wroth and Windle (1975) ( $s_v = 0.34$ ).

The final parameters used to determine the stress path followed by a soil element during pressuremeter loading are presented in the following table:

Test	$(t/s)_{ult}$	$\sigma'_{ho}$ kPa	$s_v$	$G_i$ kPa	$S_i$
228	0.687	207.9	0.34	67,088	535.7

Figure 6.4 shows the original data of test 228. The pressure was corrected based on calibration results and the cavity strain was defined as the ratio between the change in pressuremeter radius and the initial pressuremeter radius. The coordinates of the maximum loading point are:  $p'_{max} = 1,663.6$  kPa and  $\varepsilon_{max} = 0.1058$ . Figure 6.5 shows the calculated hyperbolic stress-strain relationship followed by any soil particle during the loading phase of the pressuremeter test. Figure 6.6 shows the variation of the mobilized shear stress ( $\tau_{mob} = t$ ) and the effective average normal stress ( $s$ ) with the cavity strain during pressuremeter expansion. Figure 6.7 shows the variation of radial and circumferential stresses with cavity strain during the loading phase of the pressuremeter test. Finally, figures 6.8 (a) and (b) show, respectively, the stress path in terms of the radial and circumferential stresses and in terms of the mobilized shear and effective average normal stresses.

Test 228 was also interpreted using the proposed methodology presented in section 6.5.4. Since the ideal installation implies in no disturbance, all loading points were used in the curve fitting procedure. The soil parameters derived from the curve fitting results are as follows ( $\phi'_{CV} = 34^\circ$ ):

Test	$\phi'$ ( $^\circ$ )	$\nu$ ( $^\circ$ )	$\sigma'_{ho}$ kPa	$G_i$ kPa
228	40.8	8.6	224.4	39,602

The values of the peak friction angle, dilation angle and effective horizontal stress are comparable to the values used earlier to calculate the stress path. On the other hand, the value of the shear modulus determined using the hyperbolic model is too low. Since all loading points were used in the curve

fitting procedure, the first points of the experimental loading curve forced the analytical curve to have such a low initial slope. However, when the curve fitting is performed using only the loading points with cavity strain greater than 4%, the derived shear modulus was comparable to the unload-reload shear modulus reported by Bellotti et al (1987). The following table presents the soil parameters determined by the proposed methodology when only the experimental loading points with cavity strain greater than 4% was used to perform the curve fitting:

Test	$\phi'$ (°)	$\nu$ (°)	$\sigma'_{ho}$ kPa	$G_i$ kPa
228	39.3	6.6	153.7	73,443

These results suggest that even for ideal installation the initial slope of the experimental loading curve is unrealistically low. So, the initial loading points can not be used for curve fitting purposes. Figures 6.9 (a) and (b) show, respectively, the matching between the analytical and experimental curves when all loading points and only points with cavity strain greater than 4% are used in the curve fitting procedure.

## 6.6 Evaluation of the constant volume friction angle

Either for the elastic perfectly plastic model or for the hyperbolic model, a knowledge of the constant volume friction angle is required to interpret drained pressuremeter tests (Hughes et al, 1977; Houlsby et al, 1986; Manassero, 1989; Robertson, 1982). Since the constant volume friction angle does not depend on the initial soil density, it can be determined from laboratory plane strain tests using disturbed samples. The values of the constant volume friction angle for most granular soils were found to vary within a narrow range (30° to 40°). Robertson (1982) suggested an initial estimation of  $\phi'_{CV}$  from the table presented in the next page. It was also suggested to assign lower values for well rounded particles and higher values for angular particles.

Soil Type	$\phi'_{cv}$
Well graded gravel-sand silt	40°
Uniform coarse sand	37°
Well graded medium sand	37°
Uniform medium sand	34°
Well graded fine sand	34°
Uniform fine sand	30°

The associated error in the interpreted soil parameters is generally small when the value of the constant volume friction angle is assumed. This is consistent with the acceptable accuracy of any curve fitting methodology. In fact, if no laboratory data is available, an average value of 35° can be assumed for the purpose of the preliminary evaluation of the soil parameters.

## 6.7 Interpretation of drained SBPT data

To validate the hyperbolic model as a good representation of the sand response, SBPT data from calibration chamber and from in situ tests will be interpreted. A comparison will be made with the interpreted parameters using the elastic perfectly plastic model.

### 6.7.1 Calibration chamber tests (Bellotti et al, 1987)

As presented in section 6.5.5, Bellotti et al (1987) presented the results of 48 SBPT's performed on Ticino sand and on Hokksund sand in the calibration chamber at ENEL-CRIS (Milan, Italy). The tests were grouped into two types: (a) ideal installation (25 tests); and (b) self-bored (23 tests). To check the capabilities of the pressuremeter analytical equations derived based on the elastic perfectly plastic and hyperbolic models, five self-bored tests will be analyzed.

- Interpretation using the hyperbolic model

The tests chosen to be interpreted using the methodology described in section 6.5.4. were: (a) test 238; (b) test 246; (c) test 247; (d) test 252; and (e)

test 260. These chosen tests cover a range of relative density from 43% to 89% and were performed in four types of Ticino sand (TS-4, TS-5, TS-6 and TS-8) with effective horizontal stress ranging from 53 kPa to 147 kPa. The OCR imposed varied from 1 to 4.19. A summary of the general calibration chamber conditions after sample consolidation is presented in the following table:

Test n°	Sand type	$D_{RC}$ %	$\gamma_d$ kN/m <sup>3</sup>	OCR	$\sigma'_{vo}$ kPa	$\sigma'_{ho}$ kPa	$K_0$	$u_o$ kPa
238	TS-4	74.8	15.79	2.83	101.0	83.39	0.828	5.89
246	TS-5	43.0	14.72	1.00	102.0	52.97	0.523	6.87
247	TS-5	43.0	14.80	4.19	190.3	147.15	0.776	6.87
252	TS-6	75.0	15.79	1.00	101.0	52.97	0.518	6.87
260	TS-8	89.0	16.29	1.00	131.5	78.48	0.595	6.87

Plots showing the comparison between the measured experimental loading curves and the curves fitted analytically, for each test, are shown in figures 6.9 to 6.18. The reader is referred to Bellotti et al (1987) if additional information on the tests is necessary. For all the tests, the maximum dynamic shear modulus ( $G_0$ ) was determined by resonant column tests. From unload-reload loops, the shear moduli ( $G_{ur}$  and  $G_{ur_0}$ ) were determined directly from the measured pressuremeter data.  $G_{ur}$  is the measured unload-reload shear modulus and  $G_{ur_0}$  is the unload-reload shear modulus corrected for stress level. To determine the peak friction angle and the dilation angle, all the tests were analyzed by the proposed methodology and by three other methods of pressuremeter interpretation: (a) Hughes et al (1977); (b) Robertson and Hughes (1986); and (c) Manassero (1989). The method developed by Manassero (1989) had its earlier version presented in 1987 (Politecnico di Torino, Italy). The peak friction angle for plane strain mode of deformation ( $\phi_P^{PS}$ ) was also calculated from the peak friction angle determined in laboratory triaxial tests ( $\phi_P^{TX}$ ) (Manassero, 1989). The average effective lift-off pressure ( $p'_o$ ) was determined from the measured values for each individual arm in the pressuremeter cell (total of three arms). The constant volume friction angle, determined from laboratory tests, was 34°. All derived parameters for Ticino sand are presented in the following two tables. The first

table presents the shear moduli, the effective lift-off pressure ( $p'_o$ ) and the initial effective initial horizontal stress in the calibration chamber ( $\sigma'_{ho}$ ) reported by Bellotti et al (1987), and the initial effective horizontal stress and the initial tangent shear modulus determined from the same tests using the proposed method of interpretation.

Source	Bellotti et al (1987)					Prop.Method	
Test n°	$\sigma'_{ho}$ kPa	$p'_o$ kPa	$G_0$ MPa	$G_{ur}$ MPa	$G_{ur_0}$ MPa	$\sigma'_{ho}$ kPa	$G_i$ MPa
238	83.39	44.12	91.0	49.3	39.5	52.1	702.0
246	52.97	12.94	59.7	22.1	18.7	10.5	54.8
247	147.15	11.66	94.3	35.5	32.3	8.2	134.2
252	52.97	66.64	74.9	35.8	27.8	21.8	872.8
260	78.48	20.93	97.4	41.7	34.3	29.2	66.9

The second table presents the peak friction angles and the dilation angles determined by the methods previously mentioned and by the proposed methodology.

Meth.	Lab.	Hughes (77)		Rob.(86)		Manas.(89)		Prop.Method	
Test n°	$\phi_P^{PS}$ ( $\phi_P^{TX}$ )	$\phi'$ (°)	$v$ (°)	$\phi'$ (°)	$v$ (°)	$\phi'$ (°)	$v$ (°)	$\phi'_{ult}$ (°)	$v$ (°)
238	49.3	32.6	-1.7	37.6	4.8	32.7	-1.6	30.0	-4.8
246	42.7	36.3	2.8	39.9	7.8	-	-	40.8	8.5
247	41.4	55.3	29.0	-	-	48.6	19.2	44.9	14.1
252	50.3	38.4	5.5	41.6	10.2	39.0	6.2	32.0	-2.3
260	50.4	41.2	9.1	44.0	13.0	53.0	25.6	44.5	12.9

• Interpretation using the elasto-plastic model

An interpretation based on the elastic perfectly plastic stress-strain relationship was performed using the methodology described in section 6.4.4. This method was developed to give an idea about the differences on the interpreted parameters compared to the hyperbolic based methodology. Test 260 was selected to serve as an example for such comparison. The interpreted parameters are presented in the following table:

Meth.	Hyperbolic model				Elastic plastic model			
	$\sigma'_{ho}$ kPa	$G_i$ MPa	$\phi'_{ult}$ (°)	$\nu$ (°)	$\sigma'_{ho}$ kPa	$G_i$ MPa	$\phi'$ (°)	$\nu$ (°)
260	29.2	66.9	44.5	12.9	40.0	46.0	43.0	11.5

A plot showing the comparison between the experimental loading curve and the analytical curve is shown in figure 6.19

### 6.7.2 In situ test (Fahey and Carter, 1991)

Fahey and Carter (1991) presented results of one SBPT performed in alluvial sand below the water table. The test was carried out 15.5 m deep, which is about 8m below the water table. The constant volume friction angle for this sand is reported to be 35°. The sand parameters derived by Fahey and Carter (1991) and interpreted using the hyperbolic and the elastic plastic models are presented in the next table:

Fahey & Carter (1991)				Hyperbolic model				Elastic plastic model			
$\sigma'_{ho}$ kPa	$G$ MPa	$\phi'$ (°)	$\nu$ (°)	$\sigma'_{ho}$ kPa	$G_i$ MPa	$\phi'_{ult}$ (°)	$\nu$ (°)	$\sigma'_{ho}$ kPa	$G$ MPa	$\phi'$ (°)	$\nu$ (°)
120	130	45	13	44	121	46	14	95	46	45	13

The proposed methodologies used to interpret the test are presented in section 6.4.4 and 6.5.4. Plots showing the comparison between the measured experimental loading curves and the curves fitted analytically, for this test, are shown in figures 6.21 and 6.22.

## 6.8 Discussion of the interpreted parameters

The hyperbolic and the elastic perfectly plastic models were used to derive soil parameters from drained SBPT's carried out in calibration chamber and in situ.

### 6.8.1 Calibration chamber tests (hyperbolic model)

The interpretation methodology was applied to three ranges of cavity strain:

(a) all loading points; (b) last half loading points; and (c) very last loading points. For all tests the parameters determined using the very last loading points were chosen as the most representative of the tested soil, and will be discussed here. All the interpreted results are presented in section 6.7.1.

• Test 238

Figure 6.10 shows the original loading curve of test 238 in terms of effective cavity pressure and cavity strain. The test appears to be of good quality, although some creep occurred in the unload-reload loops. Figure 6.11 shows the curve matching between the experimental and analytical curves. The curve matching is very good for the entire range of cavity strain. It appears that very small disturbance occurred during pressuremeter insertion. While the friction angles and the dilation angles compare well with the values derived from other methods, the shear modulus derived is almost 8 times greater than the dynamic shear modulus determined from the resonant column tests. There is no apparent reason for such discrepancy. The sample has a high relative density and the earth pressure coefficient is very close to 1.0.

• Test 246

Figure 6.12 shows the original loading curve of test 246 in terms of effective cavity pressure and cavity strain. Figure 6.13 shows the curve matching between the analytical and experimental curves. A very good matching was achieved over the entire range of cavity strain. Notice that the relative position of the experimental and analytical curves is the opposite to the position shown in figure 6.11. It suggests that the type of disturbance caused during pressuremeter insertion in test 246 is different from the type of disturbance caused in test 238. The derived value of the shear modulus has the same magnitude as the dynamic shear modulus. The friction and dilation angles compare well with the values derived using the other methods. The effective initial horizontal stress determined by the proposed method is very close to the measured lift-off pressure ( $p'_o$ ), even though the curve fitting was performed taking into account just the very last experimental loading points. The sample is loose and the earth pressure coefficient at rest is low. The small horizontal stress may explain why such loose sample had a dilatant



response.

• Test 247

Figure 6.13 shows the original loading curve of test 247 in terms of effective cavity pressure and cavity strain. This test was carried out in the same type of sand (TS-5) as test 246. The sample was overconsolidated and the earth pressure coefficient at rest is close to 1.0. Figure 6.15 shows the curve matching between the experimental and the analytical curves. Since the matching is very poor for the early loading points, some significant amount of disturbance may have occurred during pressuremeter insertion. The difficulty of penetration may be the reason for such disturbance, and is consistent with the high values of the initial effective vertical and horizontal stresses. The friction angle derived using the proposed method is smaller than the friction angle derived by the other methods, even though its value is relatively high. On the other hand, the hyperbolic shear modulus exceeds the dynamic shear modulus by a factor of almost 1.5. This response may be explained by the high confining pressures.

• Test 252

Figure 6.16 shows the original loading curve of test 252 in terms of effective cavity pressure and cavity strain. The sample is dense and normally consolidated. The earth pressure coefficient at rest is low. With such characteristics, the expected volumetric soil response in this test should be dilatant. Nevertheless, the interpreted friction angle based on the hyperbolic model was smaller than the constant volume friction angle. This implies contractive soil response during shear. This result is not consistent with the results from the other interpretation methods. Moreover, the derived shear modulus was more than 10 times greater than the dynamic shear modulus. There is no apparent reason for such discrepancy. The curve matching is presented in figure 6.17.

• Test 260

Figure 6.18 shows the original loading curve of test 260 in terms of effective cavity pressure and cavity strain. This test appears to be a good quality test. The curve matching shown in figure 6.19 confirms that the disturbance during

pressuremeter installation was kept to a minimum in this test. The sample is dense and normally consolidated. The friction angle and the dilation angle derived using the hyperbolic model are fairly consistent with the values determined by the other methods. The initial tangent shear modulus is also consistent with the dynamic shear modulus determined from the resonant column tests.

- Final comments on the interpreted parameters

Out of five tests analyzed, just two had inconsistent parameters derived - test 238 and test 252. It is interesting to note that both tests were carried out in dense samples and appear to have contractant response during the shearing process, based on the interpreted parameters. The hyperbolic initial shear moduli for both tests were 8 to 10 times the dynamic shear moduli. The shear moduli derived are unacceptably high. The reason for such inconsistency is not apparent. The other three tests were interpreted using the same methodology and the results were comparable to the results from the other methods. To sum up, the derived pressuremeter loading equation has the capability to simulate the pressuremeter loading curve using the parameters derived from SBPT performed in calibration chamber. However, in case of contractant response some inconsistencies were noticed. More tests from other calibration chambers must be analyzed to confirm the applicability of the proposed methodology.

#### 6.8.2 Calibration chamber test (elasto-plastic model)

The Ticino sand test 260 was also interpreted using the elastic perfectly plastic model. The results were very consistent with the results derived using the other methods and using the hyperbolic model. Figure 6.20 shows the final curve matching for test 260 using the elastic perfectly plastic model. The equivalent elastic shear modulus is smaller than the hyperbolic initial shear modulus as could be expected. More tests must be interpreted to confirm the consistency of the elastic perfectly plastic model.

### 6.8.3 In situ test (hyperbolic model)

The interpreted parameters from the test presented by Fahey and Carter (1991) using the hyperbolic model is reported in section 6.7.2. Figure 6.21 shows the original pressuremeter data in terms of effective cavity pressure and cavity strain. Figure 6.22 shows the curve matching between the analytical and the experimental curves. Only the very 'last loading points were used in the curve fitting procedure. As reported by Fahey and Carter (1991), the early portion of the loading curve was badly disturbed during the pressuremeter installation. Figure 6.22 confirms the presence of such disturbance. There is no matching whatsoever between the analytical and the experimental curve at the early part of the loading curve. The interpreted parameters using the hyperbolic model are very close to the parameters reported by Fahey and Carter (1991). The only exception is the effective initial horizontal stress. The value presented by Fahey and Carter (1991) for the initial effective horizontal stress was assumed known for this test depth. To additionally validate the proposed methodology presented in section 6.5.4 other in situ tests must be interpreted.

### 6.8.4 In situ test (elastic plastic model)

The test presented by Fahey and Carter (1991) was also analyzed using the elastic perfectly plastic model. The table presented in section 6.7.2 shows the final soil parameters. Figure 6.23 shows the curve matching between the analytical and the experimental curves. The matching is very good over the last loading points. The early part of the analytical loading curve does not match the experimental curve. The implication is that the soil was severely disturbed during pressuremeter installation. As could be expected, the equivalent elastic shear modulus is smaller than the hyperbolic initial shear modulus. In general, the results of the interpretation using the elastic perfectly plastic model are very consistent with the results presented by Fahey and Carter (1991) and with the results using the hyperbolic model. To confirm such consistency, more in situ tests must be analyzed to allow the methodology presented in section 6.4.4 to be applicable to geotechnical design.

## 6.9 Comments on pressuremeter unloading data in sands

- A complete pressuremeter test should include recorded data for: (a) the loading phase; (b) the unloading phase; and (c) the unload-reload or the reload-unload loops. When the pressuremeter test is undrained, the shear strengths mobilized during loading and unloading are correlated through parameter  $R_{\tau}$ . The interpretation methodology presented in Chapters 4 and 5 has considered  $R_{\tau} = 2.0$  in order to evaluate the initial horizontal stress. For drained tests, the mobilized shear stress during loading never reaches its critical value (i.e. shear strength) once the mean normal stress increases continuously. The higher the mean normal stress, the higher is the value of the shear strength at failure. The shear stress ratio ( $t/s$ ) is a better representation of the mobilized strength during the loading phase of a drained pressuremeter test than just the shear stress. However, for drained unloading, the pressuremeter measurement of the soil response is complicated for at least two other phenomena: (a) free movement of the pore water pressure; and (b) soil arching. The effective radial pressure during unloading goes to zero almost immediately. The range of strain to reach the zero effective radial stress is commonly less than 3%. Even within this small range of cavity strain the granular material instead of mobilizing its shear strength, it transfers the existing shear stress to the adjacent soil creating an arching effect. It means that the soil does not follow the pressuremeter membrane during unloading for a large range of cavity strain. Consequently, it is very difficult to accept that the friction angle mobilized during pressuremeter unloading has any relationship with the friction angle mobilized during the loading phase. In the mathematical derivation of the pressuremeter analytical equations, Houlsby et al (1986) have used the assumption that the friction angle mobilized during unloading is the same as the friction angle mobilized during loading. However, it was recognized by them, during the use of their proposed method, that the friction angle mobilized during unloading is more likely to be the constant volume friction angle rather than the peak friction angle. Actually, it is difficult to take into account the arching phenomenon during the mathematical derivations. With soil arching it is almost impossible to infer the amount of shear strength mobilized. It has been recognized that during drained

pressuremeter unloading the free pore water is responsible for closing the pressuremeter membrane (Wroth, 1984).

- As mentioned earlier, soil arching during cavity contraction of a drained pressuremeter test is another physical response embedded in the experimental measurements taken by the pressuremeter arms. Since the arching phenomenon is difficult to be accounted for during the mathematical derivations, the unloading pressuremeter data cannot be used to evaluate the mobilized soil strength. Consequently, derived parameters using analytical equations are meaningless if the entire unloading curve is considered. This consequence was recognized by Houlsby et al (1986). On the other hand, if just the early part of the contraction curve is considered, no reliable information on the soil strength can be obtained from analytical methods, once the soil arching has already started. The importance of the unloading curve of a drained pressuremeter test is related to the shear modulus, similar to the unload-reload loops.

- Finally, the conclusion that could be drawn from the above comments is that for drained pressuremeter tests very little information on soil parameters, other than modulus, can be derived from the unloading phase of the test using analytical equations.

## **6.10 Conclusions**

The same philosophy to interpret undrained pressuremeter data has been used to interpret drained SBPT's. This philosophy includes: (a) mathematical derivation of analytical pressuremeter equations based on principles of Solid Mechanics; (b) assumption that the pressuremeter data carry useful information on the actual soil behaviour, and (c) use of a mathematical curve fitting technique to derive a set of soil parameters.

Since the information on the soil response recorded during a drained pressuremeter test has its own peculiarities, the methodologies proposed for interpretation of drained SBPT's differ from the methodology proposed for interpretation of undrained tests. However, some similarities also exist. For

instance, the presence of a disturbed annulus around the pressuremeter caused by a poor installation makes the analytical curve match just the last loading points of the experimental data. One important difference between the drained and undrained methodologies is the role of the unloading pressuremeter data. For undrained tests, the unloading phase of the test is essential to the interpretation methodology. Information on the undrained strength and on the deformation modulus are derived from unloading data. However, for drained tests, the unloading curve plays a minor role on the derivation of the soil parameters because of the two other phenomena that occur simultaneously: (a) soil arching; and (b) free flow of water. Consequently, just the early portion of the unloading curve is meaningful for the shear modulus. Therefore, the entire unloading curve has the same utility as the small unload-reload loops. The proposed method does not consider this part of the pressuremeter test.

Two methodologies to interpret drained SBPT's have been presented in this chapter: (a) interpretation based on the elastic perfectly plastic model; and (b) interpretation based on the hyperbolic model. Analytical equations to simulate the loading portion of a drained SBPT have been derived for both models. The methodologies were used to interpret pressuremeter tests performed in calibration chamber and in situ sand deposits. Although the number of tests interpreted is limited, both methodologies have yielded soil parameters comparable to other methods. However, the soil parameters derived from calibration chamber tests were less consistent than the soil parameters derived from the in situ analyzed. More tests must be interpreted using the proposed methodologies to confirm the consistency of the derived soil parameters before any attempt to use the derived parameters for design purposes is made.

In summary, the proposed methodologies to interpret drained SBPT's are very simple to understand and easy to apply. The soil models used in the derivations are the main reason for the high degree of simplicity achieved. The derived set of soil parameters confirms that the models can capture the essential behaviour of the granular material. Additional validation of the presented methodologies may be required before they are used by practitioner engineers.

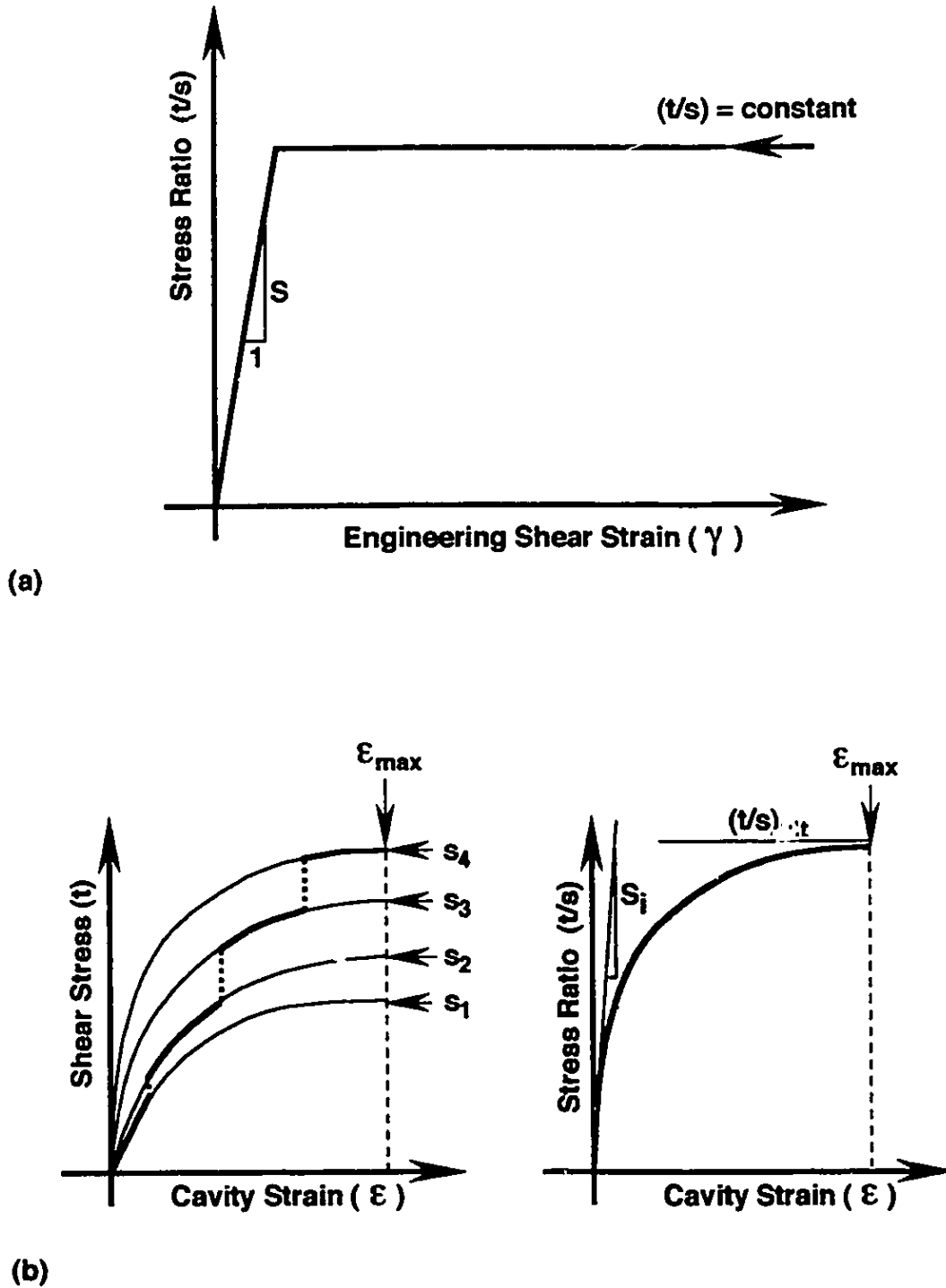


Figure 6.1 Soil models for drained response: (a) Elastic-perfectly plastic model; (b) Hyperbolic model.

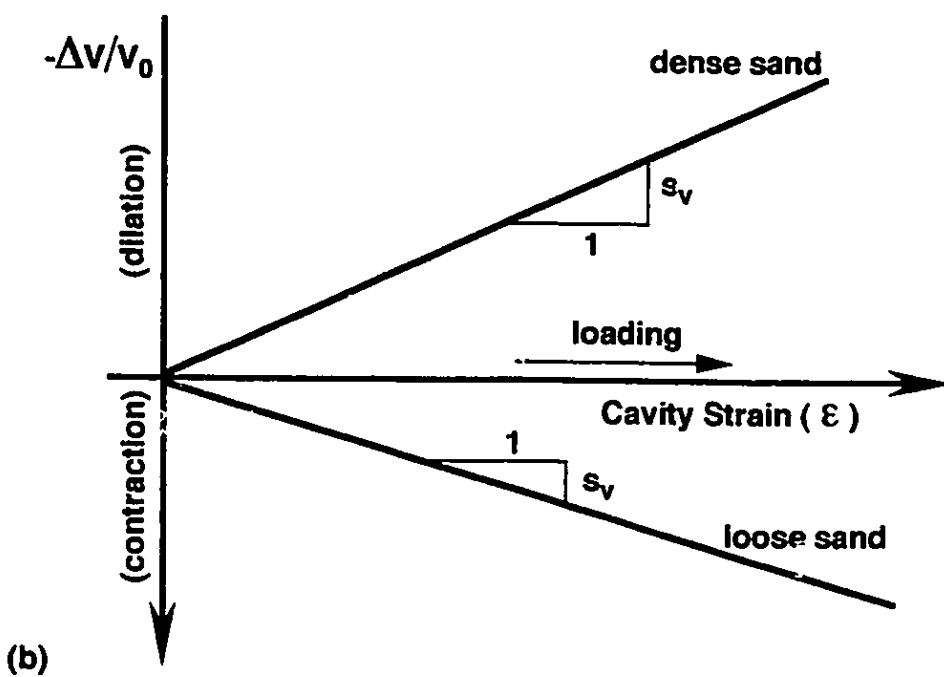
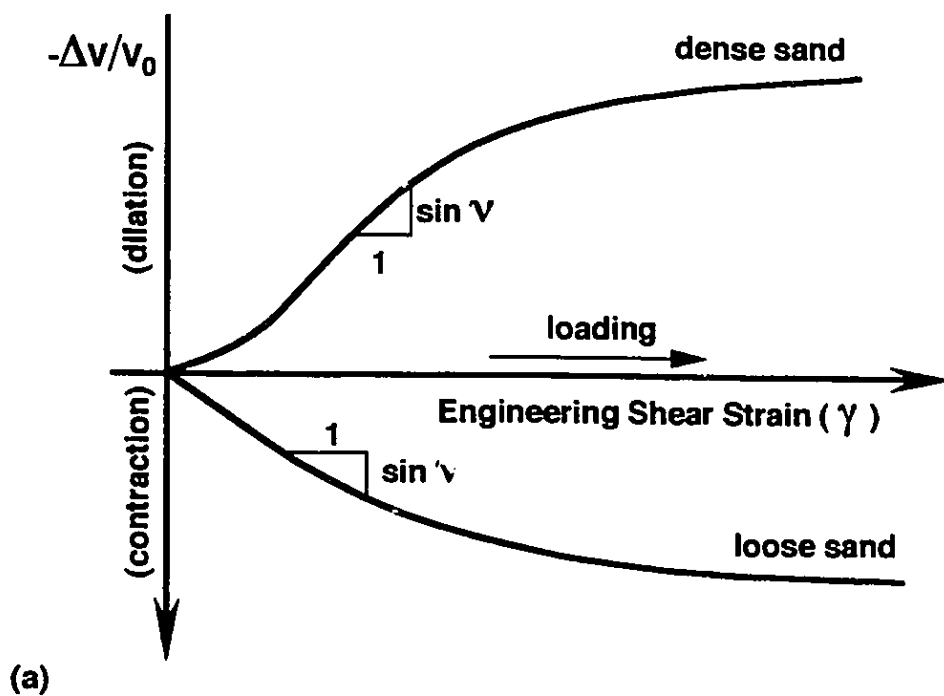
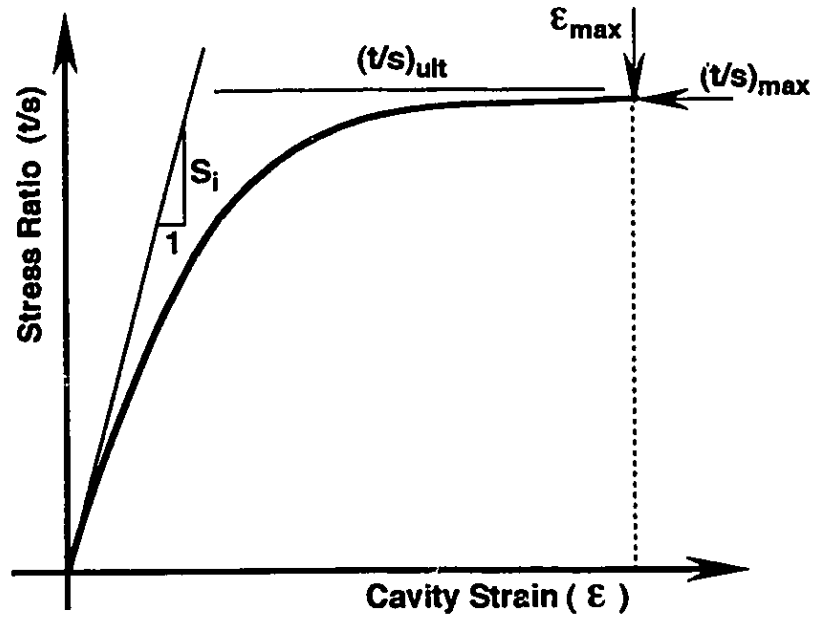
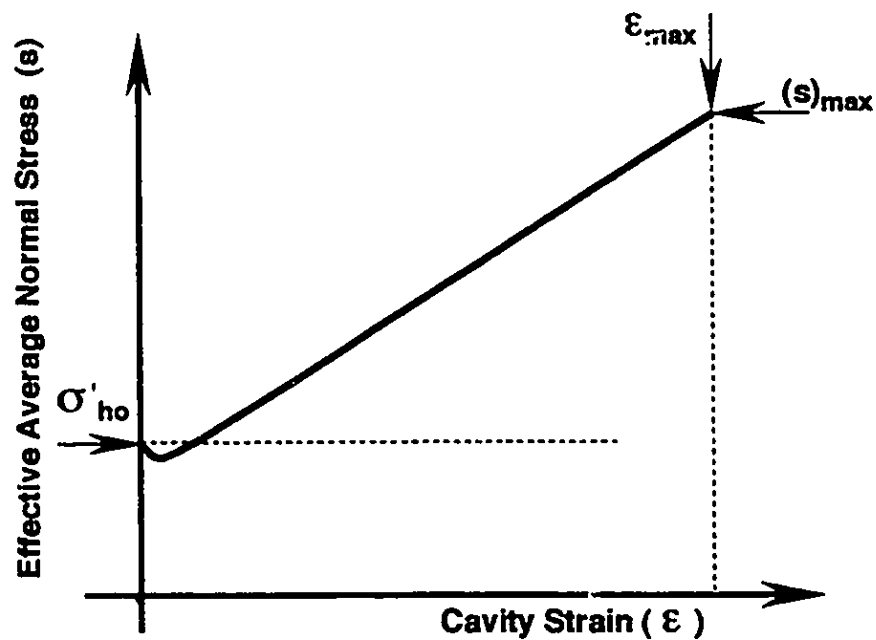


Figure 6.2 Volumetric strain relationship: (a) In terms of shear strain; (b) In terms of cavity strain.





(a)



(b)

Figure 6.3 Hyperbolic model: (a) Stress - strain relationship; (b) Variation of the effective average normal stress with cavity strain.

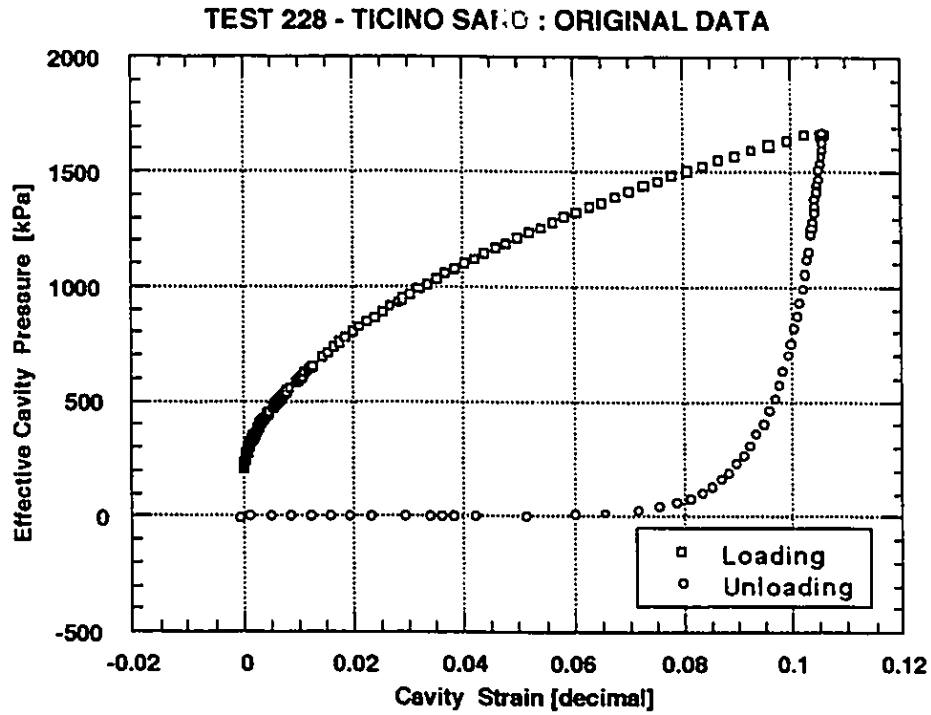


**Figure 6.4 Test 228 - Ticino sand: Original data.**

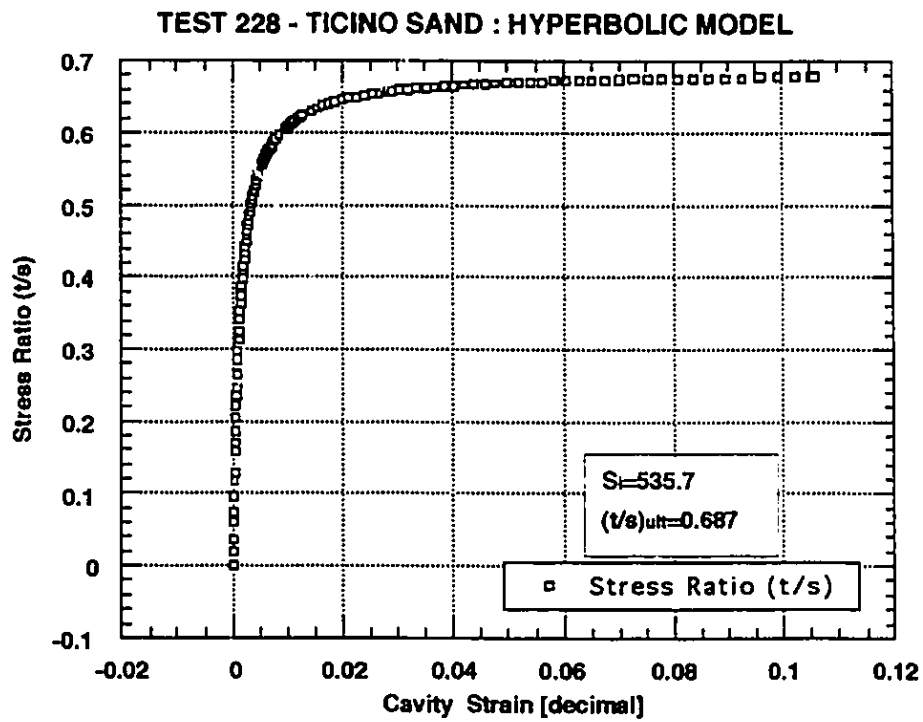


**Figure 6.5 Test 228 - Ticino sand: Hyperbolic stress-strain relationship.**

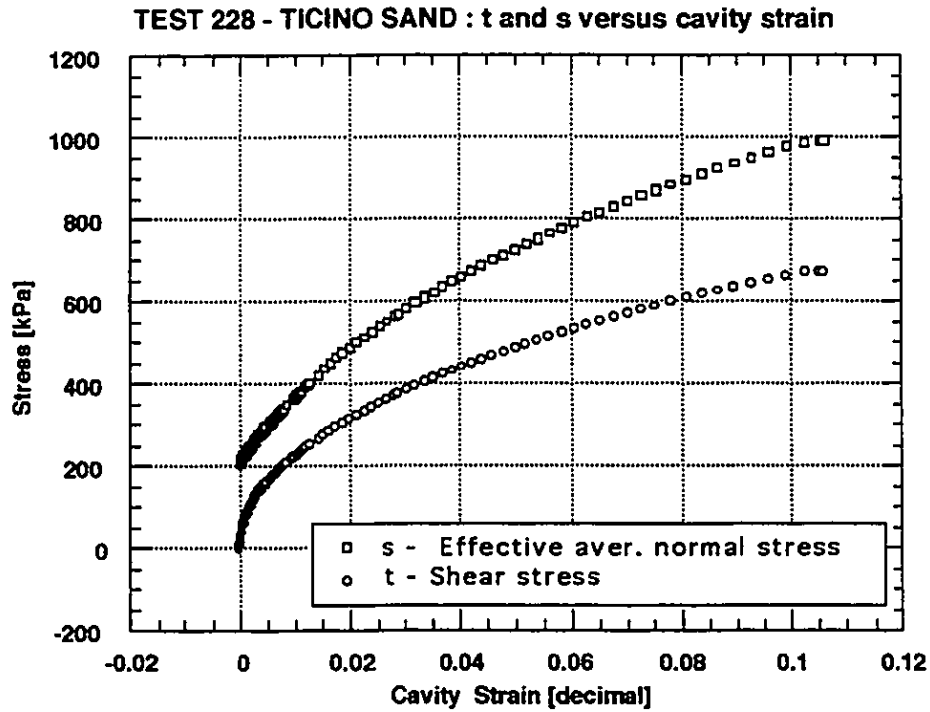


**Figure 6.6 Test 228 - Ticino sand: Mobilized shear stress and effective average normal stress.**

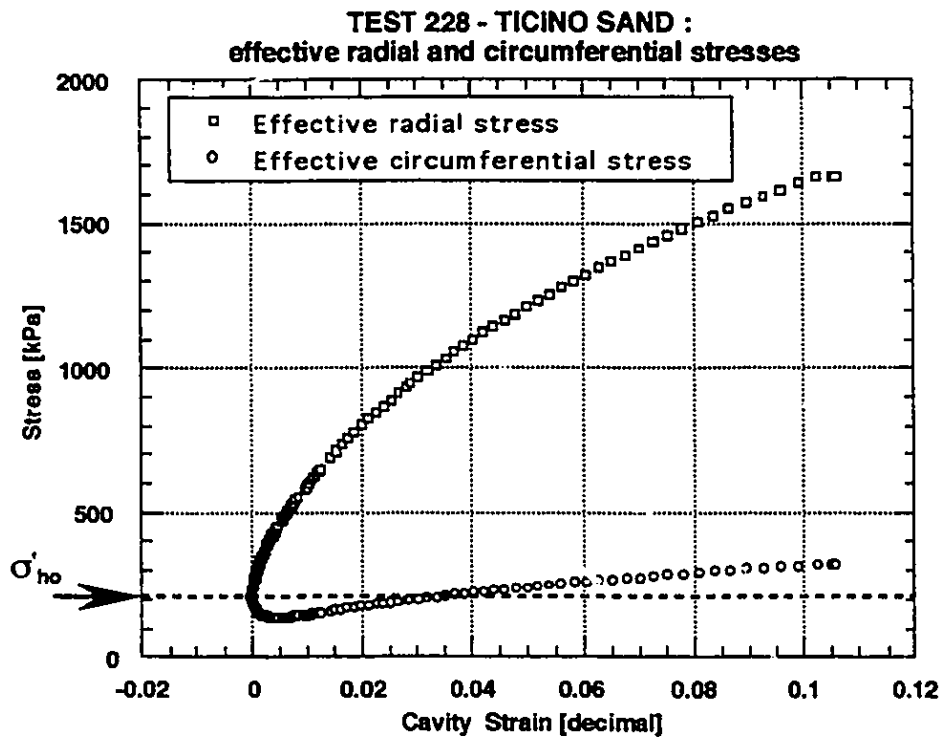


**Figure 6.7 Test 228 - Ticino sand: Radial and circumferential stresses.**

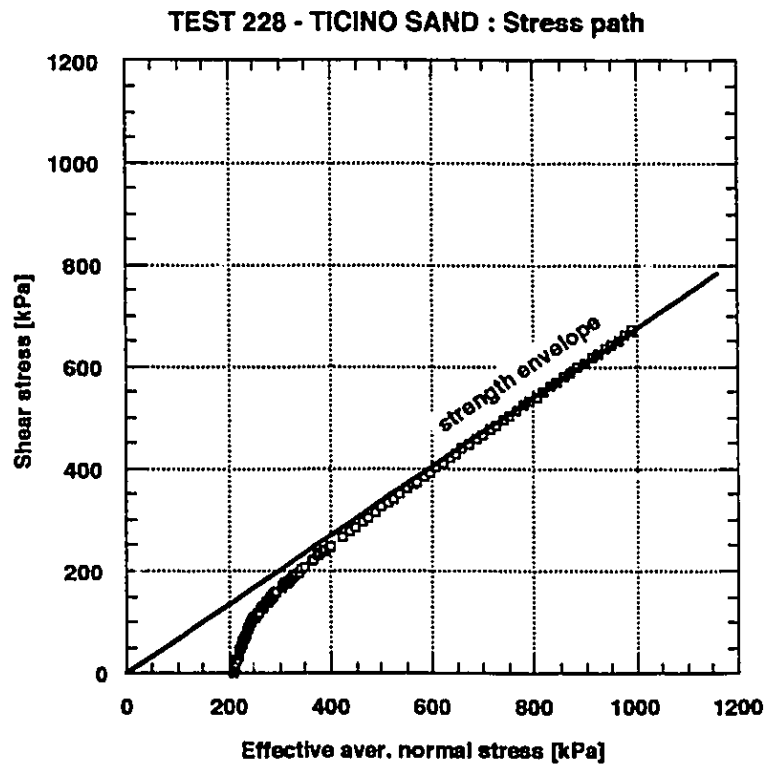
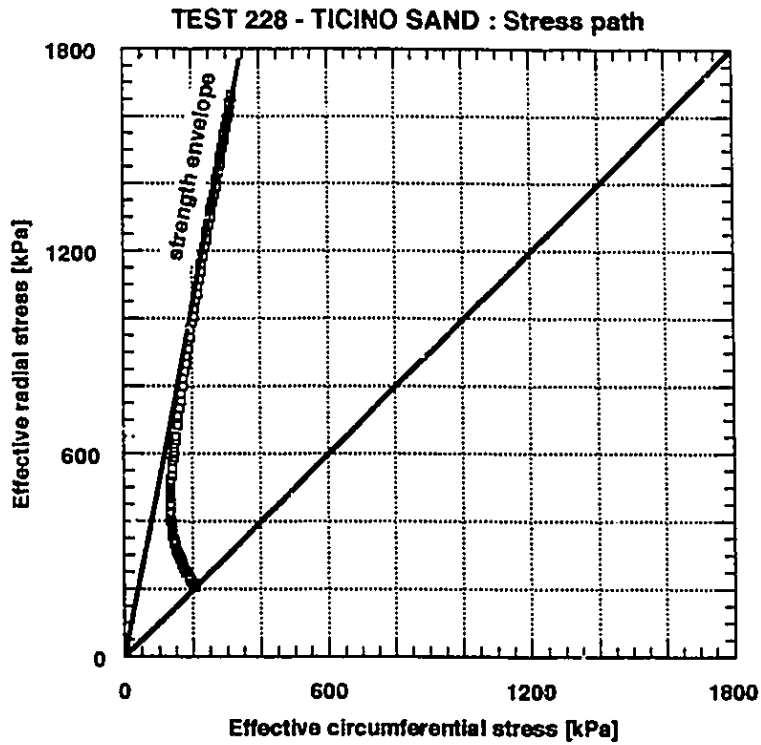
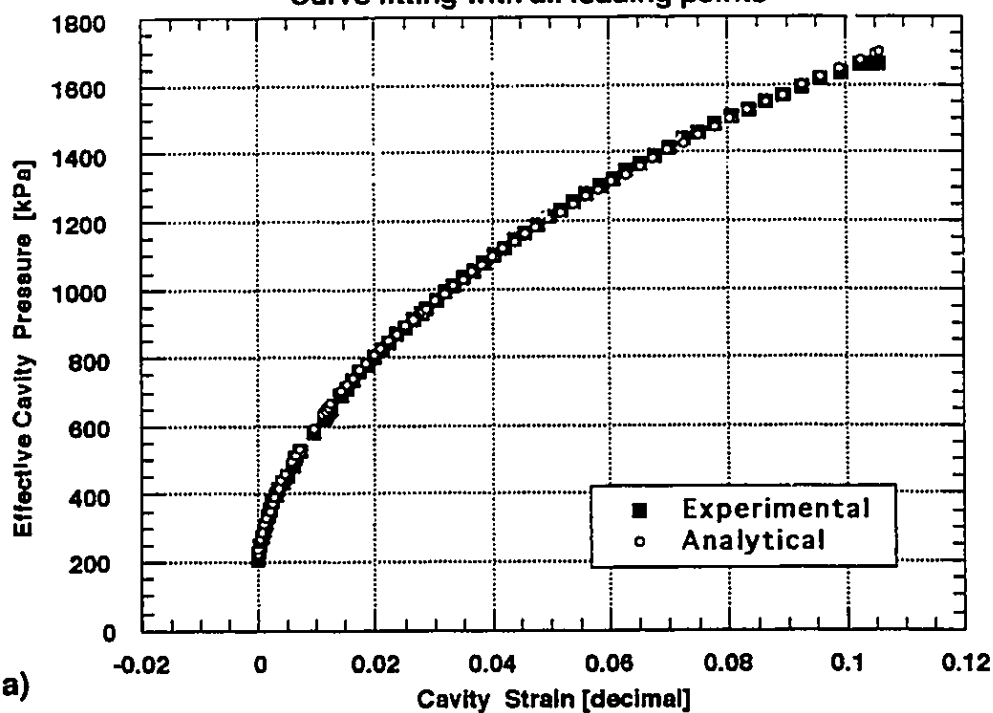


**Figure 6.8** Test 228 - Ticino sand: (a) Stress path  $\sigma_r$  versus  $\sigma_\theta$ ; (b) Stress path  $t$  versus  $s$ .

TEST 228 - TICINO SAND  
Curve fitting with all loading points



TEST 228 - TICINO SAND  
Curve fitting with  $\epsilon > 4\%$  loading points

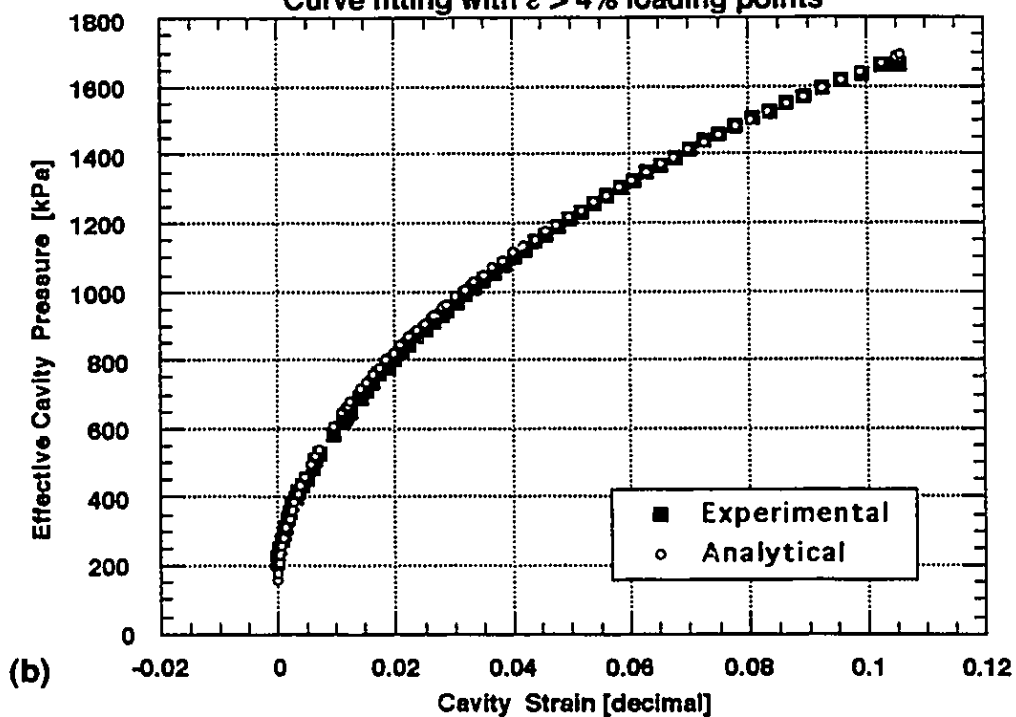
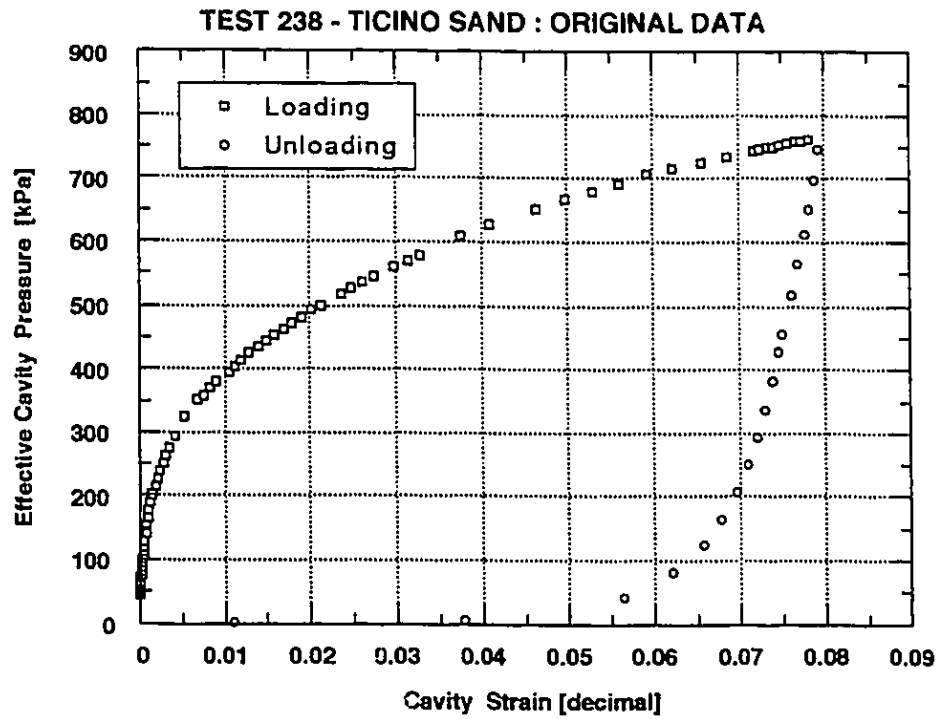
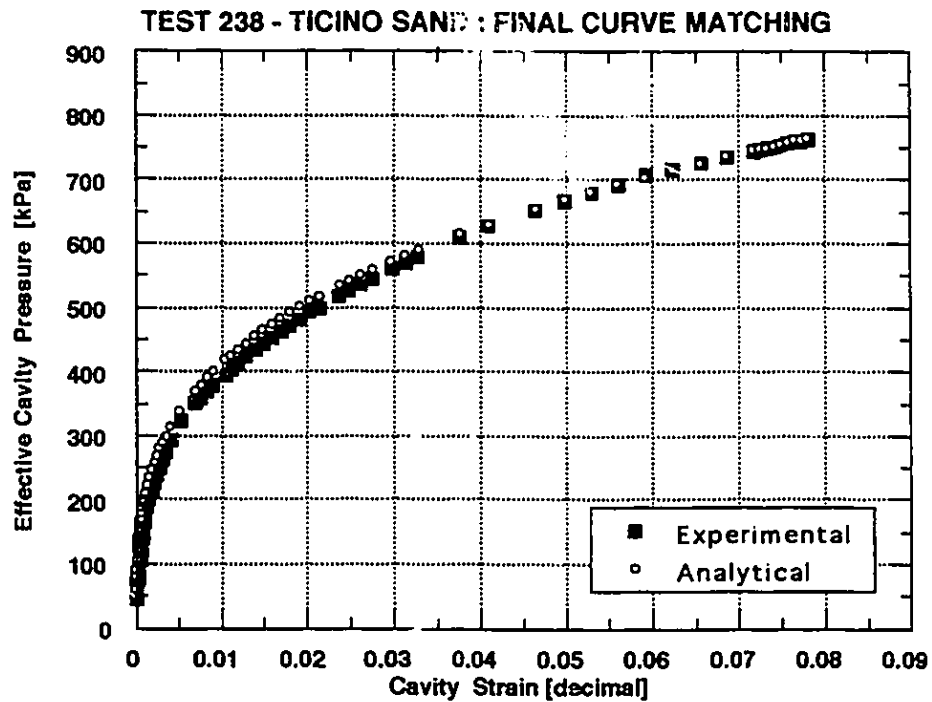


Figure 6.9 Test 228 - Ticino sand: (a) All loading points fitted;  
(b) Only points with  $\epsilon > 4\%$  fitted.



**Figure 6.10 Test 238 - Ticino sand: Original data.**



**Figure 6.11 Test 238 - Ticino sand: Final curve matching.**

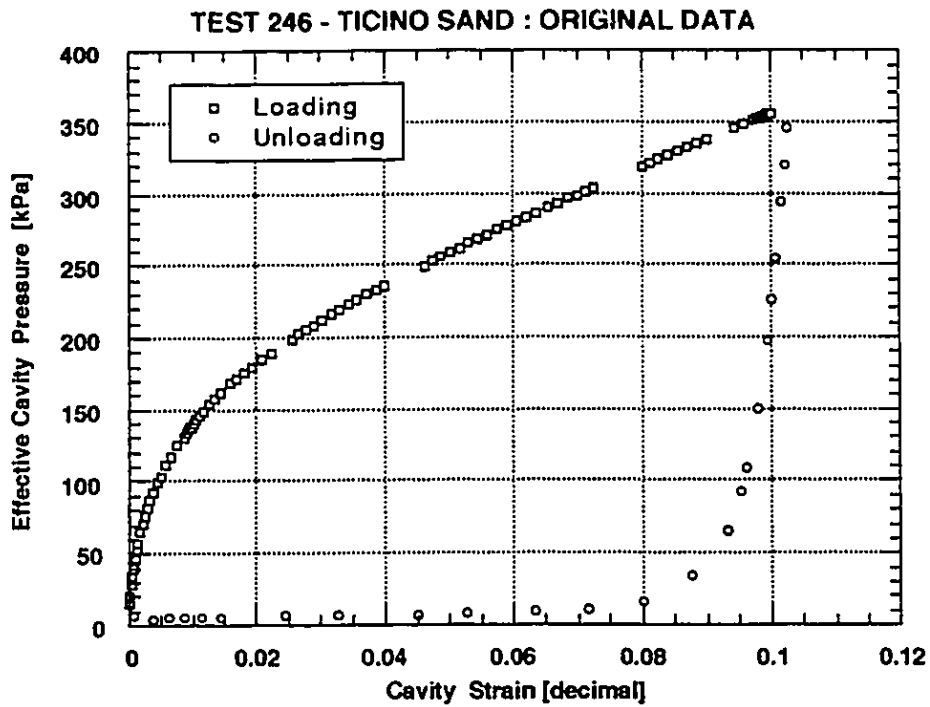


**Figure 6.12 Test 246 - Ticino sand: Original data.**

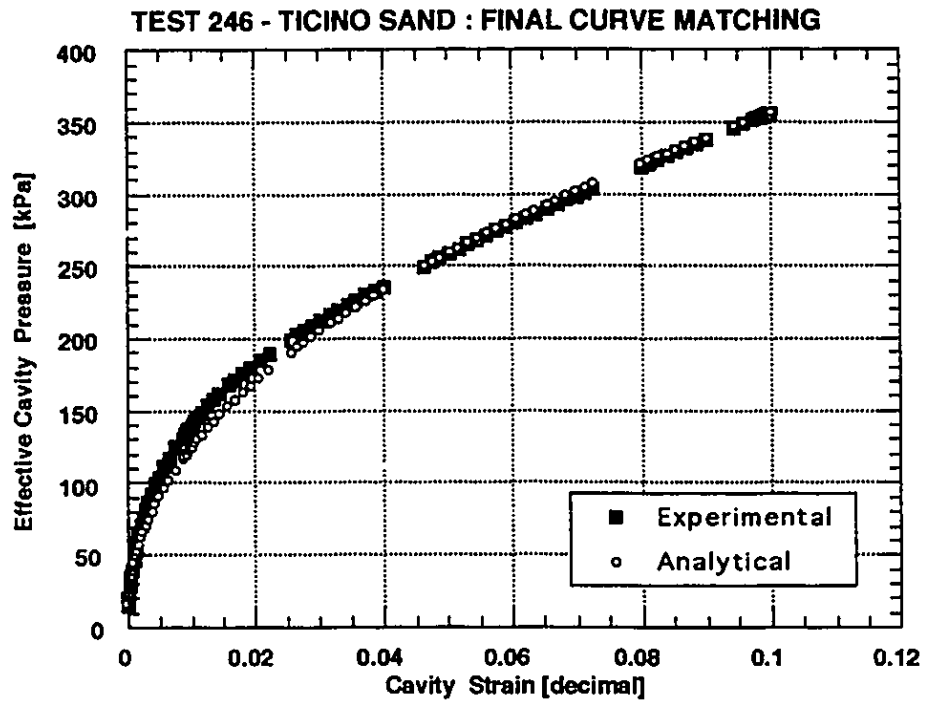


**Figure 6.13 Test 246 - Ticino sand: Final curve matching.**

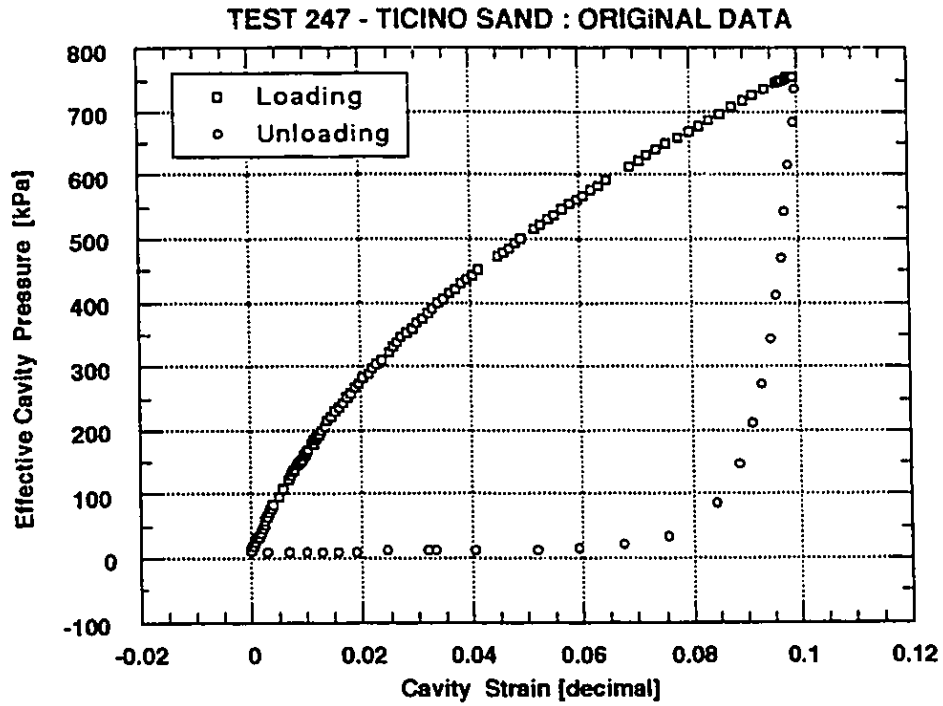


**Figure 6.14 Test 247 - Ticino sand: Original data.**

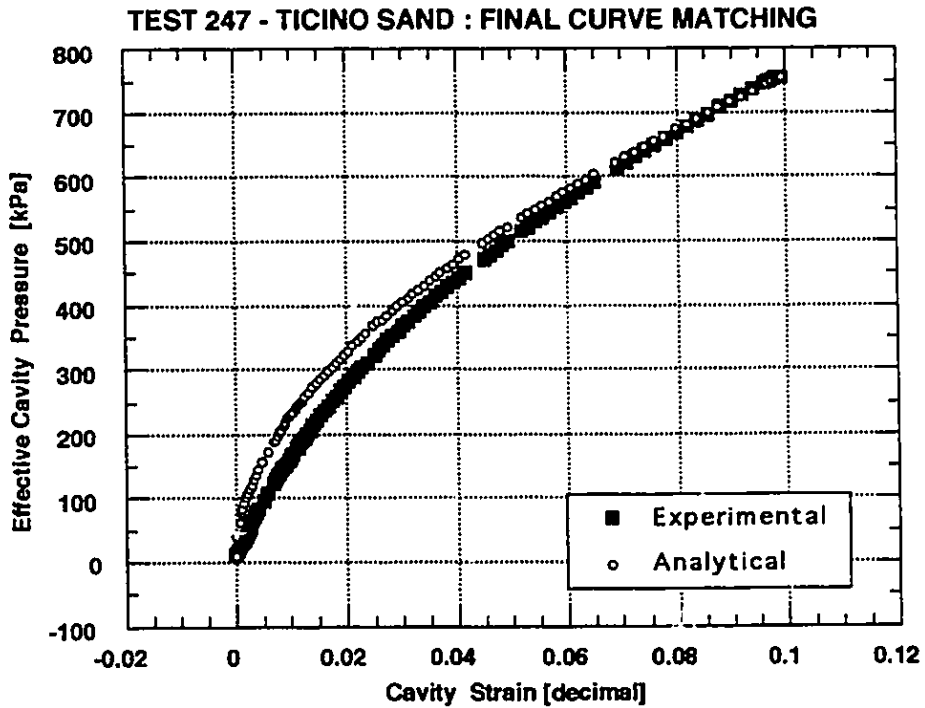


**Figure 6.15 Test 247 - Ticino sand: Final curve matching.**



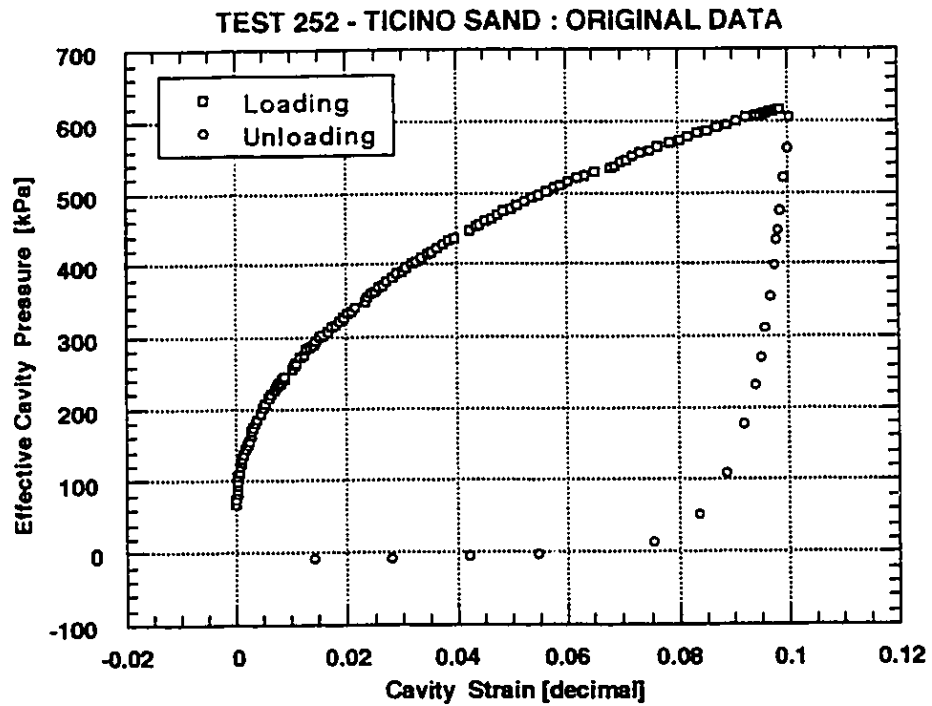


**Figure 6.16 Test 252 - Ticino sand: Original data.**

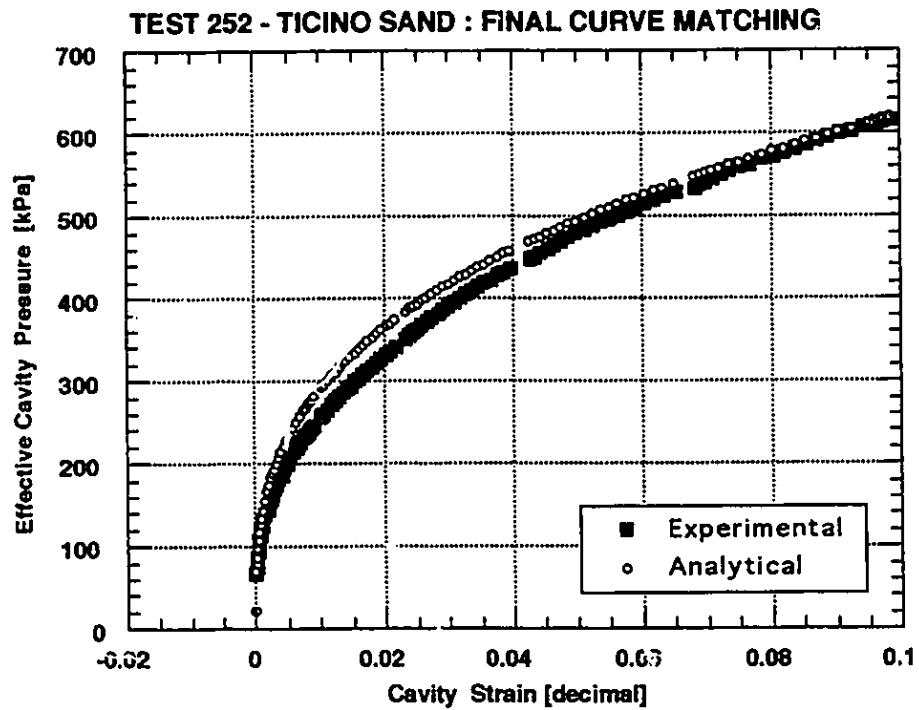


**Figure 6.17 Test 252 - Ticino sand: Final curve matching.**

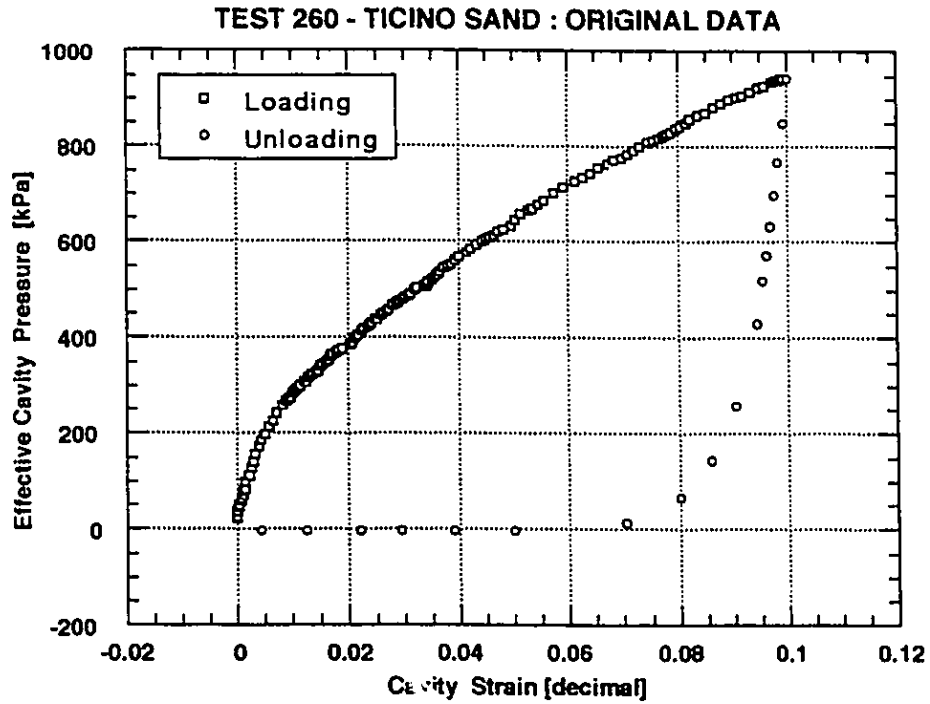


**Figure 6.18 Test 260 - Ticino sand: Original data.**

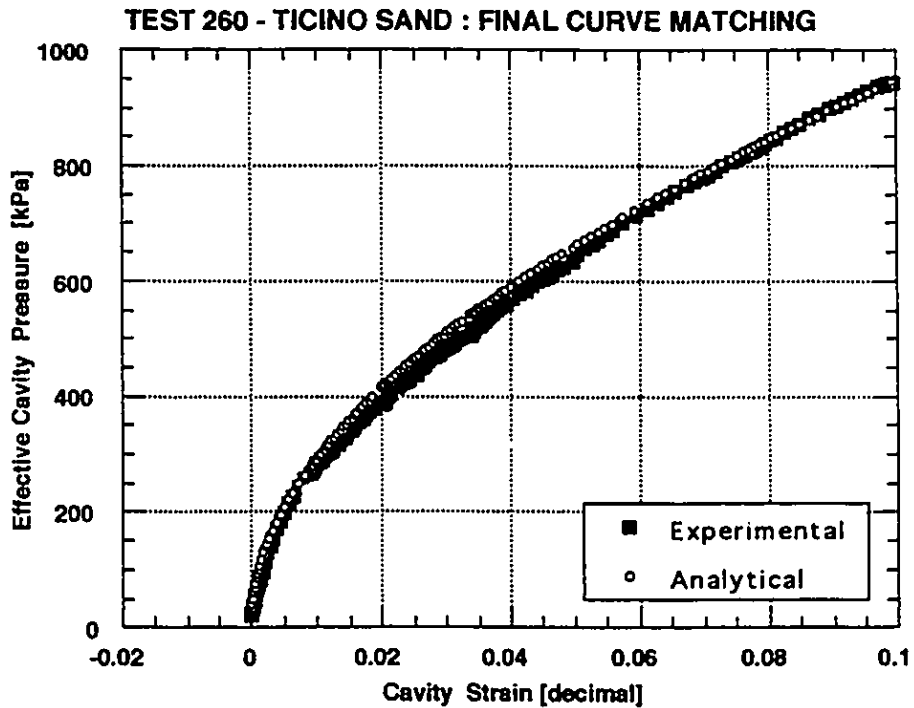


**Figure 6.19 Test 260 - Ticino sand: Final curve matching.**

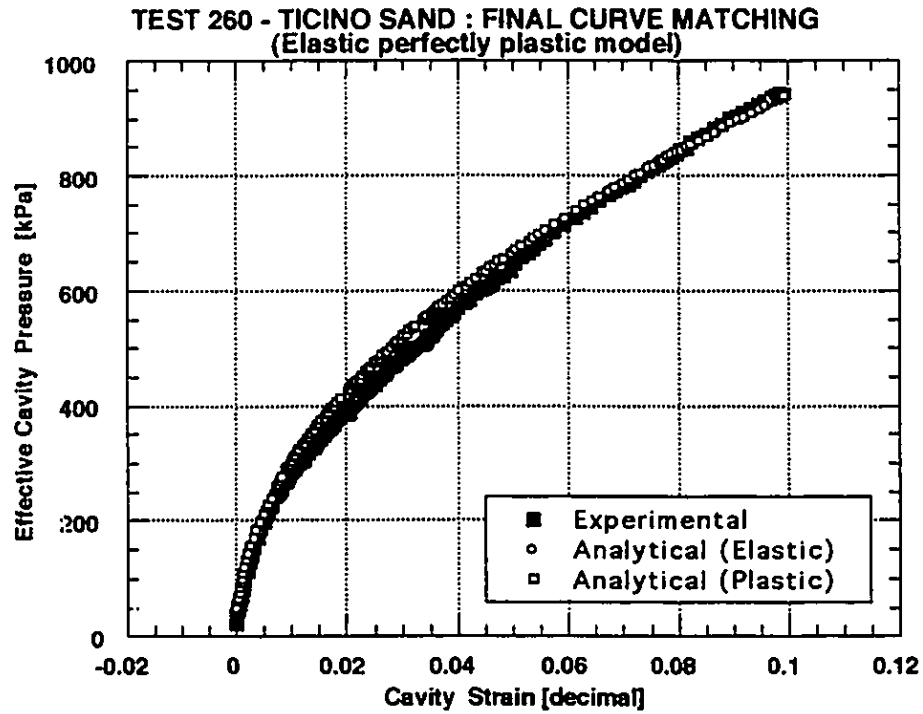


**Figure 6.20 Test 260 - Ticino sand: Final curve matching (Elasto-plastic model).**

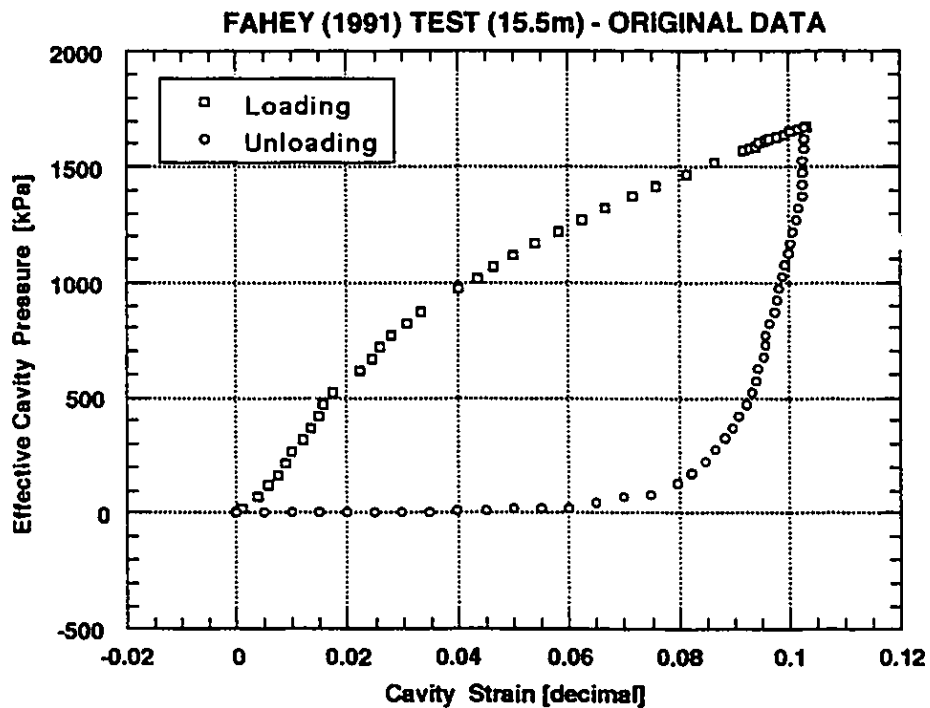


**Figure 6.21 Fahey (1991) test (15.5m): Original data.**

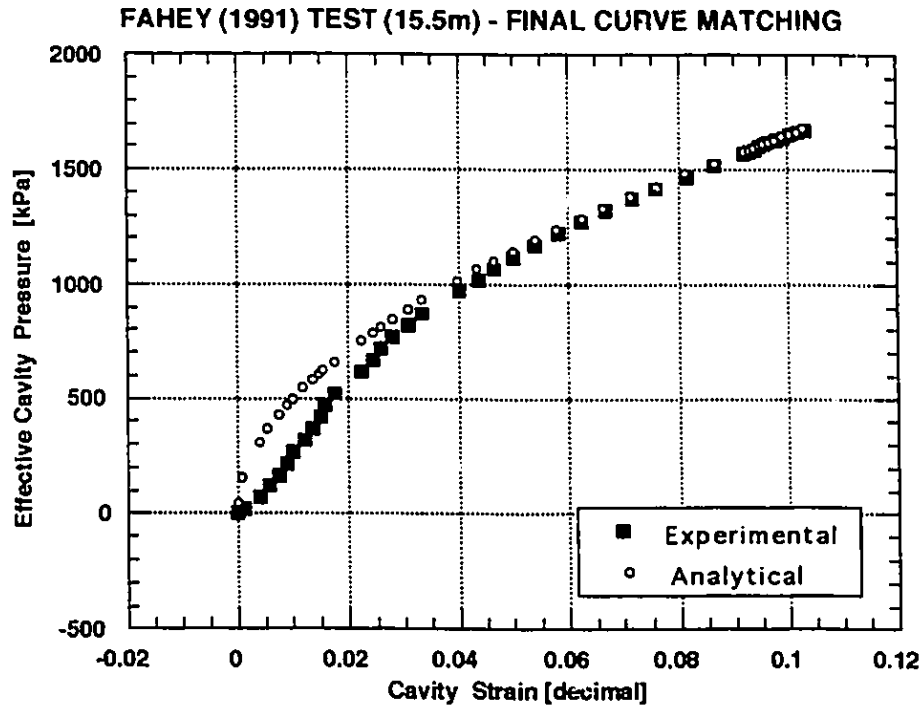


**Figure 6.22** Fahey (1991) test (15.5m): Final curve matching.

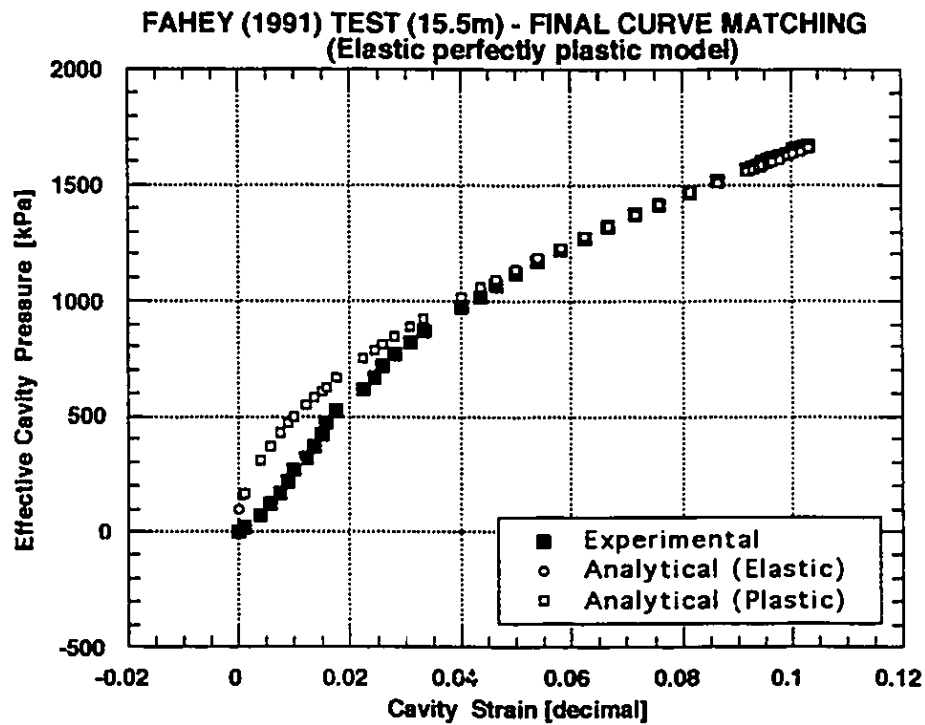


**Figure 6.23** Test 260 - Fahey (1991) Test (15.5m): Final curve matching (Elastic-plastic model).

## CHAPTER 7

### CONCLUSIONS AND SUGGESTIONS FOR FURTHER RESEARCH

#### 7.1 Introduction

Interpretation of pressuremeter tests is the main subject of this study. The mathematical derivation of the pressuremeter analytical equations can be done using small strain or large strain analyses. However, both give similar results when small strain pressuremeter tests are interpreted. Therefore, the large strain pressuremeter analytical equations are more adequate to interpret undrained pressuremeter tests (undrained soil response) irrespective of the amount of soil straining during the test. For drained tests (sand response) just small strain analysis was developed in this study.

Recognizing the potential of pressuremeter devices and the limitations of laboratory tests, this study was developed to meet the following main objectives:

- (1) Develop a new approach to determine constitutive parameters for soils from pressuremeter data;
- (2) Introduce nonlinear response in the stress-strain constitutive relationship for cohesive and cohesionless soils;
- (3) Keep the new approach as simple as possible, so that engineers can readily apply the method to geotechnical design;
- (4) Provide a contribution to the geotechnical science in terms of an analytical study to interpret field and laboratory pressuremeter results.

The first contribution of this research was the interpretation of SBPT results in clays, and validation of the proposed methodology was done based on SBPT's in Fucino clay reported by AGI (1991). The second contribution of this study was a tentative extension of the proposed methodology to the PBPT and the FDPT. Finally, following the same approach, an interpretation methodology to interpret SBPT data in sand was developed. Initial validation of this methodology was provided using calibration chamber results of SBPT's in Ticino sand, reported by Bellotti et al (1987).

More than one dozen interpretation methodologies have been presented and commented in Chapter 2. All of them use the cavity expansion theory (cylindrical or spherical). This theory constitutes the core of the theoretical background used to solve the pressuremeter problem. This review has shown that few interpretation methods, within the group of the pre-defined constitutive law (Group I), deal with nonlinear aspect of the stress-strain relationship. Also, only three of the presented approaches are concerned with the unloading stage of the pressuremeter test (Houlsby 1986 and 1988, Jefferies 1988). Additionally, the reliance on the entire loading curve of the SBPT is another point for criticism. Although the self-boring technique can theoretically eliminate soil disturbance during the installation phase, some unknown degree of perturbation exists in the soil around the probe after insertion. All these three aspects - soil non linearity, loading and unloading data, and possible disturbance during the pressuremeter installation, will be considered by the interpretation methodology developed and proposed in this study.

## **7.2 Proposed methodologies**

The development of the interpretation methodologies to derive soil parameters from pressuremeter data was presented in Chapters 4, 5, and 6. Many researchers have developed methods to interpret pressuremeter results since the early 60's. Some methodologies have become popular in geotechnical design. However, restrictive assumptions and unrepeatable mathematical techniques are important drawbacks of these interpretation methods. Nonlinear soil behaviour in the form of a hyperbolic function relating shear stress and cavity strain has been proposed in this study to have a more realistic representation of the soil response. Analytical equations are derived for both loading and unloading portions of the pressuremeter test. Using curve fitting technique as the mathematical tool, soil parameters are then derived from pressuremeter experimental data. The approach is applied for both drained and undrained soil responses.

The commonly used version of the SBP is limited to soil deformations that

rarely exceed 15%, measured as cavity strain (change in pressuremeter radius divided by initial radius). Hence, it is reasonable to derive the pressuremeter analytical equations to simulate both pressuremeter expansion and contraction curves, using the small strain analysis. On the other hand, the updated versions of the FDP are able to expand to around 50% of their original initial radius. The PBPT requires a pre-drilled hole for device installation. The pre-drilling procedure always causes some soil unloading, forming an annulus of perturbed soil around the pressuremeter. Hence, large straining during the subsequent pressuremeter test is needed until the natural soil response can be recorded. Consequently, large strain analysis is required to derive the pressuremeter analytical equations to simulate both pressuremeter expansion and contraction curves for the FDPT and PBPT.

#### 7.2.1 Undrained pressuremeter tests interpreted using small strain analysis

The methodology to interpret undrained SBPT results in clays was presented in Chapter 4. The method incorporates the unloading portion of the pressuremeter test to derive the initial shear modulus and undrained shear strength. The soil response is represented by a hyperbolic relationship between the shear stress and circumferential strain. The method accepts that some level of disturbance may exist for the SBPT loading results and, hence, only the later part of the loading curve should be used to derive the value of the in situ horizontal stress. To apply the proposed interpretation methodology a value for the ratio of the undrained shear strength in unloading and loading ( $R_{\tau}$ ) must be known. A value of 2.0 is recommended. To improve the interpreted results of the in-situ horizontal stress and the undrained shear strength, the ratio of undrained shear strength in unloading and loading ( $R_{\tau}$ ) should be measured on undisturbed samples, following stress paths similar to those in the pressuremeter test. The proposed interpretation method has been evaluated using 20 high quality self-boring pressuremeter results performed in the Fucino clay in Italy. The interpreted soil parameters had reasonable values when compared to other in situ and laboratory test results. In summary, the proposed interpretation method presents an acceptable framework to derive soil parameters from undrained pressuremeter tests in fine grained soils. This framework includes the complete loading and

unloading portions of the test, and it incorporates non linearity of the soil response in a simple closed-form manner.

### 7.2.2 Undrained pressuremeter tests interpreted using large strain analysis

The methodology to interpret PBPT and FDPT results in clays was presented in Chapter 5. The definition of Green strains in the Lagrangian space was used to derive the large strain pressuremeter analytical equations. In this derivation, the hyperbolic stress-strain relationship was assumed to be the soil constitutive law for both pressuremeter loading and unloading. The complete soil behaviour using this model is very simple and depends on just two parameters - initial tangent shear modulus and ultimate undrained shear strength. Nonlinear stress-strain relationships, like the hyperbolic model, have proved to be powerful in describing the stress-strain response of a large number of soils. Furthermore, the parameters used to describe soil behaviour are meaningful for engineering application. The derived large strain pressuremeter analytical equations - one for loading and one for unloading, require four parameters to simulate a complete pressuremeter test: (a) initial tangent shear modulus, (b) initial in situ horizontal stress; (c) ultimate undrained shear strength during loading; and (d) ultimate undrained shear strength during unloading. If a relationship between the undrained shear strength in unloading and loading is assumed known, three soil parameters can be derived from a large strain pressuremeter test. The interpretation methodology considers the experimental unloading pressuremeter curve as the least disturbed by the device insertion. The shear modulus and the undrained shear strength in unloading can be estimated using the least square error curve fitting technique. Assuming that the maximum pressure measured in the pressuremeter test is the true limit pressure, the third parameter (initial horizontal stress) can be evaluated using the limit pressure equation. Further validation is necessary to confirm this latter step since horizontal stresses derived by this method appear to be overestimated. However, the shear modulus and the undrained shear strength derived from the unloading curve by the proposed methodology appear to be useful parameters for engineering design. The shape of the FDPT curves is different when soft and stiff undrained soils are tested. As presented by Howie (1991)



the shape of the FDPT curve for soft soils can be not much different from the shape of the SBPT curve. In this case, the large strain pressuremeter analytical equations can be used in conjunction with the interpretation philosophy presented in Chapter 4. All three parameters can then be derived. On the other hand, if the FDPT is performed in stiff soils, the loading curve may not present any information on the initial horizontal stress. In this case, the limit pressure has to be used according to the methodology described in 5.6.5 if the horizontal stress is to be evaluated. Hence, it is important that the pressuremeter be expanded to a strain level sufficient to reach a pressure close to the limit pressure of the undisturbed soil.

### 7.2 3 Drained pressuremeter tests interpreted using small strain definition

The same philosophy to interpret undrained pressuremeter data has been used to interpret drained SBPT's. This philosophy includes: (a) mathematical derivation of analytical pressuremeter equations based on principles of Solid Mechanics; (b) assumption that the pressuremeter data carry useful information on the actual soil behaviour, and (c) use of a mathematical curve fitting technique to derive a set of soil parameters. One important difference between the drained and undrained methodologies is the role of the unloading pressuremeter data. For undrained tests, the unloading phase of the test is essential to the interpretation methodology. Information on the undrained strength and on the deformation modulus is derived from unloading data. However, for drained tests, the unloading curve plays a minor role in the derivation of the soil parameters because of the two other phenomena that occur simultaneously: (a) soil arching; and (b) free flow of water. Consequently, just the early portion of the unloading curve is meaningful for soil modulus. Two methodologies to interpret drained SBPT's have been presented in Chapter 6: (a) interpretation based on the elastic-perfectly plastic model; and (b) interpretation based on the hyperbolic model. Analytical equations to simulate the loading portion of a drained SBPT have been derived for both models. The methodologies were used to interpret pressuremeter tests performed in the calibration chamber and in situ sand deposits. Although limited in number of tests interpreted, both methodologies have yielded soil parameters comparable to other methods. However, the soil

parameters derived from calibration chamber tests were less consistent than the soil parameters derived from the in situ test analyzed. More tests must be interpreted using the proposed methodologies to confirm the consistency of the derived soil parameters before any attempt to use the derived parameters for design purposes is made.

### **7.3 Summary**

Interpretation of in situ tests can be very difficult because of the unknown boundary conditions. To be included in the geotechnical design routine, the in situ test must have a simple and accurate methodology of interpretation. The pressuremeter test is, perhaps, one of the few in situ tests that has well-defined boundary conditions. Another advantage is the possibility of using a theory based on Solid Mechanics principles - cavity expansion theory, to derive closed-form solutions for the pressuremeter problem. The loading and unloading pressuremeter curves can, therefore, be simulated using analytical equations. Solutions for the drained and undrained problems were presented in this study. The undrained problem was solved using small and large strain analyses, while the drained problem was solved using just the small strain analysis. The solutions were based on the hyperbolic stress-strain relationship with no soil volumetric change for undrained tests, and linear volumetric change relationship for drained tests. Based on these solutions, interpretation methodologies for drained and for undrained tests were presented. For both types of tests, the early portion of the pressuremeter loading curve is assumed not to represent the undisturbed soil response. Just the last points of the loading curve are used for soil parameter interpretation purposes. The unloading pressuremeter curve plays a major role in the methodology to interpret undrained tests. Information on soil strength and soil modulus can be derived from the unloading data. For pressuremeter tests, such as FDPT and PBPT, which have the loading data badly disturbed the unloading data is essential for soil parameters interpretation. The proposed methodology to interpret undrained pressuremeter tests relies on the unloading data to derive the undrained shear strength and the shear modulus of the soil tested. On the other hand, due to the soil arching and the free pore water flow phenomena, the unloading portion of the pressuremeter drained

test may not be used to derive the drained soil strength. For this reason, the proposed methodologies for interpreting drained SBPT's do not take into account the unloading data. All derived equations are presented and the curve fitting technique is performed using a commercially available microcomputer software. This allows any geotechnical company to use the proposed methods. Simplicity, accuracy, and reliability have been essential features of the proposed methodologies pursued since the conception of this whole work. Also, these are the features sought by practitioner engineers in any interpretation method of in situ tests to help them derive soil parameters and use those parameters in geotechnical design.

#### **7.4 Suggestions for further research**

Three complementary areas of research can be identified when dealing with the pressuremeter test. One area would be the development of the equipment. A lot of laboratory and field work has been done in this respect in England, France, Canada, the USA, Australia, Italy, and other countries around the world (Withers et al, 1986, Baguelin et al, 1978, Briaud et al, 1983, Campanella et al, 1990, Fahey, 1991, Ghionna et al 1983). The second area of research on the pressuremeter test would deal with the test procedures. Strain controlled, stress controlled and holding tests constitute the focus of past studies on test techniques (Fioravante, 1988, Pyrah et al, 1985, Bellotti et al, 1986). Finally, the third area of pressuremeter related research is the development of interpretation methods to derive soil parameters from the pressuremeter data. The following are suggestions for further research.

##### **7.4.1 Equipment development**

- Cone-pressuremeter with seismic measurements.
- Improvement of measurement accuracy for pressure and strains.
- Improvement of measurement accuracy of pore water pressure.

##### **7.4.2 Field test procedures**

- Perform SBPT, FDPT, and PBPT at the same site and same depth.

- Measure limit pressure from undrained SBPT, FDPT, and PBPT.
- Perform multiple subsequent expansions and contractions of the pressuremeter cell.
- Perform stress and strain controlled pressuremeter tests with emphasis on creep and consolidation measurements.

#### 7.4.3 Interpretation of pressuremeter data

- Obtain closed-form solutions using other soil models.
- Perform finite element analysis for cavity expansion with strain-softening materials.
- Perform finite element analysis for loading and unloading undrained pressuremeter tests.

## BIBLIOGRAPHY

1. A.G.I. - Associazione Geotecnica Italiana 1991. Geotechnical characterization of Fucino clay. X European Conference on Soil Mechanics and Foundation Engineering - Florence, Italy. 1: pp.27-40.
2. Anderson, W.F. and Pyrah, I.C. 1986. Undrained strength and deformation parameters from pressuremeter test results. The pressuremeter and Its Marine Applications: Second International Symposium - Texas, USA. pp.324-338.
3. Anderson, W.F., Pyrah, I.C. and Haji-Ali, F. 1986. Pressuremeter testing of normally consolidated clays - The effects of varying test technique. Engineering Geology - Special Publication. N°2: pp.125-132.
4. Arnold, M. 1981. An empirical evaluation of pressuremeter test data. Canadian Geotechnical Journal. 18: pp.455-459.
5. Baguelin, F., Jezequel, J.F. and Shields, D.H. 1978. The pressuremeter and foundation engineering. Series on Rock and Soil Mechanics, Trans Tech Publications. 2: N°4.
6. Baguelin, F., Jezequel, J.F., Mee, E.L. and Mehaute, A.L. 1972. Expansion of cylindrical probes in cohesive soils. Journal of the Soil Mechanics and Foundations Division - ASCE. 98: pp.1129-1142.
7. Battaglio, M., Ghionna, V., Jamiolkowski, M. and Lancellotta, R. 1981. Interpretation of self-boring pressuremeter tests in clays. 10th ICSMFE - Stockholm, Sweden. 2: pp.433-438.
8. Belkacemi, S. 1988. Laboratory study in a calibration chamber of a pressuremeter test on clay. Ph.D. Thesis - Tufts University, Massachusetts, USA.
9. Bellotti, R., Crippa, V., Ghionna, V.N., Jamiolkowski, M. and Robertson, P.K. 1987. Self-boring pressuremeter in pluvially deposited sands. Technical Report - ENEL CRIS, Milan, Italy.
10. Bellotti, R., Ghionna, V., Jamiolkowski, M., Lancellotta, R. and Manfredini, G. 1986. Deformation characteristics of cohesionless soils from in situ tests. In Situ '86 -Use of In Situ Tests in Geotechnical Engineering - Virginia, USA. pp.47-73.
11. Bellotti, R., Ghionna, V., Jamiolkowski, M., Robertson, P.K. and Peterson, R.W. 1988. Interpretation of moduli from self-boring pressuremeter tests in sand. Geotechnique. 39: N°2 pp.269-292.
12. Benoit, J., Oweis, S. and Leung, A. 1990. Self-boring pressuremeter

- testing of the Hackensack Meadows varved clays. Proceedings of the Third International Symposium on Pressuremeters - Oxford, England. pp.85-104.
13. Briaud, J.L. and Cosentino, P.J. 1990. Pavement design with the pavement pressuremeter. Proceedings of the Third International Symposium on Pressuremeters - Oxford, England. pp.401-413.
  14. Briaud, J.L. and Lytton, R.L. 1983. Obtaining moduli from cyclic pressuremeter tests. Journal of the Geotechnical Engineering - ASCE. 109: pp.657-665.
  15. Briaud, J.L., Tucker, L.M. and Makarim, C.A. 1986. Pressuremeter standard and pressuremeter parameters. The pressuremeter and Its Marine Applications: Second International Symposium - Texas, USA. pp.303-323.
  16. Burgess, N.C. 1975. The University of Alberta pressuremeter. M.Sc. Thesis - University of Alberta, Alberta, Canada.
  17. Campanella, R.G., Howie, J.A., Sully, J.P. and Robertson, P.K. 1990. Evaluation of Cone Pressuremeter Tests in Soft Cohesive Soils. Proceedings of the Third International Symposium on Pressuremeters - Oxford, England. pp.125-135.
  18. Clough, G.W., Briaud, J.L. and Hughes, J.M.O. 1990. The development of pressuremeter testing. Proceedings of the Third International Symposium on Pressuremeters - Oxford, USA. pp.25-45.
  19. Coutinho, A.G.F.S. 1990. Radial expansion of cylindrical cavities in sandy soil: application to pressuremeter tests. Canadian Geotechnical Journal. 67: pp.737-748.
  20. Denby, G.M. 1978. Self-boring pressuremeter study of the San Francisco Bay mud. Ph.D. Thesis - Stanford University, California, USA.
  21. Drucker, D.C. 1987. Comments on the Modeling of the Behavior of Sand. Proceedings of the International Workshop on Constitutive Equations for Granular Non-Cohesive Soils - Ohio, USA. pp.695-697.
  22. Duncan, J.M. and Chang, C.Y. 1970. Nonlinear analysis of stress and strain in soils. Journal of the Soil Mechanics and Foundation Division - ASCE. 96: SM5 pp.1629-1653.
  23. Eisenstein, Z. and Morrison, N.A.. 1973. Prediction of foundation deformations in Edmonton using as in situ pressure probe. Canadian Geotechnical Journal. 10: pp.193-209.
  24. Ervin, M.C. 1983. The pressuremeter in geotechnical investigations. Proceedings of an extension course on in situ testing for geotechnical

investigations - Sidney, Australia. pp.49-63.

25. Fahey, M. and Carter, J.P. 1991. Finite element simulation of the pressuremeter test in sand using a Mohr-Coulomb model with non-linear elasticity. Research Report - The University of Western Australia. RR N° G1023:
26. Ferreira, R.S. and Robertson, P.K. 1992. Interpretation of undrained self-boring pressuremeter test results incorporating unloading. Submitted and accepted to be published in Canadian Geotechnical Journal.
27. Fioravante, V. 1988. Interpretazione delle prove pressiometriche in argille con particolare riferimento alla fase di holding. Dottorato di Ricerca in Ingegneria Geotecnica - Politecnico di Torino, Torino, Italy.
28. Fukagawa, R. and Iizuka, A. 1990. Effects of drainage on interpretation of pressuremeter tests in clay. Proceedings of the Third International Symposium on Pressuremeter - Oxford, England. pp.189-198.
29. Fyffe, S., Reid, W.M. and Summers, J.B. 1986. The push-in pressuremeter. The pressuremeter and Its Marine Applications: Second International Symposium - Texas, USA. pp.22-37.
30. Gambin, M.P. 1990. The history of pressuremeter practice in France. Proceedings of the Third International Symposium on Pressuremeters - Oxford, England. pp.5-24.
31. Ghionna, V., Jamiolkowski, M., Lacasse, S., Ladd, C.C., Lancellotta, R. and Lunne T. 1983. Evaluation of self-boring pressuremeter. Symposium International - In Situ Testing, Paris, France. 2: pp.293-301.
32. Ghionna, V.N. 1990. Limit pressure in expansion of cylindrical cavity in sand. Proceedings of the Third International Symposium on Pressuremeters - Oxford, England. pp.149-158.
33. Ghionna, V.N., Jamiolkowski, M. and Lancellotta, R. 1982. Characteristics of saturated clays as obtained from SBP tests. Symposium on the Pressuremeter and Its Marine Applications - Paris, France. pp.165-185.
34. Gibson, R.E. and Anderson, W.F. 1961. In-situ measurement of soil properties with the pressuremeter. Civil Engineering and Public Works Review, London, England. 56: pp.615-618.
35. Hardin, B.O. and Drnevich, V.P. 1972. Shear modulus and damping in soils: Measurement and parameters effects. Journal of the Soil Mechanics and Foundation Division - ASCE. 98: SM6: pp.603-624.
36. Houlsby, G.T. and Yu, H.S. 1990. Finite element analysis of the cone-

- pressuremeter test. Proceedings of the Third International Symposium on Pressuremeters - Oxford, England. pp.221-230.
37. Houlsby, G.T., Clarke, B.G. and Wroth, P. 1986. Analysis of the unloading of a pressuremeter in sand. The pressuremeter and Its Marine Applications: Second International Symposium - Texas, USA. pp.245-262.
38. Houlsby, G.T. and Withers, N.J. 1988. Analysis of the cone pressuremeter test in clay. *Geotechnique*. 38: N°4 pp.575-587.
39. Howie, J.A. 1991. Factors affecting the analysis and interpretation of full-displacement pressuremeter tests. Ph.D. Thesis - University of British Columbia, British Columbia, Canada.
40. Huang, A.B., Holtz, R.D. and Chameau, J.L. 1991. Laboratory study of pressuremeter tests in clays. *Journal of Geotechnical Engineering - ASCE*. 117: N°10. pp.1549-1567.
41. Hughes, J.M.O. 1982. Interpretation of pressuremeter tests for the determination of the elastic shear modulus. *Updating Subsurface Samplings of Soils and Rocks and their In Situ Testing - California, USA*. pp.279-289.
42. Hughes, J.M.O. and Robertson, P.K. 1985. Full displacement pressuremeter testing in sands. *Canadian Geotechnical Journal*. 22: No.3:
43. Hughes, J.M.O., Wroth, C.P. and Windle, D. 1977. Pressuremeter Tests in Sands. *Geotechnique*. 27: N°4 pp.455-477.
44. Jamiolkowski, M. and Lancellotta, R. 1977a. Remarks on the use of self-boring pressuremeter in three Italian clays. *Revista Italiana Geotecnica*. 11: N°3.
45. Jamiolkowski, M. and Lancellotta, R. 1977b. On the reliability of the strength and deformation characteristics as deduced from the self-boring pressuremeter tests. IX ICSMFE - Tokyo, Japan. Discussion.
46. Jefferies, M.G. 1988. Determination of horizontal geostatic stress in clay with self-bored pressuremeter. *Canadian Geotechnical Journal*. 25: pp.559-573.
47. Jewell, R.J., Fahey, M. and Wroth, P. 1980. Laboratory studies of the pressuremeter test in sand. *Geotechnique*. 30: pp.507-531.
48. Juran, I. and Mahmoodzadegan, B. 1989. Interpretation procedure for pressuremeter tests in sand. *Journal of Geotechnical Engineering - ASCE*. 115: N°11 pp.1617-1632.
49. Kondner, R.L. 1963. Hyperbolic stress-strain response: cohesive soil.



- Journal of the Soil Mechanics and Foundation Division - ASCE. 89: pp.115-143.
50. Kondner, R.L., Zelasko, J.S. 1963. A hyperbolic stress-strain formulation for sands. Proceedings of the Second Pan-American Conference on Soil Mechanics and Foundation Engineering - Sao Paulo, Brazil. pp.289-324.
  51. Lacasse, S., D'orazio, T.B. and Bandis, C. 1990. Interpretation of self-boring and push-in pressuremeter tests. Proceedings of the Third International Symposium on Pressuremeters - Oxford, England. pp.273-285.
  52. Ladanyi, B. 1961. Étude théorique et expérimentale de l'expansion dans un sol pulvérulent d'une cavité présentant une symétrie sphérique ou cylindrique. Annales des Travaux Public de Belgique N°.2-4. pp81.
  53. Ladanyi, B. 1963. Evaluation of pressuremeter tests in granular soils. Proceedings of the Second Pan-American Conference on Soil Mechanics and Foundation Engineering - Sao Paulo, Brazil. pp.3-20.
  54. Ladanyi, B. 1972. In situ determination of undrained stress-strain behavior of sensitive clays with the pressuremeter. Canadian Geotechnical Journal. 9: pp.313-319.
  55. Ladanyi, B. 1972b. Interpretation of pressuremeter test results in frozen soils. NRCC-DBR, Canada, Internal Report N°.401. pp118.
  56. Law, K.T. and Eden, W.J. 1982. Effects of soil disturbance in pressuremeter tests. Updating Subsurface Sampling of Soils and Rocks and their In Situ Testing - California, USA. pp.291-303.
  57. Mair, R.J. and Wood, D.M. 1987. Pressuremeter testing - Methods and interpretation. CIRIA Ground Engineering Report: In situ testing - Butterworths. pp.160.
  58. Manassero, M. 1989. Stress-strain relationships from drained self-boring pressuremeter tests in sands. Geotechnique. 39: pp.293-307.
  59. Morrison, N.A. 1972. Investigation of foundation deformation using in situ probe. M.Sc. Thesis - University of Alberta, Alberta, Canada.
  60. Palmer, A.C. 1972. Undrained plane-strain expansion of a cylindrical cavity in clay: a simple interpretation of the pressuremeter test. Geotechnique. 22: pp.451-457.
  61. Prapaharan, S. 1987. Effects of disturbance, strain rate and partial drainage on pressuremeter test results in clay. Ph.D. Thesis - Purdue University, Indiana, USA.

62. Prevost, J.H. and Hoeg, K. 1975. Analysis of pressuremeter in strain-softening soil. *Journal of Geotechnical Engineering - ASCE*. 101: N°GT8 pp.717-732.
63. Pyrah, I.C., Anderson, W.F. and Ali, F.H. 1985. The interpretation of pressuremeter tests: Time effects for fine-grained soils. *Fifth International Conference on Numerical Methods in Geomechanics - Nagoya, Japan*. 3: pp.1629-1636.
64. Robertson, P.K. 1982. In situ testing of soil with emphasis on its application to liquefaction assessment. Ph.D. - University of British Columbia, British Columbia, Canada.
65. Robertson, P.K. and Hughes, J.M.O. 1986. Determination of properties of sand from self-boring pressuremeter tests. *The pressuremeter and Its Marine Applications: Second International Symposium - Texas, USA*. pp.283-302.
66. Rowe, P.W. 1962. The stress dilatancy relation for static equilibrium for any assembly of particles in contact. *Proc. R. Soc., Series A*. 269: pp.500-527.
67. Rowe, P.W. 1972. Stress-strain relationship for particulate materials at equilibrium. *Proceedings of the Specialty Conference on the performance of earth supported structures - Purdue University, Indiana, USA*. pp.327-359.
68. Salgado, F.M.G.A. 1990. Analysis procedures for caisson-retained island type structures. Ph.D. Thesis - University of British Columbia, British Columbia - Canada.
69. Sayed, M.S. and Hamed, M.A. 1988. Pressuremeter test and disturbance effects. *Journal of Geotechnical Engineering - ASCE*. 114: N°5 pp.631-637.
70. Terzaghi, K. and Peck, R.B. 1948. *Soil mechanics in engineering practice*. John Wiley & Sons Inc., New York.
71. Vesic, A.S. 1972. Expansion of cavities in infinite soil mass. *Journal of the Soil Mechanics and Foundation Division - ASCE*. 98: pp.265-289.
72. Vucetic, M. and Dobry, R. 1991. Effect of soil plasticity on cyclic response. *Journal of Geotechnical Engineering*. 117: pp.89-107.
73. Williams, D.J. 1986. Evaluation of different soil tests for determining design parameters. *Interpretation of Field Testing for Design Parameters - Adelaide, Australia*. pp.174-179.

74. Withers, N.J., Howie, J. and Robertson, P.K. 1989. Performance and analysis of cone-pressuremeter tests in sands. *Geotechnique*. 39: N°3 pp.433-454.
75. Withers, N.J., Schaap, L.H.J. and Dalton, C.P. 1986. The development of a full-displacement pressuremeter. *The Pressuremeter and Its Marine Applications: Second International Symposium - Texas, USA*. pp.38-56.
76. Wood, D.M. 1990. Strain-dependent moduli and pressuremeter tests. *Geotechnique, Technical Note*. 40: N°3: pp.509-512.
77. Wood, D.M. 1990. Strain-dependent moduli and pressuremeter tests. *Geotechnique, Discussion*. 41: N°4 pp.621-626.
78. Wroth, C.P. 1975. In situ measurement of initial stresses and deformation characteristics. *Proceedings of the Conference on In situ Measurement of Soil Properties - North Carolina, USA*. 2: pp.181-230.
79. Wroth, C.P. 1984. The interpretation of in situ soil tests. *Geotechnique*. 34: pp.449-489.
80. Wroth, C.P. 1982. British experience with the self-boring pressuremeter. *Symposium on the Pressuremeter and Its Marine Applications - Paris, France*. pp.143-163.
81. Wroth, C.P. and Windle, D. 1975. Analysis of the pressuremeter test allowing for volume change. *Geotechnique*. 25: N°3 pp.598-604.
82. Yeung, S.K. and Carter, J.P. 1990. Interpretation of the pressuremeter test in clay allowing for membrane end effects and material non-homogeneity. *Proceedings of the Third International Symposium on Pressuremeters - Oxford, England*. pp.199-208.

**APPENDIX - A****TYPES OF PRESSUREMETER DEVICES**

The task of expanding a cavity within all soil or rock types cannot be accomplished with just one type of pressuremeter device. For example, the pre-bored, also called the Menard type pressuremeter, is difficult to use in medium to soft clay soil or medium to loose saturated sand. In addition, due to its capabilities, a pressuremeter test is considered so powerful that several devices with special characteristics are necessary to deal with the many problems or conditions encountered, e.g. (a) testing a particular type of soil or rock; (b) minimizing disturbance caused during insertion; (c) avoiding excessive test costs; (d) avoiding excessive influence of the operator on the results; (e) being flexible enough to be used on-shore and off-shore; and (f) allowing the use of theoretical background in result interpretation.

To solve such a broad range of problems, four types of pressuremeter devices are currently used: (a) pre-bored pressuremeter (PBP) also called Menard type; (b) self-boring pressuremeter (SBP); (c) push-in pressuremeter (PIP); and (d) full-displacement pressuremeter (FDP).

The first two types are mostly used on-shore and are responsible for the great majority of pressuremeter test results. The third type has a specific off-shore application, and the last one has the ability to link some advantages of the cone penetration test (CPT) and the pressuremeter test.

**A.1 Pre-bored (Menard type) pressuremeter (PBP)**

The pre-bored pressuremeter test is performed in a pre-drilled hole. Most of the design rules based on the PBP originated from Menard's work in the early 60's. The problem of soil disturbance is the most significant factor affecting PBPT results. Investigation by Menard and the Laboratoire Central de Ponts et Chaussées (LCPC) in France have led to the development of standard procedures for this type of test. A complete description of these procedures is given in Baguelin et al (1978). The quality of foundation design using the

Menard type pressuremeter is often very good providing the tests are carried out according to the standard methods using standard equipment in soils similar to those that have been studied in the development of the empirical design rules. In medium to stiff clays and soft rocks, where installation procedure is easier and a good test hole can be formed, the results are usually more repeatable. However, in soft saturated soils, disturbance can be significant and test results are not always repeatable. Full details of the various factors affecting PBPT results are given by Baguelin et al (1978). An ideal pre-bored pressuremeter test result is presented in figure A-1.

### A.2 Self-boring pressuremeter (SBP)

Efforts to minimize soil disturbance led to the development of self-boring devices in the early 70's. The self-boring pressuremeter is self-bored into the ground. This improvement resulted in a series of developments related to the theoretical interpretation of the SBPT. However, the process of installation by current SBP's is not always efficient (Clough, 1990) and is often subject to problems, resulting in some disturbance especially in very stiff soils. Hence, most SBPT results are subject to some unknown degree of disturbance, and the level of disturbance tends to increase with increasing soil stiffness. Soil disturbance during installation of the SBP has the greatest effect on the shape of the initial loading portion of the pressuremeter curve. An ideal self-boring pressuremeter test result with no soil disturbance is presented in figure A-2.

### A.3 Push-in pressuremeter (PIP)

Developed in the UK in the late 70's, the push-in pressuremeter became available commercially in 1980. Specially designed for off-shore operation, the PIP is similar to a sampling tube with an unrestricted passage through its hollow cylinder body (Mair and Wood, 1987). Although some soil is recovered within the instrument during the insertion procedure, unavoidable disturbance is generated, stressing the soil into which it is being pushed. For this reason the interpretation of its results using available techniques to determine undrained shear strength and in situ horizontal stress are not recommended

(Lacasse, 1990). A push-in pressuremeter test result with common soil disturbance is presented in figure A-3.

#### A.4 Full-displacement pressuremeter (FDP)

Initially intended to overcome some difficulties in performing pressuremeter tests in the off-shore environment, the full-displacement pressuremeter also called the cone pressuremeter is still under development. The first prototype became available in 1983 and a limited number of tests were performed, both on-shore and off-shore sites. Developed to be performed during a cone penetration operation, the FDPT is attractive because of the following advantages: (a) the large soil disturbance caused by insertion can be repeatable and is not operator dependent; (b) measurement of deformation properties by the pressuremeter can immediately be related to the measurements of the cone penetration resistance at the same depth; (c) deformation properties can give useful information for the design of laterally loaded piles which are commonly used in off-shore structures (Withers, 1986). As expected, the installation process makes the soil largely overstressed; hence, a larger expansion capacity should be provided to the pressuremeter so that the intact soil response can be recorded. A full unloading curve should be provided during the FDPT and the interpretation of the test results can be based primarily on this contraction phase (Houlsby and Withers, 1988). An ideal full-displacement pressuremeter test result is presented in figure A-4.

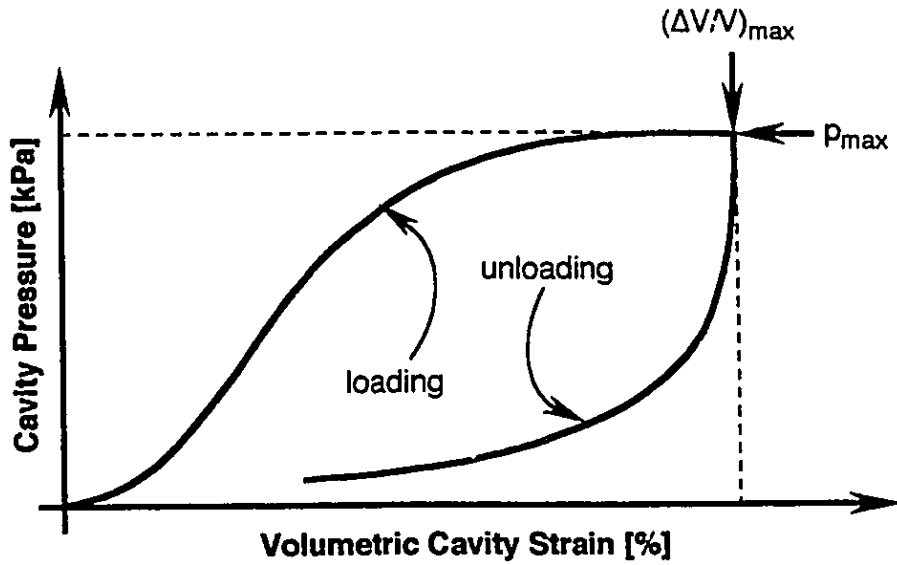


Figure A - 1 Ideal results of the field PBPT.

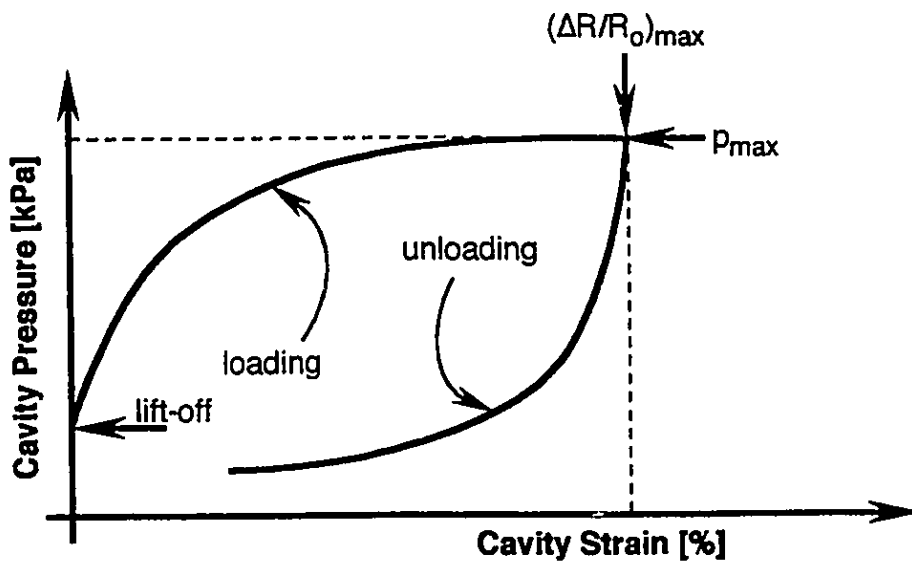


Figure A - 2 Ideal results of the field SBPT.

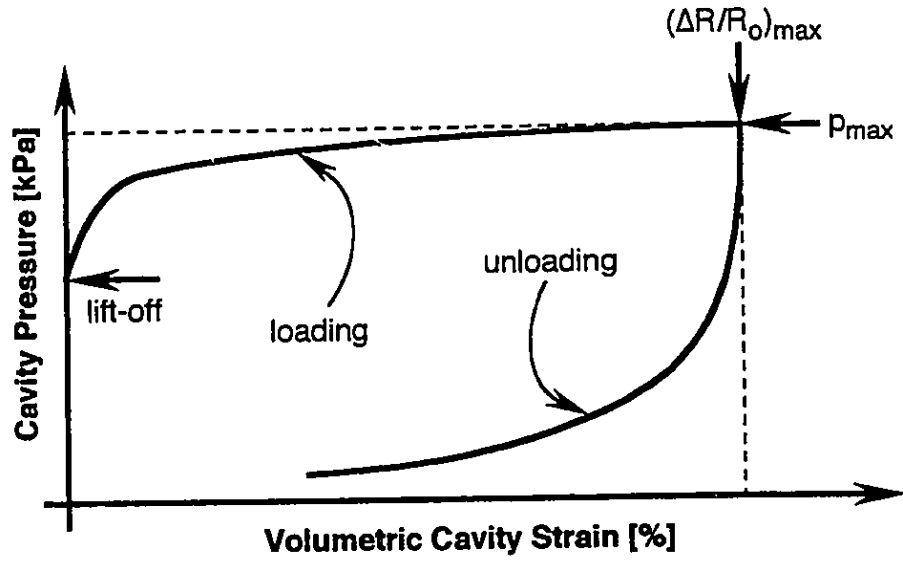


Figure A - 3 Ideal results of the field PIPT.

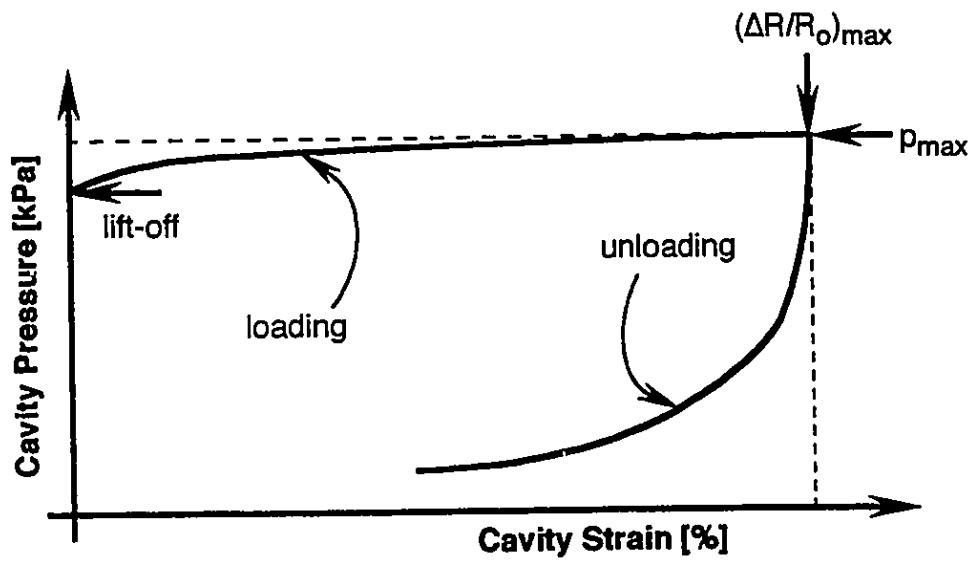


Figure A - 4 Ideal results of the field FDPT.



**APPENDIX - B****PRESSUREMETER RELATED THESES AND DISSERTATIONS**

Since the early 70's, the pressuremeter has been the subject of research in many Universities and Research Institutes around the world. Several countries, besides England and France, have given important contributions. This interest was driven by its potential to improve geotechnical design.

Pressuremeter devices have been constructed and used not only to yield empirical information, but also to determine soil and rock constitutive parameters for more sophisticated analyses, such as finite element methods.

A list of pressuremeter related dissertations and theses is given below starting with the earliest academic work on the subject. Although limited in number, this list is intended to help identify the nature of the research and places where these studies have been developed.

1. Menard, L. 1957. An apparatus for measuring the strength of soils in place. M.Sc. Dissertation. University of Illinois, USA.
2. Ladanyi, B. 1961. Étude théorique et expérimentale de l'expansion dans un sol pulvérulent d'une cavité présentant une symétrie sphérique ou cylindrique. Annales des Travaux Public de Belgique No.2-4. pp81.
3. Morrison, N.A. 1972. Investigation of foundation deformation using in situ pressure probe. M.Sc. Thesis. University of Alberta, Canada.
4. Hughes, J.M.O. 1973. An instrument for the in situ measurement of the properties of soft clays. Ph.D. Thesis. University of Cambridge, UK.
5. Hartman, J.P. 1974. Finite element parametric study of vertical strain influence factors and the pressuremeter test to estimate the settlement of footings in sand. Ph.D. Thesis. University of Florida, USA.

6. Laier, J.E. 1974. Effects of pressuremeter probe length-diameter ratio and borehole disturbance on pressuremeter test results in dry sand. Ph.D. Thesis. University of Florida, USA.
7. Al-Awkati, Z. 1975. On problem of soil bearing capacity at depth. Ph.D. Thesis. Duke University, USA.
8. Burgess, N.C. 1976. The University of Alberta pressuremeter. M.Sc. Thesis. University of Alberta, Canada.
9. Windle, D. 1976. In situ testing of soils with a self-boring pressuremeter. Ph.D. Thesis. University of Cambridge, UK.
10. Denby, G.M. 1978. Self-boring pressuremeter study of the San Francisco Bay mud. Ph.D. Thesis. Stanford University, USA.
11. Briaud, J.-L. 1979. The pressuremeter: Application to pavement design. Ph.D. Thesis. University of Ottawa, Canada.
12. Fahey, M. 1980. A study of the pressuremeter test in dense sand. Ph.D. Thesis. University of Cambridge, UK.
13. Huang, W.F. 1980. LLT pressuremeter in Bangkok clay. M.Eng, Dissertation. Asian Institute of Technology, Thailand.
14. Steussy, D.K. 1980. Development of SBP for efficient use in clays. Geotechnical Engineering Thesis. University of Texas, USA.
15. Clarke, B.G. 1981. In situ testing of clays using Cambridge self-boring pressuremeter. Ph.D. Thesis. University of Cambridge, UK.
16. Degenne, P. 1981. Expansion d'une cavite cylindrique dans des sols très compressibles et très déformables. M.Sc. Dissertation. Ecole Polytechnique Montreal, Canada.

17. Sellgren, E. 1981. Friction piles in non-cohesive soils: Evaluation from pressuremeter tests. Ph.D. Thesis. Chalmers University of Technology, Gothenburg.
18. Surya, I. 1981. Application of the LLT pressuremeter test to soil engineering problems in Bangkok clay. M.Eng. Dissertation. Asian Institute of Technology, Thailand.
19. Robertson, P.K. 1982. In situ testing of soil with emphasis on its application to liquefaction assessment. Ph.D. Thesis. University of British Columbia, Canada.
20. Benoit, J. 1983. Analysis of self-boring pressuremeter tests in soft clay. Ph.D. Thesis. Stanford University, USA.
21. Eldridge, T.L. 1983. Pressuremeter tests in sands : Effects of dilation. M.Sc. Dissertation. University of British Columbia, Canada.
22. Kauschinger, J.L. 1983. Evaluation and implementation of Prevost's total stress model. Ph.D. Thesis. University of Texas, USA.
23. Pavlakis, M. 1983. Prediction of foundation behaviour in residual soils from pressuremeter tests. Ph.D. Thesis. University of Witwatersrand, South Africa.
24. Smith, T.D. 1983. Pressuremeter design method for single piles subjected to static lateral load. Ph.D. Thesis. Texas A&M University, USA.
25. Khaleque, M.A. 1984. Correlation of pressuremeter, vane, and Dutch cone tests on Bangkok clay. M.Eng. Dissertation. Asian Institute of Technology, Thailand.
26. Negussey, D. 1984. An experimental study of the small strain response of sand. Ph.D. Thesis. University of British Columbia, Canada.

27. Brown, P.T. 1985. Predicting laterally loaded pile capacity using the pressuremeter. M.Sc. Dissertation. University of British Columbia, Canada.
28. Chang, C.C. 1985. Correlation of soil parameters from pressuremeter test with index properties and compressibility characteristics of Bangkok clay. M.Eng. Dissertation. Asian Institute of Technology, Thailand.
29. Jain, S.K. 1985. Analysis of the pressuremeter test by FEM formulation of the elasto-plastic consolidation. Ph.D. Thesis. Virginia P.I. and State University, USA.
30. Ruj, N.. 1985. Correlation of pressuremeter test, Dutch cone test, and Standard penetration test in first stiff clay and first sand layers in Bangkok clay. M.Eng. Dissertation. Asian Institute of Technology, Thailand.
31. Ameratunga, J.J.P. 1986. A numerical assessment of pressuremeter testing in soft rock. Ph.D. Thesis. Monash University, Australia.
32. Huang, A.B. 1986. Laboratory pressuremeter experiments in clay soils. Ph.D. Thesis. Purdue University, USA.
33. Yan, L. 1986. Numerical studies of some aspects with pressuremeter tests and laterally loaded piles. M.Sc. Dissertation. University of British Columbia, Canada.
34. Cosentino, P.J. 1987. Pressuremeter moduli for airport pavement design. Ph.D. Thesis. Texas A.M. University, USA.
35. Haberfield, C.M. 1987. The performance of the pressuremeter and socketed piles in weak rock. Ph.D. Thesis. Monash University, Australia.
36. Mayu, P. 1987. Determining parameters for stiff clays and residual soils using self-boring pressuremeter. Ph.D. Thesis. Virginia P.I. and State University, USA.

37. Prapaharan, S. 1987. Effects of disturbance, strain rate and partial drainage on pressuremeter test results in clay. Ph.D. Thesis. Purdue University, USA.
38. Belkacemi, S. 1988. Laboratory study in a calibration chamber of a pressuremeter test on silt. Ph.D. Thesis. Tufts University, USA.
39. Fioravante, V.. 1988. Interpretation of the pressuremeter test in clay with emphasis on holding stage. Ph.D. Thesis. Politecnico di Torino, Italy.
40. Yeung, S.K. 1988. Application of cavity expansion model in geotechnical engineering. Ph.D. Thesis. University of Sidney, Australia.
41. Atwood, M.J. 1989. Investigation of jetting insertion procedure for rapid deploying a self-boring pressuremeter in soft clays. M.Sc. Dissertation. University of New Hampshire, USA.
42. Hers, I. 1989. The analysis and interpretation of the cone pressuremeter in cohesive soil. M.Sc. Dissertation. University of British Columbia, Canada.
43. Powell, J.J.M. 1989. In situ testing of stiff clays. Ph.D. Thesis. University of London (Imperial College), UK.
44. Salgado, F.M. 1989. Analysis procedures for caisson-retained island type structures. Ph.D. Thesis. University of British Columbia, Canada.
45. Lien, B. 1990. Anisotropic behaviour and cylinder expansion of pressuremeter in stiff soils. Ph.D. Thesis. Virginia P.I. and State University, USA.
46. Pappas, J.L. 1990. Determination of parameters for stiff soils by pressuremeter testing. Ph.D. Thesis. Virginia P.I. and State University, USA.

47. Schnaid, F. 1990. A study of the cone pressuremeter test in sand. Ph.D. thesis. University of Oxford, UK.
48. Yu, H.S. 1990. Cavity expansion theory and its application to the analysis of the pressuremeter. Ph.D. Thesis. University of Oxford, UK.
49. Howie, J.A. 1991. Factors affecting the analysis and interpretation of full-displacement pressuremeter tests. Ph.D. Thesis. University of British Columbia, Canada.

## APPENDIX C

### FUCINO CLAY - V2 SBPT's - INTERPRETATION RESULTS

#### C.1 Introduction

Since the late 70's, important contributions have been made in Italy to a better understanding of the pressuremeter test. Some studies have dealt with self-boring pressuremeter test in clays (Battaglio et al, 1981; Ghionna et al, 1982; Fioravante, 1988) and in sands (Bellotti et al, 1988; Manassero, 1989; Ghionna, 1990). Both in situ and laboratory (calibration chamber) tests have been used for this purpose.

Fioravante(1988) presented 36 SBPT results performed in clay at Fucino Site in two boreholes - V1 and V2. The first test, V1P01 (2m), was performed on May 11, 1987 and the last test, V2P20 (38m), on June 1<sup>st</sup>, 1987. The device used was the Camkometer N.770512. Additional information on this test program can be found in Fioravante(1988).

#### C.2 Interpretation results

From the SBPT results presented by Fioravante(1988) 20 tests from borehole V2 were interpreted using the methodology presented in chapter 4. For each test two figures are presented. The first figure shows the interpretation template used to obtain the clay parameters. The second one shows two plots. The first plot shows the curve fitting of the unload phase of the test. The second one shows the final plot that permits an overall appreciation of the curve matching for both phases of each SBPT, loading and unloading. Figures C-01 to C-20 show the interpreted results of the Fucino clay.

#### C.3 Comments on the interpreted results

- Firstly, a comment on the experimental test results presented by Fioravante(1988) is necessary. For the loading phase of the tests, the complete loading curve was presented, from the lift-off pressure to the

maximum loading pressure reached during the test. However, the unloading phase was shown partially, from the maximum pressure to the lift-off pressure. It means that the soil response during unloading for pressures smaller than the lift-off pressure was omitted. The lack of information on the complete unloading response has just a marginal effect on the interpreted soil parameters. During the interpretation procedure, presented in chapter 4, the points that deviate from the true response are generally identified and discarded. However, the complete unloading curve, from the maximum expansion of the membrane to its complete contraction, is always recommended for all pressuremeter tests.

- For all the experimental SBPT results analyzed, the curve matching for the unloading phase of the tests was excellent. From this curve fitting two parameters were derived - the initial tangent shear modulus and the ultimate undrained shear strength during unloading. For the Fucino clay the derived small strain unloading pressuremeter equation can easily follow the unloading experimental curves and yields acceptable values for the derived soil parameters. The matching of the analytical and experimental loading curves, however, shows some discrepancies.
- A very good matching of the loading curves was obtained for the tests: V2P02, V2P04, V2P05, V2P11, V2P13, V2P14, V2P15, V2P16, V2P18, and V2P19. Depending on the improvement of the curve matching either one of the following options was considered during the curve fitting procedure: (a) last half of the loading points; (b) last quarter of the loading points; and (c) just the very last points. For case (c), the number of fitted loading points was increased by interpolating additional points, in order to avoid a correlation factor out of the range [0,1] during the least square error calculation. The following tests had the curve fitting done just to the very last points of the experimental loading curve: V2P06, V2P07, V2P08, V2P09, V2P10, V2P12, V2P17, and V2P20.
- Tests V2P01 and V2P03 are examples of poor fitting using the last half of the experimental loading points. The first test was too shallow so that the actual mode of failure in situ does not agree with the mode of failure assumed



for the analytical equations derivation. For shallow depths the vertical stress can become the minor principal stress during the pressuremeter test. The test V2P03 was used just to present an example on the deviation of the final analytical loading pressure if the last half of the experimental loading points were used during the curve fitting procedure.

- One important reason for the poor matching between the analytical and experimental loading curves is the presence of a variable degree of disturbance during the device insertion and during the test itself. The relative position of the analytical and the experimental loading curves can qualitatively suggest what type of disturbance occurred during the test. Just the two most common types of disturbance will be considered here: (a) oversized hole, and (b) undersized hole. For example, figure C - 17 (b2) shows the analytical loading curve above the experimental curve. One possible explanation for such situation is the disturbance caused by a very small borehole oversizing. In this case the soil is partially unloaded and the lift-off pressure is smaller than the in situ initial horizontal stress. The opposite is shown in figure C - 10 (b2). The analytical curve is below the experimental curve. In this situation the explanation could be a disturbance caused by undersized borehole. The lift-off pressure is greater than the initial in situ horizontal stress. Subsequent drainage is likely to occur due to the high pore pressures generated. So, a greater deformation modulus was recorded as the soil response. Although it is not possible to quantify the amount of generated disturbance during a SBPT, the indication above can be helpful during the interpretation procedure.

- The final derived soil parameters were compared to the soil parameters determined using other in situ and laboratory tests reported by AGI (1991). Figures 4.12, 4.13, and 4.14 show the comparison of the Fucino clay parameters varying with depth.

## PRESSUREMETER INTERPRETATION TEMPLATE - CLAYS

TEST ID Fucino clay - Test V2P01

DEPTH [m] 2.0 LIFT-OFF [kPa] 7.85

Loading :  $p_{max}$  [kPa] 139.0  $\epsilon_{max}$  [dec] 0.105

Unloading :  $p_{max}$  [kPa] 139.0  $\epsilon_{max}$  [dec] 0.105

### STEP # 1 - UNLOADING (Best fit with two parameters)

(a) All unloading points

$\tau_{ult}^*$  = \_\_\_\_\_ Graph Page \_\_\_\_\_

$2G_i$  = \_\_\_\_\_

(b) (some data points removed) Discard the last points

$\tau_{ult}^*$  = 50.9 Graph Page Figure C - 01 (b1)

$2G_i$  = 9,145.0

### STEP # 2 - LOADING (Best fit with one parameter $R_c=2.0$ )

(a) All loading points

$\sigma_{ho}$  = \_\_\_\_\_ Graph Page \_\_\_\_\_

(b) Strain range (first option) Last half  
 $\sigma_{ho}$  = 37.0 Graph Page Figure C - 01 (b2)

(c) Strain range (second option) Last quarter  
 $\sigma_{ho}$  = \_\_\_\_\_ Graph Page \_\_\_\_\_

(d) Strain range (third option) Interpolate points at the very last end  
 $\sigma_{ho}$  = \_\_\_\_\_ Graph Page \_\_\_\_\_

### STEP # 3 - SUMMARY

(a) First strain range selected: Step # 2 option (b)

$\tau_{ult}^*$  = 50.9  $\tau_{ult}$  = 25.5 Graph Page Figure C - 01 (b2)

$2G_i$  = 9,145.0  $\sigma_{ho}$  = 37.0

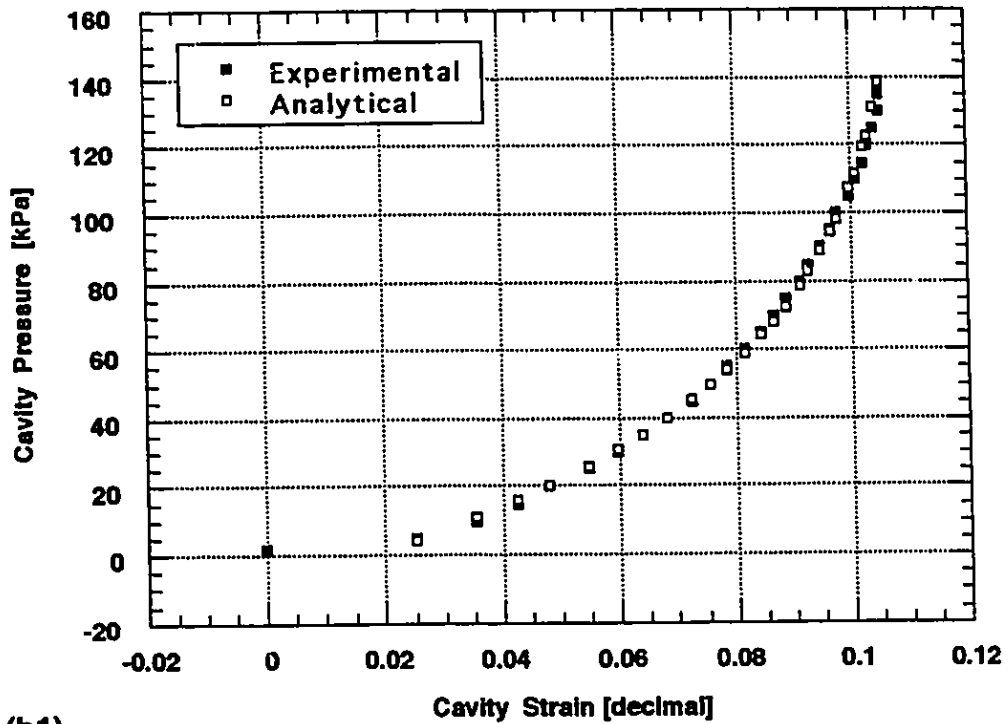
(b) Second strain range selected

$\tau_{ult}^*$  = \_\_\_\_\_  $\tau_{ult}$  = \_\_\_\_\_ Graph Page \_\_\_\_\_

$2G_i$  = \_\_\_\_\_  $\sigma_{ho}$  = \_\_\_\_\_

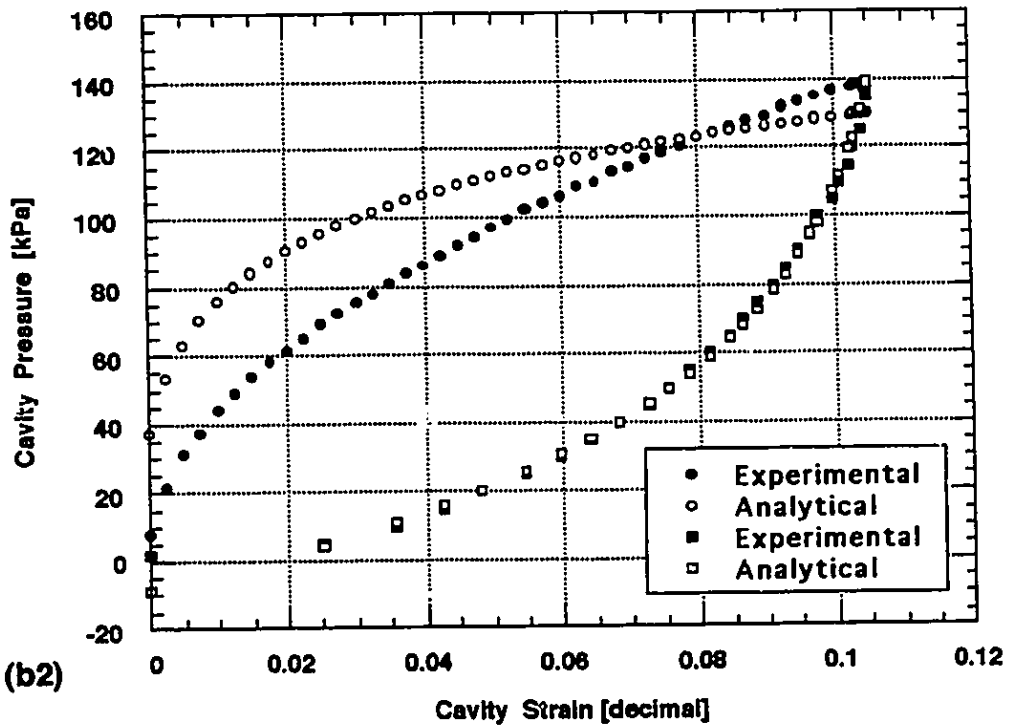
Figure C - 01 (a) Fucino clay test V2P01: Interpretation template.

Fucino Clay - Test V2P01 - Unload Fitting



(b1)

Fucino Clay - Test V01 - Final Plot



(b2)

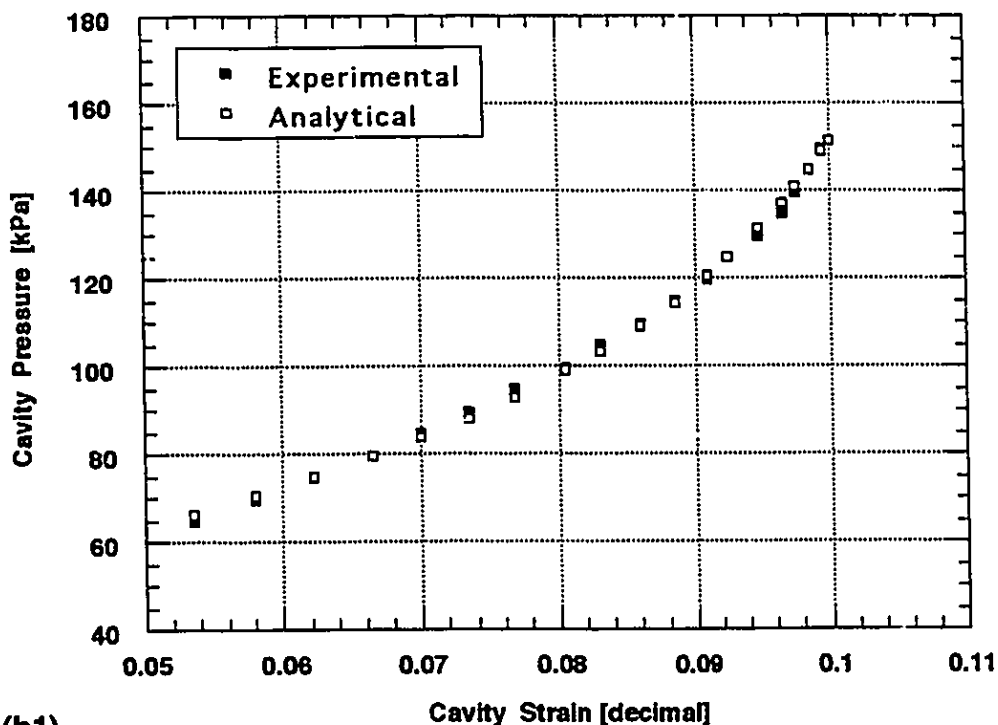
Figure C - 01 (b) Fucino clay test V2P01: (b1) Unload fitting; (b2) Final plot

## PRESSUREMETER INTERPRETATION TEMPLATE - CLAYS

TEST ID	Fucino clay - Test V2P02		
DEPTH [m]	3.5	LIFT-OFF [kPa]	64.73
Loading :	p <sub>max</sub> [kPa] <u>154.73</u>	ε <sub>max</sub> [dec] <u>0.10</u>	
Unloading :	p <sub>max</sub> [kPa] <u>151.73</u>	ε <sub>max</sub> [dec] <u>0.10</u>	
<b>STEP # 1 - UNLOADING (Best fit with two parameters)</b>			
<b>(a) All unloading points</b>			
	τ <sub>ult</sub> <sup>*</sup> = 50.7	Graph Page	<u>Figure C - 02 (b1)</u>
	2G <sub>i</sub> = 5,235.6		
<b>(b) (some data points removed)</b>			
	τ <sub>ult</sub> <sup>*</sup> =	Graph Page	_____
	2G <sub>i</sub> =		
<b>STEP # 2 - LOADING (Best fit with one parameter R<sub>c</sub>=2.0)</b>			
<b>(a) All loading points</b>			
	σ <sub>ho</sub> =	Graph Page	_____
<b>(b) Strain range (first option) Last half</b>			
	σ <sub>ho</sub> = 77.3	Graph Page	<u>Figure C - 02 (b2)</u>
<b>(c) Strain range (second option) Last quarter</b>			
	σ <sub>ho</sub> =	Graph Page	_____
<b>(d) Strain range (third option) Interpolate points at the very last end</b>			
	σ <sub>ho</sub> =	Graph Page	_____
<b>STEP # 3 - SUMMARY</b>			
<b>(a) First strain range selected: Step # 2 option (b)</b>			
	τ <sub>ult</sub> <sup>*</sup> = 50.7	τ <sub>ult</sub> = 25.4	Graph Page <u>Figure C - 02 (b2)</u>
	2G <sub>i</sub> = 5,235.6	σ <sub>ho</sub> = 77.3	
<b>(b) Second strain range selected</b>			
	τ <sub>ult</sub> <sup>*</sup> =	τ <sub>ult</sub> =	Graph Page _____
	2G <sub>i</sub> =	σ <sub>ho</sub> =	

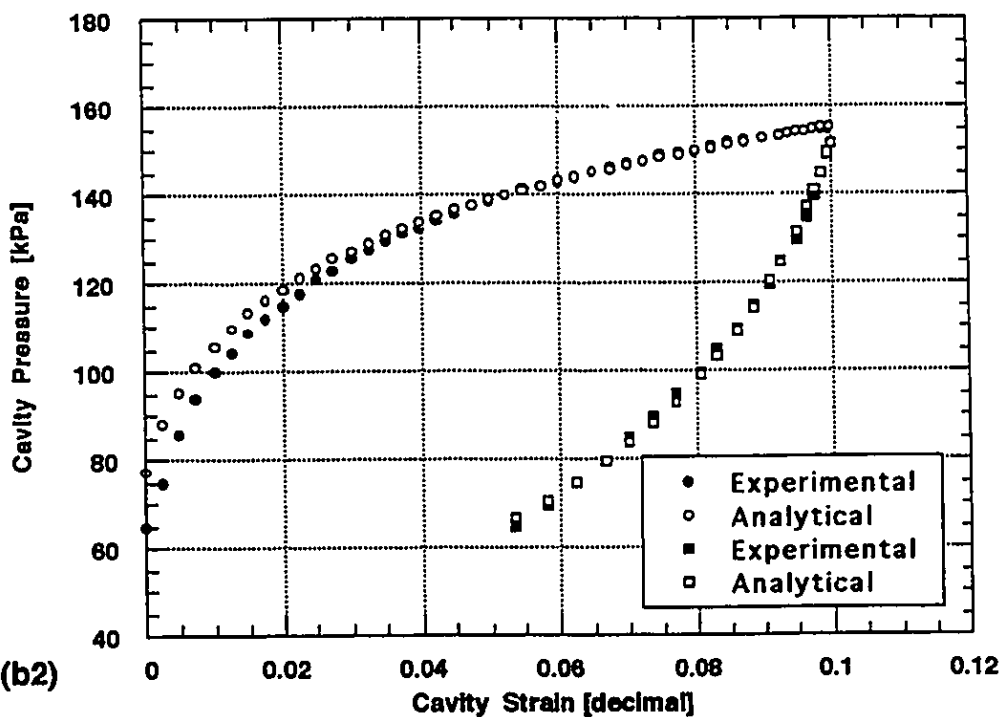
Figure C - 02 (a) Fucino clay test V2P02: Interpretation template.

Fucino Clay - Test V2P02 - Unload Fitting



(b1)

Fucino Clay - Test V2P02 - Final Plot



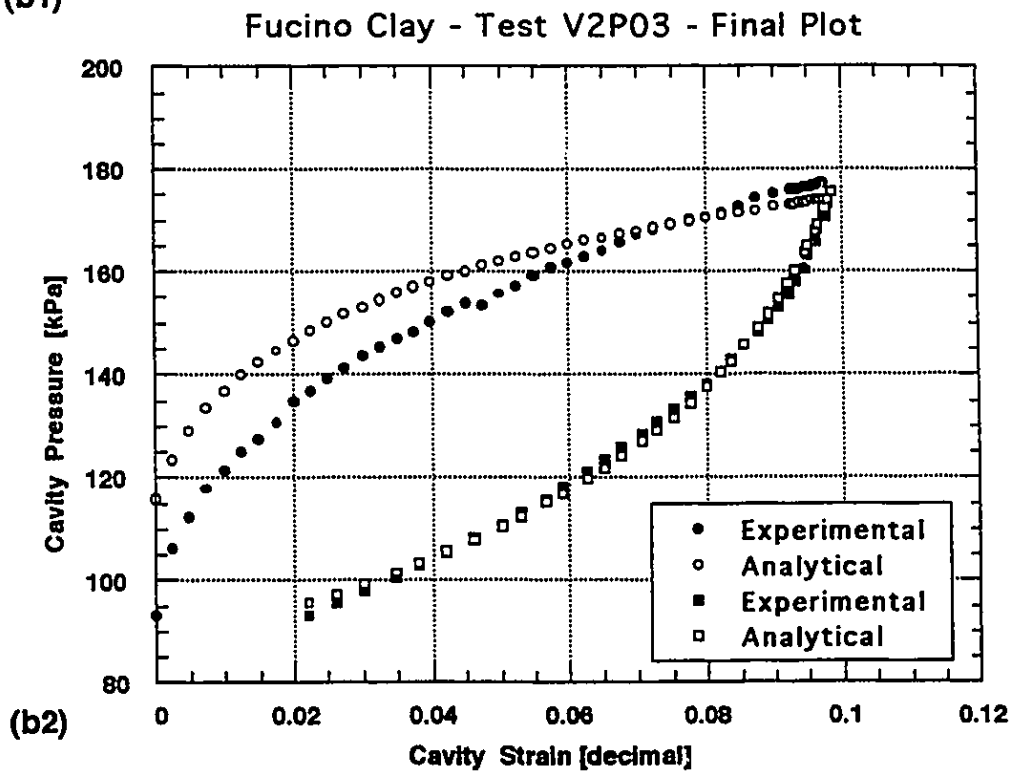
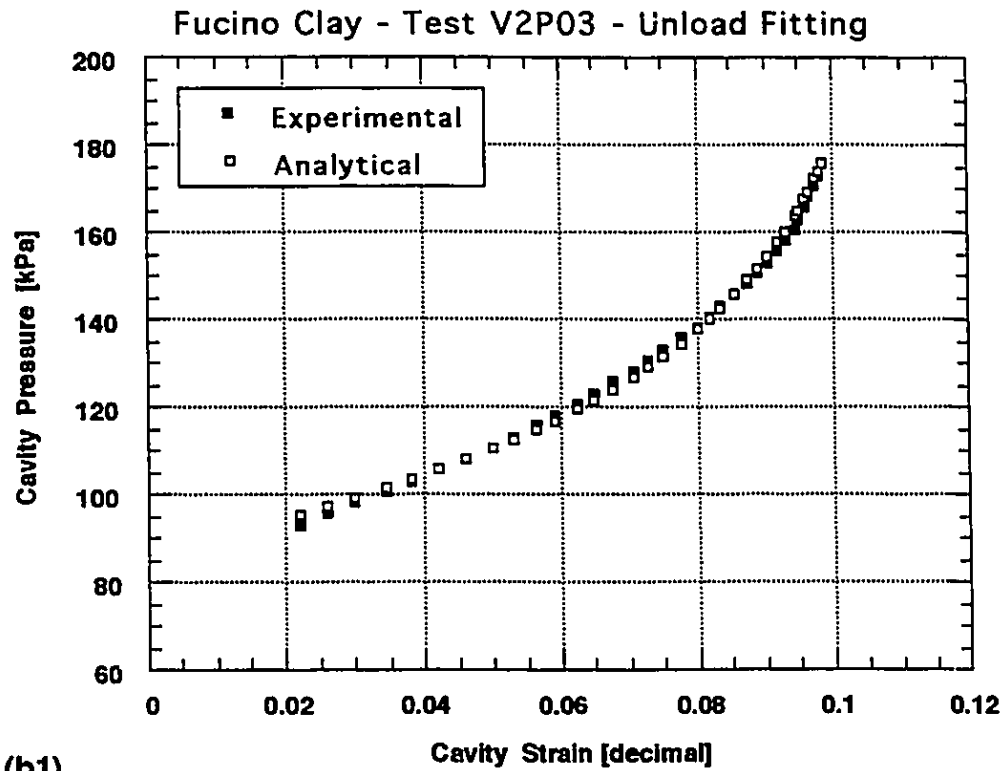
(b2)

Figure C - 02 (b) Fucino clay test V2P02: (b1) Unload fitting; (b2) Final plot

## PRESSUREMETER INTERPRETATION TEMPLATE - CLAYS

<b>TEST ID</b>	<b>Fucino clay - Test V2P03</b>			
<b>DEPTH [m]</b>	5.0	<b>LIFT-OFF [kPa]</b>	93.17	
<b>Loading :</b>	<b>p<sub>max</sub> [kPa]</b>	177.17	<b>ε<sub>max</sub> [dec]</b>	0.0975
<b>Unloading :</b>	<b>p<sub>max</sub> [kPa]</b>	175.67	<b>ε<sub>max</sub> [dec]</b>	0.0985
<b>STEP # 1 - UNLOADING (Best fit with two parameters)</b>				
<b>(a) All unloading points</b>				
	<b>τ<sub>ult</sub>' =</b>	38.8	<b>Graph Page</b>	<b>Figure C - 03 (b1)</b>
	<b>2G<sub>i</sub> =</b>	3,831.6		
<b>(b) (some data points removed)</b>				
	<b>τ<sub>ult</sub>' =</b>		<b>Discard the last point</b>	
	<b>2G<sub>i</sub> =</b>		<b>Graph Page</b>	
<b>STEP # 2 - LOADING (Best fit with one parameter R<sub>c</sub>=2.0)</b>				
<b>(a) All loading points</b>				
	<b>σ<sub>ho</sub> =</b>		<b>Graph Page</b>	
<b>(b) Strain range (first option) Last half</b>				
	<b>σ<sub>ho</sub> =</b>	115.6	<b>Graph Page</b>	<b>Figure C - 03 (b2)</b>
<b>(c) Strain range (second option) Last quarter</b>				
	<b>σ<sub>ho</sub> =</b>		<b>Graph Page</b>	
<b>(d) Strain range (third option) Interpolate points at the very last end</b>				
	<b>σ<sub>ho</sub> =</b>		<b>Graph Page</b>	
<b>STEP # 3 - SUMMARY</b>				
<b>(a) First strain range selected: Step # 2 option (b)</b>				
	<b>τ<sub>ult</sub>' =</b>	38.8	<b>τ<sub>ult</sub> =</b>	19.4
	<b>2G<sub>i</sub> =</b>	3,831.6	<b>σ<sub>ho</sub> =</b>	115.6
<b>(b) Second strain range selected</b>				
	<b>τ<sub>ult</sub>' =</b>		<b>τ<sub>ult</sub> =</b>	
	<b>2G<sub>i</sub> =</b>		<b>σ<sub>ho</sub> =</b>	
			<b>Graph Page</b>	

**Figure C - 03 (a) Fucino clay test V2P03: Interpretation template.**



**Figure C - 03 (b) Fucino clay test V2P03: (b1) Unload fitting; (b2) Final plot**

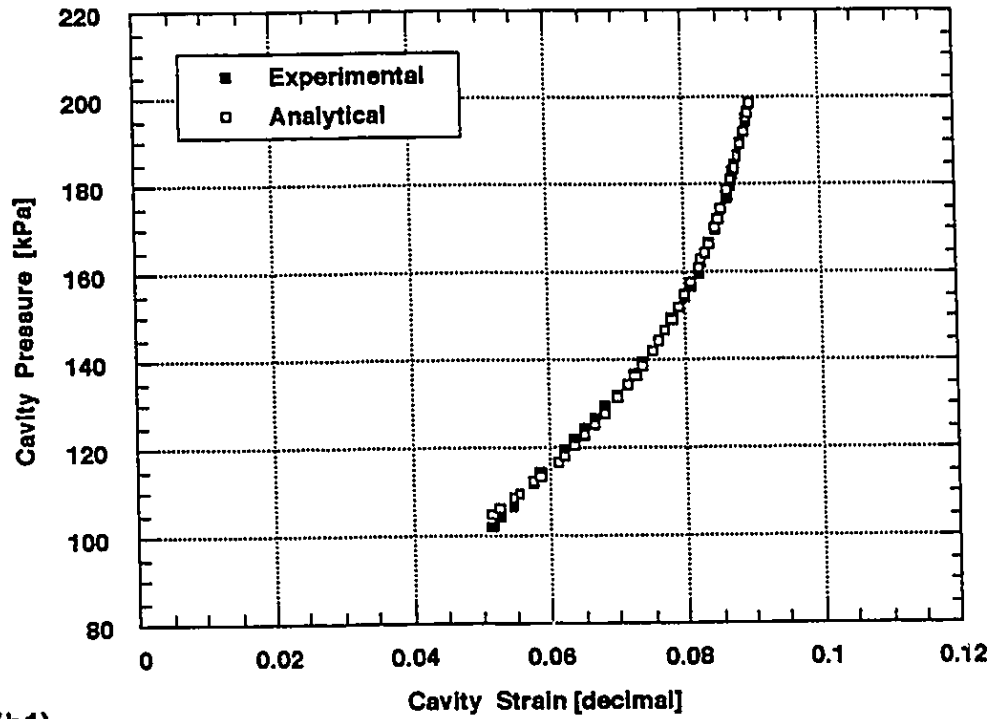
## PRESSUREMETER INTERPRETATION TEMPLATE - CLAYS

TEST ID	Fucino clay - Test V2P04		
DEPTH [m]	6.5	LIFT-OFF [kPa]	101.99
Loading :	$p_{\max}$ [kPa] 199.59	$\epsilon_{\max}$ [dec]	0.0875
Unloading :	$p_{\max}$ [kPa] 198.49	$\epsilon_{\max}$ [dec]	0.09
<b>STEP # 1 - UNLOADING (Best fit with two parameters)</b>			
<b>(a) All unloading points</b>			
	$\tau_{ult}^* = 51.6$	Graph Page	Figure C - 04 (b1)
	$2G_i = 7,475.5$		
<b>(b) (some data points removed)</b>			
	$\tau_{ult}^* =$	Graph Page	_____
	$2G_i =$		
<b>STEP # 2 - LOADING (Best fit with one parameter <math>R_c=2.0</math>)</b>			
<b>(a) All loading points</b>			
	$\sigma_{ho} =$	Graph Page	_____
<b>(b) Strain range (first option) Last half</b>			
	$\sigma_{ho} = 116.3$	Graph Page	Figure C - 04 (b2)
<b>(c) Strain range (second option) Last quarter</b>			
	$\sigma_{ho} =$	Graph Page	_____
<b>(d) Strain range (third option) Interpolate points at the very last end</b>			
	$\sigma_{ho} =$	Graph Page	_____
<b>STEP # 3 - SUMMARY</b>			
<b>(a) First strain range selected: Step # 2 option (b)</b>			
	$\tau_{ult}^* = 51.6$	$\tau_{ult} = 25.8$	Graph Page
	$2G_i = 7,475.5$	$\sigma_{ho} = 116.3$	Figure C - 04 (b2)
<b>(b) Second strain range selected</b>			
	$\tau_{ult}^* =$	$\tau_{ult} =$	Graph Page
	$2G_i =$	$\sigma_{ho} =$	_____

Figure C - 04 (a) Fucino clay test V2P04: Interpretation template.

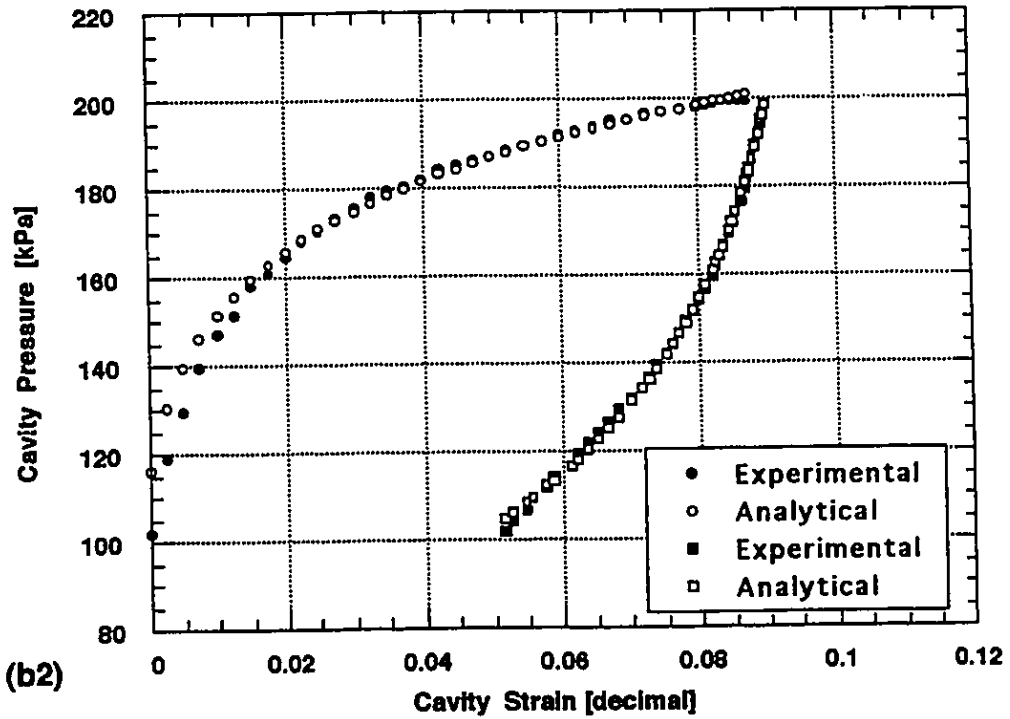


Fucino Clay - Test V2P04 - Unload Fitting



(b1)

Fucino Clay - Test V2P04 - Final Plot



(b2)

Figure C - 04 (b) Fucino clay test V2P04: (b1) Unload fitting; (b2) Final plot

## PRESSUREMETER INTERPRETATION TEMPLATE - CLAYS

TEST ID Fucino clay - Test V2P05

DEPTH [m] 8.0 LIFT-OFF [kPa] 125.53

Loading :  $p_{\max}$  [kPa] 240.53  $\epsilon_{\max}$  [dec] 0.095

Unloading :  $p_{\max}$  [kPa] 240.53  $\epsilon_{\max}$  [dec] 0.098

### STEP # 1 - UNLOADING (Best fit with two parameters)

#### (a) All unloading points

$\tau_{ult}^* = 55.4$  Graph Page Figure C - 05 (b1)  
 $2G_i = 9,645.8$

#### (b) (some data points removed)

$\tau_{ult}^* =$  Graph Page \_\_\_\_\_  
 $2G_i =$

### STEP # 2 - LOADING (Best fit with one parameter $R_\tau=2.0$ )

#### (a) All loading points

$\sigma_{ho} =$  Graph Page \_\_\_\_\_

#### (b) Strain range (first option) Last half

$\sigma_{ho} =$  Graph Page \_\_\_\_\_

#### (c) Strain range (second option) Last quarter

$\sigma_{ho} =$  Graph Page \_\_\_\_\_

#### (d) Strain range (third option) Interpolate points at the very last end

$\sigma_{ho} = 143.7$  Graph Page Figure C - 05 (b2)

### STEP # 3 - SUMMARY

#### (a) First strain range selected: Step # 2 option (d)

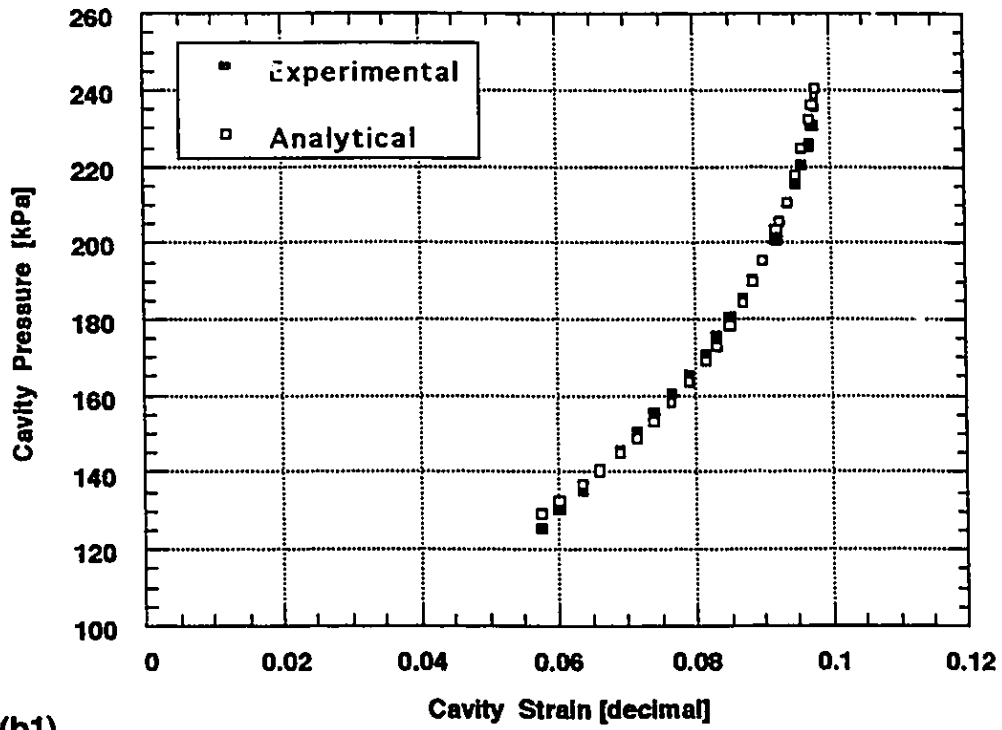
$\tau_{ult}^* = 55.4$   $\tau_{ult} = 27.7$  Graph Page Figure C - 05 (b2)  
 $2G_i = 9,645.8$   $\sigma_{ho} = 143.7$

#### (b) Second strain range selected

$\tau_{ult}^* =$   $\tau_{ult} =$  Graph Page \_\_\_\_\_  
 $2G_i =$   $\sigma_{ho} =$

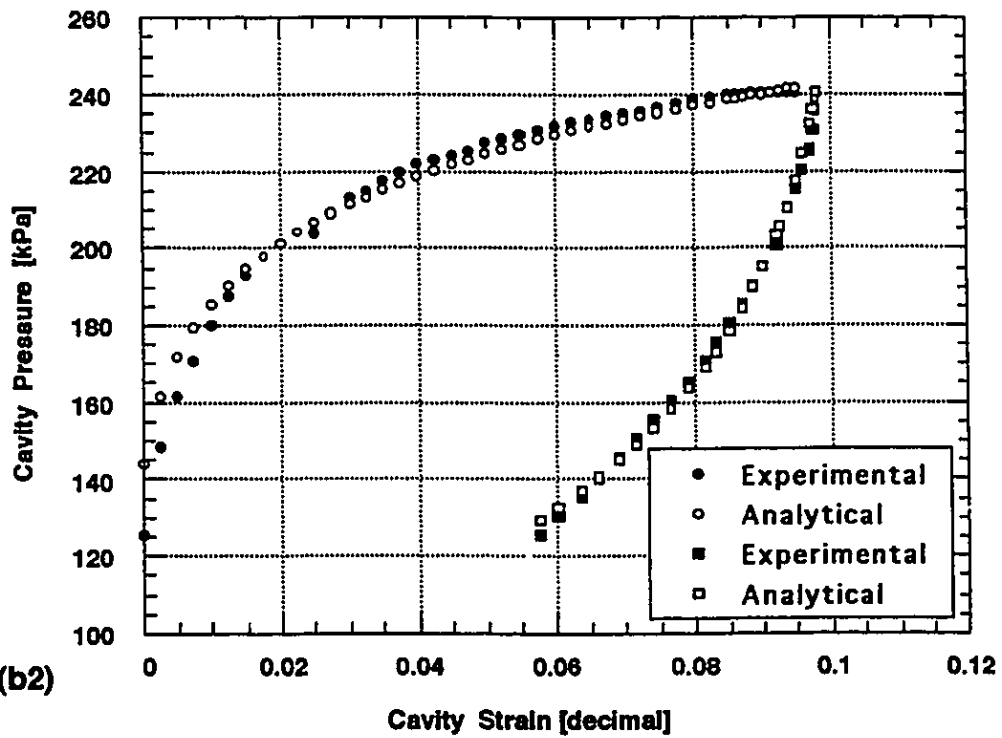
Figure C - 05 (a) Fucino clay test V2P05: Interpretation template.

Fucino Clay - Test V2P05 - Unload Fitting



(b1)

Fucino Clay - Test V2P05 - Final Plot



(b2)

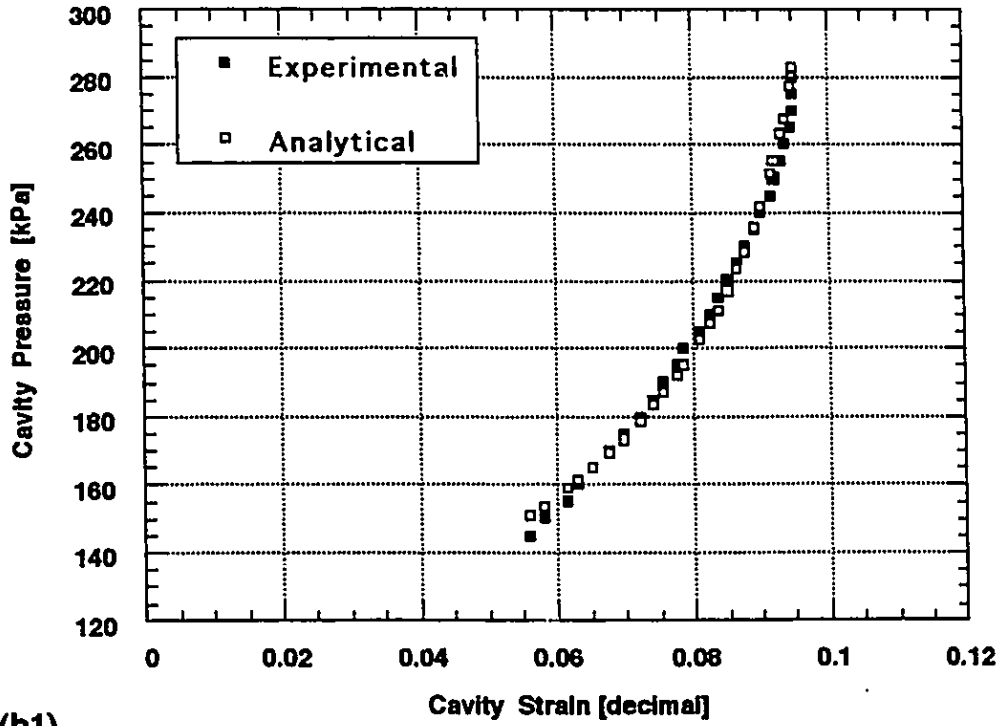
Figure C - 05 (b) Fucino clay test V2P05: (b1) Unload fitting; (b2) Final plot

## PRESSUREMETER INTERPRETATION TEMPLATE - CLAYS

TEST ID	Fucino clay - Test V2P06		
DEPTH [m]	9.5	LIFT-OFF [kPa]	145.14
Loading :	p <sub>max</sub> [kPa] 285.14	ε <sub>max</sub> [dec] 0.0925	
Unloading :	p <sub>max</sub> [kPa] 283.14	ε <sub>max</sub> [dec] 0.095	
<b>STEP # 1 - UNLOADING (Best fit with two parameters)</b>			
<b>(a) All unloading points</b>			
	τ <sub>ult</sub> <sup>*</sup> = 62.1	Graph Page	Figure C - 06 (b1)
	2G <sub>i</sub> = 12,923.5		
<b>(b) (some data points removed)</b>			
	τ <sub>ult</sub> <sup>*</sup> =	Graph Page	_____
	2G <sub>i</sub> =		
<b>STEP # 2 - LOADING (Best fit with one parameter R<sub>c</sub>=2.0)</b>			
<b>(a) All loading points</b>			
	σ <sub>ho</sub> =	Graph Page	_____
<b>(b) Strain range (first option) Last half</b>			
	σ <sub>ho</sub> =	Graph Page	_____
<b>(c) Strain range (second option) Last quarter</b>			
	σ <sub>ho</sub> = 170.4	Graph Page	Figure C - 06 (b2)
<b>(d) Strain range (third option) Interpolate points at the very last end</b>			
	σ <sub>ho</sub> =	Graph Page	_____
<b>STEP # 3 - SUMMARY</b>			
<b>(a) First strain range selected: Step # 2 option (c)</b>			
	τ <sub>ult</sub> <sup>*</sup> = 62.1	τ <sub>ult</sub> = 31.1	Graph Page
	2G <sub>i</sub> = 12,923.5	σ <sub>ho</sub> = 170.4	Figure C - 06 (b2)
<b>(b) Second strain range selected</b>			
	τ <sub>ult</sub> <sup>*</sup> =	τ <sub>ult</sub> =	Graph Page
	2G <sub>i</sub> =	σ <sub>ho</sub> =	_____

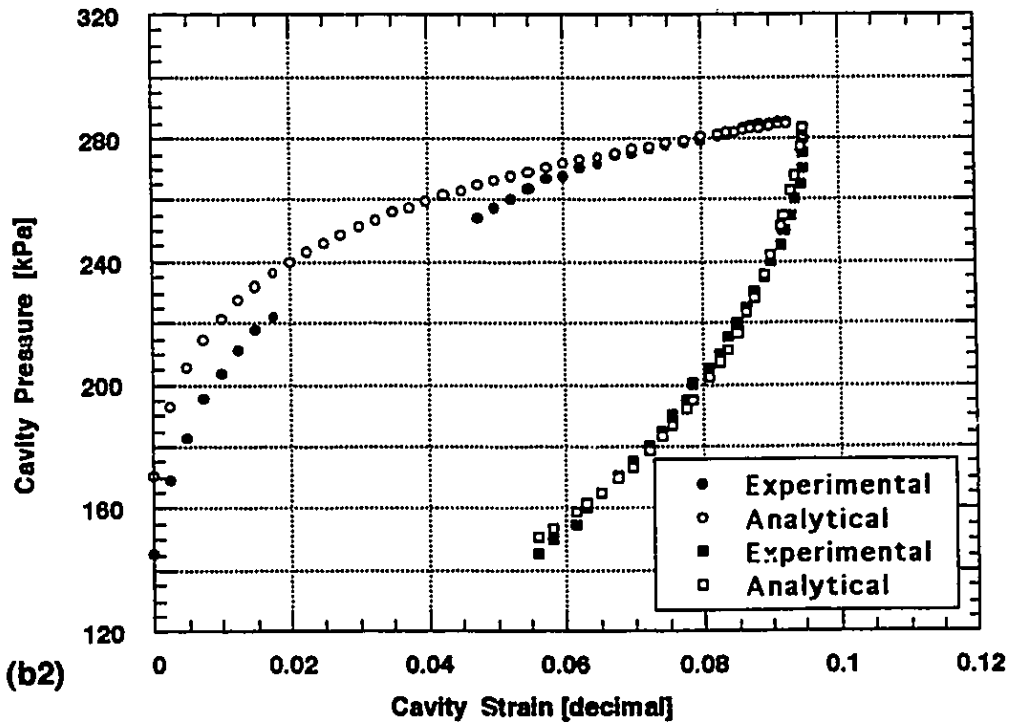
Figure C - 06 (a) Fucino clay test V2P06: Interpretation template.

Fucino Clay - Test V2P06 - Unload Fitting



(b1)

Fucino Clay - Test V2P06 - Final Plot



(b2)

Figure C - 06 (b) Fucino clay test V2P06: (b1) Unload fitting; (b2) Final plot

## PRESSUREMETER INTERPRETATION TEMPLATE - CLAYS

TEST ID Fucino clay - Test V2P07

DEPTH [m] 11.0 LIFT-OFF [kPa] 167.7

Loading :  $p_{\max}$  [kPa] 309.2  $\epsilon_{\max}$  [dec] 0.095

Unloading :  $p_{\max}$  [kPa] 307.7  $\epsilon_{\max}$  [dec] 0.095

### STEP # 1 - UNLOADING (Best fit with two parameters)

#### (a) All unloading points

$$\tau_{ult}^* = 82.7$$

Graph Page Figure C - 07 (b1)

$$2G_i = 10,430.0$$

#### (b) (some data points removed)

$$\tau_{ult}^* =$$

Graph Page \_\_\_\_\_

$$2G_i =$$

### STEP # 2 - LOADING (Best fit with one parameter $R_c=2.0$ )

#### (a) All loading points

$$\sigma_{ho} =$$

Graph Page \_\_\_\_\_

#### (b) Strain range (first option)

Last half

$$\sigma_{ho} =$$

Graph Page \_\_\_\_\_

#### (c) Strain range (second option)

Last quarter

$$\sigma_{ho} =$$

Graph Page \_\_\_\_\_

#### (d) Strain range (third option) Interpolate points at the very last end

$$\sigma_{ho} = 176.6$$

Graph Page Figure C - 07 (b2)

### STEP # 3 - SUMMARY

#### (a) First strain range selected: Step # 2 option (d)

$$\tau_{ult}^* = 82.7 \quad \tau_{ult} = 41.4$$

Graph Page Figure C - 07 (b2)

$$2G_i = 10,430.0 \quad \sigma_{ho} = 176.6$$

#### (b) Second strain range selected

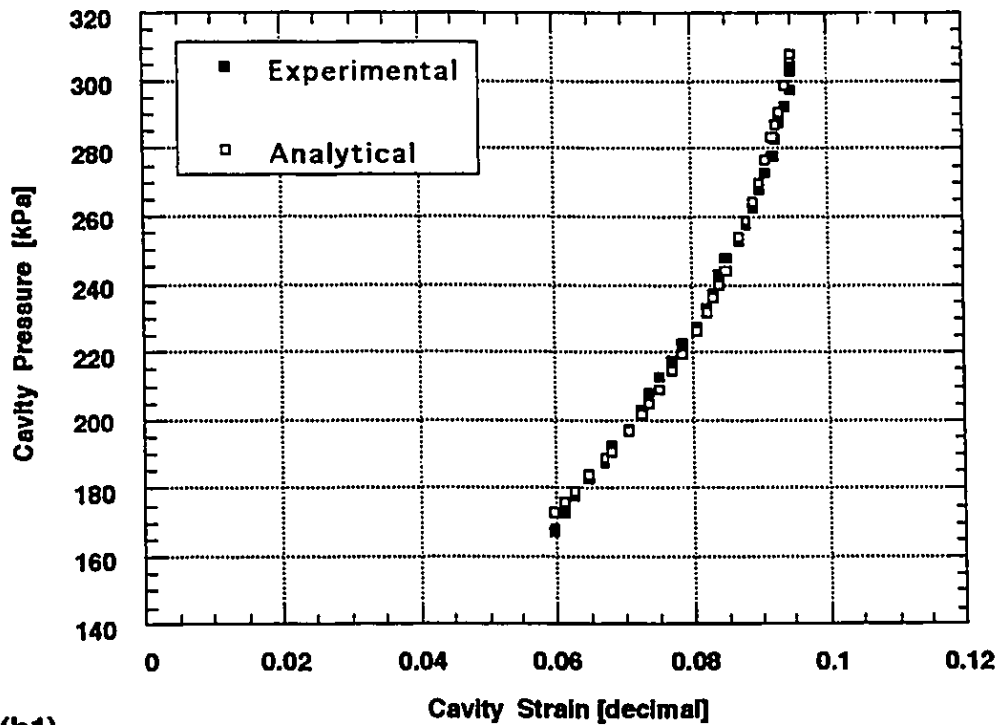
$$\tau_{ult}^* = \quad \tau_{ult} =$$

Graph Page \_\_\_\_\_

$$2G_i = \quad \sigma_{ho} =$$

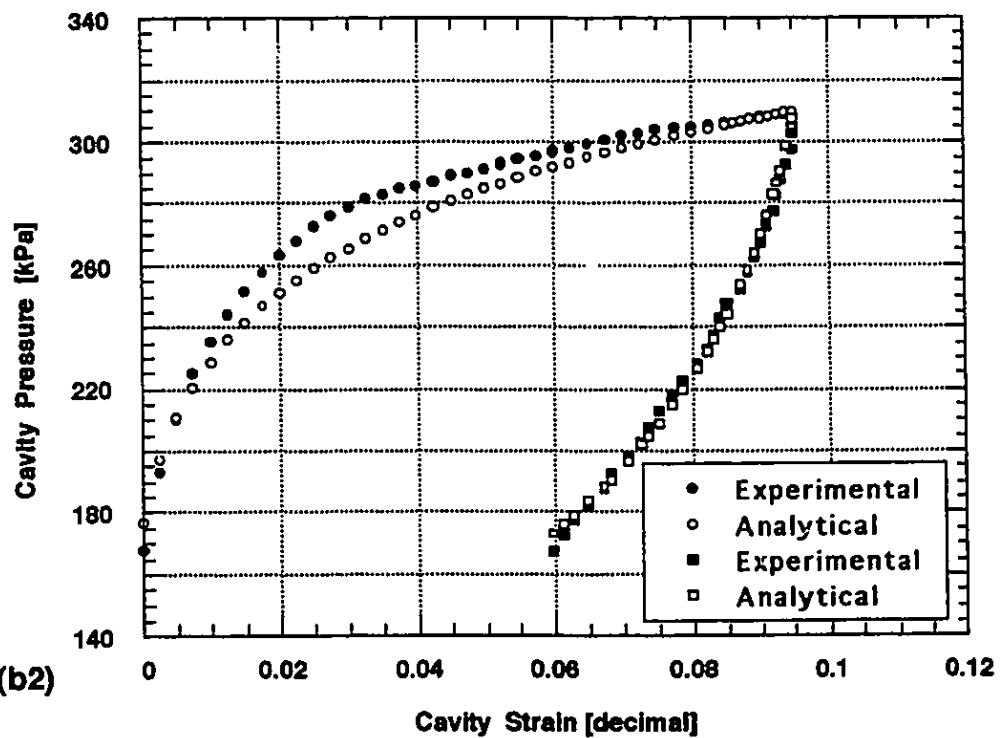
Figure C - 07 (a) Fucino clay test V2P07: Interpretation template.

Fucino Clay - Test V2P07 - Unload Fitting



(b1)

Fucino Clay - Test V2P07 - Final Plot



(b2)

Figure C - 07 (b) Fucino clay test V2P07: (b1) Unload fitting;  
(b2) Final plot

## PRESSUREMETER INTERPRETATION TEMPLATE - CLAYS

TEST ID Fucino clay - Test V2P08

DEPTH [m] 14.0 LIFT-OFF [kPa] 207.91

Loading :  $p_{max}$  [kPa] 387.91  $\epsilon_{max}$  [dec] 0.0985

Unloading :  $p_{max}$  [kPa] 387.91  $\epsilon_{max}$  [dec] 0.0985

### STEP # 1 - UNLOADING (Best fit with two parameters)

#### (a) All unloading points

$$\tau_{ult}^* = 105.8$$

Graph Page Figure C - 08 (b1)

$$2G_i = 12,580.5$$

#### (b) (some data points removed)

$$\tau_{ult}^* =$$

Graph Page \_\_\_\_\_

$$2G_i =$$

### STEP # 2 - LOADING (Best fit with one parameter $R_p=2.0$ )

#### (a) All loading points

$$\sigma_{ho} =$$

Graph Page \_\_\_\_\_

#### (b) Strain range (first option)

Last half

$$\sigma_{ho} =$$

Graph Page \_\_\_\_\_

#### (c) Strain range (second option)

Last quarter

$$\sigma_{ho} =$$

Graph Page \_\_\_\_\_

#### (d) Strain range (third option) Interpolate points at the very last end

$$\sigma_{ho} = 219.1$$

Graph Page Figure C - 08 (b2)

### STEP # 3 - SUMMARY

#### (a) First strain range selected: Step # 2 option (d)

$$\tau_{ult}^* = 105.8 \quad \tau_{ult} = 52.9$$

Graph Page Figure C - 08 (b2)

$$2G_i = 12,580.5 \quad \sigma_{ho} = 219.1$$

#### (b) Second strain range selected

$$\tau_{ult}^* = \quad \tau_{ult} =$$

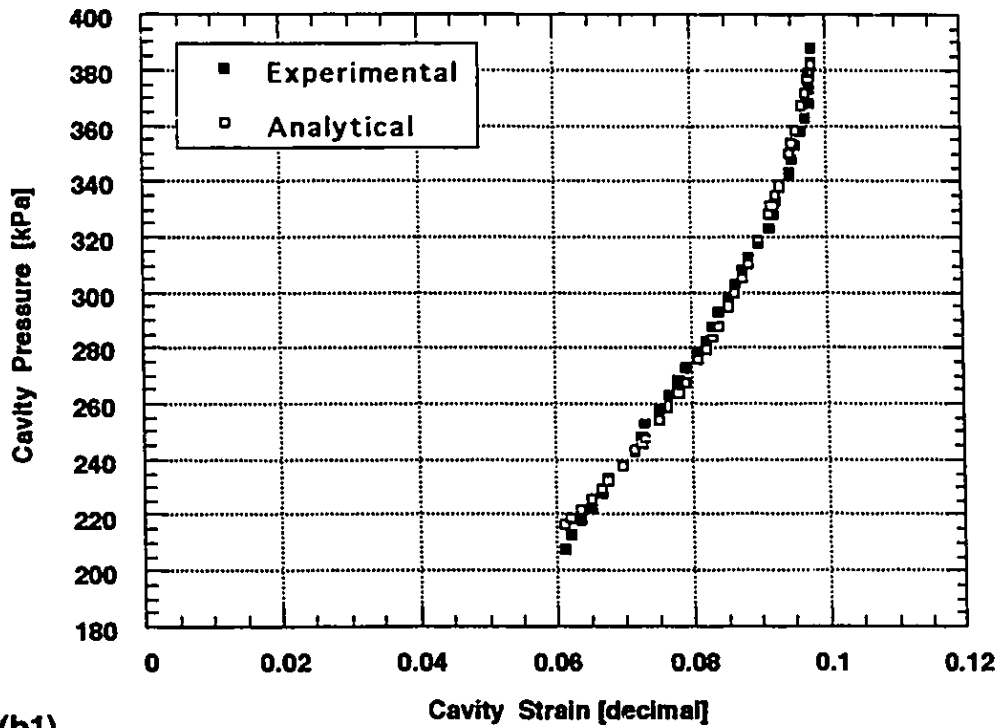
Graph Page \_\_\_\_\_

$$2G_i = \quad \sigma_{ho} =$$

Figure C - 08 (a) Fucino clay test V2P08: Interpretation template.

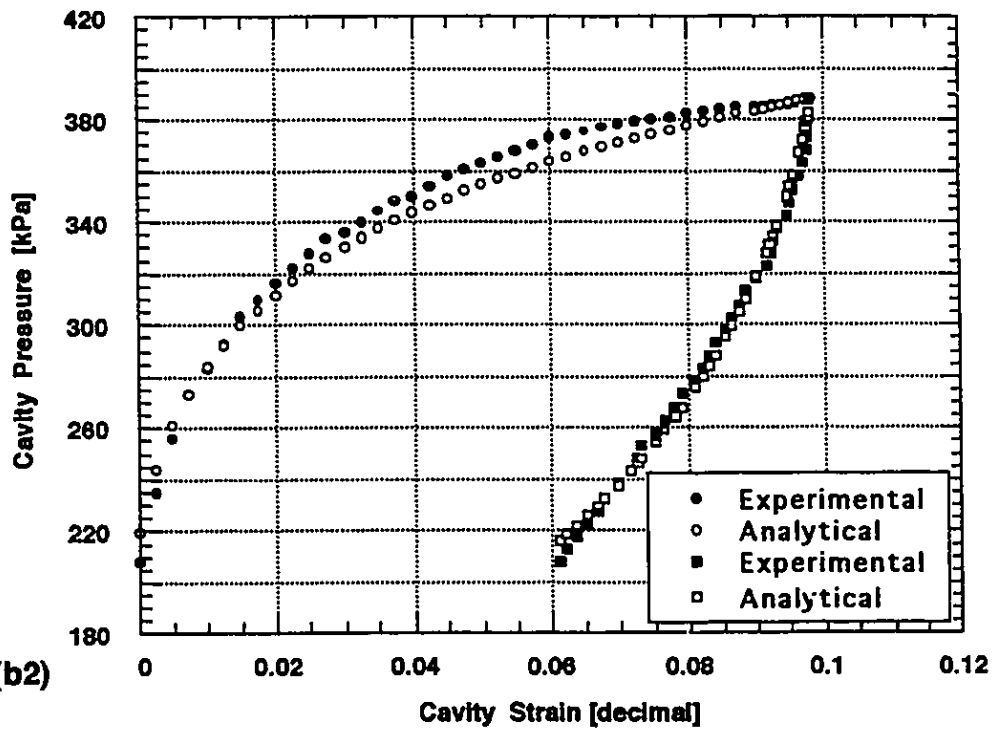


Fucino Clay - Test V2P08 - Unload Fitting



(b1)

Fucino Clay - Test V2P08 - Final Plot



(b2)

Figure C - 08 (b) Fucino clay test V2P08: (b1) Unload fitting; (b2) Final plot

## PRESSUREMETER INTERPRETATION TEMPLATE - CLAYS

TEST ID Fucino clay - Test V2P09

DEPTH [m] 16.0 LIFT-OFF [kPa] 246.16

Loading :  $p_{\max}$  [kPa] 444.16  $\epsilon_{\max}$  [dec] 0.10

Unloading :  $p_{\max}$  [kPa] 441.16  $\epsilon_{\max}$  [dec] 0.102

### STEP # 1 - UNLOADING (Best fit with two parameters)

#### (a) All unloading points

$$\tau_{ult}^* = 169.9$$

Graph Page Figure C - 09 (b1)

$$2G_i = 10,139.8$$

#### (b) (some data points removed)

$$\tau_{ult}^* =$$

Graph Page \_\_\_\_\_

$$2G_i =$$

### STEP # 2 - LOADING (Best fit with one parameter $R_c=2.0$ )

#### (a) All loading points

$$\sigma_{ho} =$$

Graph Page \_\_\_\_\_

#### (b) Strain range (first option)

Last half

$$\sigma_{ho} =$$

Graph Page \_\_\_\_\_

#### (c) Strain range (second option)

Last quarter

$$\sigma_{ho} =$$

Graph Page \_\_\_\_\_

#### (d) Strain range (third option) Interpolate points at the very last end

$$\sigma_{ho} = 227.5$$

Graph Page Figure C - 09 (b2)

### STEP # 3 - SUMMARY

#### (a) First strain range selected: Step # 2 option (d)

$$\tau_{ult}^* = 169.9 \quad \tau_{ult} = 85.0$$

Graph Page Figure C - 09 (b2)

$$2G_i = 10,139.8 \quad \sigma_{ho} = 227.5$$

#### (b) Second strain range selected

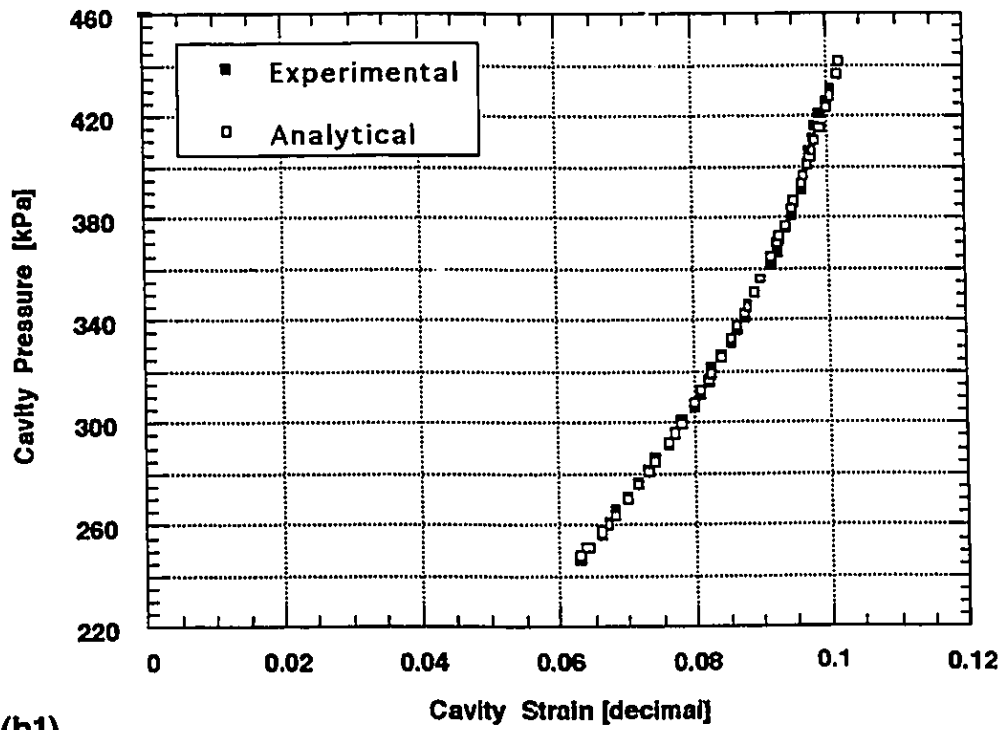
$$\tau_{ult}^* = \quad \tau_{ult} =$$

Graph Page \_\_\_\_\_

$$2G_i = \quad \sigma_{ho} =$$

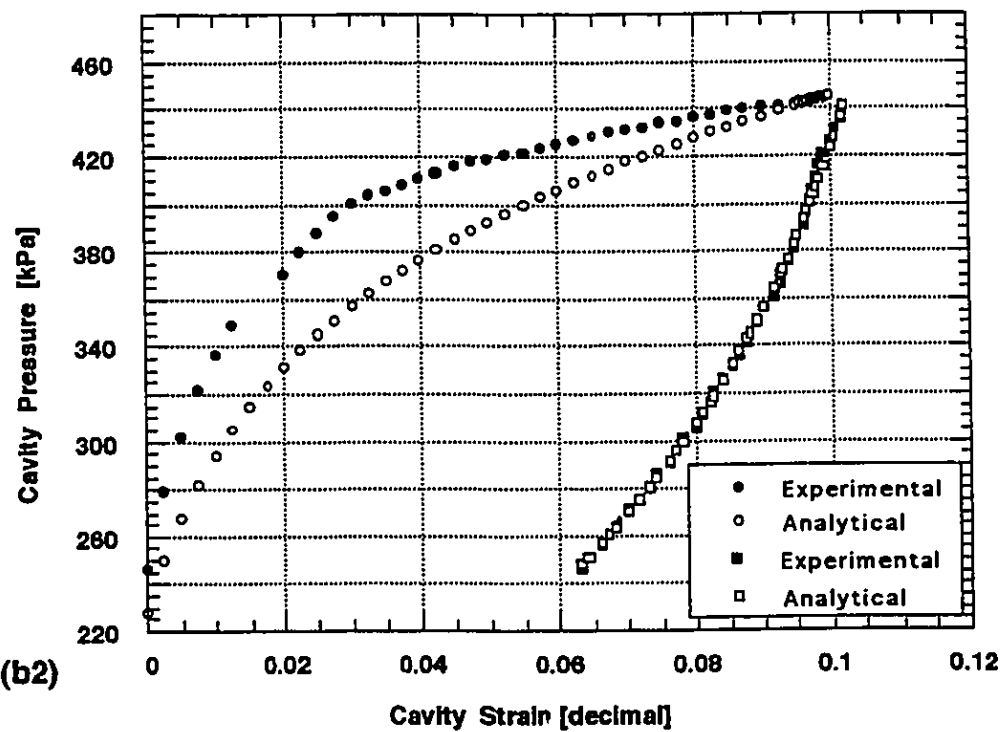
Figure C - 09 (a) Fucino clay test V2P09: Interpretation template.

## Fucino Clay - Test V2P09 - Unload Fitting



(b1)

## Fucino Clay - Test V2P09 - Final Plot



(b2)

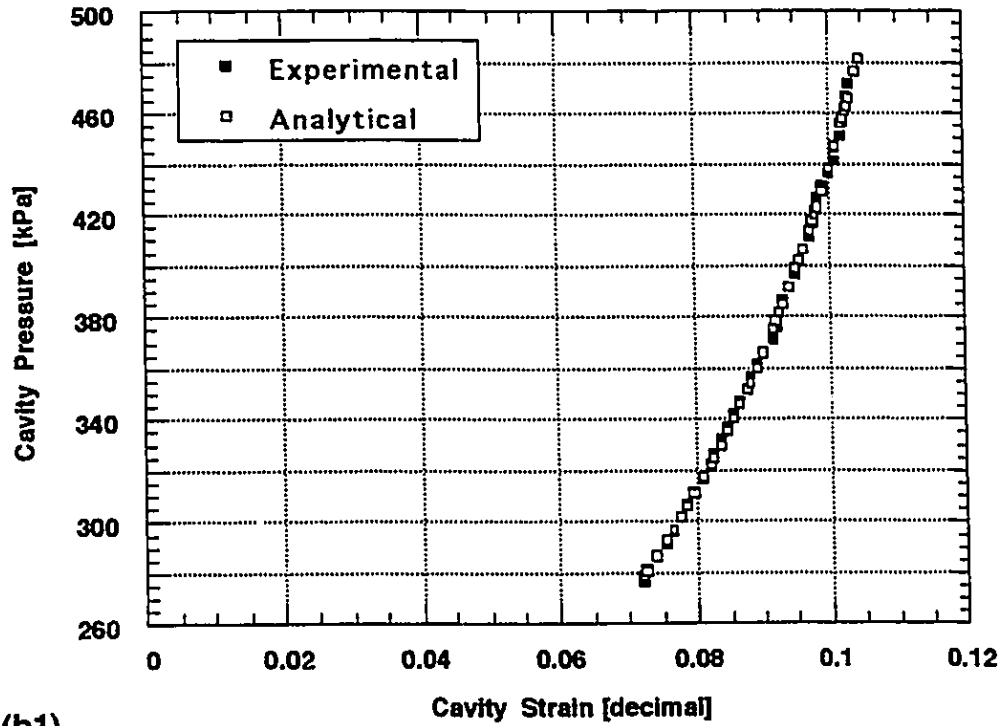
Figure C - 09 (b) Fucino clay test V2P09: (b1) Unload fitting; (b2) Final plot

## PRESSUREMETER INTERPRETATION TEMPLATE - CLAYS

TEST ID	Fucino clay - Test V2P10		
DEPTH [m]	18.0	LIFT-OFF [kPa]	276.56
Loading :	P <sub>max</sub> [kPa] <u>491.06</u>	ε <sub>max</sub> [dec] <u>0.105</u>	
Unloading :	P <sub>max</sub> [kPa] <u>481.56</u>	ε <sub>max</sub> [dec] <u>0.1045</u>	
<b>STEP # 1 - UNLOADING (Best fit with two parameters)</b>			
<b>(a) All unloading points</b>			
	τ <sub>ult</sub> <sup>*</sup> = 201.0	Graph Page	<u>Figure C - 10 (b1)</u>
	2G <sub>i</sub> = 11,903.7		
<b>(b) (some data points removed)</b>			
	τ <sub>ult</sub> <sup>*</sup> =	Graph Page	_____
	2G <sub>i</sub> =		
<b>STEP # 2 - LOADING (Best fit with one parameter R<sub>c</sub>=2.0)</b>			
<b>(a) All loading points</b>			
	σ <sub>ho</sub> =	Graph Page	_____
<b>(b) Strain range (first option) Last half</b>			
	σ <sub>ho</sub> =	Graph Page	_____
<b>(c) Strain range (second option) Last quarter</b>			
	σ <sub>ho</sub> = 234.4	Graph Page	<u>Figure C - 10 (b2)</u>
<b>(d) Strain range (third option) Interpolate points at the very last end</b>			
	σ <sub>ho</sub> =	Graph Page	_____
<b>STEP # 3 - SUMMARY</b>			
<b>(a) First strain range selected: Step # 2 option (c)</b>			
	τ <sub>ult</sub> <sup>*</sup> = 201.0	τ <sub>ult</sub> = 100.5	Graph Page <u>Figure C - 10 (b2)</u>
	2G <sub>i</sub> = 11,903.7	σ <sub>ho</sub> = 234.4	
<b>(b) Second strain range selected</b>			
	τ <sub>ult</sub> <sup>*</sup> =	τ <sub>ult</sub> =	Graph Page _____
	2G <sub>i</sub> =	σ <sub>ho</sub> =	

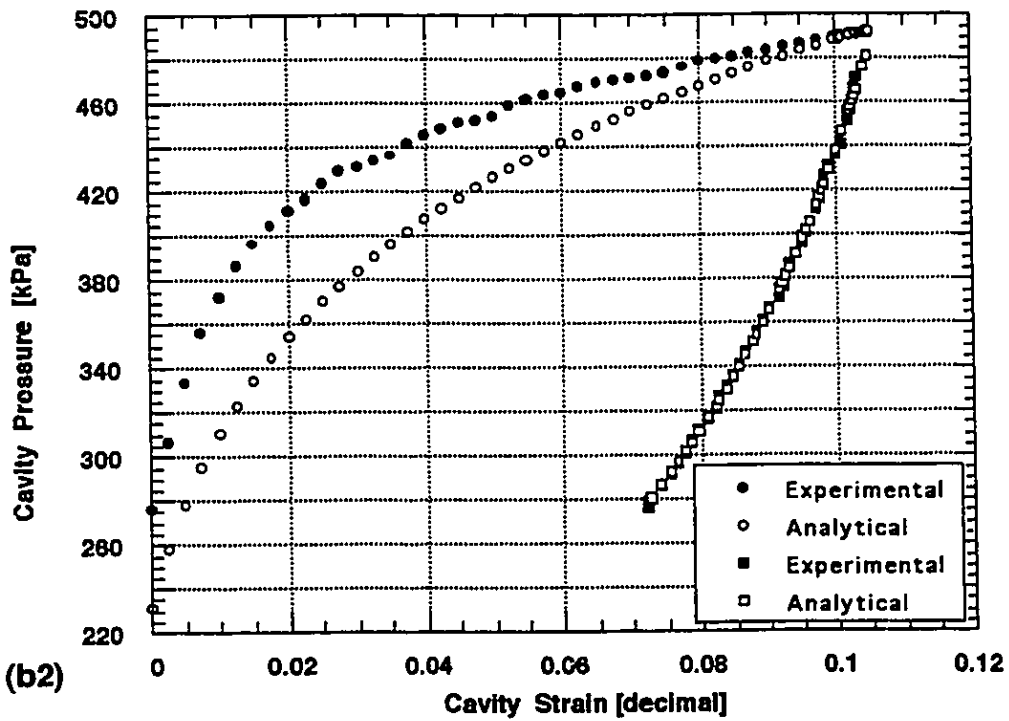
Figure C - 10 (a) Fucino clay test V2P10: Interpretation template.

Fucino Clay - Test V2P10 - Unload Fitting



(b1)

Fucino Clay - Test V2P10 - Final Plot



(b2)

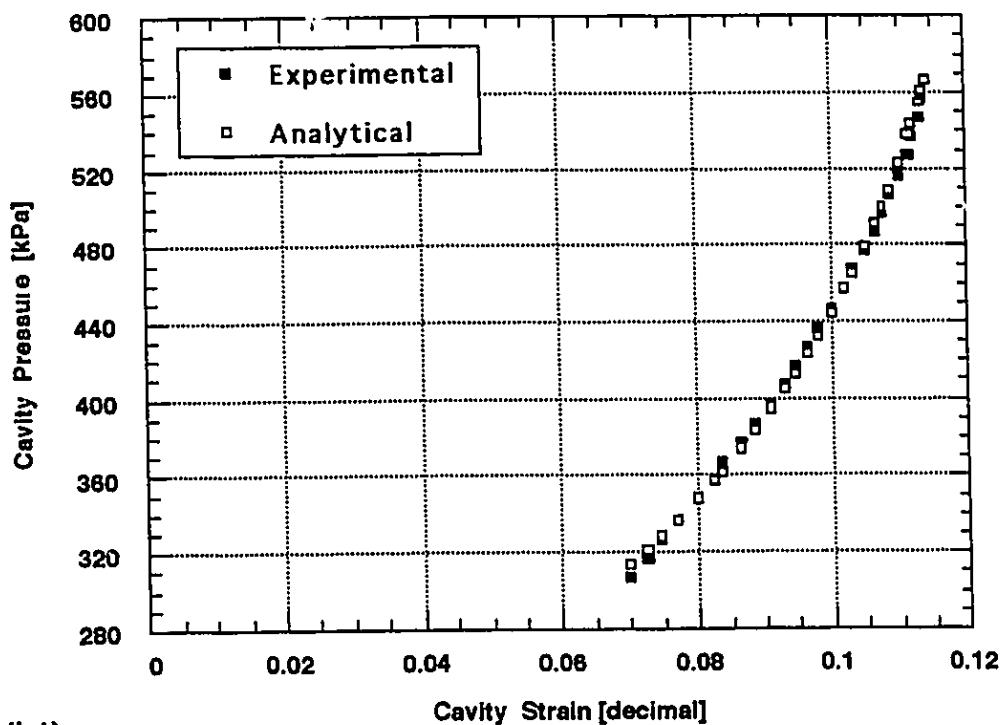
Figure C - 10 (b) Fucino clay test V2P10 (b1) Unload fitting; (b2) Final plot

## PRESSUREMETER INTERPRETATION TEMPLATE - CLAYS

TEST ID	Fucino clay - Test V2P11		
DEPTH [m]	20.0	LIFT-OFF [kPa]	306.96
Loading :	p <sub>max</sub> [kPa] <u>586.96</u>	ε <sub>max</sub> [dec] <u>0.105</u>	
Unloading :	p <sub>max</sub> [kPa] <u>566.96</u>	ε <sub>max</sub> [dec] <u>0.114</u>	
<b>STEP # 1 - UNLOADING (Best fit with two parameters)</b>			
<b>(a) All unloading points</b>			
	τ <sub>ult</sub> <sup>*</sup> = 182.8	Graph Page	Figure C - 11 (b1)
	2G <sub>i</sub> = 13,861.9		
<b>(b) (some data points removed)</b>			
	τ <sub>ult</sub> <sup>*</sup> =	Graph Page	_____
	2G <sub>i</sub> =		
<b>STEP # 2 - LOADING (Best fit with one parameter R<sub>c</sub>=2.0)</b>			
<b>(a) All loading points</b>			
	σ <sub>ho</sub> =	Graph Page	_____
<b>(b) Strain range (first option) Last half</b>			
	σ <sub>ho</sub> =	Graph Page	_____
<b>(c) Strain range (second option) Last quarter</b>			
	σ <sub>ho</sub> =	Graph Page	_____
<b>(d) Strain range (third option) Interpolate points at the very last end</b>			
	σ <sub>ho</sub> = 328.2	Graph Page	Figure C - 11 (b2)
<b>STEP # 3 - SUMMARY</b>			
<b>(a) First strain range selected: Step # 2 option (d)</b>			
	τ <sub>ult</sub> <sup>*</sup> = 182.8	τ <sub>ult</sub> = 91.4	Graph Page <u>Figure C - 11 (b2)</u>
	2G <sub>i</sub> = 13,861.9	σ <sub>ho</sub> = 328.2	
<b>(b) Second strain range selected</b>			
	τ <sub>ult</sub> <sup>*</sup> =	τ <sub>ult</sub> =	Graph Page _____
	2G <sub>i</sub> =	σ <sub>ho</sub> =	

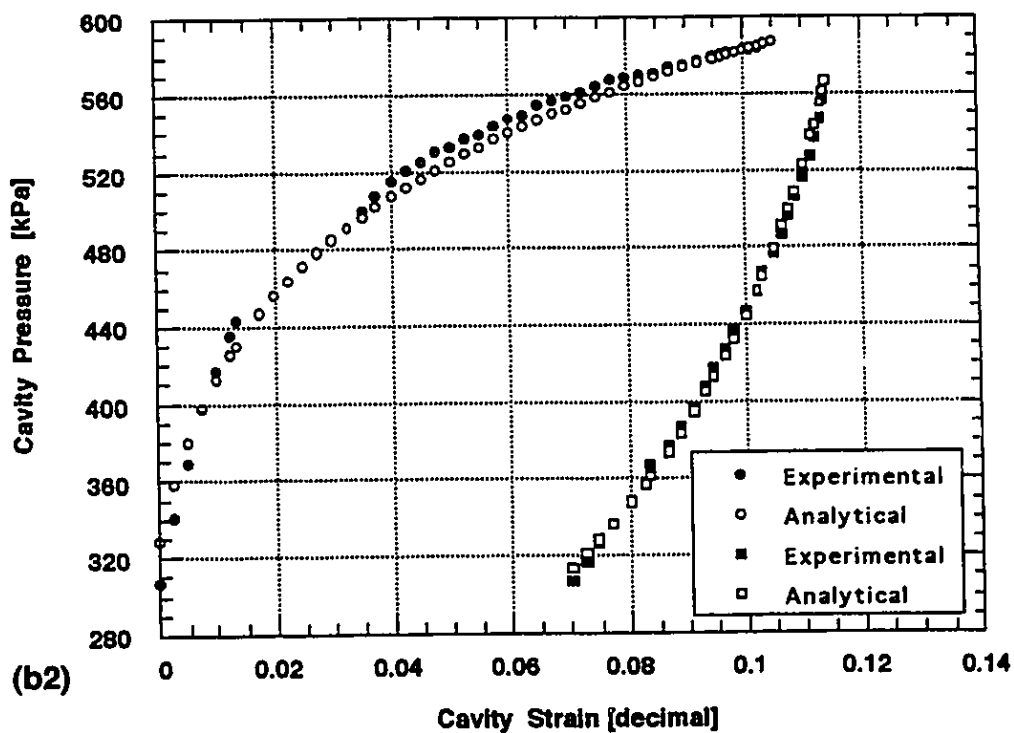
Figure C - 11 (a) Fucino clay test V2P11: Interpretation template.

Fucino Clay - Test V2P11 - Unload Fitting



(b1)

Fucino Clay - Test V2P11 - Final Plot



(b2)

Figure C - 11 (b) Fucino clay test V2P11 (b1) Unload fitting; (b2) Final plot

## PRESSUREMETER INTERPRETATION TEMPLATE - CLAYS

TEST ID Fucino clay - Test V2P12

DEPTH [m] 22.0 LIFT-OFF [kPa] 338.34

Loading :  $p_{max}$  [kPa] 668.34  $\epsilon_{max}$  [dec] 0.099

Unloading :  $p_{max}$  [kPa] 655.34  $\epsilon_{max}$  [dec] 0.1023

**STEP # 1 - UNLOADING (Best fit with two parameters)**

(a) All unloading points

$\tau_{ult}^* = 241.4$  Graph Page Figure C - 12 (b1)

$2G_i = 18,498.2$

(b) (some data points removed)

$\tau_{ult}^* =$  Graph Page \_\_\_\_\_

$2G_i =$

**STEP # 2 - LOADING (Best fit with one parameter  $R_\tau=2.0$ )**

(a) All loading points

$\sigma_{ho} =$  Graph Page \_\_\_\_\_

(b) Strain range (first option) Last half

$\sigma_{ho} =$  Graph Page \_\_\_\_\_

(c) Strain range (second option) Last quarter

$\sigma_{ho} =$  Graph Page \_\_\_\_\_

(d) Strain range (third option) Interpolate points at the very last end

$\sigma_{ho} = 333.2$  Graph Page Figure C - 12 (b2)

**STEP # 3 - SUMMARY**

(a) First strain range selected: Step # 2 option (d)

$\tau_{ult}^* = 241.4$   $\tau_{ult} = 120.7$  Graph Page Figure C - 12 (b2)

$2G_i = 18,498.2$   $\sigma_{ho} = 333.2$

(b) Second strain range selected

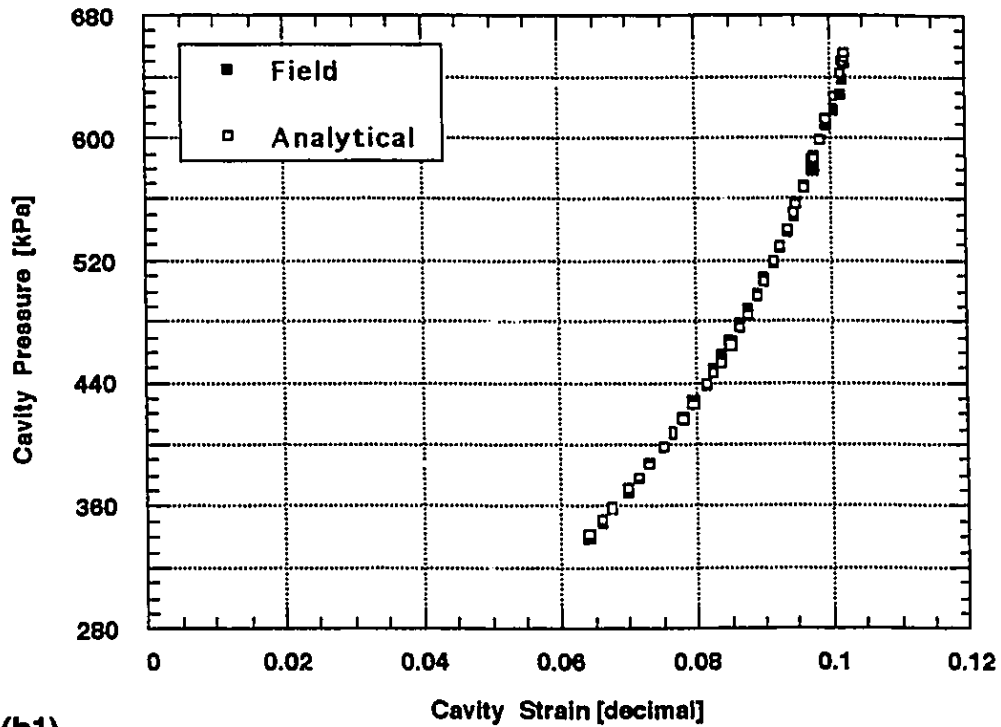
$\tau_{ult}^* =$   $\tau_{ult} =$  Graph Page \_\_\_\_\_

$2G_i =$   $\sigma_{ho} =$

Figure C - 12 (a) Fucino clay test V2P12: Interpretation template.

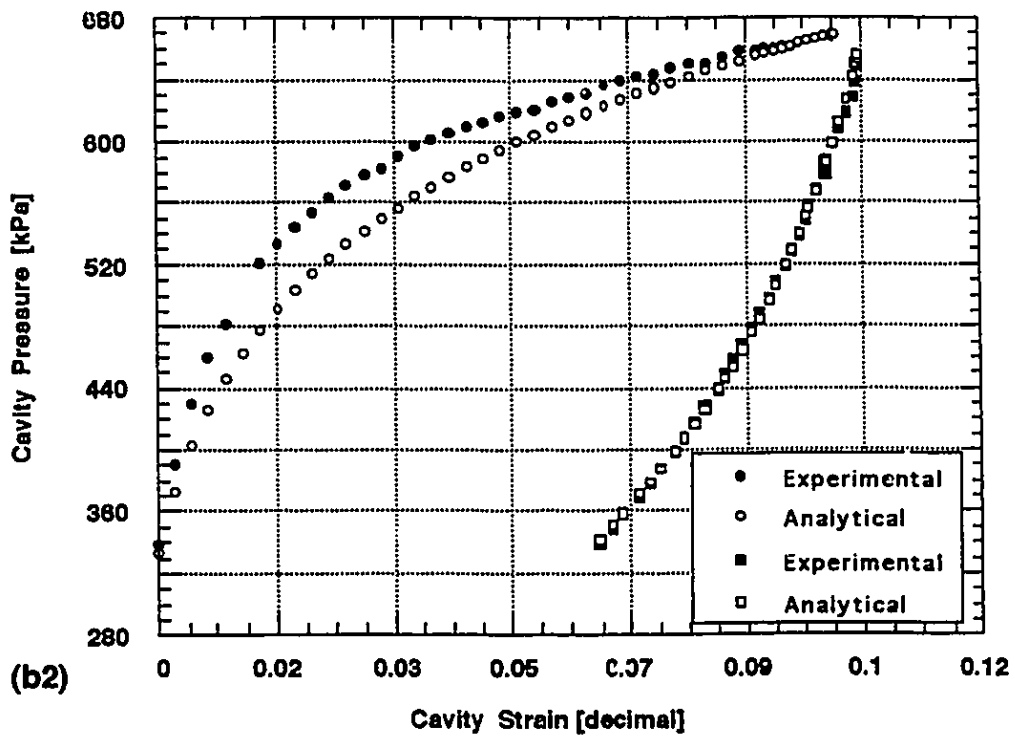


Fucino Clay - Test V2P12 - Unload Fitting



(b1)

Fucino Clay - Test V2P12 - Final Plot



(b2)

Figure C - 12 (b) Fucino clay test V2P12 b1) Unload fitting; (b2) Final plot

## PRESSUREMETER INTERPRETATION TEMPLATE - CLAYS

TEST ID Fucino clay - Test V2P13

DEPTH [m] 24.0 LIFT-OFF [kPa] 367.76

Loading :  $p_{max}$  [kPa] 713.76  $\epsilon_{max}$  [dec] 0.095

Unloading :  $p_{max}$  [kPa] 707.76  $\epsilon_{max}$  [dec] 0.099

**STEP # 1 - UNLOADING (Best fit with two parameters)**

(a) All unloading points

$\tau_{ult}^* = 209.0$  Graph Page Figure C - 13 (b1)

$2G_i = 20,612.9$

(b) (some data points removed)

$\tau_{ult}^* =$  Graph Page \_\_\_\_\_

$2G_i =$

**STEP # 2 - LOADING (Best fit with one parameter  $R_r=2.0$ )**

(a) All loading points

$\sigma_{ho} =$  Graph Page \_\_\_\_\_

(b) Strain range (first option) Last half

$\sigma_{ho} =$  Graph Page \_\_\_\_\_

(c) Strain range (second option) Last quarter

$\sigma_{ho} =$  Graph Page \_\_\_\_\_

(d) Strain range (third option) Interpolate points at the very last end

$\sigma_{ho} = 403.3$  Graph Page Figure C - 13 (b2)

**STEP # 3 - SUMMARY**

(a) First strain range selected: Step # 2 option (d)

$\tau_{ult}^* = 209.0$   $\tau_{ult} = 104.5$  Graph Page Figure C - 13 (b2)

$2G_i = 20,612.9$   $\sigma_{ho} = 404.3$

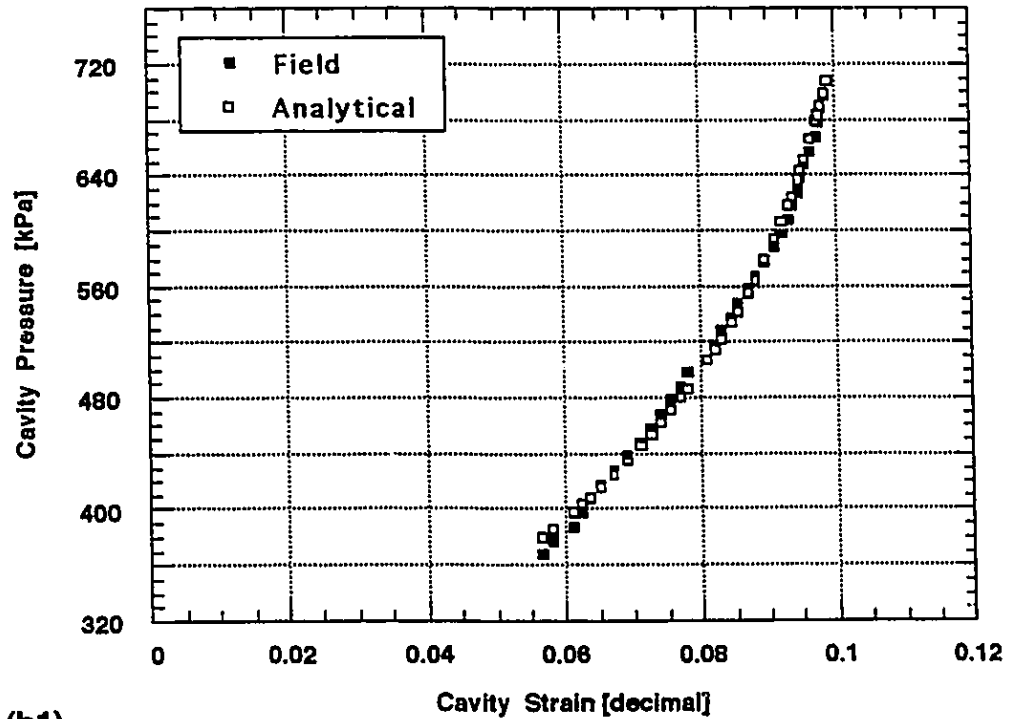
(b) Second strain range selected

$\tau_{ult}^* =$   $\tau_{ult} =$  Graph Page \_\_\_\_\_

$2G_i =$   $\sigma_{ho} =$

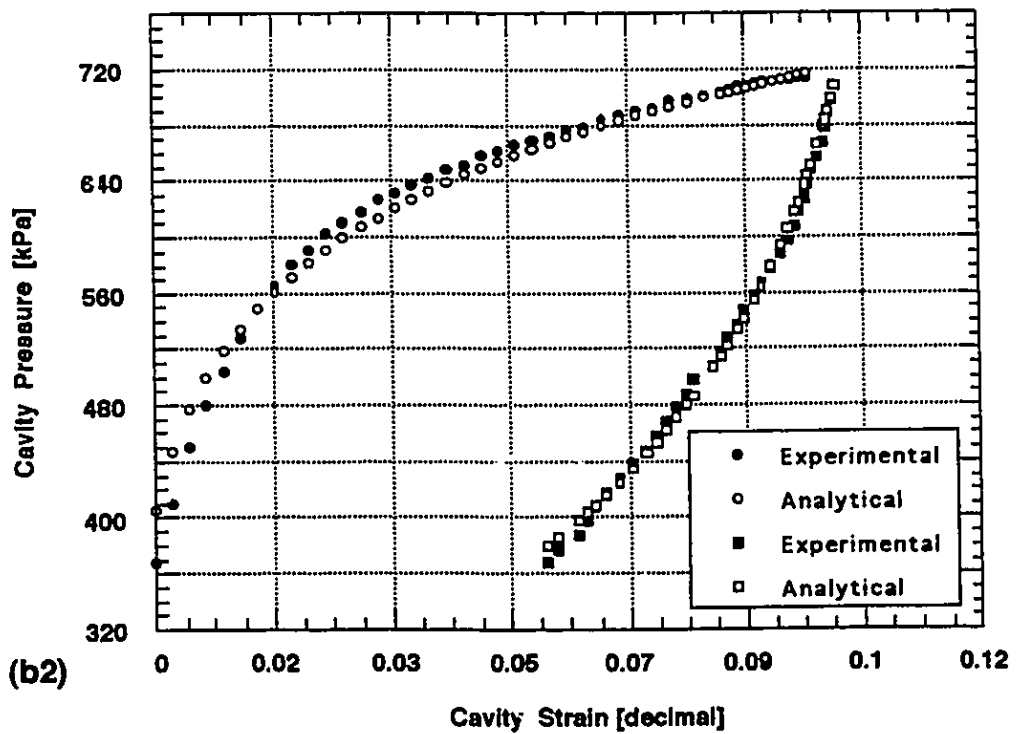
Figure C - 13 (a) Fucino clay test V2P13: Interpretation template.

Fucino Clay - Test V2P13 - Unload Fitting



(b1)

Fucino Clay - Test V2P13 - Final Plot



(b2)

Figure C - 13 (b) Fucino clay test V2P13 (b1) Unload fitting; (b2) Final plot

## PRESSUREMETER INTERPRETATION TEMPLATE - CLAYS

TEST ID Fucino clay - Test V2P14

DEPTH [m] 26.0 LIFT-OFF [kPa] 409.93

Loading :  $P_{max}$  [kPa] 792.53  $\epsilon_{max}$  [dec] 0.1025

Unloading :  $P_{max}$  [kPa] 779.93  $\epsilon_{max}$  [dec] 0.1074

**STEP # 1 - UNLOADING (Best fit with two parameters)**

(a) All unloading points

$\tau_{ult}^* = 233.0$  Graph Page Figure C - 14 (b1)

$2G_i = 22,377.0$

(b) (some data points removed)

$\tau_{ult}^* =$  Graph Page \_\_\_\_\_

$2G_i =$

**STEP # 2 - LOADING (Best fit with one parameter  $R_c=2.0$ )**

(a) All loading points

$\sigma_{ho} =$  Graph Page \_\_\_\_\_

(b) Strain range (first option) Last half

$\sigma_{ho} =$  Graph Page \_\_\_\_\_

(c) Strain range (second option) Last quarter

$\sigma_{ho} =$  Graph Page \_\_\_\_\_

(d) Strain range (third option) Interpolate points at the very last end

$\sigma_{ho} = 441.7$  Graph Page Figure C - 14 (b2)

**STEP # 3 - SUMMARY**

(a) First strain range selected: Step # 2 option (d)

$\tau_{ult}^* = 233.0$   $\tau_{ult} = 116.5$  Graph Page Figure C - 14 (b2)

$2G_i = 22,377.0$   $\sigma_{ho} = 441.7$

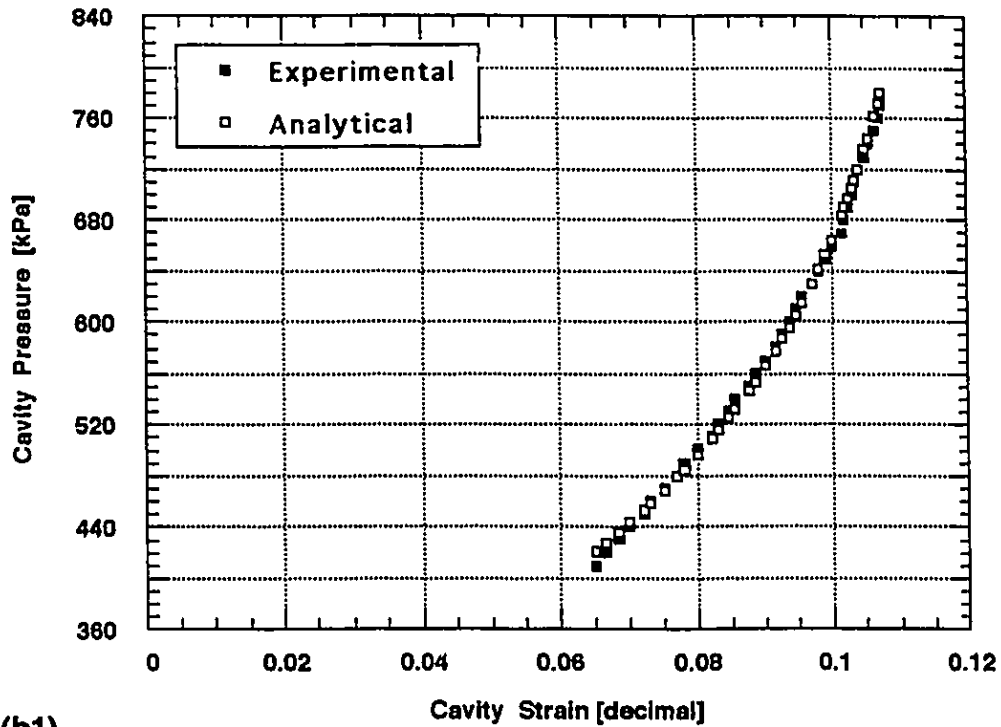
(b) Second strain range selected

$\tau_{ult}^* =$   $\tau_{ult} =$  Graph Page \_\_\_\_\_

$2G_i =$   $\sigma_{ho} =$

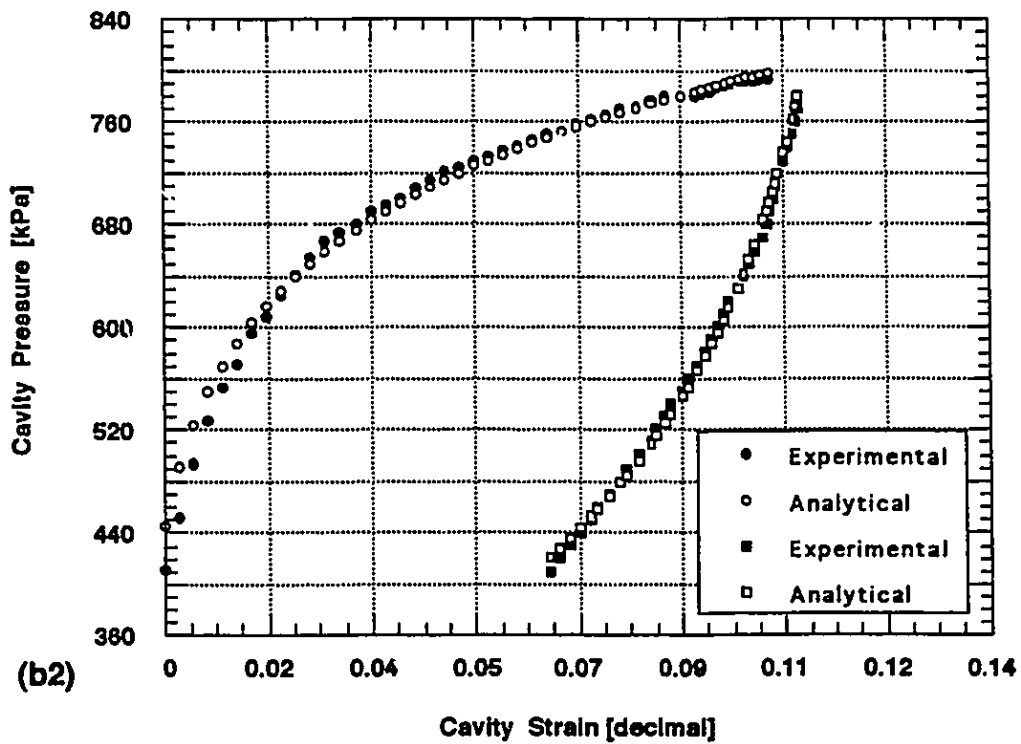
Figure C - 14 (a) Fucino clay test V2P14: Interpretation template.

Fucino Clay - Test V2P14 - Unload Fitting



(b1)

Fucino Clay - Test V2P14 - Final Plot



(b2)

Figure C - 14 (b) Fucino clay test V2P14 (b1) Unload fitting; (b2) Final plot

## PRESSUREMETER INTERPRETATION TEMPLATE - CLAYS

TEST ID Fucino clay - Test V2P15

DEPTH [m] 28.0 LIFT-OFF [kPa] 424.64

Loading :  $p_{\max}$  [kPa] 836.64  $\epsilon_{\max}$  [dec] 0.1065

Unloading :  $p_{\max}$  [kPa] 824.64  $\epsilon_{\max}$  [dec] 0.107

### STEP # 1 - UNLOADING (Best fit with two parameters)

#### (a) All unloading points

$\tau_{ult}^* = 250.6$  Graph Page Figure C - 15 (b1)

$2G_i = 25,395.1$

#### (b) (some data points removed)

$\tau_{ult}^* =$  Graph Page \_\_\_\_\_

$2G_i =$

### STEP # 2 - LOADING (Best fit with one parameter $R_c=2.0$ )

#### (a) All loading points

$\sigma_{ho} =$  Graph Page \_\_\_\_\_

#### (b) Strain range (first option) Last half

$\sigma_{ho} = 453.1$  Graph Page Figure C - 15 (b2)

#### (c) Strain range (second option) Last quarter

$\sigma_{ho} =$  Graph Page \_\_\_\_\_

#### (d) Strain range (third option) Interpolate points at the very last end

$\sigma_{ho} =$  Graph Page \_\_\_\_\_

### STEP # 3 - SUMMARY

#### (a) First strain range selected: Step # 2 option (b)

$\tau_{ult}^* = 250.6$   $\tau_{ult} = 125.3$  Graph Page Figure C - 15 (b2)

$2G_i = 25,395.1$   $\sigma_{ho} = 453.1$

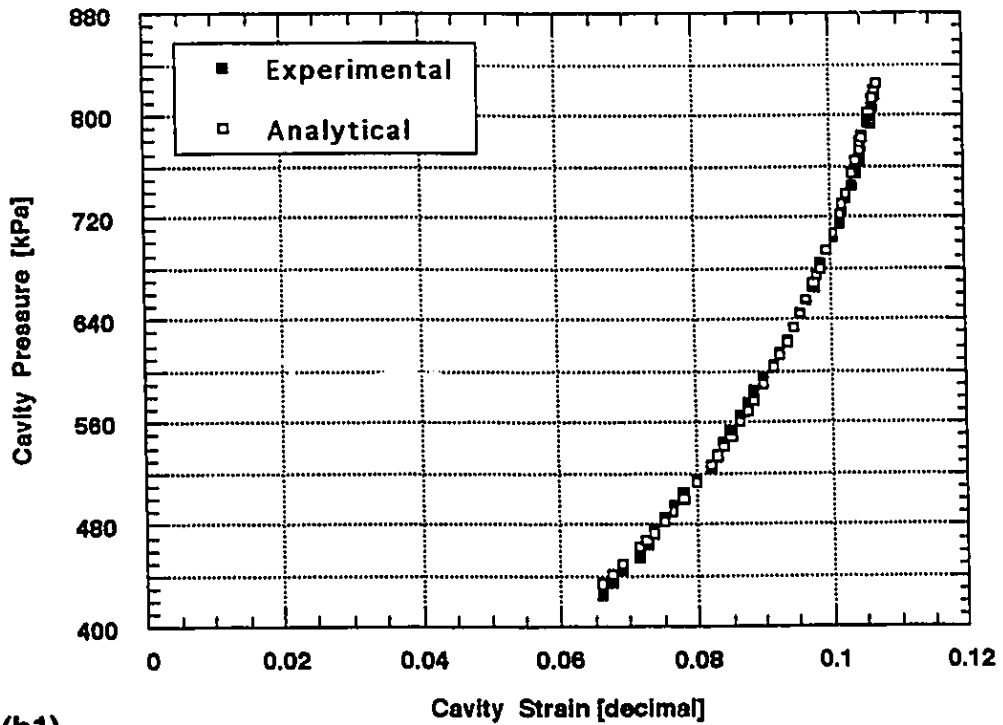
#### (b) Second strain range selected

$\tau_{ult}^* =$   $\tau_{ult} =$  Graph Page \_\_\_\_\_

$2G_i =$   $\sigma_{ho} =$

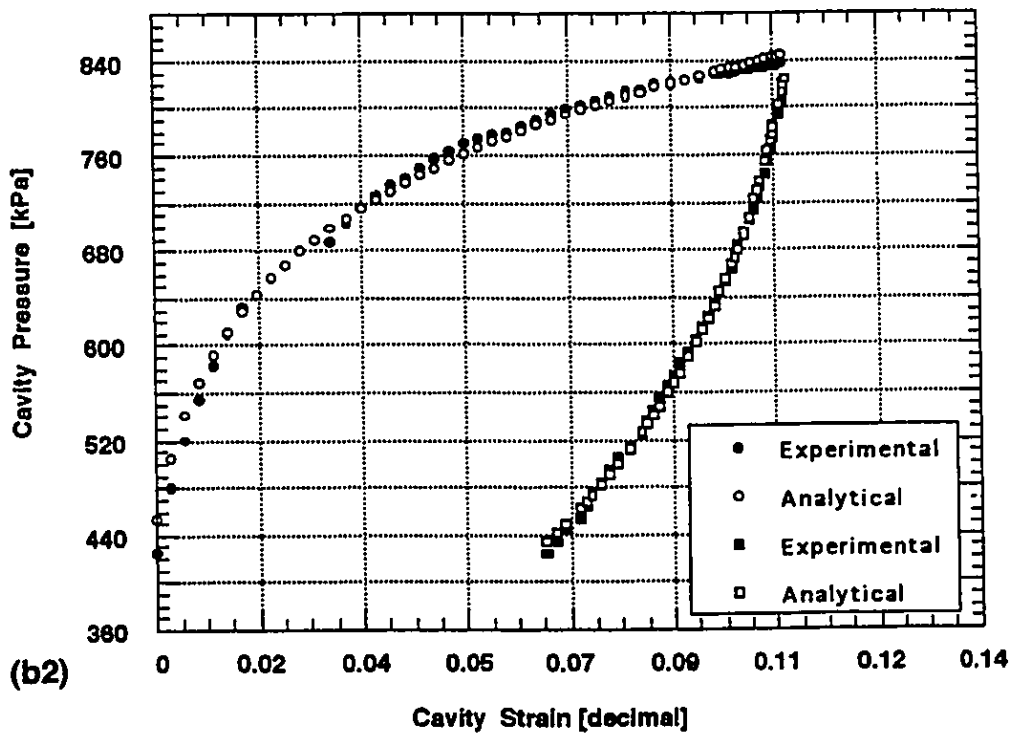
Figure C - 15 (a) Fucino clay test V2P15: Interpretation template.

Fucino Clay - Test V2P15 - Unload Fitting



(b1)

Fucino Clay - Test V2P15 - Final Plot



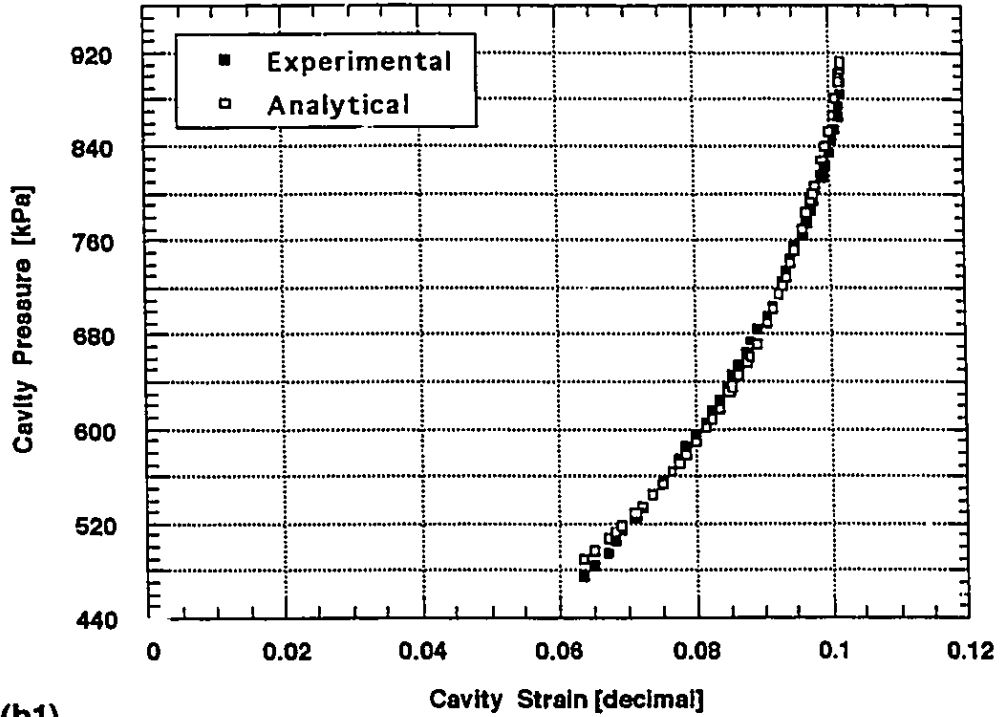
(b2)

Figure C - 15 (b) Fucino clay test V2P15 (b1) Unload fitting; (b2) Final plot



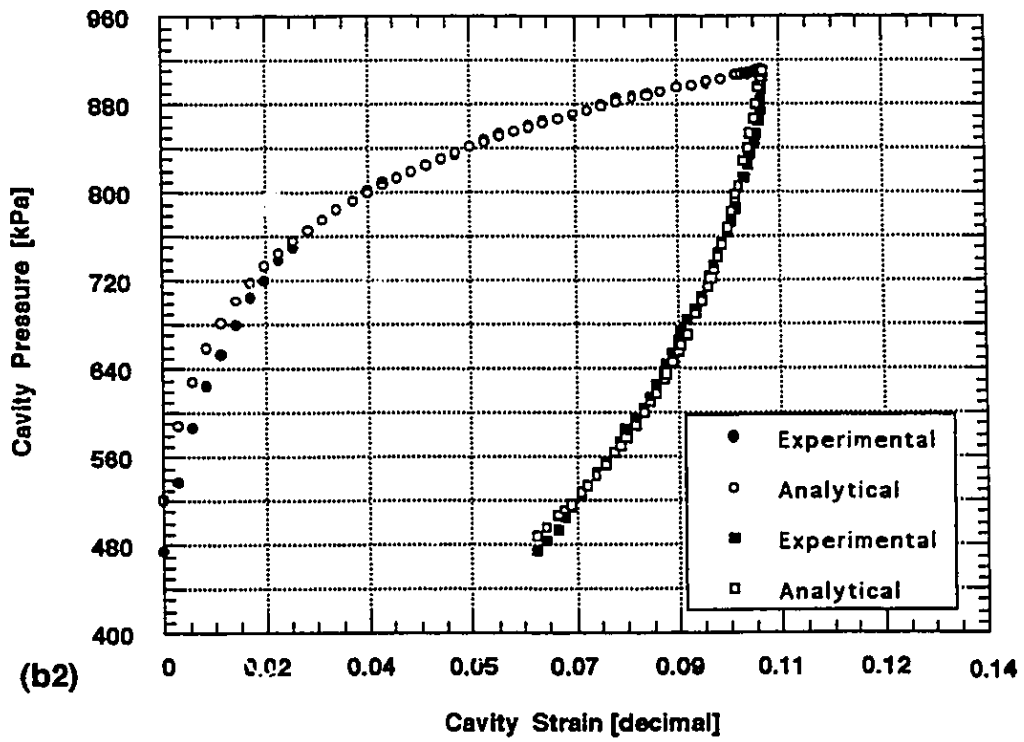


Fucino Clay - Test V2P16 - Unload Fitting



(b1)

Fucino Clay - Test V2P16 - Final Plot



(b2)

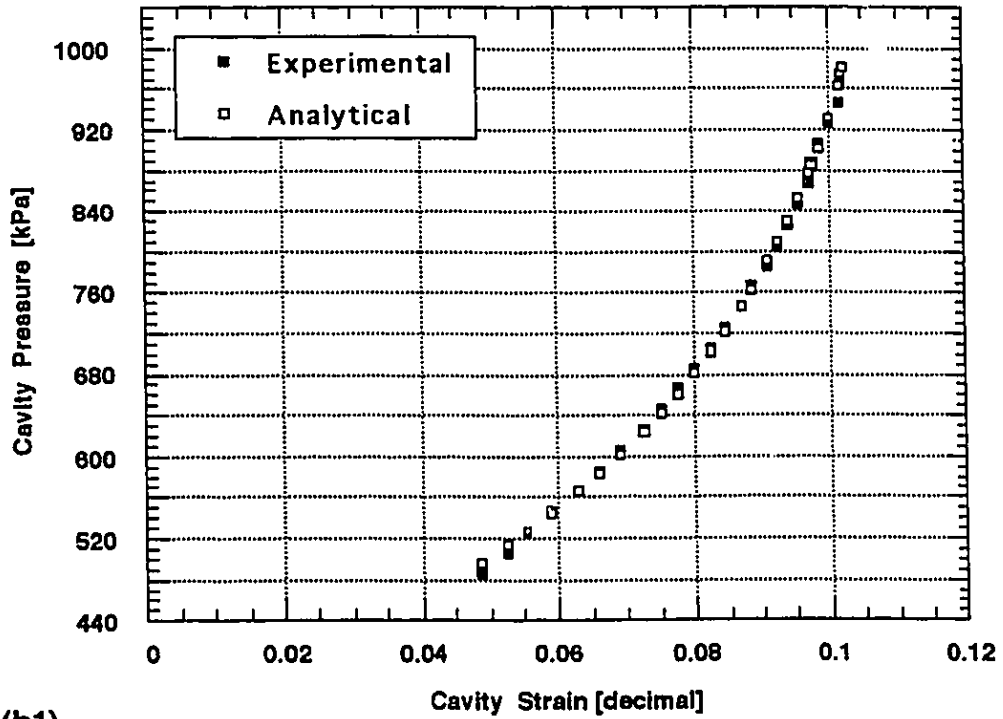
Figure C - 16 (b) Fucino clay test V2P16 (b1) Unload fitting; (b2) Final plot

## PRESSUREMETER INTERPRETATION TEMPLATE - CLAYS

TEST ID	Fucino clay - Test V2P17		
DEPTH [m]	32.0	LIFT-OFF [kPa]	486.43
Loading :	p <sub>max</sub> [kPa] 989.43	ε <sub>max</sub> [dec] 0.0975	
Unloading :	p <sub>max</sub> [kPa] 981.43	ε <sub>max</sub> [dec] 0.1023	
<b>STEP # 1 - UNLOADING (Best fit with two parameters)</b>			
<b>(a) All unloading points</b>			
	τ <sub>ult</sub> <sup>*</sup> = 284.8	Graph Page	Figure C - 17 (b1)
	2G <sub>i</sub> = 26,332.3		
<b>(b) (some data points removed)</b>			
	τ <sub>ult</sub> <sup>*</sup> =	Graph Page	_____
	2G <sub>i</sub> =		
<b>STEP # 2 - LOADING (Best fit with one parameter R<sub>c</sub>=2.0)</b>			
<b>(a) All loading points</b>			
	σ <sub>ho</sub> =	Graph Page	_____
<b>(b) Strain range (first option) Last half</b>			
	σ <sub>ho</sub> =	Graph Page	_____
<b>(c) Strain range (second option) Last quarter</b>			
	σ <sub>ho</sub> =	Graph Page	_____
<b>(d) Strain range (third option) Interpolate points at the very last end</b>			
	σ <sub>ho</sub> = 568.1	Graph Page	Figure C - 17 (b2)
<b>STEP # 3 - SUMMARY</b>			
<b>(a) First strain range selected: Step # 2 option (d)</b>			
	τ <sub>ult</sub> <sup>*</sup> = 284.8	τ <sub>ult</sub> = 142.4	Graph Page
	2G <sub>i</sub> = 26,332.3	σ <sub>ho</sub> = 568.1	Figure C - 17 (b2)
<b>(b) Second strain range selected</b>			
	τ <sub>ult</sub> <sup>*</sup> =	τ <sub>ult</sub> =	Graph Page
	2G <sub>i</sub> =	σ <sub>ho</sub> =	_____

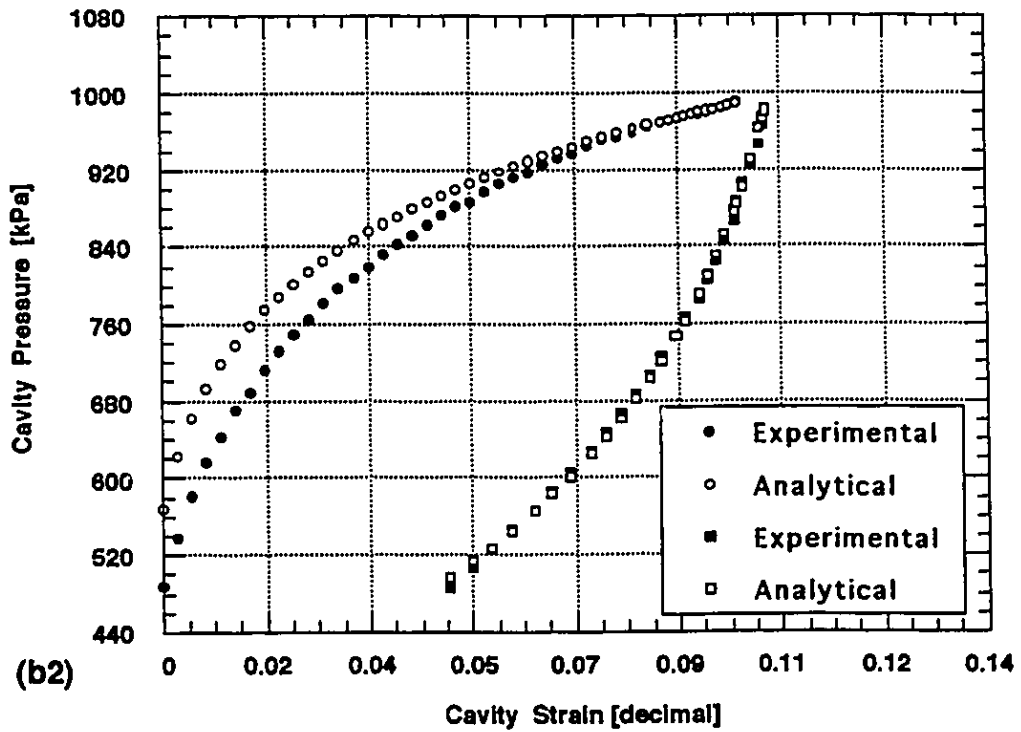
Figure C - 17 (a) Fucino clay test V2P17: Interpretation template.

Fucino Clay - Test V2P17 - Unload Fitting



(b1)

Fucino Clay - Test V2P17 - Final Plot



(b2)

Figure C - 17 (b) Fucino clay test V2P17 (b1) Unload fitting; (b2) Final plot

## PRESSUREMETER INTERPRETATION TEMPLATE - CLAYS

TEST ID Fucino clay - Test V2P18

DEPTH [m] 34.0 LIFT-OFF [kPa] 497.21

Loading :  $p_{max}$  [kPa] 953.21  $\epsilon_{max}$  [dec] 0.099

Unloading :  $p_{max}$  [kPa] 944.21  $\epsilon_{max}$  [dec] 0.1025

**STEP # 1 - UNLOADING (Best fit with two parameters)**

(a) All unloading points

$\tau_{ult}^* = 254.2$  Graph Page Figure C - 18 (b1)

$2G_i = 28,235.7$

(b) (some data points removed)

$\tau_{ult}^* =$  Graph Page \_\_\_\_\_

$2G_i =$

**STEP # 2 - LOADING (Best fit with one parameter  $R_c=2.0$ )**

(a) All loading points

$\sigma_{ho} =$  Graph Page \_\_\_\_\_

(b) Strain range (first option) Last half

$\sigma_{ho} =$  Graph Page \_\_\_\_\_

(c) Strain range (second option) Last quarter

$\sigma_{ho} =$  Graph Page \_\_\_\_\_

(d) Strain range (third option) Interpolate points at the very last end

$\sigma_{ho} = 555.1$  Graph Page Figure C - 18 (b2)

**STEP # 3 - SUMMARY**

(a) First strain range selected: Step # 2 option (d)

$\tau_{ult}^* = 254.2$   $\tau_{ult} = 127.1$  Graph Page Figure C - 18 (b2)

$2G_i = 28,235.7$   $\sigma_{ho} = 555.1$

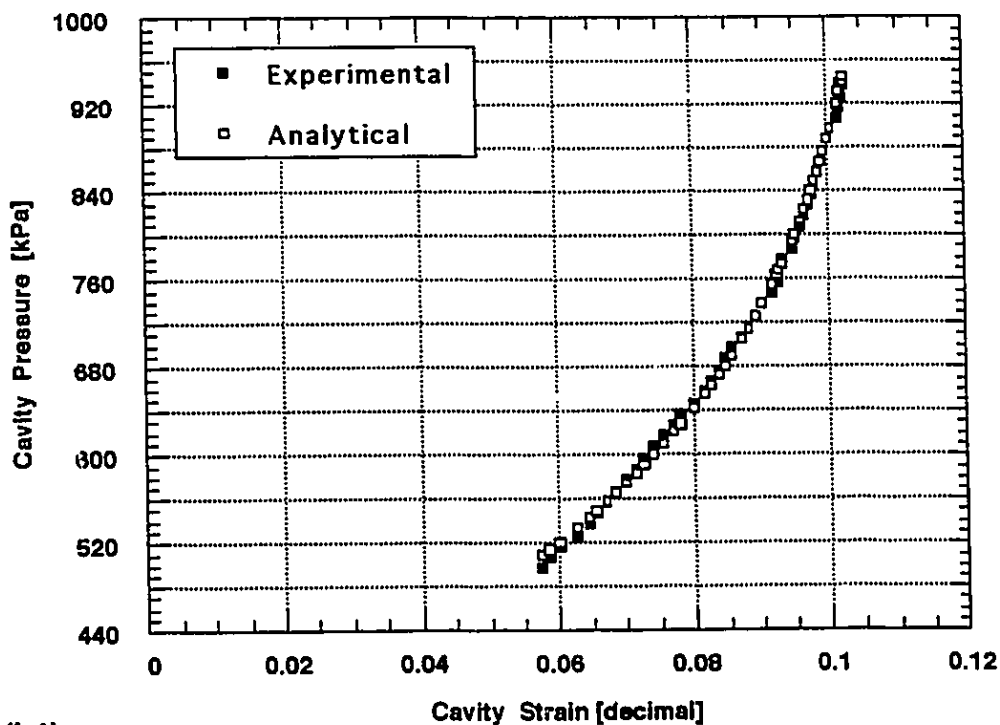
(b) Second strain range selected

$\tau_{ult}^* =$   $\tau_{ult} =$  Graph Page \_\_\_\_\_

$2G_i =$   $\sigma_{ho} =$

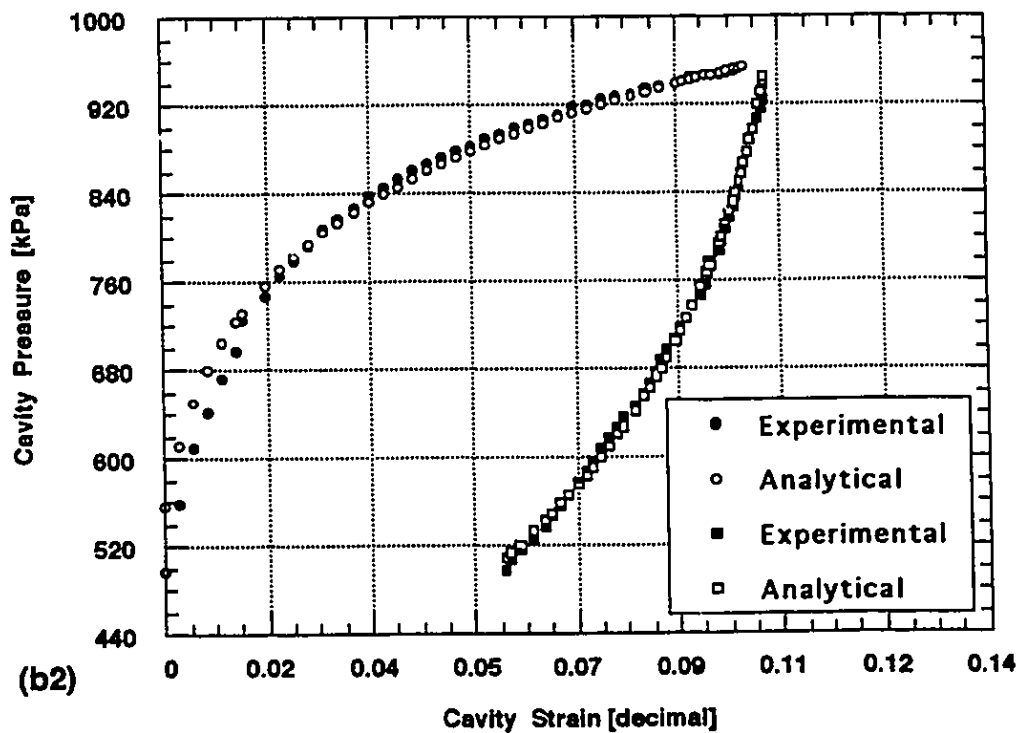
Figure C - 18 (a) Fucino clay test V2P18: Interpretation template.

Fucino Clay - Test V2P18 - Unload Fitting



(b1)

Fucino Clay - Test V2P18 - Final Plot



(b2)

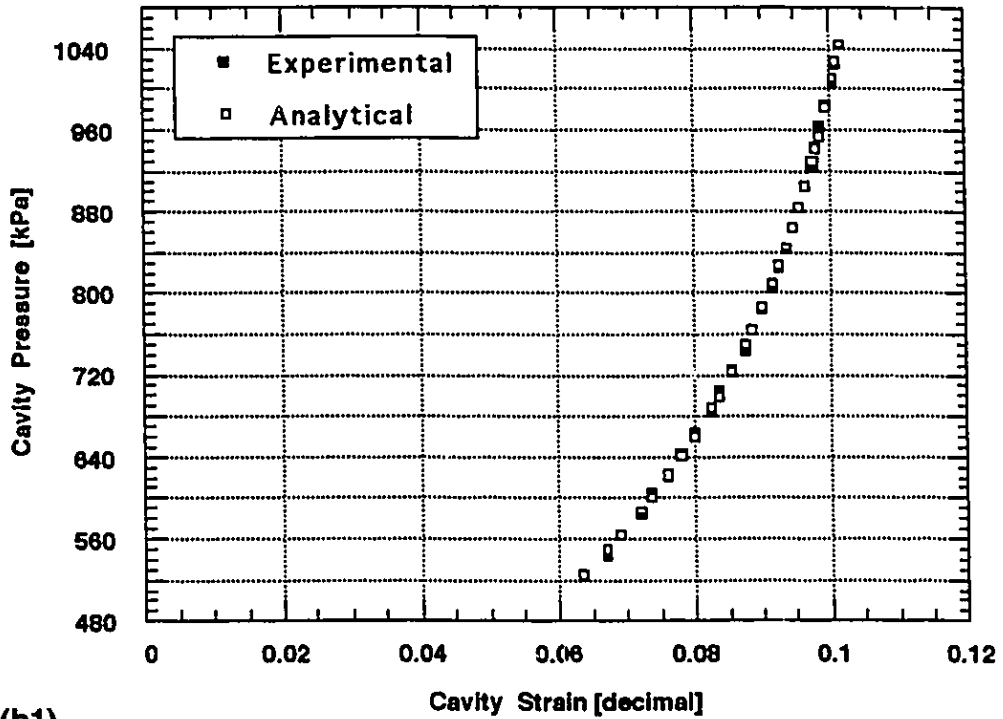
Figure C - 18 (b) Fucino clay test V2P18 (b1) Unload fitting; (b2) Final plot

## PRESSUREMETER INTERPRETATION TEMPLATE - CLAYS

TEST ID	Fucino clay - Test V2P19		
DEPTH [m]	36.0	LIFT-OFF [kPa]	524.67
Loading :	p <sub>max</sub> [kPa] 1,056.67	ε <sub>max</sub> [dec] 0.0985	
Unloading :	p <sub>max</sub> [kPa] 1,044.67	ε <sub>max</sub> [dec] 0.1015	
<b>STEP # 1 - UNLOADING (Best fit with two parameters)</b>			
<b>(a) All unloading points</b>			
	τ <sub>ult</sub> <sup>*</sup> = 314.7	Graph Page	Figure C - 19 (b1)
	2G <sub>i</sub> = 38,424.9		
<b>(b) (some data points removed)</b>			
	τ <sub>ult</sub> <sup>*</sup> =	Graph Page	_____
	2G <sub>i</sub> =		
<b>STEP # 2 - LOADING (Best fit with one parameter R<sub>c</sub>=2.0)</b>			
<b>(a) All loading points</b>			
	σ <sub>ho</sub> =	Graph Page	_____
<b>(b) Strain range (first option) Last half</b>			
	σ <sub>ho</sub> =	Graph Page	_____
<b>(c) Strain range (second option) Last quarter</b>			
	σ <sub>ho</sub> =	Graph Page	_____
<b>(d) Strain range (third option) Interpolate points at the very last end</b>			
	σ <sub>ho</sub> = 549.8	Graph Page	Figure C - 19 (b2)
<b>STEP # 3 - SUMMARY</b>			
<b>(a) First strain range selected: Step # 2 option (d)</b>			
	τ <sub>ult</sub> <sup>*</sup> = 314.7	τ <sub>ult</sub> = 157.4	Graph Page Figure C - 19 (b2)
	2G <sub>i</sub> = 38,424.9	σ <sub>ho</sub> = 549.8	
<b>(b) Second strain range selected</b>			
	τ <sub>ult</sub> <sup>*</sup> =	τ <sub>ult</sub> =	Graph Page _____
	2G <sub>i</sub> =	σ <sub>ho</sub> =	

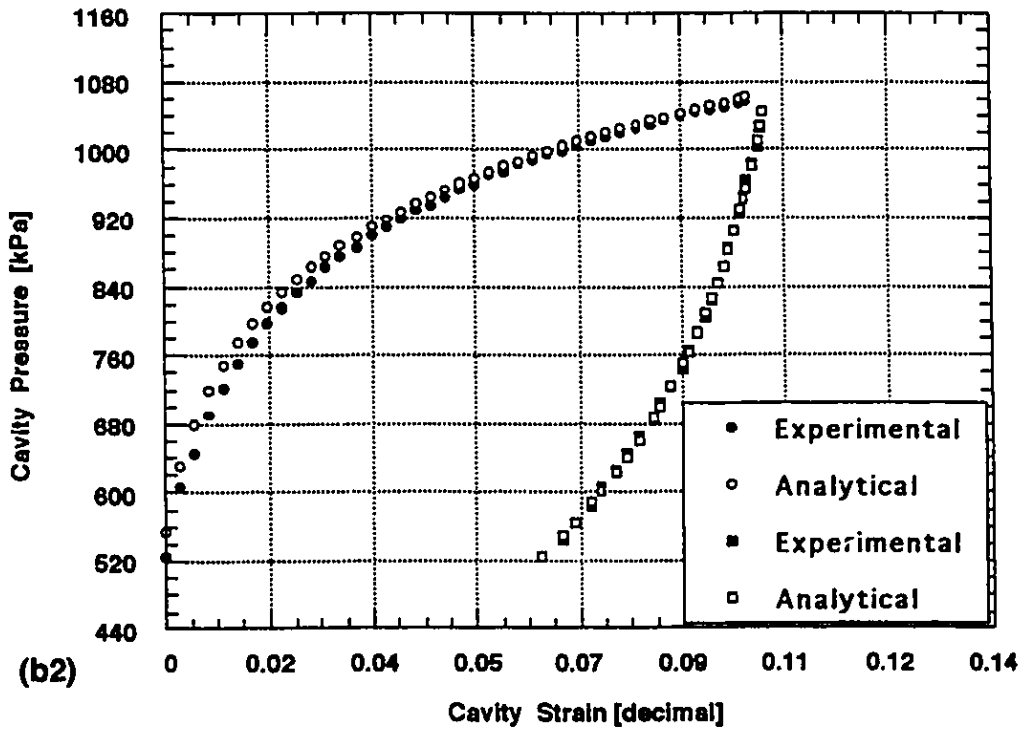
Figure C - 19 (a) Fucino clay test V2P19: Interpretation template.

Fucino Clay - Test V2P19 - Unload Fitting



(b1)

Fucino Clay - Test V2P19 - Final Plot



(b2)

Figure C - 19 (b) Fucino clay test V2P19 (b1) Unload fitting; (b2) Final plot

## PRESSUREMETER INTERPRETATION TEMPLATE - CLAYS

TEST ID Fucino clay - Test V2P20

DEPTH [m] 38.0 LIFT-OFF [kPa] 567.83

Loading :  $p_{max}$  [kPa] 1,142.83  $\epsilon_{max}$  [dec] 0.1025

Unloading :  $p_{max}$  [kPa] 1,127.83  $\epsilon_{max}$  [dec] 0.1045

### STEP # 1 - UNLOADING (Best fit with two parameters)

#### (a) All unloading points

$\tau_{ult}^* = 291.2$  Graph Page Figure C - 20 (b1)

$2G_i = 32,392.9$

#### (b) (some data points removed)

$\tau_{ult}^* =$  Graph Page \_\_\_\_\_

$2G_i =$

### STEP # 2 - LOADING (Best fit with one parameter $R_c=2.0$ )

#### (a) All loading points

$\sigma_{ho} =$  Graph Page \_\_\_\_\_

#### (b) Strain range (first option) Last half

$\sigma_{ho}^* =$  Graph Page \_\_\_\_\_

#### (c) Strain range (second option) Last quarter

$\sigma_{ho} =$  Graph Page \_\_\_\_\_

#### (d) Strain range (third option) Interpolate points at the very last end

$\sigma_{ho} = 681.3$  Graph Page Figure C - 20 (b2)

### STEP # 3 - SUMMARY

#### (a) First strain range selected: Step # 2 option (d)

$\tau_{ult}^* = 291.2$   $\tau_{ult} = 145.6$  Graph Page Figure C - 20 (b2)

$2G_i = 32,392.9$   $\sigma_{ho} = 681.3$

#### (b) Second strain range selected

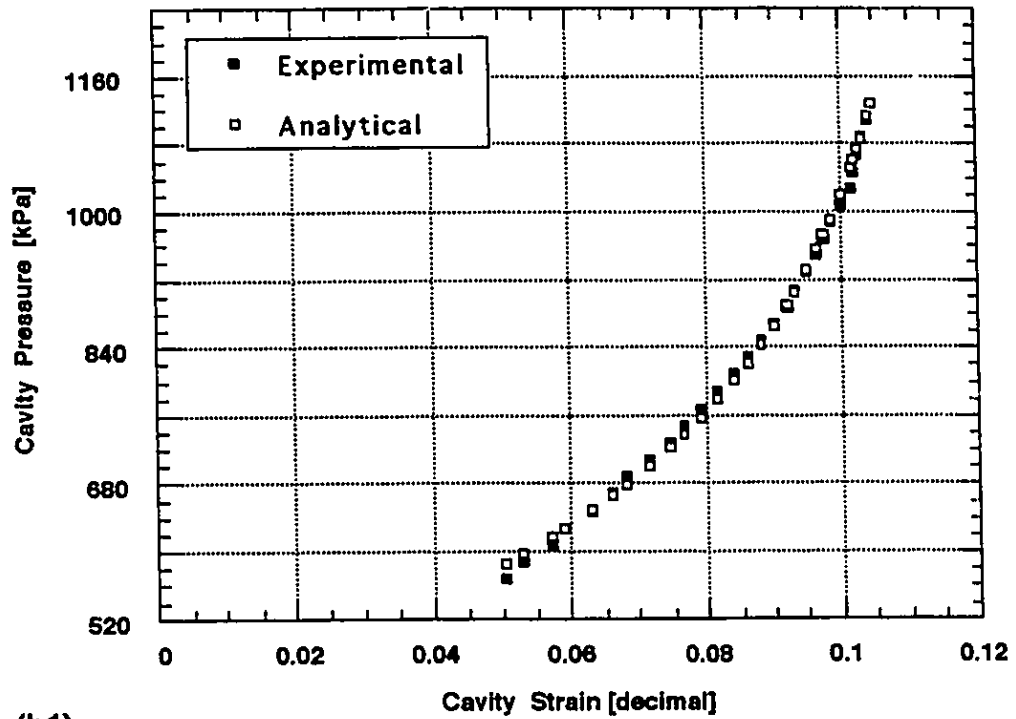
$\tau_{ult}^* =$   $\tau_{ult} =$  Graph Page \_\_\_\_\_

$2G_i =$   $\sigma_{ho} =$

Figure C - 20 (a) Fucino clay test V2P20: Interpretation template.

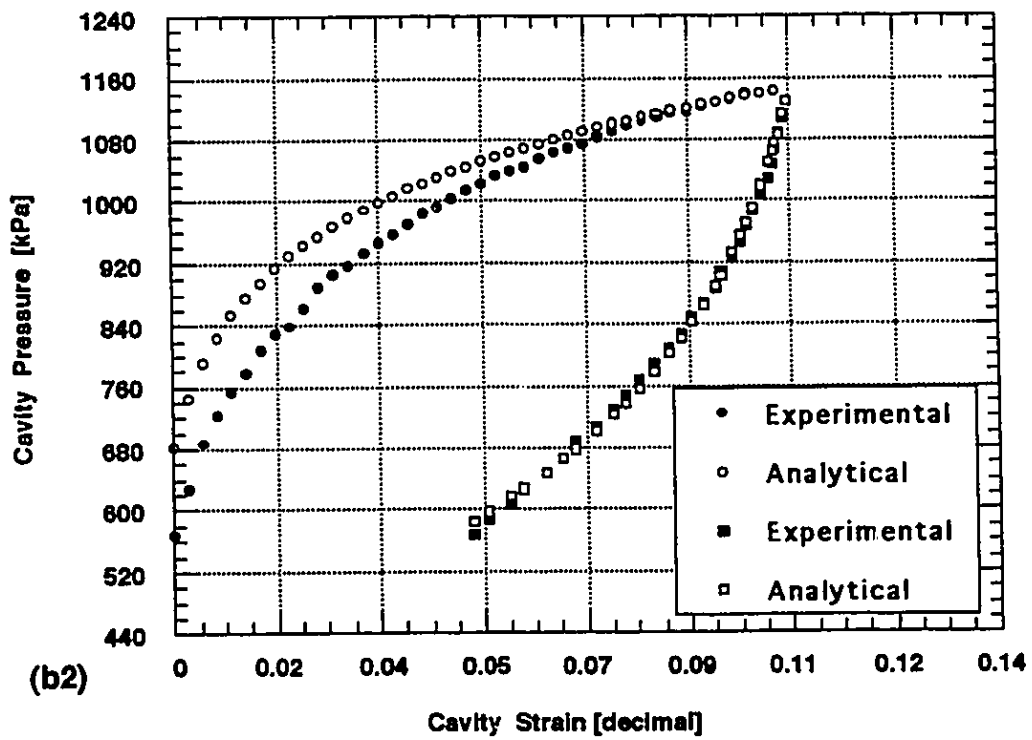


Fucino Clay - Test V2P20 - Unload Fitting



(b1)

Fucino Clay - Test V2P20 - Final Plot



(b2)

Figure C - 20 (b) Fucino clay test V2P20 (b1) Unload fitting; (b2) Final plot